MECHANICAL DEFORMATION OF THE INTERMETALLIC COMPOUND, NiAl

A Thesis Submitted for

the Degree of

Doctor of Philosophy

in the

University of London

by

RICHARD TERRY PASCOE

Department of Metallurgy

Imperial College of Science and Technology

London University

October, 1966

ABSTRACT

Single crystals of the intermetallic compound NiAl have been grown by the Bridgman and strain-anneal techniques. Their deformation behaviour in compression has been studied, and compared with polycrystals, as a function of temperature, strain-rate, composition, orientation and grain size.

All crystals with compression axes remote from $[\bar{0}01]$ slipped in an $[00\bar{1}]$ direction, the slip plane was dependent on temperature and orientation. Constraining slip on these primary systems resulted in the operation of other deformation modes. These included slip in $[\bar{1}11]$ and $[\bar{0}11]$ directions, kinking and a martensitic transformation. The observed slip systems were compared with the energies and mobilities of the corresponding dislocations calculated from anisotropic elasticity theory.

The temperature and strain-rate dependence of flow stress was divided into three distinct regions. Below 0.2 T_m and above 0.4 T_m the rate controlling processes were strongly thermally activated; a temperature independent process was observed at intermediate temperatures. The flow stress of polycrystals was controlled by the motion of $\underline{a}[\bar{1}00]$ dislocations, and showed a similar temperature dependence to single crystals that slipped in a $[\bar{1}00]$ direction. These crystals were generally much softer than those with $[\bar{0}01]$ axes.

The rate controlling process at low temperatures was consistent with a model of the nucleation of dislocation kink pairs against the

Peierls-Nabarro stress, but there was evidence for a further process operating at low stresses. The intermediate temperature process was associated with solid solution hardening caused by the lattice defects present in non-stoichiometric compositions. Several deformation mechanisms appeared to operate at high temperatures, these involved the climb or cross-slip of dislocations around obstacles.

Polycrystals retained some deformability to 77°K. The brittle nature of the material was explained by the high stress required to cause dislocation motion because sufficient slip systems were available for general ductility.

CONTENTS.

Chapter 1 Introduction and Literature Survey.

1.1. Introduction.

Intermetallic compounds which remain fully ordered to their melting points form a class of material which has, as yet, received little attention. Most of their physical and mechanical properties are still unexplored. This neglect seems to be due to experimental difficulties in preparing and handling these materials, and to their lack of industrial application. The growing requirements for new and special materials has led to increased interest in these compounds, some for their superconducting properties, some as semiconductors, and others as the basis of high strength, high temperature alloys.

NiAl has one of the simplest crystal structures of all intermetallic compounds, that of CsCl. It is therefore a useful material on which to try to build an understanding of these compounds, and to perfect the techniques for handling them. This compound has a relatively high melting point (up to 1638°C), a good resistance to oxidation (below 1100°C) and high strength. Thus it has considerable potential as a useful high temperature material, particularly as its two constituents are metals in common use which are readily available at a reasonable cost. In common with other materials envisaged for high temperature applications, such as ceramics, cermets and some refractory metals, NiAl suffers from the disadvantages that it is brittle at low temperatures, whilst its strength at elevated temperatures is low.

Although industrial exploitation of the useful properties of NiAl has been hampered by low temperature brittleness, and the lack of "workability", some applications have already been found for the material. Attempts have been made to use the corrosion resistant properties to protect gas turbine blades, but the protective layer was not sufficiently adherent and was susceptible to spalling on cyclic heating. Other applications include high density exothermic sprayed coatings (Sheppard, 1963) and resistance heating elements.

In addition to these possible industrial applications NiAl is also of considerable fundamental interest. The compound is stable across a wide range of composition, the formula NiAl describing the perfect stoichiometric structure on which this phase is based. Different defect structures are observed on either side of this stoichiometric composition. Additional nickel atoms are able to substitute for aluminium, but extra aluminium atoms prefer to occupy aluminium sites, leading to vacancy formation on the nickel sublattice. Thus this compound is ideal for comparing the effects of substitutional and vacancy defects on mechanical and physical properties.

At the start of this investigation NiAl was known to be hard and brittle at low temperatures, but the only useful quantitative information available was the hardness values of Westbrook (1956). There was no reliable data on the atomic mechanisms of slip.

The object of the present research was to make a general survey of the deformation behaviour of single and polycrystalline NiAl. This was to be achieved by studying, in detail, the slip processes and

deformation mechanisms in an alloy of equiatomic composition. These were to be compared with similar measurements on polycrystals of non-stoichiometric composition, to determine the hardening mechanisms and other effects of the defect structure. It was hoped that in this way the reasons for the low temperature brittleness and low strength at elevated temperatures would be found, and some insight gained into the deformation characteristics of materials of this type.

1.2. The Crystal Structure and Order of NiAl.

1.2.1. The Nickel-Aluminium Phase Diagram.

The nickel-aluminium phase diagram was first investigated by Gwyer (1908), who measured the solidus and liquidus temperatures over the full range of compositions, but was unable to determine accurately the solid phases present or their range of homogeneity.

The X-ray investigation of Bradley and Taylor (1937) established the composition range of the phases present at room temperature, including the β (NiAl) intermetallic compound. Inaccuracies in these diagrams, largely in the α' (Ni_3Al) phase region, were revealed by further studies, using conventional techniques, (e.g. Fink and Wiley, (1934) working on aluminium rich alloys; Alexander and Vaughn (1937); and Phillips (1942), who studied ternary alloys with iron and silicon). The currently accepted phase diagram for the system (Hansen, 1958) is shown in Fig 1.1.

The β phase, with which this investigation was concerned, exists about the stoichiometric composition NiAl (50 at % Al = 31.5 wt % Al). The phase is stable over a wide composition range, from 41.5 to 55 at % Al (i.e. 24.5 to 36 wt % Al) at room temperature. The homogeneity range gradually widens with increasing temperature. The stoichiometric composition has a congruent melting point at 1638°C; deviations from this composition result in a decrease in the liquidus temperature, and an even sharper drop in the solidus temperature. Thus alloys near the limit of the phase field solidify over a wide range of temperature.

1.2.2. The Crystal Structure of NiAl.

NiAl has a CsCl (B.2) crystal structure with a maximum lattice parameter of 2.887 Å (Bradley and Taylor, 1937). This is an ordered body-centred cubic structure (Fig 1.2), consisting of two interpenetrating simple cubic lattices, one of nickel and one of aluminium atoms, with the corner atoms of one of the cubic sublattices located at the centre of the other. The Bravais lattice is simple cubic with two atoms per lattice point.

Bradley and Taylor (1937) investigated the variations of density and lattice parameter with composition, and found that the density increased with increasing nickel content across the entire phase field, but that the lattice parameter showed a maximum near the stoichiometric composition. They explained this result in terms of different defect structures on either side of stoichiometry. Nickel rich alloys are simple solid solutions of nickel in NiAl; the smaller, heavier nickel atoms substitute for aluminium atoms, resulting in a rise in density and a decrease in lattice parameter. Aluminium atoms prefer to occupy aluminium atomic sites. Since there are equal numbers of each type of atomic site in the CsCl lattice this leads to a surplus of vacancies on nickel sites in aluminium rich alloys, and causes a decrease in both density and lattice parameter. This explanation has been confirmed by measurements of the intensities of X-ray reflections.

The variation of lattice parameter with composition has since been investigated by Cooper (1963 A) who confirmed most of the earlier observations, but found that the maximum lattice parameter was

displaced to the aluminium rich side of the equi-atomic composition; the maximum lattice spacing was found to be 2.8864 ($\pm$ 0.0006) Å at 51 at % Al. This displacement was explained by the substitution of up to 1.5 at % Al on nickel sites before significant vacancy formation started.

Aluminium-rich compositions have been compared with γ brass by Bradley and Taylor and found to be similar in colour, fracture and extreme brittleness. The δ brass structure may be derived from the CsCl structure of β brass by stacking together twenty seven body-centred cubic unit cells, removing two copper atoms, and rearranging slightly to form a large unit cell of fifty-two atoms. Aluminium-rich NiAl is very similar except that nickel atoms are removed randomly, retaining the cubic symmetry. The composition at which the δ brass electron-to-atom ratio of 21:13 occurs lies within the NiAl homogeneity range.

The unusual defect structure has been explained by the electron theory and the Hume-Rothery rules of alloy phases (Lipson and Taylor, 1939, Hume-Rothery and Raynor, 1962). In the body-centred cubic phases the Fermi surface touches the Brillouin zone at an electron-to-atom (e/a) ratio of 1.48. The phase should be stable up to this value, although in practice ratios of 1.5 and higher are observed. Normally when the critical e/a ratio is reached the phase field terminates, but in some compounds, including NiAl, the single phase region may be extended to higher apparent electron concentrations by the formation of a defect structure in which the number of electrons

per unit cell does not exceed the critical value.

NiAl may be classed as an electron compound because the atomic sizes differ by only 14% and a body centred cubic compound is observed at e/a = 1.5 (aluminium is tri-valent and transition metals are normally given a valency of zero). The addition of further aluminium atoms to stoichiometric NiAl would raise e/a above the permitted level if substitution for nickel occurred. Thus the extra aluminium atoms occupy aluminium atomic sites, which leads to excess vacancies (over the normal thermal concentration) on nickel sites, but maintains the number of electrons in each unit cell at a constant value of three. Cooper has shown that there is, in practice, some solid solution of aluminium on nickel sites, and the observed maximum number of electrons per unit cell is 3.04.

An alternative explanation of the defect structure is based on size effects. The larger aluminium atoms will not fit into nickel sites without causing considerable strain. To differentiate between the effects of size and electron concentration Lipson and Taylor (1939) studied the effects of ternary additions on the defect structure. The addition of iron, which has the same size and valency as nickel, was found to have no effect; a maximum lattice spacing still occurred at 50 at % Al. When copper, which is the same size as nickel and is divalent, was added vacancy formation was observed even with a deficiency of aluminium. There was however a breakdown of quantitative agreement in copper alloys: e/a ratios of up to 3.38 were observed, and contours of constant number of atoms per unit cell coincided with

lines of constant aluminium content, suggesting that the atomic size factor is also of considerable importance. Measurements in Fe-Cu-Al alloys containing 50 at % Al showed that the number of vacant sites increased with copper content.

There has been considerable discussion as to whether the vacancies are clustered or distributed randomly. West (1964) has studied nuclear magnetic resonance in NiAl and found evidence of clustering of vacancies, which was not indicated by the X-ray measurements of Cooper (1963). Nuclear magnetic resonance is however more sensitive to changes in nearest neighbours (Cooper, 1964), and thus it is possible that the vacancies are clustered into small aggregates which would be consistent with both observations.

1.2.3. The Degree of Order and its Variation with Temperature in NiAl.

Whilst the evidence for a high degree of order in NiAl near room temperature is overwhelming the situation with regard to high temperature order is confused and the results are conflicting.

Room temperature X-ray measurements on NiAl, comparing the intensities of fundamental and superlattice lines, indicated a high degree of order (Cooper, 1963 B); as did the nuclear magnetic resonance measurements of West (1964) and West and Drain (1965), and the thermodynamic measurements of Steiner and Komarck (1964) (degree of disorder 4×10^{-4}). Electron density measurements by Ageev and Guseva (1949) and Cooper (1963 B) indicated that there is a transfer of charge to the short bond position, but no electron transfer between the atoms

associated with these bonds. Thus there is a degree of covalent bonding between the nickel and aluminium atoms, but no ionic contribution to the binding. This covalent bonding is responsible for the high ordering parameter, and the associated large values of reduction in volume and heat of mixing. (Kubachewski and Caterall 1956). Heats of formation of nickel-aluminium alloys have been measured calorimetrically by Kubachewski (1958), a maximum value of 14 Kcal $(g.\ atom)^{-1}$ was found in stoichiometric and aluminium-rich alloys, decreasing to 12 Kcal $(g.\ atom)^{-1}$ in a 60 at % Ni alloy. Further evidence for strong ordering forces is the observed operation of a $\underline{[100]}$ slip direction (see 1.3.1.).

Although some of the information regarding high temperature ordering is contradictory it is now generally accepted that NiAl is ordered to its melting point. Evidence for this is:

i) The strong ordering at low temperatures

ii) Bradley (1951) studied the system Ni-Fe-Al metallographically, and found that two β' phases, one disordered and the other ordered, were present in some ternary alloys, but that NiAl was single phase at all temperatures.

iii) A number of physical properties, which are dependent upon the degree of order, have been measured as a function of temperature, and no significant changes have been found, although it is possible that the change of some of the properties on disordering would be too small to be detected. Physical properties measured include the elastic constants up to 800°C (Wasilewski, 1966); slip systems up to 800°C

(Ball and Smallman, 1966 A); resistivity up to 1200°C (Guseva, 1951); and diffusion coefficients in the range 1050-1350°C (Berkowitz et al. 1954).

Room temperature X-ray measurements (Bradley and Taylor, 1937, Cooper, 1963 A) indicated that an improvement in the resolution of X-ray reflections could be obtained by slow cooling. This was attributed to the retention of high temperature disorder by rapid cooling, but as the effect was most marked with a {310} doublet, which is a fundamental line and not affected by ordering, the difference is probably due to quenching strains. Isaichew and Mirekskii (1940) reported significant disordering and vacancy formation as low as 900°C and that the ordering reaction could not be supressed by quenching. This result was checked by Guseva (1951) who detected no change up to 900°C by using high temperature X-ray measurements. The specific heat of the isomorphous compound CoAl, which is very similar to NiAl in its physical properties, was measured by Tret'yakov and Khomyakov (1959) using continuous adiabatic heating; a sharp change observed at 800°C was thought to be due to disordering.

The viscosity of molten nickel-aluminium alloys has been determined by Vertman and Samarin (1961) who found a maximum in the viscosity of the equiatomic composition which they attributed to short range order persisting into the liquid state. This result must be treated with caution because only a few measurements were made in the NiAl phase field, and these were all made in the temperature range 1600-1700°C, thus the degree of superheat varied considerably, and was a minimum at the equiatomic composition.

1.2.4. The Thermodynamics of Ordered Alloys

There has, as yet, been no systematic investigation into the thermodynamic properties of intermetallic compounds or the nickel-aluminium system. However the heat of formation of NiAl has been discussed with respect to the structure and stability of this compound; and Steiner and Komarek (1964) have measured the thermodynamic activities of aluminium in Ni-Al alloys and found a change of three orders of magnitude in the β-region which they attributed to the high stability of this phase.

One property which is of great importance when considering slip in ordered alloys is the energy of ordering, $\underline{v}$, which is defined as the change in energy when one atom is exchanged for another on a wrong site i.e.

$$v = v_{AB} - \tfrac{1}{2}(v_{AA} - v_{BB}) \qquad (1.1)$$

where $\underline{v}_{AB}$ is the bonding energy between unlike atoms and $\underline{v}_{AA}$ and $\underline{v}_{BB}$ are the bond energies between like atoms.

If $\underline{v}$ is negative then the ordered structure will be stable at low temperatures. At higher temperatures the entropy contribution to the ordering energy becomes significant, due to the difference in configurational entropy between an ordered and disordered state, ($\underline{S}$) and a critical temperature (T_c) may be reached where the free energy of ordering is zero.

i.e. $v = S\ T_c$

At this temperature an order-disorder transition will occur.

There have been numerous attempts to estimate $\underline{v}$ theoretically. Mott (1937) has attempted to calculate it for β-brass from the electron theory of metals, and Shimoji (1960) has extended this to more complex cases. These treatments give an order of magnitude correlation with the observed results.

Other attempts have been made to obtain a value of this parameter, but have proved mathematically difficult and an exact solution has only been obtained for simple two dimensional lattices (Krivoglaz and Smirov 1964). A number of simplified approximation methods have been used to obtain solutions for real three-dimensional lattices. The earliest of these was the theory of Bragg and Williams (1935), who used statistical methods to derive relationships between temperature, ordering energy and the degree of long range order. This theory predicts that for a CsCl structure the ordering energy will be related to the critical ordering temperature by

$$v = A\, k\, T_c \qquad (1.2)$$

It should be noted that various applications of the Bragg-Williams theory to CsCl structures employ differing values of the constant $\underline{A}$, values of $\frac{1}{4}$ and 4 are commonly used. This discrepancy is due to differences in the definition of $\underline{v}$. If $\underline{v}$ is the difference in bond energy between like and unlike atom $A = \frac{1}{4}$, but if $\underline{v}$ is defined as the energy gain on exchanging an atom with one on a "wrong" site then

A = 4, since this operation involves the cutting of sixteen unlike bonds.

A number of other approximation methods have been used since, and have been reviewed by Muto and Takagi (1955). Most of these theories predict relationships between the ordering energy and transition temperature of the form:

$$\frac{k\,T_c}{v} = \text{constant.}$$

The results of various theories for CsCl structures are listed by Guttman (1956) and Kriŵoglaz and Smirov (1964).

When compared with experimental results these theories meet with varying degrees of success. Most will predict the form of the temperature dependence of the long range order parameter or the specific heat, but these calculations involve the use of an experimentally determined critical temperature. Very little experimental information is available, although some calorimetric measurements of the ordering energy have been made by summing the latent heat of ordering (where the transformation is first order) and the heat evolved in the anomalous heat capacity region below the ordering temperature.

The ordering energy in β-brass has been measured by Sykes and Wilkinson (1937) and found to have a value between 0.024 and 0.028 eV $atom^{-1}$ (i.e. 0.550 to 0.645 Kgal $g\text{-}atom^{-1}$). If the Bragg-Williams theory is used to calculate this energy change, assuming that half the

nearest neighbour atoms are of the "wrong" type in the random disordered alloy, a value of 0.032 eV atom^{-1} is found. An alternative theory due to Bethe (1935) takes into account short range order which persists above the critical temperature, and predicts a value of 0.031 eV atom^{-1}. Although neither theoretical result lies within the experimental values, they may be considered to show reasonable agreement, particularly when it is realised that the errors in the experimental determination are considerable and that the material used would not be in a fully ordered state.

Since no one theory will predict the observed ordering energies the Bragg-Williams result will be used in future calculations. In determining the ordering energy of a material which remains ordered to its melting point a difficulty arises in not knowing the critical temperature. In such cases a lower limit for the critical temperature - the melting point - is normally used. Thus for stoichiometric NiAl (T_m = 1910^{o}K) $\underline{v}$ = 0.082 eV atom^{-1}.

1.2.5. The Stability of the CsCl lattice

Several intermetallic compounds with the CsCl lattice undergo transformations on cooling, indicating that the CsCl structure is unstable at low temperatures. Compounds which transform martensitically include AuCd, CuZn (Westbrook, 1960) and nickel-rich NiAl (Alexander and Vaughn, 1937). NiTi, which has a crystal structure similar to CsCl (Wang et al., 1965), has a martensite transformation near room temperature. This transition is thought to be the cause of

the relatively large ductility (up to 15% tensile elongation) of TiNi at room temperature.

The transformation in NiAl has been observed only in quenched alloys with a high nickel content. Crystallographic relationships in this and other martensite structures have been studied by Ball (1964) using electron microscopy. The appearance at fracture surfaces of NiAl martensite was studied by Guard and Turkalo (1960).

1.3. Crystallography of Deformation of Compounds with the CsCl Lattice.

1.3.1. The Dependence of the Slip Direction on Ordering Energy.

The direction of slip in compounds with the CsCl structure varies markedly with the degree of ordering and the character of the atomic bonding. Compounds such as CuZn and FeCo have the same slip direction as b.c.c. metals, i.e. $\langle 111 \rangle$, whilst the ionic crystals, CsBr and Tl (Br, I), and some intermetallic compounds e.g. AuZn, CuCd and NiAl, have a $\langle 100 \rangle$ slip direction. This behaviour is readily understood for b.c.c. metals and ionic crystals if the normal criterion for choosing the slip direction is applied, that is that slip occurs in the most close packed direction, i.e. with the shortest Burgers vector, $\underline{b}$. The shortest vector in the body centred cubic structure is $\frac{1}{2}\underline{a}\langle 111 \rangle$, thus the observed slip direction is predominantly $\langle 111 \rangle$. In ionic crystals there is a further requirement that overall electrical neutrality must be maintained. The operation of a $\frac{1}{2}\underline{a}\langle 111 \rangle$ Burgers vector would involve a positive ion moving to a negative site (or vice versa), therefore the shortest vector which fulfils this additional condition is $\underline{a}\langle 100 \rangle$; $\langle 100 \rangle$ is the observed slip direction.

In a superlattice the passage of a single $\frac{1}{2}\underline{a}\langle 111 \rangle$ dislocation would similarly lead to disordering. To minimise the energy increase so caused Koehler and Seitz (1947) proposed that dislocations in superlattices are in the form of superdislocations, the passage of which would leave no net disordering. A superdislocation in a CsCl lattice would consist of two $\frac{1}{2}\underline{a}\langle 111 \rangle$ imperfect dislocations joined by a

region of anti-phase boundary (APB). It can be seen that the total translation produced by such an array is $\underline{a}\langle 111\rangle$; and as the elastic energy of a dislocation is proportional to $\underline{b}^2$, the total elastic energy of the array is less than that of an $\underline{a}\langle 111\rangle$ unit dislocation. Such dislocations have been seen in partially ordered FeCo by Marcinkowski and Chessin (1964) using electron microscopy; their apparent absence in other CsCl compounds has been explained by the difficulty of resolving the small width of the ribbon of APB. This width, $\underline{w}$, is determined by an equilibrium between the surface energy of the APB ($\underline{E}_{APB}$) and the interaction energy between the imperfect dislocations ($\underline{E}_{int}$).

Assuming the entropy term associated with this configuration is small (Cottrell, 1951), the total free energy, $\underline{G}$, of the array is:

$$G = E_1 + E_2 + E_{int} + E_{APB} \tag{1.3}$$

where $\underline{E}_1$ and $\underline{E}_2$ are the elastic energies of the two imperfect dislocations of Burgers vector $\underline{b}_1$ and $\underline{b}_2$.

The interaction energy per unit length of dislocation line is given by (Cottrell, 1951):

$$E_{int} = \frac{K\, b_1\, b_2}{2\pi}\left[\ln\left(\frac{R}{w}\right) - n\right] \tag{1.4}$$

where $\underline{K}$ is a function of the elastic moduli.

$\underline{R}$ the conventional outer cut-off radius.

$\underline{n}$ a geometrical factor (= 1 for a screw dislocation and $\frac{1}{2}$ for edge dislocations on the same slip plane).

Brown and Herman (1956) in a calculation of the equilibrium spacing of superdislocations have shown that:

$$E_{APB} = NS^2(v_{AA} + v_{BB} - 2\,v_{AB}) \qquad (1.5)$$

where $\underline{N}$ is the number of atoms in the slipped part of one slip plane

$\underline{S}$ is the degree of long range order

$\underline{v}_{AA}$, $\underline{v}_{BB}$ and $\underline{v}_{AB}$ are bond energies as defined in Eqn 1.1

From equations 1.1 and 1.2

$$(v_{AA} + v_{BB} - 2\,v_{AB}) = \frac{k\,T_c}{2}$$

The number of atoms $\underline{N}$ per unit length in the APB,

$$= \frac{w}{\alpha a^2}$$

where $\underline{a}$ is the lattice spacing.

$\underline{\alpha}$ is a geometrical factor determined by the density of packing in the slip plane and the number of unlike bonds broken. Flinn (1960) has shown that for a fault on a plane (h k l) where

h ⩾ k ⩾ l in a CsCl lattice

$$\alpha = \frac{h}{\sqrt{h^2 + k^2 + l^2}}$$

Substituting these values in 1.5

$$E_{APB} = \frac{w}{\alpha a^2} \cdot S^2 \cdot \frac{k T_c}{2} \qquad (1.6)$$

$$\therefore \quad G = E_1 + E_2 + \frac{K b_1 b_2}{2\pi}\left[\ln\left(\frac{R}{w}\right) - n\right] + \frac{w S^2 k T_c}{2 \alpha a^2} \qquad (1.7)$$

At the equilibrium width

$$\frac{dG}{dw} = -\frac{K b_1 b_2}{2\pi} \cdot \frac{1}{w} + \frac{S^2 k T_c}{2 \alpha a^2} = 0$$

$$w = \frac{K b_1 b_2 a^2 \alpha}{\pi k T_c S^2} \qquad (1.8)$$

If typical values of $\underline{b}$, $\underline{k}$ and $\underline{T}_c$ are inserted in eqn. 1.8 $\underline{w}$ for screw dislocations on a {110} plane in both NiAl and CuZn is found to be $\sim$ 25 Å assuming $\underline{S} = 1$; this separation would be very difficult to resolve in an electron microscope. Marcinkowski (1962) has calculated the separation in FeCo (S = 0.59) and found a value of 125 Å, compared with 123 Å measured experimentally (Marcinkowski and Chessin, 1964).

Too much faith cannot be placed on the absolute value of the spacing because of the difficulties in measuring ordering energies (see 1.2.4.), and because this calculation takes no account of the

energy of the dislocation core. This could be of considerable importance in NiAl and CuZn where $\underline{w}$ is not large compared with the size of the core.

Not all CsCl structure intermetallic compounds, however, slip in a $\langle 111 \rangle$ direction; many show a preference for $\langle 100 \rangle$ particularly if there is some degree of ionic (e.g. LiTl and MgTl) or covalent bonding (e.g. NiAl) present. Rachinger and Cottrell (1956) attempted to correlate slip directions and ordering energy. They assumed a critical value of $\underline{E}_{APB}$ ($\underline{E}_c$) which exerts a force on the dislocation equal to the theoretical strength of the lattice.

$$\text{i.e. } E_c = \alpha \mu b \qquad (1.9)$$

where μ is the shear modulus

$\alpha\mu$ is the theoretical shear strength ($\alpha \simeq 1/30$)

If typical values for NiAl are inserted in eqn. 1.9 ($\mu = 2 \times 10^{12}$ dyne cm^{-2}, $\underline{b} = \frac{1}{2}\underline{a}\ 111 = 2.6 \times 10^{-8}$ cm) a value of the critical APB energy is found to be $\sim 1.5 \times 10^{3}$ erg cm^{-2}. The energy of the APB in NiAl, calculated from eqn. 1.6, is 220 erg cm^{-2}; this is well below the critical value, and a $\langle 111 \rangle$ primary slip direction should be observed. Thus this theory is not in quantitative agreement with the experimental findings because the operation of a $\langle 100 \rangle$ slip direction in NiAl is now well established (Ball and Smallman, 1966; Wasilewski and Rozner, 1966).

1.3.2. Determination of Slip Systems by Anisotropic Elasticity Theory.

Ball and Smallman (1966 B) have estimated the energies and mobilities of various dislocation arrays using anisotropic elasticity theory. These were calculated for unit dislocations with Burgers vectors $\underline{a}\langle 100\rangle$, $\underline{a}\langle 110\rangle$ and $\underline{a}\langle 111\rangle$ using the equations of Eshelby (1949):

$$\text{Energy} : E = \frac{k\,b^2}{4\pi} \ln\left(\frac{R}{r_o}\right) \qquad (1.10)$$

$$\text{Mobility} : S = 4\pi \frac{\zeta}{b} \exp\left(-2\pi \frac{\zeta}{b}\right) \qquad (1.11)$$

where $\underline{K}$ is a function of the elastic moduli and direction of the dislocation line in an anisotropic medium.

$\underline{R}$ and $\underline{r_o}$ are the conventional outer and inner cut-off radii

$\underline{\zeta}$ is the dislocation width defined by:

$$\zeta = \frac{b}{2} \cdot \frac{K}{C} \cdot \frac{d}{b}$$

where $\underline{C}$ is the shear modulus in the slip direction

$\underline{d}$ is the spacing between glide planes.

Since the energy of an $\underline{a}\langle 111\rangle$ dislocation may sometimes be reduced by the formation of a superdislocation the energies of these arrays were calculated using equation 1.3. It was assumed that the mobility of a superdislocation was greater than that of an $\underline{a}\langle 111\rangle$ unit dislocation.

In CsBr the $\underline{a}\langle 100\rangle$ dislocation was found to be the most stable

and mobile because dissociation into a superdislocation was prohibited by electrostatic interactions. In CuZn a superdislocation was shown to have a lower energy than the most stable unit dislocation, which was $\underline{a}\langle 100\rangle$. The lowest energy configuration in NiAl, even when dissociations were considered, was an $\underline{a}\langle 100\rangle$ unit dislocation. These low energy configurations agreed with the experimentally observed slip directions. The observed slip planes were shown to be those on which the dislocation mobility was highest.

Although the theory of Ball and Smallman gives reasonable agreement between predicted and observed slip systems in the three materials studied, its extension to other CsCl structures has been limited by the lack of information on elastic moduli. The application of anisotropic elasticity theory to other crystal structures has not been very successful. Foreman (1955) noted that although the theory predicted various slip planes in face centre cubic metals, slip was always observed on close packed planes. An $\underline{a}\langle 100\rangle$ dislocation was shown to have the lowest energy in niobium by Reid (1966), who has also observed slip in a $\langle 100\rangle$ direction in this metal, but only under very specific conditions.

1.3.3. Twinning.

Cahn and Coll (1961) studied twinning in the ordered b.c.c. structure compound Fe_3Al and found that it only occurred in a relatively disordered matrix. They noted that twinning did not occur with a long range order parameter greater than about 0.5.

These observations were in agreement with the predictions of Laves (1952) who showed that the operation of the normal b.c.c. twinning elements (twinning plane $\{112\}$, and a $\langle 111 \rangle$ shear direction) should lead to an increased number of "wrong" bonds across the twin plane and therefore disordering. The $\{112\}$ plane is the only low index plane in which a simple translation can give a twinned structure in a b.c.c. lattice. It was also pointed out that the twinned structure so caused would constitute an ordered tetragonal lattice, so it would be more accurate to describe the process, if it did occur, as a martensitic transformation.

Marcinkowski and Fisher (1963) calculated the stresses required to cause twinning and slip in the CsCl lattice. They showed that the stress necessary to move a twinning dislocation is up to twenty times greater than that required for superdislocation motion, but the twinning stress should be more strongly dependent on the degree of long range order.

1.4. Mechanical and Physical Properties of Intermetallic Compounds and Body-Centred Materials.

1.4.1. General Survey of the Properties of Intermetallic Compounds.

There have been numerous reviews of the properties of intermetallic compounds and ordered alloys. The structural aspects have been treated by Muto and Takagi (1955), and by Guttman (1956). Collongues (1956) has discussed typical phase diagrams of intermetallic compounds, and the consequences of deviations from stoichiometry.

The mechanical properties of intermetallic compounds was the subject of an international symposium in 1959, and the literature before this date was reviewed by Westbrook (1960). This symposium marked a turning point in the study of the deformation of intermetallics. Most prior investigations were of an empirical nature, utilising simple tests such as hardness determinations and corrosion resistance to explore the potentialities of these materials. An extensive list of investigations of this type is given by Paine et al. (1960).

Progress since 1959 has been considerable. Tensile or compression tests have been made on pure single and polycrystals of many materials; and the results related to dislocation and atomic structure, as determined by electron microscopy and other techniques. The effects of order on the mechanical properties have been reviewed recently by Stoloff and Davies (1966), and the properties of engineering importance (strength and brittleness) by Westbrook (1965).

1.4.2. Ionic Crystals with a CsCl Structure.

Ionic crystals have been used as models for studying the deformation properties of metals, because their transparent nature, and etching characteristics, allow dislocation distribution and mobility to be determined readily. Ionic crystals with the CsCl structure have not received as much attention as those with the NaCl structure because they are more difficult to prepare and handle.

The slip system was first determined to be $\{110\}\langle 100\rangle$ in thallium bromoiodide (Tl (Br, I)) by Smakula and Klein (1951). This system has been confirmed in CsBr by Johnson and Pask (1964), and in CsI by Urusovskaya and Thyagarajan (1965). Amelinckx (1961) studied decorated dislocation networks in CsBr, and noted numerous three fold nodes, indicative of dislocation reactions of the type:

$$a\,[100] + a\,[010] \rightleftharpoons a[110]$$

This shows that the reaction to form an $a[110]$ dislocation should involve no increase in energy, which is in agreement with the conclusions of Ball and Smallman (1966 B). None of these investigations considered the effects of temperature on deformation behaviour, although Johnson and Pask showed that the room temperature slip systems were maintained up to 300°C.

If CsBr is strained along a $\langle 100\rangle$ axis the shear stress resolved along each slip direction is zero, so an alternative deformation mechanism must operate. This is produced by kinking which has been

seen by Johnson and Pask in CsBr, and by Urusovskaya and Thyagarjan in CsI.

Kinking was first observed by Orowan (1942), in a single crystal of cadmium compressed with its axis parallel to the basal (slip) plane. The kinks appeared as non-crystallographic bands in the compressed rod and their formation was accompanied by a sharp relaxation in the applied stress. Orowan suggested that this might be a completely new deformation mechanism. A detailed investigation of zinc by Hess and Barnett (1949) revealed that a kink is a special form of deformation band, caused by the movement of primary dislocations. Large local concentrations of dislocations of the same sign lead to bending (Fig 1.3). These dislocations were thought to move under the influence of the applied stress and local inhomogeneities. Hess and Barrett also showed that the sharp load drops could be suppressed by using a very hard machine, and that kinks could be made to form gradually.

Blasdale and King (1965) studied the tensile kinking of cadmium and noted that the greatest number of kinks occurred near room temperature and in high purity material. They suggested that tensile kinks could not be explained by local stress irregularities because of the reproducibility with which they were obtained.

The dislocation etching characteristics of CsI should have allowed the dislocation structure of the kinks to be studied; but Urusovokaya and Thyagarajan found that the dislocation density in the bands was so high that local configurations could not be determined.

1.4.3. The Body-Centred Cubic Metals.

The properties of body-centred cubic metals are currently the subject of considerable research effort, and several reviews have appeared recently, e.g. Allen (1964). This interest is concentrated on the low temperature properties, and most of the detailed treatments have been concerned with this range, e.g. Conrad (1963), Christian and Masters (1964).

Slip is normally observed in a $\langle 111 \rangle$ direction, and on any plane which contains this direction - $\{110\}$ at very low temperatures, but normally on $\{110\}$ $\{112\}$ or $\{123\}$, depending on orientation. At higher temperatures slip has been observed on apparently non-crystallographic planes, which contain the slip direction (Foxall and Duesbury, 1965). Cross-slip is very profuse and slip traces wavy, except at very low temperatures. Electron microscope observations have shown that significant numbers of a $\langle 100 \rangle$ and a $\langle 110 \rangle$ dislocations may be formed in some b.c.c. metals during deformation (Dingley and Hale, 1966).

The other important feature of the deformation behaviour of the b.c.c. metals is their high strength at low temperatures. This decreases rapidly with increasing temperature (or decreasing strain-rate), and is due to the operation of a strongly thermally-activated process. At intermediate temperatures (approx 0.2 to 0.5 Tm) the flow stress is relatively independent of strain-rate and temperature. A further thermally-activated process, with the flow stress exponentially dependent on temperature, is observed at high temperatures. The explanations of these various regions, and their

significance in the deformation behaviour of NiAl will be considered later.

Another feature of these metals is the dependence of the mechanical properties on purity, particularly in vanadium, molybdenum and tungsten. This is reflected by strain-ageing effects, internal friction peaks, and low temperature brittleness. A further contribution to the brittleness comes from the high flow stress at low temperatures, and from the associated twinning (cf. 1.5.2.).

1.4.4. CsCl Superlattices which Exhibit an Order-Disorder Transformation.

FeCo and β-brass (CuZn) are typical of the compounds which exhibit an order-disorder transition. The former can be obtained in a disordered state at room temperature, but the ordering reaction in CuZn cannot be suppressed by quenching. Slip occurs in the highly ordered state by the movement of $\langle 11\bar{1} \rangle$ superdislocations, but a reduction of in the degree of order favours the motion of $\frac{1}{2}$ a $\langle 111 \rangle$ unit dislocations.

The temperature dependence of the flow stress of these alloys has received considerable attention, both theoretical and experimental. Cottrell (1953) was first to consider the effects of the size of anti-phase domains on flow stress, and concluded that it should show a maximum at a critical domain size (about 20 Å). Brown (1959) extended this treatment to the temperature dependence of the flow stress, in an ordered b.c.c. lattice, and concluded that it was of the form:

$$\sigma = N k T S^2 / 4 b$$

Using the notation of 1.3

The experimentally determined curve (Fig 1.4) shows a peak of this form superimposed on the normal temperature dependence observed in b.c.c. materials. This peak is associated with a change of deformation mechanism from the motion of superdislocations to unit dislocations (Stoloff and Davies, 1964).

Work hardening characteristics are also modified by the presence of long-range order, Typical experimental results have been shown by Marcinkowski and Chessin (1964) for ordered and disordered FeCo. Ordered alloys show higher rates of work hardening, in agreement with the theoretical predictions of Flinn (1960) and Vidoz and Brown (1962). This increase has been explained by the inhibition of cross-slip by extended superdislocations, and by the destruction of long-range order by the motion of jogged superdislocations. The inhibition of cross slip is indicated by a marked change in the appearance of slip traces in in FeCo, from wavy in the disordered state to straight and planar when ordered (Stoloff and Davies (1964)).

1.4.5. Properties of AgMg.

AgMg, which is isomorphous with NiAl, has received considerable attention as a model CsCl structure. It has a lower melting point than NiAl (820°C compared with 1638°C) and therefore becomes ductile at a lower temperature; defect structures on either side of the

stoichiometric composition are of the substitutional type. The slip systems in AgMg are $\{123\}\langle 111\rangle$ and occasionally $\{112\}\langle 111\rangle$ (Rachinger and Cottrell, 1956; Mukherjee and Dorn, 1964; Kurfman, 1965).

The earliest systematic deformation studies were the microhardness measurements of Westbrook (1957); these were made over the full range of stability, i.e. from 39 to 65 at % Mg, and from -196 to 800°C. The temperature dependence of the logarithm of the hardness for any composition could be divided into two approximately linear regions, in agreement with earlier work on pure metals (Westbrook, 1953), and the iron-group aluminides (Westbrook, 1956). At low temperatures a minimum was observed in hardness isotherms at the equiatomic composition; but at elevated temperatures (above about 0.65 Tm or 400°C) the hardness at the stoichiometric composition was the highest. This behaviour was explained by a change in the role of the lattice defects. At low temperatures they harden by hindering slip, whereas at high temperatures they soften by enhancing diffusion.

A detailed study of the effects of deformation conditions on the tensile flow stress of AgMg was made by Wood and Westbrook (1962), and similar behaviour observed. At all temperatures a local minimum flow stress was observed at the stoichiometric composition; but at high temperatures the lowest values were those near the extremes of the single phase region. Three distinct deformation processes were observed, depending on temperature and strain rate:

i) Temperatures up to 100°C, deformation was primarily by slip. The flow stress was not markedly dependent on temperature.

ii) 100-300°C, deformation by slip but dominated by dislocation interactions with solute atoms, indicated by sharp yield points and jerky flow. Deviations from linear log. flow stress-temperature plots occurred in this region.

iii) Above 300°C, deformation by slip but the rate controlled by diffusion processes, characterised by a marked temperature dependence of flow stress (Wood, 1961).

Tensile properties were also studied by Terry and Smallman (1964) who found a small dependence of flow stress on grain size; and that, unlike b.c.c. metals, the friction stress was relatively independent of temperature and strain rate - below 0.45 $\frac{T}{T_m}$ (200°C i.e. mechanisms i) and ii) above). No serrations were observed on the stress-strain curve between 100 and 300°C, it was in this range that the friction stress became temperature dependent (Fig 1.5). They confirmed the hardening effects of deviations from stoichiometry.

In contrast Mukherjee and Dorn (1964) found that the temperature dependence of the flow stress of single crystals was steep below room temperature. This study was extended to cover a wide range of temperatures (-269 to 650°C) and strain rates (10^{-6} to 10^{4} sec^{-1}) and five different regions identified (Mukherjee et al., 1965):

i) A low temperature thermally activated region. (A)

ii) A high temperature thermally activated region. (B)

iii) An athermal region at low strain rates and intermediate temperatures. (C)

iv) A region of increasing flow stress with increasing temperature. (D)

v) At very high strain rates the flow stress was independent of temperature and varied with the strain-rate. (E)

The above index letters refer to Fig 1.5. The operative deformation processes could not be determined unambiguously, except in region i) where the mechanism appeared to be the thermally activated nucleation of dislocation kinks across a Peierls barrier (Dorn and Rajnak, 1964). Creep in the range 460 to 555°C was studied separately (Mukherjee and Dorn, 1965). The pre-exponential term and activation energy were shown to be consistent with a model of the rate controlling process being the viscous glide of dislocations, modified by the presence of anti-phase boundaries.

These results are very different to those obtained on polycrystalline material by Wood and Westbrook, and Terry and Smallman (see Fig 1.5). There is no obvious explanation for this discrepancy; critical experimental conditions, such as strain rate, purity, and composition, appeared to be comparable.

Terry and Smallman (1963) extended the work hardening theory of Vidoz and Brown (1962), by comparing the effects of A.P.B energy on flow stress at high and low temperatures. They showed that ordering should lead to a decrease in the temperature, $\underline{T}_c$, at which the change to diffusion controlled flow occurs. $\underline{T}_c$ for AgMg is 0.45 $\underline{T}_m$ compared with about 0.65 $\underline{T}_m$ in pure metals. Terry and Smallman predicted, and observed, a linear relationship between $\underline{1/T}_c$ and $\underline{\ln \dot{\epsilon}}$ (where $\dot{\epsilon}$ is the

strain rate). $\underline{T}_c$ was found to be independent of composition, which is not unreasonable, in view of the small variation, with composition, of the activation energy of self-diffusion (Domian and Aaronson, 1964).

Deviations from stoichiometry have a marked effect on the ductility of AgMg (Wood, 1961). Silver-rich compositions have some ductility at all temperatures down to - 196°C; magnesium-rich alloys are completely brittle below 200°C. This difference has been attributed to grain boundary segregation (Westbrook and Wood, 1963 A). Kurfman (1965) noted that the ductility in bending, of slightly silver-rich AgMg, was strongly dependent on surface preparation at room temperature, and that this notch sensitivity disappeared at 200°C. This suggests that the brittleness is associated with the ease with which dislocation motion can blunt cracks rather than grain boundary effects.

Robinson and Bever (1965) studied the effects of strain on electrical resistivity and the stored energy of deformation by means of solution calorimetry. They noted that the magnitude of these properties increased continuously with strain at 25°C, but reached a plateau at 165°C; and that the stored energy of deformation for any given strain was greater than in any other known material. They explained these effects by deformation induced disordering, and the plateau by simultaneous ordering at the higher temperature. The greater disordering observed in non-stoichiometric alloys was thought to be due to the increased width of superdislocations in these compositions.

1.4.6. The Properties of NiAl.

The earliest study of the mechanical properties of NiAl was the comprehensive survey of hardness as a function of temperature and composition by Westbrook (1956). As in AgMg the temperature dependence of the logarithm of the hardness could be divided into two linear regions. The critical temperature, T_c, was dependent on composition, and increased continuously with increasing nickel content; this effect was attributed to the increasing metallic nature of the bonding. Hardness isotherms showed a minimum at the stoichiometric composition at all temperatures up to 800°C. Vacancy defects were found to be more potent as hardening agents, compared with substitutional atoms (Fig 1.6).

Grala (1960), whilst concerned mainly with microstructural and fabrication problems, made some tensile and stress-rupture tests on large grain size NiAl in the as-cast condition. This material was completely brittle at low temperatures; a peak in the temperature dependence of the ultimate tensile strength, at 650°C, coincided with the onset of ductility. Imai and Kumazawa (1959) prepared NiAl by sintering nickel and aluminium powder, and concluded that the compound in this form was inferior in strength to cermets, but had superior resistance to thermal shock.

Since the start of the present work the results of several other investigations into the properties of NiAl have been published. These results will be described in the relevant sections of Chapters 3 and 4. The investigations include those of:

Westbrook et al. (1964) on the effects of hot working and grain refining.

Ball and Smallman (1964-6) on electron microscopy and the mechanical deformation of stoichiometric single crystals, and of polycrystals of several compositions.

Wasilewski and various coworkers (1964-6) on the elasticity and plastic deformation of stoichiometric single and polycrystals.

Lautenslager et al. (1965) who compressed polycrystals of various grain sizes and composition in the temperature range 700-900°C.

Mohanty and Wert (1963) investigated, by X-rays, the structure of heavily cold worked (ground) NiAl. They noted significant $\{211\}$ faulting, from a comparison of the apparent particle sizes in the $\langle 110 \rangle$ and $\langle 100 \rangle$ directions. The degree of order measured in a cold worked sample was 0.96. A further study of peak widths by Mohanty (1966) revealed that significant $\{110\}$ A.P.B.s were not formed in NiAl, although the occurrence of other types of fault could not be discounted.

1.4.7. Grain Boundaries in Intermetallic Compounds and the Pest Phenomenon.

A major drawback of many intermetallic compounds, which has limited their usefulness, is their susceptibility to failure by "pesting". This is the tendency to severe intergranular attack which may eventually lead to complete disintegration of the material. The

pest has been observed in numerous intermetallic compounds (Westbrook and Wood, 1963 B); particularly silcidies, beryllides and aluminides, including AgMg and NiAl containing excess of the electronegative element. Westbrook and Wood (1963 A) showed that conditions which lead to the occurrence of pesting also caused anomalous hardening in the grain boundary regions. A detailed investigation of the compound NiGa by Seybolt and Westbrook (1964) showed that this hardening was associated with the presence of dissolved oxygen. They suggested that the hardening was due to a concentration of oxygen atoms at the grain boundaries, although the exact mechanism was uncertain, and no precipitates were seen. Turner et al. (1966) detected precipitates at grain boundaries in NiAl containing excess aluminium (Ni 54 at % Al); these were identified as aluminium suboxide Al_2O. On exposure to the atmosphere for several days this highly unstable phase transformed to the stable oxide, α-Al_2O_3, which reduced intergranular cohesion because of its powdery form.

The study of Turner et al. forms a part of the present investigation and a copy of the published letter is included in this thesis. The results will not be considered further, as the work has not been extended beyond that published.

From a consideration of the experimental data it would appear that the phenomena associated with the pest effect could be explained by a mechanism of oxide precipitation, involving several stages, similar to those observed in precipitation hardening systems. An

initial high temperature anneal would take oxygen into solid solution, this would involve no grain boundary hardening. Further annealing at a lower temperature could lead to precipitate formation, which would occur preferentially at grain boundaries. The form of these precipitates would be dependent on annealing conditions; short times and a low degree of supersaturation could cause clustering, and explain the observations of Seybolt and Westbrook. Other conditions could lead to precipitation of the oxide with the lowest oxygen content, and explain the observations of Turner et al. Under normal conditions these unstable complexes and precipitates could oxidise to a more stable form, and the volume expansion and physical form of the new precipitates lead to disintegration.

1.5. Factors Influencing Brittleness.

1.5.1. Independent Slip Systems.

Von Mises (1928) was first to show that five independent shear modes are required if a polycrystalline material is to deform macroscopically by slip. This condition, which was also examined by Taylor (1938), arises because a general strain must be able to change the shape of any grain in a random manner, so that the continuity of stress and of material across the grain boundary is not destroyed. The strain may be described by six components of the general strain tensor, of which only five are independent if the volume of material is assumed to remain constant on straining. Since one component of the strain tensor corresponds to the operation of a single slip system five independent slip systems are required for general deformation.

This requirement is of considerable importance to the deformation of polycrystalline aggregates. Fewer than five independent slip systems can result in individual grains being unable to conform to the required change of shape and may lead to the opening of voids at grain boundaries.

Methods of determining the number of slip systems, and their interdependence, have been formalised by Groves and Kelly (1963) and by Kocks (1964). A slip system is shown to be independent if its operation results in a change of shape that cannot be produced by a suitable combination of slip on other systems. Slip systems can only be interdependent if slip directions within a single plane can be added

as vectors or if combinations of systems correspond to pure rotation with no translation.

Groves and Kelly showed that if a b.c.c. structure, ordered or otherwise, slips in a [11] direction five independent systems should be available and the material should be ductile. Slip systems in the CsCl lattice have been considered by Copley (1963) and in detail by Ball and Smallman (1966 B). They showed that the operation of a (110)[00] system permits only three independent systems, which cannot be augmented by cross-slip or pencil glide in an [00] direction.

Groves and Kelly noted that a material with fewer than five independent slip systems would not necessarily be brittle. General deformation could occur if the stresses required to cause slip on other independent slip systems were smaller than those required to propagate cracks.

1.5.2. Atomic Mechanisms of Fracture.

The availability of five independent slip systems does indicate that a material must be ductile because two dislocation processes - plastic deformation and cracking - compete for the relief of stress concentrations. If cracks are able to propagate at a stress smaller than that required for plastic deformation the material will fail in a brittle manner.

It is generally accepted that the transition from ductile to brittle behaviour is controlled by the propagation of cracks. However this criterion requires crack nuclei to be available to propagate.

Numerous mechanisms have been postulated for the nucleation of cracks by dislocation motion e.g. Cottrell (1958) proposed that cracks could nucleate at grain boundary pile ups or at the intersection of slip bands.

The conditions necessary for the propagation of cleavage cracks have been considered by Meakin and Petch (1963). They showed that brittle fracture should occur if:

$$\frac{\sigma k_y d^{\frac{1}{2}}}{4\mu} \geqslant \gamma \qquad (1.12)$$

where σ is the stress

k_y relates flow stress to grain size (d) by:

$$\sigma = \sigma_1 + k_y d^{-\frac{1}{2}}$$

σ_1 is the lattice friction stress

μ is the shear modulus

γ is the surface energy

The strong temperature dependence of flow stress is responsible for the well known ductile-brittle transition temperature in b.c.c. metals.

Smith and Worthington (1965) extended this treatment to consider the number of independent slip systems - described by a mean orientation factor, $\bar{m}$. They concluded that equation 1.12 was modified to:

$$\frac{\sigma k_y d^{\frac{1}{2}}}{4\mu} + \left(1 - \frac{2}{\bar{m}}\right)\frac{\sigma \sigma_1 d}{4\mu} \geqslant \gamma \qquad (1.13)$$

When $\bar{m} = 2$ this reduces to equation 1.12. The conclusion that may be drawn from equations 1.12 and 1.13 is that high stresses, large grain sizes and high values of $\underline{k}_y$ all favour brittle behaviour, even when five independent slip systems are available. If $\bar{m} > 2$, because of the lack of slip systems or a marked texture, the importance of these parameters in determining ductility is increased further.

1.6. Plastic Deformation as a Dynamic Process.

Plastic deformation has long been recognised as a dynamic, i.e. time dependent, process. This is illustrated by the phenomenon of creep - the ability for plastic flow to continue under the influence of a constant stress. A further example of the dynamic nature is the dependence of the flow stress on temperature and strain-rate.

1.6.1. Thermally Activated Deformation.

The observed dependence of flow stress on temperature and strain-rate has led to the idea that thermal fluctuations may assist the applied stress in overcoming obstacles to slip. (Eyring, 1936; Conrad, 1964). Plastic deformation being a thermally activated process may be described by the Arrhenius type equation:

$$\dot{\epsilon} = \dot{\epsilon}_o \exp -\left(\frac{\Delta G}{kT}\right) \qquad (1.14)$$

where $\dot{\epsilon}$ is the plastic strain rate.

$\dot{\epsilon}_o$ is a parameter which depends on the number and distribution of dislocations and their vibrational frequency; it is only weakly dependent on temperature.

ΔG is the free energy of activation and depends on stress, structure and temperature.

k is Boltzmann's constant.

T is the absolute temperature.

A simplified barrier to dislocation motion, where the total

activation energy is not a function of stress, is illustrated schematically in Fig 1.7. The application of an effective stress, $\underline{\tau}^*$, moves the dislocation up the barrier to equilibrium position where the force is given by $F = \tau^* b l^*$, $\underline{l}^*$ is the length of dislocation segment involved in the thermal activation. To pass the obstacle, that is to move the dislocation forward by an activation distance $\underline{d}^*$, thermal energy $\underline{\Delta G}$ has to be supplied. This activation energy is determined by the area under the force-distance curve and the work done by the applied stress.

The stress derivative of the activation free energy, which has the dimensions of volume, is termed the activation volume, $\underline{v}^*$:

$$v^* = - \left(\frac{\partial \Delta G}{\partial \tau} \right)_T \qquad (1.15)$$

The activation volume is a parameter which may be measured experimentally and can provide useful information about the form of the barriers to dislocation motion, e.g. for the simplified barrier outlined above it may be shown that $v^* = b l^* d^*$.

Barriers to dislocation motion may be divided into two limiting categories. Those which have localised stress-fields may be overcome with the aid of thermal fluctuations if the required activation energy is of the order of $\underline{kT}$. Thermal activation could not assist a dislocation to pass an obstacle with a long range stress-field because $\underline{\Delta G}$ would be too large; this type of barrier is called athermal.

The obstacles encountered by a moving dislocation are seldom

simple. The force experienced by such a dislocation may be resolved into components due to the individual barriers. The total flow stress, $\underline{\sigma}$, is thus the sum of two terms:

$$\underline{\sigma} = \underline{\sigma}^{*} + \underline{\sigma}_{\mu} \qquad (1.16)$$

The thermally activated component, $\underline{\sigma}^{*}$, is dependent on temperature and strain rate and is due to the short range interactions. The athermal component $\underline{\sigma}_{\mu}$ varies with temperature only through changes in the shear modulus. The temperature and strain-rate dependence of $\underline{\sigma}$ arising from equation 1.16 is shown schematically in Fig 1.8.

1.6.2. Experimental Evaluation of the Activation Parameters.

In order to gain an understanding of the deformation behaviour of any material it is necessary to know the nature of the obstacles which control the rate of motion of the dislocations. It is, in principle, possible to obtain this information from a comparison of the experimentally measured values of the activation energy and volume, and their dependence on stress, temperature and dislocation structure, with theoretical models of possible obstacles.

The processes that occur when a dislocation encounters a real barrier with a short range stress-field are complex and cannot be described by exact force-distance relationships. The rate equation used in practice is based on the assumption that the distribution of activation energies throughout the crystal may be replaced by a single

equivalent activation energy, ΔG. The mean velocity, u, of a dislocation line which is continuously halted is then given by (Christian and Masters, 1964 B)

$$u = p \nu_o \exp -\left(\frac{\Delta G}{kT}\right) \tag{1.17}$$

where p is the distance moved after a successful activation and ν_o is a frequency factor.

The macroscopic strain-rate, $\dot{\epsilon}$, is defined by

$$\dot{\epsilon} = \phi b \rho u \tag{1.18}$$

where ϕ is an orientation factor and ρ is the density of mobile dislocations.

Alternatively

$$\dot{\epsilon} = \phi b \frac{NA}{p} u$$

where N is the effective number of dislocation sites per unit volume at which the dislocation is halted and A is the area of glide plane swept out by this dislocation after a successful nucleation. If this value is substituted for u in equation 1.17 equation 1.14 is obtained, where $\dot{\epsilon}_o$ is a structure sensitive constant depending on N, A and ν_o.

Several analyses have been developed to calculate the activation

parameters from experimental data. These are all based on rate equations of the same form as 1.14 and 1.17. There is, however, considerable confusion in the literature about which thermodynamic function is measured. Basinski (1957) and Conrad and Wiedersich (1960) have determined relationships for activation enthalpy, while Schoeck (1965) has derived similar equations for activation free energy. Christian and Masters (1964 B) noted the confusion between free energy and enthalpy and concluded that the difference was insignificant in view of the small entropy of activation.

Schoeck (1965) determined the activation free energy by considering the work done when a section of dislocation line is moved a small distance against the combined effects of a short-range barrier and an internal stress, $\underline{\sigma}_i$, represented by a second stationary dislocation. The total work is made up of terms due to the work done on the dislocations by the applied and internal stresses, the localised atomic misfit, and the movement of the point of action of the applied force. If the motion is assumed to occur isothermally and reversibly the change in Gibbs free energy may be calculated from the usual thermodynamic relationships. The free energy change in moving the dislocation to the saddle-point, from where it may move freely under the influence of the applied stress, can then be obtained by integration as

$$\Delta G = \Delta g\,(\underline{\tau}^*) - \underline{\tau}^* v^* \qquad (1.19)$$

where $\Delta g\ (\tau^*)$ is a free energy term due to localised atomic misfit and the second term is the work done by the stress in moving the dislocation to the saddle-point configuration.

It is possible to measure experimentally an activation energy for dislocation motion, Q, defined by:

$$Q = k\,T^2 \left(\frac{\partial \log \dot{\epsilon}/\dot{\epsilon}_o}{\partial T} \right)_\tau \tag{1.20}$$

If the rate equation 1.14 is assumed, it may be shown that:

$$Q = \Delta G - T\left(\frac{\partial \Delta G}{\partial T}\right)_\tau \tag{1.21}$$

Therefore $Q = \Delta H$, the enthalpy of activation because

$$\left(\frac{\partial \Delta G}{\partial T}\right)_\tau = -\Delta S$$

Combining equations 1.19 and 1.21 Schoeck showed that:

$$\Delta G = Q + T\,\frac{\partial \mu}{\partial T}.\,\frac{\tau_i}{\mu}\,v^* + T\left(\frac{\partial \Delta G}{\partial T}\right)_{\tau^*} \tag{1.22}$$

$$\text{or} \quad \Delta G = \left(Q + T\,\frac{\partial \mu}{\partial T}.\,\frac{\tau}{\mu}\,v^*\right)\left(1 - \frac{T}{\mu}.\,\frac{\partial \mu}{\partial T}\right)^{-1} \tag{1.23}$$

where μ is the shear modulus.

The activation free energy can be determined from experimental

data because each of the terms in equations 1.22 and 1.23 can be measured. The activation volume may be obtained from equations 1.14 and 1.15 as

$$v^* = k\,T\left(\frac{\partial \log \dot{\epsilon}/\dot{\epsilon}_o}{\partial \tau}\right)_T$$

which involves the structure sensitive term $\dot{\epsilon}_o$. The problem of variations of $\dot{\epsilon}_o$ can be avoided if differential tests are made, changing the stress or strain-rate so rapidly that the structure, and hence the pre-expontial term, remains constant, The activation volume then becomes

$$v^* = k\,T\left(\frac{\partial \log \dot{\epsilon}}{\partial \tau}\right)_T \qquad (1.24)$$

Similarly

$$Q = \Delta H = k\,T^2\left(\frac{\partial \log \dot{\epsilon}}{\partial T}\right)_\tau$$

This relationship is suitable for measuring $\underline{\Delta H}$ from creep tests, where the effects of a temperature change on strain-rate can be studied. In a compression test, using a cross-head moving at constant speed, strain-rate cannot be varied independently of temperature; $\underline{\Delta H}$ can however be measured from a modified expression

$$\Delta H = -\,T\left(\frac{\partial \tau}{\partial T}\right)_{\dot{\epsilon}} v^* \qquad (1.25)$$

if all measurements are made at constant structure.

The analysis which is more generally employed is that of Conrad and Wiedersich (1960) who derived the enthalpy of activation as:

$$H = - k T^2 \left(\frac{\partial \log \dot{\epsilon}}{\partial \tau}\right)_T \left[\left(\frac{\partial \tau}{\partial T}\right)_{\dot{\epsilon}} - \frac{\tau_i}{\mu} \cdot \frac{\partial \mu}{\partial T}\right] \qquad (1.26)$$

Schoeck has shown that this calculation is in error and that equation 1.26 more nearly describes the activation free energy (cf. eqn 1.22). However it may be noted that if $\underline{\tau}_i \ll \underline{\mu}$ and $\frac{\partial \mu}{\partial T}$ is small compared with $\frac{\partial \tau}{\partial T}$ equation 1.26 approximates to equation 1.25, and for practical purposes the differences between the analyses may be ignored.

Activation Parameters at Low Stresses.

Back jumps - the motion of the dislocation line against the applied stress - may contribute significantly to the applied strain-rate under some conditions. The rate equation (1.17) may be modified to account for this process (Christian and Masters, 1964 B) to

$$u = p \nu b \left[\exp - \left(\frac{\Delta G}{kT}\right) - \exp - \left(\frac{\Delta G_b}{kT}\right)\right] \qquad (1.27)$$

where $\underline{\Delta G}$ and $\underline{\Delta G_b}$ are respectively the free energies of activation in the forward and backward directions. If these are replaced by $(\Delta G_o - v^* \tau^*)$ and $(\Delta G_o + v^* \tau^*)$ then equation 1.27 becomes

$$u = 2 p \nu_o \sinh \left(\frac{v^* \tau^*}{kT}\right) \exp - \left(\frac{\Delta G_o}{kT}\right) \qquad (1.28)$$

If $v^* \tau^* \gg kT$ this reduces to equation 1.17.

Alefeld (1962) considered the effects of back-jumps on the activation parameters, by replacing equation 1.17 with 1.28, and concluded that equation 1.24 defined an effective activation volume, v^*_{eff}, related to the true volume by

$$v^*_{eff} = v^* \coth\left(\frac{v^* \tau^*}{kT}\right) \qquad (1.29)$$

The correction factor may explain some of the high activation volumes observed at low stresses and high temperatures, because it tends to infinity at low $v^* \tau^*$. The correction may be made graphically. Schoeck (1965) showed that the frequency of back-jumps should be negligible for the majority of deformation processes and that equations 1.27 to 1.29 need not be used.

When applying the analysis outlined above it is conventional to omit the Δ in the change of energy and entropy terms, e.g. ΔH is often written as H. This convention will be followed in chapters 4 and 5, and it should be noted that any thermodynamic function measured is a relative, and not absolute, value.

1.6.3. Dislocation Dynamics.

An alternative approach to the dynamic properties of dislocations stems from direct measurements of the stress dependence of dislocation velocity. These measurements, made using etch pit techniques on LiF (Johnston and Gilman, 1959) and Fe - 3% Si (Stein and Low, 1960),,

indicated that an empirical relationship existed between stress and velocity ($\underline{u}$) of the form

$$u = \left(\frac{\tau}{\tau_o}\right)^m \tag{1.30}$$

where $\underline{\tau_o}$ and $\underline{m}$ are constants for a given material and temperature.

Guard (1961) showed that it should be possible to measure the dislocation velocity exponent, $\underline{m}$, from change of strain-rate experiments. Since the strain-rate may be written as equation 1.18

$$\dot{\epsilon} = \phi \rho b u$$

by taking logs and differentiating

$$\frac{\partial \log \dot{\epsilon}}{\partial \log \tau} = \frac{\partial \log \rho}{\partial \log \tau} + \frac{\partial \log u}{\partial \log \tau}$$

$$= \frac{\partial \log \rho}{\partial \log \tau} + m \tag{1.31}$$

It should therefore be possible to measure $\underline{m}$ from the same change of strain-rate tests that were used to determine $\underline{v}^*$ (eqn 1.24) if the same assumption is made - that structure, represented by $\underline{\rho}$, is constant.

Guard tried to measure $\underline{m}$ in Fe - 3% Si by this method and found that it had almost twice the value obtained by direct measurements.

However Johnston and Stein (1963) showed that if the apparent value was extrapolated to zero strain the results corresponded closely to those obtained by direct methods in both LiF and Fe - 3% Si. The apparent value of $\underline{m}$ is normally given the symbol $\underline{m}'$

$$\text{i.e. } m' = \frac{\partial \log \dot{\epsilon}}{\partial \log \tau} \qquad (1.32)$$

The reasons for the discrepancy between $\underline{m}$ and $\underline{m}'$ have been discussed by Christian (1964) who concluded that it was not due to an immediate increase in ρ on changing the strain rate. The difference was more probably due to equation 1.30 being an over simplification, and a re-definition in terms of an effective stress (that was not increased by work-hardening) would be more realistic.

Although the empirical relationship between dislocation velocity and stress, indicated by equation 1.30, fits the experimental data over a limited range of stress it can have little physical significance because it places no upper limit on the velocity. Gilman (1960) has proposed an alternative empirical relationship

$$u = u_o \exp - \left(D/\tau \right) \qquad (1.33)$$

where u_o is a limiting velocity near that of sound and D is a characteristic drag stress. A relationship of this type has been observed in several materials (Gilman, 1965) and its use has permitted an explanation of the flow stress and work hardening behaviour of these

materials (Gillis and Gilman, 1965 A and B). Since neither $\underline{D}$ or $\underline{u}_o$ can be determined without direct measurements of dislocation velocity this approach could not be applied to the present investigation.

Whilst the validity of $\underline{m}$ is limited and its physical significance is in doubt it does have some usefulness in determining the form of the stress-strain curve at small plastic strains, particularly with regard to an initial yield point; hence the interest in determining $\underline{m}$ by indirect means.

The occurrence of a yield point may be explained qualitatively by considering the effects of increasing dislocation density on the flow stress at constant strain-rate. Combining equations 1.18 and 1.30.

$$\dot{\epsilon} = \rho b (\tau/\tau_o)^m \qquad (1.34)$$

When plastic flow commences with a low mobile dislocation density ($\underline{\rho}$) the dislocation velocity, and hence the stress, must increase to accommodate the applied strain rate. Once flow has started $\underline{\rho}$ may be increased by dislocation multiplication, and the required stress decreased. This may result in a yield point with suitable values of $\underline{m}$, $\underline{\rho}$ and rate of work hardening.

Hahn (1962) and Johnston (1962) have developed, from equation 1.34, relationships between flow stress and strain as a function of $\underline{m}$, $\underline{\rho}$, $\underline{\dot{\epsilon}}$ and the rates of dislocation multiplication and of work-hardening. Johnston also considered the effects of machine hardness which Hahn neglected. Numerical solutions were obtained for

these equations, using a computer. It was found that the occurrence of a yield point was favoured by small values of $\underline{m}$ and $\underline{\rho}$; typical theoretical stress-strain curves for many experimental conditions are given in both papers.

The value of $\underline{\rho}$ may be small because of a low initial dislocation density (as in germanium) or because the majority of dislocations are strongly locked and therefore immobile. A reduced mobile dislocation density has been used by Hahn and by Cottrell (1963) to explain the yield point in b.c.c. metals, in preference to the earlier ideas of the unpinning of locked dislocations (Cottrell, 1953).

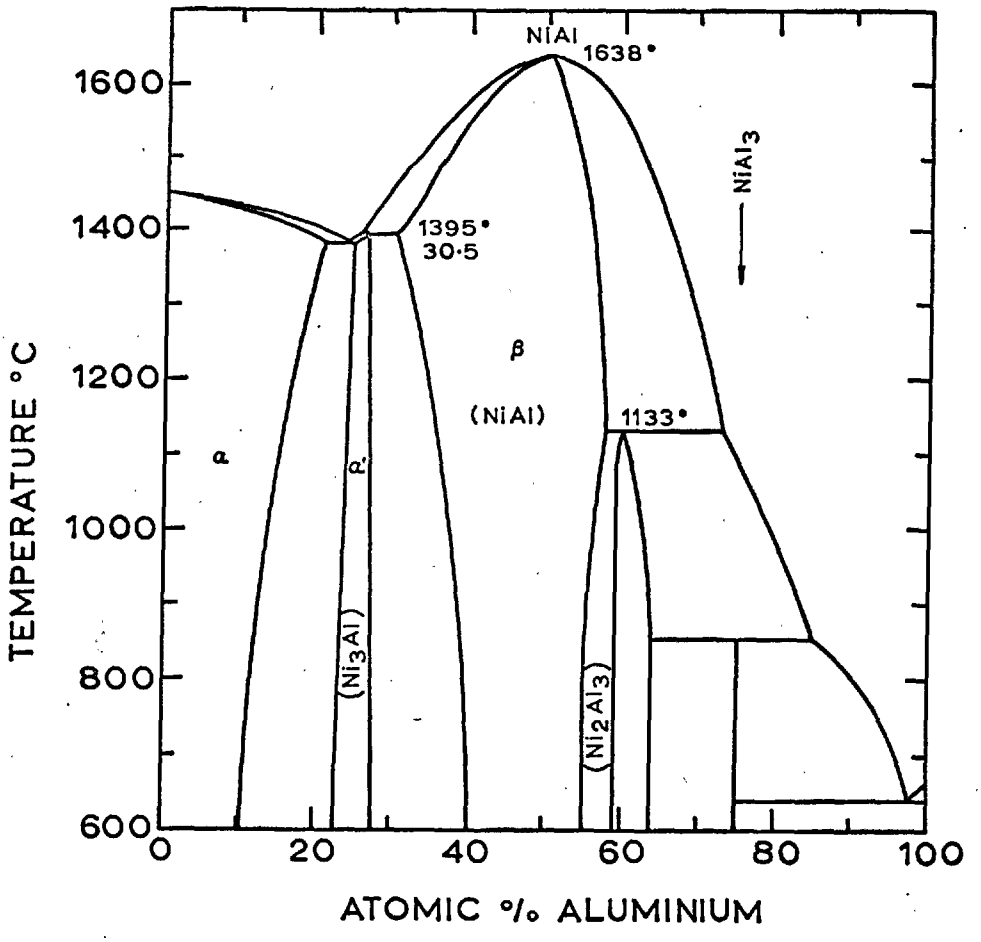

Fig 1.1. Nickel-Aluminium Phase Diagram.

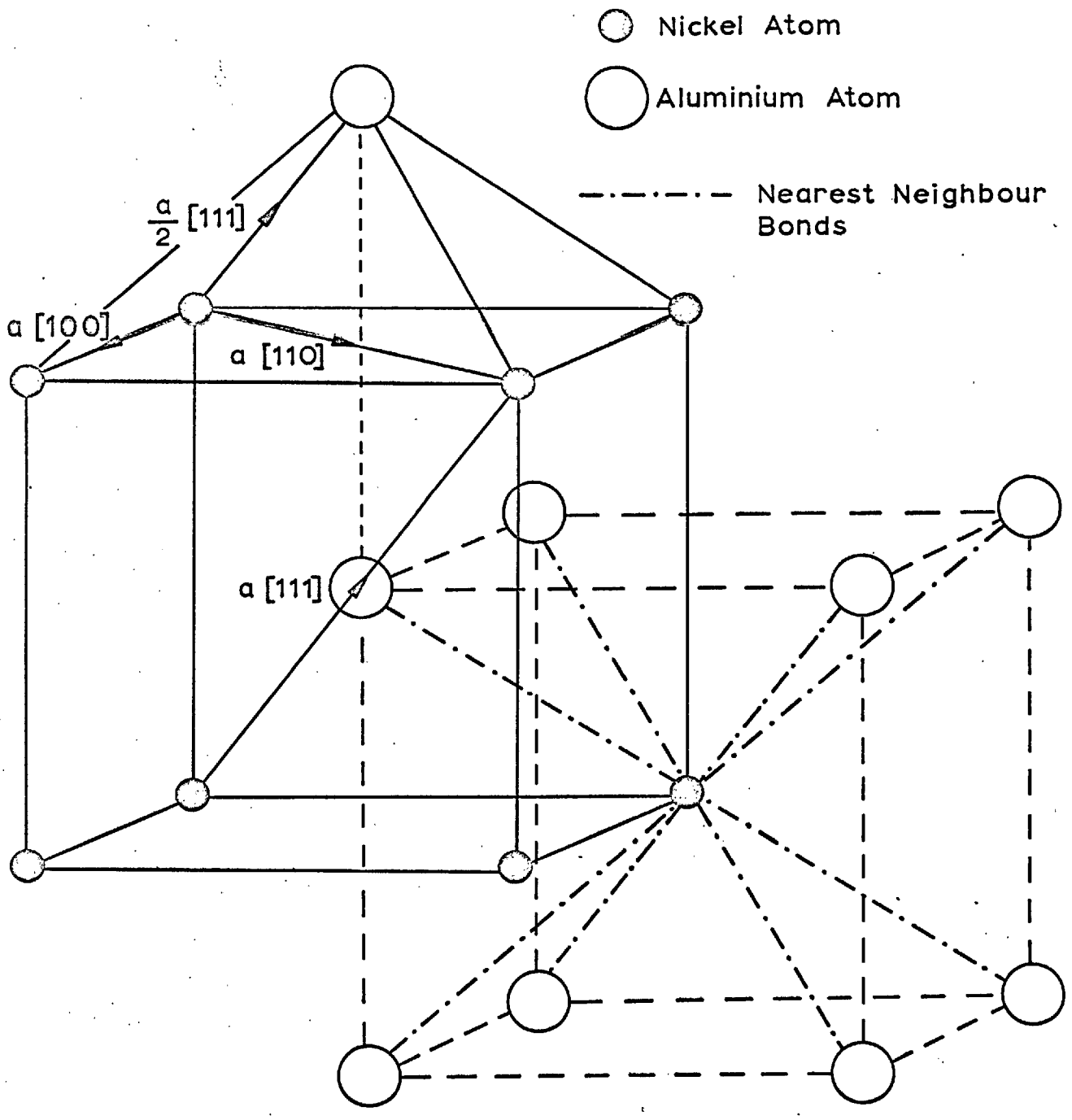

Fig 1.2 NiAl Crystal Structure showing possible Burgers vectors.

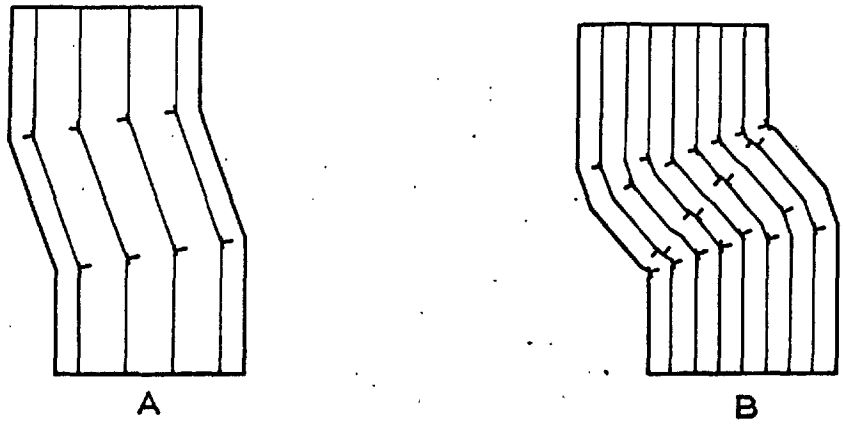

Fig 1.3 Formation of a kink by dislocations.

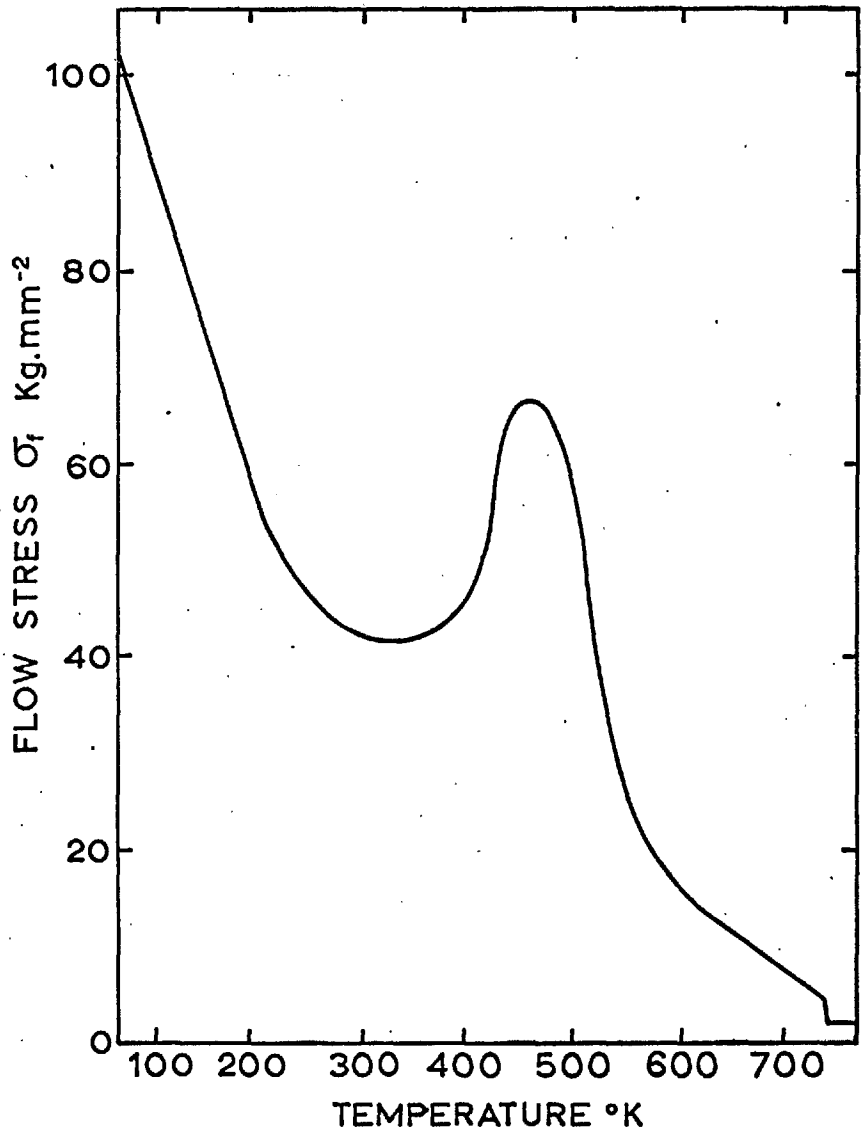

Fig 1.4 Temperature Dependence of the Flow Stress of β -Brass (Brown, 1959).

Fig 1.5 Temperature and Strain-Rate Dependence of Single Crystal [illegible] (Mukherjee et al. 1965).

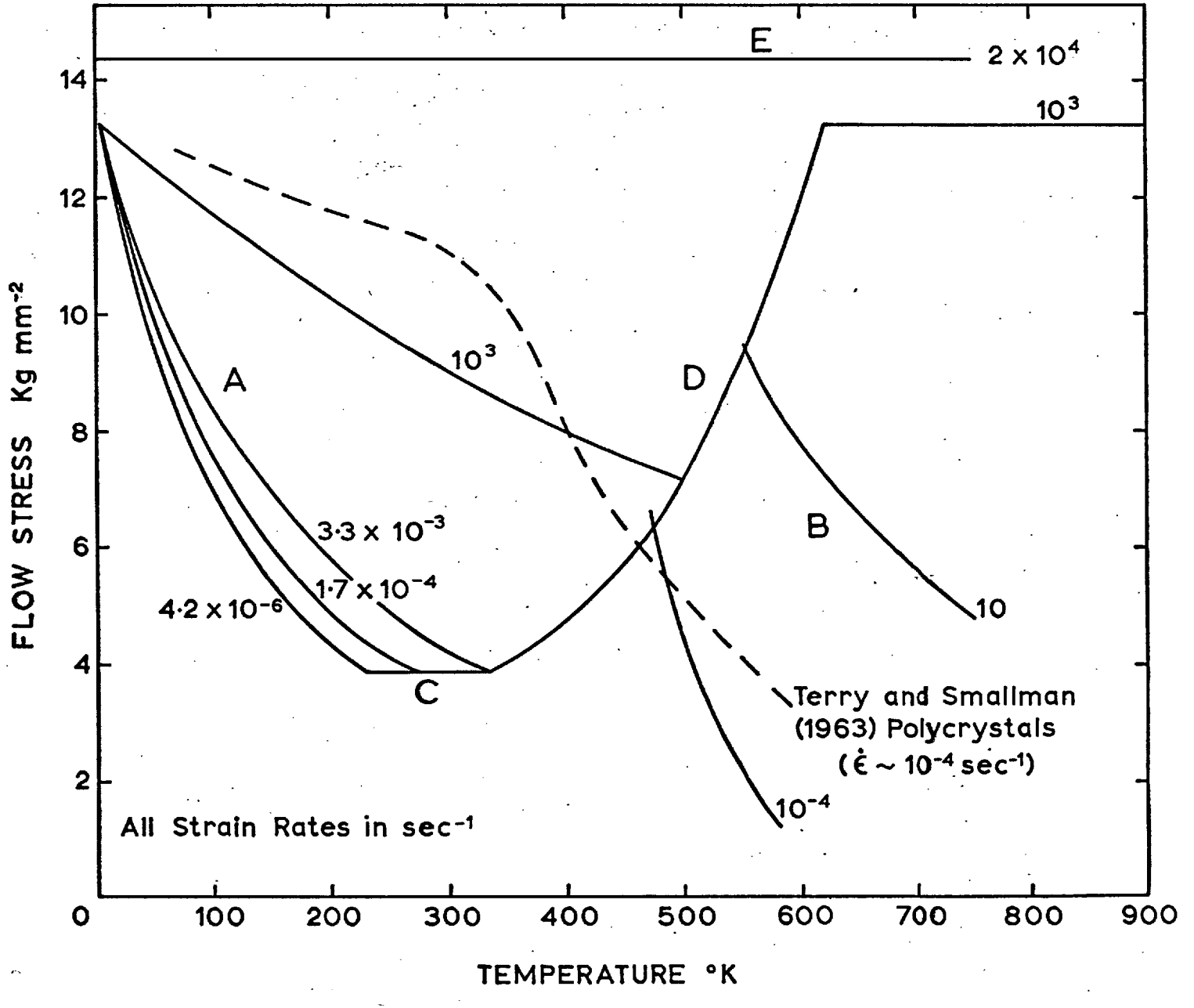

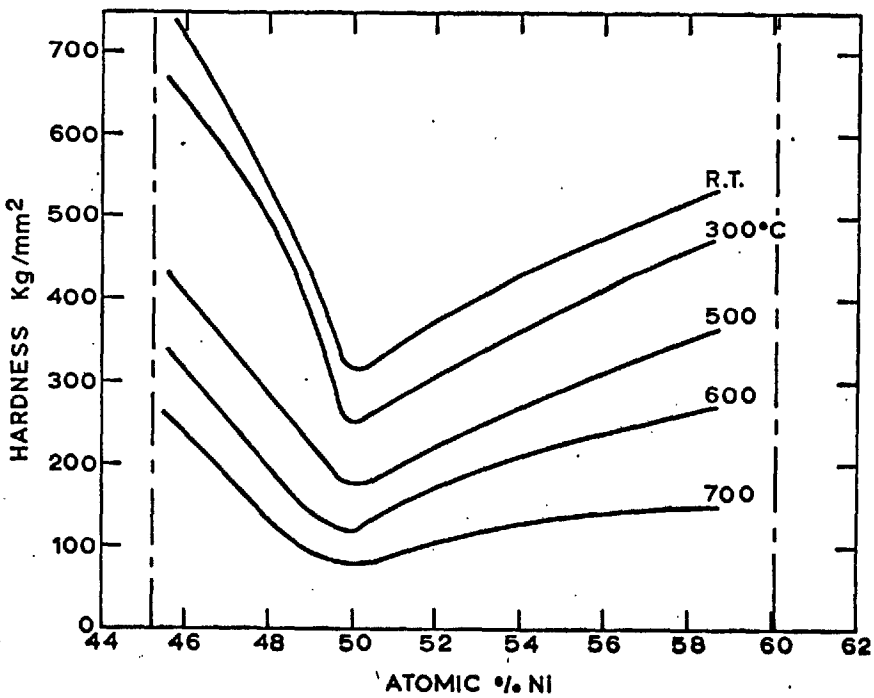

Fig 1.6 Effects of Composition on hardness isotherms of NiAl (Westbrook, 1956).

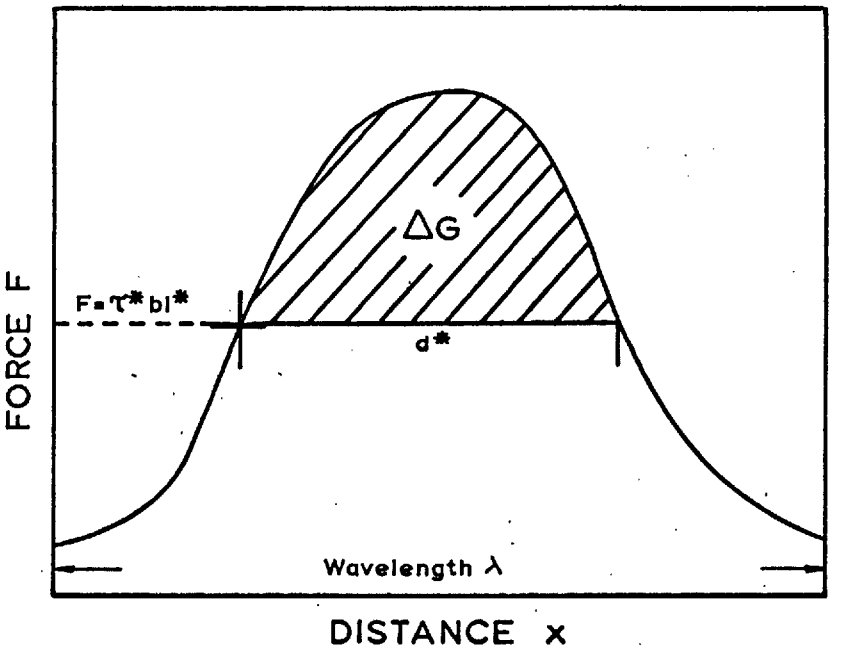

Fig 1.7 Schematic Barrier to Dislocation Motion

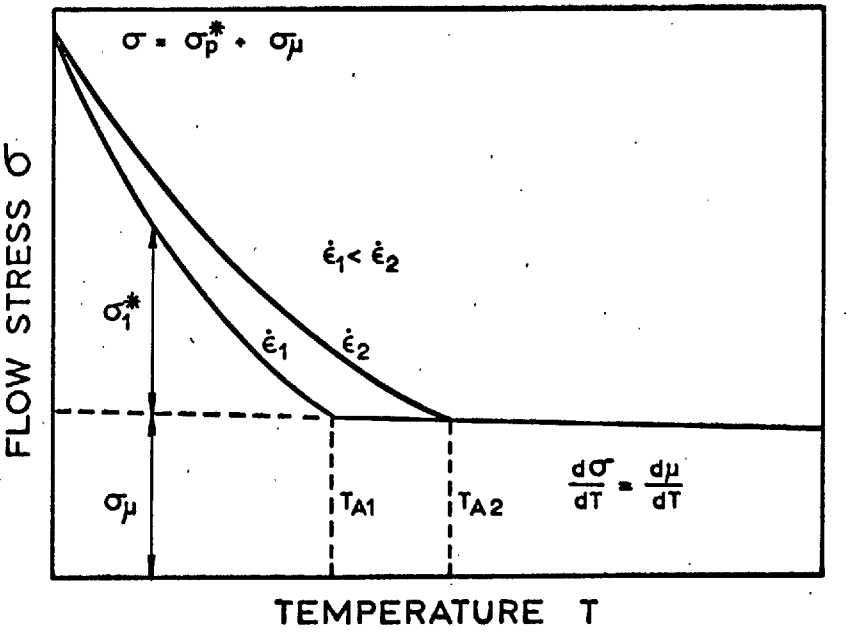

Fig 1.8 Schematic Temperature and Strain Rate Dependence Resulting from Equation 1.16

Chapter 2 Experimental Techniques.

2.1. Preparation of Materials.

2.1.1. Melting and Casting.

As-cast material was used in this investigation for some early exploratory tests and for the growth of single crystals from the melt. International Nickel Ltd produced bars of various compositions by melting together 'Mond' nickel pellets of 99.9% purity and 99.99% pure aluminium and casting in refractory moulds. To minimise atmospheric contamination each of these operations was performed under an argon atmosphere.

Further material was cast from these master alloys or from high purity nickel (99.99% pure) and aluminium (99.999% pure) using an induction melting technique. The charge was contained in a water-cooled copper boat and was heated by radio-frequency induced currents; electromagnetic levitation of the charge prevented contamination of the molten metal by the crucible material, whilst the water cooling helped to reduce the effects of the violently exothermic heat of mixing. Gaseous contamination was minimised by rigorous out-gassing procedures and the use of a purified argon atmosphere. One disadvantage of this method, that the charge was cast in situ and was therefore of an irregular shape, proved unimportant as it was remelted in order to grow single crystals.

2.1.2. Extrusion.

All specimens used in the study of the properties of polycrystalline NiAl were cut from fine grain-sized rod which had been extruded by International Nickel Ltd. The problems associated with the extrusion of brittle intermetallic compounds, cf. Wood (1960), were overcome by cladding the cast material in mild steel and extruding at 1200°C. Under these conditions ingots of initial diameter $1\frac{7}{8}$ in of composition near stoichiometry and at the extremes of the phase field were reduced to $\frac{1}{4}$ in square. A similar technique, using stainless steel cladding, and rolling at 1100°C, was used by Lautenslager et al. (1965) to produce fine grain NiAl.

Improved extrusion facilities have allowed some rods of near stoichiometric and nickel-rich compositions to be extruded at 1300°C to a diameter of $\frac{3}{8}$ in without the use of steel cladding; this material was used for most of the measurements on compositions containing excess nickel.

2.2. The Growth of Single Crystals.

The techniques available for the growth of single crystals have been the subject of many reviews, for example those of Honeycombe (1959) and Gilman (1963).

After a consideration of the special problems involved several of the methods described appeared feasible for use with NiAl, although at the start of this investigation there was only one known example of the growth of a NiAl single crystal. Ray and Smith (1958) produced small single crystal beads by spattering molten NiAl with short bursts of an electric arc. These were used for an X-ray investigation and were far too small (up to 1 mm dia) for mechanical testing.

The major problem with NiAl is that, although the stoichiometric alloy has a congruent melting point, small deviations from this composition result in solidification occurring over a wide temperature range (e.g. 500°C for a 54 at. % Al alloy), causing segregation and possible nucleation ahead of a growing interface. Furthermore the high temperatures involved pose further difficulties. The melting point of the compound is almost 1000°C above that of pure aluminium. Thus the high vapour pressure of alumiuium may result in a considerable loss by volatilisation in vacuum, whilst its marked affinity for oxygen and nitrogen could cause contamination in all but the purest atmospheres. Molten aluminium at temperatures near 1700°C is known to be extremely corrosive and it attacks most crucible materials, a tendency which should be reduced by its decreased thermodynamic activity in the compound (Steiner and Komarek, 1964).

Thus, for non-stoichiometric compositions, solid state techniques appear far more promising since they avoid most of these problems; although melt techniques, which seem preferable because crystals can be grown with greater control of size and orientation, should be successful for near equi-atomic compounds.

One possible technique for the growth of non-stoichiometric crystals would be to alter the composition of melt grown crystals by solid state diffusion; for example annealing at a high temperature in a vacuum should result in the loss of aluminium by vapourisation and an increase in the nickel content of crystals. The difficulties of this method - ensuring homogeneity and obtaining aluminium-rich compositions - led to the choice of a recrystallisation technique for the first attempts to grow single crystals. After some preliminary experiments the strain-anneal method was selected. It was found that whilst single crystals, large enough to deform and study crystal plasticity, could be grown by this method, a melt technique had to be used to provide sufficient material for the temperature dependence of the deformation behaviour of various orientations to be measured.

2.2.1. The Strain-Anneal Technique.

The basic features of the strain-anneal phenomenon were described by Carpenter and Elam (1922), who noted that when fine-grained recrystallised aluminium sheet was subjected to a tensile strain and annealed at a high temperature, a single crystal was produced for a tensile strain of about 2%. Smaller strains resulted in

no grain growth and larger strains produced polycrystals of varying grain size; the number of nucleation sites for new grains, and thus the grain size, were dependent upon the total strain.

A theoretical study of the factors leading to a large grain size was made by Williamson and Smallman (1953). They defined a parameter P the probability of successful nucleation, which should be small for single crystal growth, so that nucleation will be restricted to a few sites, ideally just one, and growth will occur from these sites to cover the entire specimen.

$$P \propto \frac{T_g^2 \exp -\left(\frac{Q_n}{k T_g}\right) \cdot V}{S \, v \, Q_n} \qquad (2.1)$$

or substituting for T_g

$$P \propto \frac{v^{\frac{Q_n}{Q_g}} Q_g^2 \, V}{S \, v \left\{\ln\left(1/v\right)\right\}^2 Q_n} \qquad (2.2)$$

where T_g is the temperature at which growth occurs with a steady-state velocity v

Q_n the activation energy for nucleation

Q_g the activation energy for growth

V the volume of the specimen

S the temperature gradient.

It may be seen from these relationships that to maintain a low value of $\underline{P}$ a steep temperature gradient should be moved through a strained specimen of small volume. The rate of traverse affects $\underline{P}$ through $\underline{T}_g$ and $\underline{v}$, since $\underline{P}$ is more strongly dependent upon $\underline{T}_g$ than $\underline{v}$; a reduction in traverse rate should reduce $\underline{P}$ and allow the equilibrium growth rate to be achieved at a lower temperature. The variations of grain size with strain noted by Carpenter and Elam are due to variations of $\underline{Q}_n$ and $\underline{Q}_g$ with strain.

Williamson and Smallman introduced further parameters to explain the observed dependence of $\underline{P}$ on annealing texture, which affects the relationship between $\underline{T}_g$ and $\underline{v}$, grain size, purity and recrystallisation treatment. A very important condition for single crystal growth is that the initial grain size should be fine, uniform and fully recrystallised. Whilst it was found that specimen shape was important, and that square cross section material was susceptible to inhomogeneous nucleation at the corners, no theoretical prediction could be made of the importance of these sources of nucleation. Similarly poor surface finish or irregular cross sections are likely to lead to stress concentrations and inhomogeneous strain distribution.

2.2.2. The Growth of NiAl Single Crystals by the Strain-Anneal Technique.

Before attempting to grow NiAl single crystals by the strain-anneal method a preliminary test was made to see if a sufficiently large grain size could be produced by secondary recrystallisation. A piece of hot-extruded polycrystalline NiAl was annealed for two days

at 1550°C, during which time the grain size had increased from 0.05 mm to about 1 mm (cf. Fig 2.3). Whilst this growth was considerable the final grain size was too small to allow useful single crystals to be cut from bulk specimens; this result was not surprising as it has been found that for secondary recrystallisation to be effective a heavily deformed starting material with a distinct annealing texture is required (Aust, 1963).

All information available at the start of this investigation suggested that polycrystalline NiAl was brittle at room temperature (Grala 1962, Ball 1964). It was therefore concluded that the strain required for the strain-anneal method would have to be supplied at an elevated temperature and that the specimen should then be cooled rapidly to prevent the loss by recovery of the effects of the deformation. Since no means of straining in tension at elevated temperatures was available it was decided to apply this strain in compression, using the high temperature compression facility which was being constructed.

As there was no known example of a compressive pre-strain being used in this technique some preliminary experiments were made on aluminium. Specimens were deformed in compression and annealed under conditions known to give single crystals after a tensile strain. Despite difficulties in achieving homogeneous deformation with the crude compression apparatus used the results were very encouraging, grain sizes of up to 1 cm were obtained after a strain of 1-2%.

Initially NiAl was strained with a simple compression cage fitted

to a modified, motorised, Hounsfield Tensometer and heated by a nichrome-wound resistance furnace. This arrangement proved unsatisfactory because misalignment and oxidation of the cage caused inhomogeneous deformation. However, the experience gained with this simple arrangement was useful in the design of a high temperature compression modification to the Instron testing machine, (see 2.4) and once this became available, and a suitable specimen geometry found, no great difficulty was encountered in obtaining uniform deformation. The systematic study of the temperature dependence of the mechanical properties revealed that near-stoichiometric and nickel-rich compositions could be deformed at room temperature, which was subsequently used as the pre-strain temperature in most strain-anneal experiments. Aluminium rich compositions were completely brittle at room temperature and a pre-strain temperature of 500-600°C was found necessary.

The Gradient Annealing Furnace.

The furnace for annealing the pre-strained specimens (Figs 2.1 and 2.2) was designed according to the principles suggested by Williamson and Smallman. Heating to 1500°C was provided by a silicon carbide resistance heating element (Crusilite type DM), cut with the hot zone very close to one end, and contained in a sindanyo and fire-brick box. The entire furnace was mounted on a wheeled base and drawn along rails by means of a cable wound around a rotating drum which was driven by a syncronous motor. Traversing speeds were varied by altering the

diameter of the drum or the gear-ratio between the drum and the motor. A 24 volt D.C. air-blower was used to cool the wheels and prevent sticking. The mean temperature gradient measured in a dummy specimen was $150^{\circ}C\ cm^{-1}$ for a furnace temperature $1500^{\circ}C$; the last inch of travel was within the hot zone, so that the specimen finished the anneal at constant temperature.

The specimen was contained in a stationary alumina tube mounted along the axis of the heating element. Connections for inert atmosphere, vacuum, and a measuring thermocouple were made through brass end-fittings which had facilities for water cooling and made close contact on the alumina tube by means of 'O' ring seals. A vacuum pumping unit capable of maintaining 10^{-5} torr was used to evacuate this tube prior to admitting the inert atmosphere. The annealing atmosphere, used to reduce the vapourisation of aluminium, was initially 99.995% pure argon, at a slight positive pressure (with respect to atmospheric) to ensure that any leaks were outwards. Considerable oxidation occurred with gas of this purity, so a gas purification train was added and commercial purity argon was passed through the following sequence:

i) A liquid nitrogen cold trap (available to remove condensable vapours from low boiling point gases although it was not used with argon).

ii) "Sofnolite" to remove CO_2.

iii) P_2O_5 to remove water vapour.

iv) Titanium chips at $1000^{\circ}C$ to remove oxygen (Titanium is the most

efficient getter available in a convenient form for use at 1000°C).

v) Chromium chips at 1000°C to remove nitrogen.

As further precautions the gas flow rate was reduced to the minimum required to maintain a positive pressure, and no rubber tubing was used in the train after the P_2O_5 trap. All seals were demountable ground glass cones or 'O' rings.

With the specimen within the hot zone, and the traversing motor off, the furnace was used as a conventional annealing furnace in vacuum up to 1000°C or argon up to 1500°C.

Conditions for the Growth of Single Crystals.

The results obtained were subject to considerable variation. No sharp critical strain was observed, but it was found that compared with an undeformed control specimen no grain growth occurred after a strain of less than 0.5%, and that larger strains resulted in various grain sizes. Some of these grains were sufficiently large to allow single crystals to be cut out of them. This "critical" strain of about 0.5% is small compared with that normally observed for other materials (2-3%). This difference is possibly due to the high stresses set up at the grain boundaries on deformation causing local disordering (cf. 4.5), hence increasing the stored energy of deformation and affecting Q_n and Q_g in equation 2.2. Robinson and Bever (1965) have attributed the high stored energy of deformation of AgMg, measured calorimetrically, to the local destruction of order.

A number of factors, which were thought to be important, were found to have little effect on the grain size. These included furnace temperature and surface finish, (equivalent results were obtained after grinding on silicon carbide papers and with careful electropolishing). As the initial state of the material was known to be of great importance, various initial annealing treatments were tried. It was found that after preliminary anneals which resultsd in some grain growth, the strain-anneal effect disappeared. Consequently a standard pre-anneal temperature of 1100°C was adopted for all compositions. As predicted by equation 2.1 low traverse speeds gave the best results, a speed of 0.5 cm hr^{-1} was generally used; the temperature gradient could not be altered without reconstructing the furnace.

Specimen size and geometry had a considerable effect, All specimens were cut from extruded bar, polished on fine (600 grade) silicon carbide paper and annealed for 1 hour at 1100°C. Although not recommended by Williamson and Smallman a square cross-section was adopted for ease of machining. An initial cross-section of 4.5 x 4.5 mm was used in the hope that the grain size would be large enough to cut out single crystals of any orientation, but it was always found that there were at least 3-4 grains in the cross-section. A reduction of cross-section to 2.5 x 2.5 mm resulted in a considerable improvement, and it was with specimens of this size that the largest crystals were grown.

The largest crystal produced measured 2 x 2 x 13 mm after a strain of 1.1% and is shown in Fig 2.3, together with an undeformed control

specimen which received the same annealing treatment. Large crystals have been grown in near-stoichiometric and nickel-rich compositions, but, although tests indicate that enhanced grain growth occurs after pre-straining, no useful single crystals have been grown in aluminium-rich alloys. A complicating factor in material of this latter composition is the yield drops and low initial rate of work hardening near 500°C (Fig 4.12); it was found that useful grain growth only occurred if the specimen was pre-strained at a temperature at which a high initial rate of work hardening would ensure a more homogeneous distribution of strain. This happens at about 600°C, at which temperature the rate of recovery is becoming quite appreciable, necessitating rapid cooling after deformation.

There was no obvious crystallographic relationship between the orientations of the single crystals and compression axes of the polycrystals from which they were derived. This may be seen from Fig 2.4, in which the original compression axes of the strain-anneal grown single crystals are plotted on a standard stereographic triangle. It may be noted that the distribution is fairly uniform, except that orientations with axes close to ⟨100⟩ and ⟨111⟩ seem to be unfavourable.

2.2.3. Melt Techniques.

Of the melt-techniques available for the growth of single crystals, three appeared practicable to use with stoichiometric NiAl:

i) The Czochralski method, withdrawal of a single crystal seed from a melt.

ii) The floating zone technique, passing a small molten zone along a rod at a rate which allows solidification as a single crystal behind the zone.

iii) The Bridgman method, unidirectional cooling of a melt contained in a crucible, nucleation being controlled by a seed crystal or painted end to the crucible.

The Czochralski method was not used because a large mass is required to be kept molten for long periods which leads to difficulties of crucible contamination and concentration gradients caused by the vapourisation of aluminium. The floating zone method is probably best for growing crystals of this type: Seeding is possible and contamination avoided since a crucible is not used; providing the charge is of constant cross-section vapourisation should cause no problems; all parts would be molten for the same time, thus the losses should be constant and no concentration gradient should be produced. This technique has been used by Wasilewski (1966) to grow NiAl single crystals. However the Bridgman technique was finally selected because it could be set up more conveniently with the facilities available and because of the difficulties of obtaining long lengths of rod of constant cross section. The Bridgman technique has been used by Ball (1964) to grow single crystals of NiAl, heating the charge with a molybdenum wound resistance furnace.

2.2.4. The Growth of Stoichiometric NiAl Single Crystals by the Bridgman Method.

The final form of the apparatus used to grow single crystals of stoichiometric NiAl is shown in Fig 2.5 and is similar to that used by Hall (1957) to grow single crystals of iron alloys.

The charge, irregular cross-section rods produced in the "cold boat" was contained in a tapered alumina crucible which had a pointed bottom. This was held in a cylindrical graphite susceptor, a small gap preventing the reduction of the alumina by the carbon, and mounted on a stainless steel base which was water cooled to aid uni-directional cooling and to prevent the melting of the support. This assembly, with its cooling water connections, was attached to a platform which could be lowered by two leadscrews rotated at constant speed by a small syncronous motor of high torque (30 Kg. cm).

An argon atmosphere at a pressure slightly greater than atmospheric was used to minimise aluminium losses; no gas purification was used because at the operating temperatures carbon is an efficient oxygen getter. The heated assembly and atmosphere were contained in a water cooled jacket, the inner tube of which was clear silica and the outer pyrex. These materials had the advantage of being both transparent and di electric, although the cooling was required to prevent the silica devitrifying. Connections for vacuum allowed the apparatus to be out-gassed at dull red heat and a pressure below 10^{-4} torr.

To minimise volatilisation loss and crucible contamination, a

zone about one inch high of the graphite susceptor was heated by high frequency induced currents. The charge was heated by radiation from the graphite rather than by direct induction for several reasons:

i) The efficiency of induction heating is proportional to the ratio of the diameters of heating coil and susceptor, thus considerably more power would have been required. (Wilkinson, 1963).

ii) The geometry of the charge would change on melting as would its resistance, another parameter which determines heating efficiency, this effect would have to be counteracted by constant variations of power and would make the calibration of power against temperature difficult.

iii) Differential thermal expansion could lead to cracking by heating the charge before the crucible.

As a control thermocouple could not be introduced into the melt without disturbing the supply of solid material and nucleation conditions, the temperature was controlled by the power supplied, and was found to be constant ($\pm$ 20°C) in successive calibrations. Power against temperature calibrations were made at several positions along an empty crucible using an Ir - 60% Ir / 40% Rh thermocouple introduced through a gas seal. The power required to maintain a given temperature was found to decrease as the crucible was lowered, due to changes in geometry and distance from the water cooled end.

Single crystals up to $2\frac{1}{2}$ ins long and $\frac{1}{2}$ in diameter have been successfully grown by this technique, operating at a temperature of

1700 ($\pm$ 50) ^{o}C and lowering the crucible at 0.2 mm min^{-1} (0.5 in hr^{-1}), a speed similar to those used with many other materials (Schadler, 1963). The orientations of the crystals were such that the growing face was always near to either a $\{100\}$ or a $\{110\}$ plane, i.e. the planes with the highest density of packing. Crystalline perfection, indicated by the sharpness of the spots on a Laue X-Ray back reflection photograph, was not as high as obtained with the strain-anneal technique, but after a 12 hour anneal at 1500^{o}C the results were comparable.

2.3. Specimen Preparation.

2.3.1. Cutting and Machining.

NiAl, being hard and brittle, is very difficult to machine. Conventional techniques cannot be used because all but the hardest tools are rapidly blunted, whilst the small degree of ductility of the compound prevents the use of standard ceramic techniques, because abrasive wheels soon become clogged and useless. Surface grinding has been successfully employed, but considerable care has to be taken to prevent surface cracking. Spark machining could have been used but the hardness of NiAl leads to very slow rates of erosion.

All NiAl single and polycrystalline specimens for mechanical testing were cut with a Capco Q. 35 annular diamond saw. This saw employs a thin (typically 0.008 in) circular metal blade rotating at 3-5,000 r.p.m., which is tensioned and held at the periphery and has a diamond impregnated annular cutting edge. The work-piece is mounted on a moving table with a gravity feed to maintain a constant and slow cutting rate. The main advantage of this system is that thin straight cuts can be made. There are, however, several disadvantages; the size of the work-piece is limited and normal life of the blade is short. Nevertheless good surfaces were obtained with new blades and slices as thin as 0.5 mm have been cut.

The orientation fixture supplied with this machine only rotated through $\pm$ 10° in the two required directions. An additional goniometer was made which was capable of a 360° rotation about the direction of

traverse and of a further $\pm$ 90°, hinging about a vertical axis. The mounting block, to which the specimens were fixed with a brittle resin that melts at 65°C, could be removed from the goniometer and fitted to an X-ray machine for orientation determinations; the specimen could be rotated in 90° steps for the accurate cutting of perpendicular faces. In order to cut all six faces the specimen had to be remounted after the first parallel cuts for which a flat mounting press was used to ensure that the remaining cuts were made perpendicular to the original faces.

2.3.2. Polishing and Etching.

Specimens for mechanical testing were mounted in a soluble cold setting compound and passed through the usual sequence of successively finer grades of silicon carbide papers and diamond paste in order to obtain a good mechanical polish. In general polycrystalline specimens were only polished to the 600 grade SiC paper, but single crystals, and other specimens on which surface observations were to be made, were polished to $\frac{1}{4}\mu$ diamond paste.

Electropolishing, in a solution of 79% acetic acid and 21% perchloric acid at 90 V and 1-2 A, was used to finally polish all those single crystals not used for surface observations, and for some polycrystals. It was found that electropolishing had no noticeable effect on the mechanical properties, including the strain to failure, but since it produced a slightly rippled surface it was not used when surface observations were to be made.

The distortion of the spots in Laue X-ray back reflection photographs were used as an indication of the surface damage produced by these various polishing treatments. Although it was found that the cutting operations cause some broadening of the spots, careful polishing to 1μ grade diamond paste gave results comparable with annealed or electropolished surfaces. It was therefore concluded that the retained surface damage in the depth penetrated by the X-rays was negligible. The depth of damage is small compared with most pure metals, and is probably a useful by-product of the hard and brittle nature of NiAl.

Grain boundary etchants recommended for NiAl, which include Vilella's reagent (Grala, 1960) and chromium trioxide in hydrochloric acid (Wood and Westbrook, 1960), were found to etch the compound very slowly. More rapid attack was achieved using alcoholic ferric chloride (5 g $FeCl_3$, 2 ml HCl, and 95 ml ethanol). This etch works by differential attack of various crystallographic faces and proved suitable for normal use at moderate magnifications, although relief effects and uneven attack (cf. Fig 2.3) made it less effective for high and low magnifications respectively. Grain sizes were measured after etching in this solution by the intercept method - counting the number of grain boundaries cutting a straight line of known length.

2.3.3. Annealing.

Annealing of both single and polycrystalline specimens prior to mechanical testing was often necessary to remove the effects of earlier

working or cutting operations.

All samples were annealed well within the hot zone of the gradient annealing furnace, in vacuum, inert atmosphere (normally purified argon) or air as required.

After a series of anneals at various temperatures, and for various times, the optimum annealing conditions for polycrystals, those that would give no grain growth and the maximum ductility, were determined to be 1 hour at 1100^{o}C in argon; longer anneals at higher temperatures were used to produce larger grain sizes. Since no recrystallisation problem existed for single crystals a standard annealing treatment, before mechanical testing, of 12 hours at 1500^{o}C followed by a slow cool was adopted.

2.4. Mechanical Testing.

2.4.1. Factors Influencing the Choice of Compression as the Mode of Deformation.

Compression was selected as the mode of mechanical testing for this investigation because its use allowed tests to be continued to far greater strains than would be possible in a tensile test. Sometimes plastic flow was observed under conditions that would have produced completely brittle behaviour in a tensile test. This difference is due to compressive stresses closing cracks and thus reducing their tendency to propagate. A further advantage is that compression tests require no complex grips and may be performed on small specimens of simple shape, thereby economising on material and reducing machining problems.

Of the alternative methods bend tests are difficult to analyse and provide little comparative data, their main advantage being the small loads required to cause plastic flow. Yield stresses can be very different from those measured in tensile tests, Rozner (1965) found that the flow stresses of NiAl deformed by bending were three times higher than those in tension. A number of other mechanical tests such as torsional tests and pure shear suffer from a similar lack of scope. The tensile test is generally preferred because it can provide more information about the later stages of deformation, particularly work-hardening and fracture characteristics. This is because a specimen is more stable when loaded in tension and it deforms uniformly until the onset of necking. On the other hand a specimen strained in

compression tends to buckle, and, if friction is high at the specimen-ram interface, to become barrel shaped. These effects may be minimised by the careful selection of specimen geometry and lubricants for the compression surface, which enable work hardening characteristics to be studied at least up to moderate strains (10-20%). Due to the tendency for cracks to close the interpretation of fracture data in compression is difficult.

2.4.2. Considerations in the Design of the High Temperature Compression Apparatus.

To permit deformation in compression existing apparatus had to be modified. This, together with the requirements of constructional materials and temperature imposed limitations on the design and performance of the high temperature compression apparatus.

All tests were performed in an Instron testing machine model TT-CM; the design of which was such that the strain had to be applied by the downward motion of a moving beam, and the resulting load measured by a downward pull on a load cell located above this. Thus a jig had to be constructed which allowed a downward motion of the crosshead to produce a compressive stress in the specimen and a tensile stress on the load cell. Alternative systems, using compression load cells or the "reverse loading" facility which are available for the Instron, were rejected because of the difficulty of adjusting the compression faces and maintaining axiality of loading at elevated temperatures.

A major problem in the design of apparatus for high temperature mechanical testing is the choice of materials, particularly for the components which will be subjected to high stresses at elevated temperatures. Apart from the refractory metals, which oxidise rapidly and would have to be protected by a continuous inert atmosphere, the only materials which are sufficiently strong at elevated temperatures are ceramics, which have limited ductility and can, therefore, only be loaded in compression. However considerations of mechanical stability, and the design of the jig outlined above, require most of the frame to be loaded in tension.

For the rapid attainment of thermal and mechanical equilibrium the furnace should heat only the specimen. This ideal is impossible to achieve because heat losses through the specimen ends will give rise to thermal gradients, which are usually minimised by employing long furnaces. Thus the length of the furnace, like the design of the loading frame, has to be a compromise between two conflicting requirements.

All the above requirements were essentially fulfilled by the compression cage and furnace described in sections 2.4.3. and 2.4.4. The apparatus consisted of a small 1000°C furnace fitted in a loading frame. The load was transmitted to the specimen by rams fitting inside the furnace and attached to the frame. The advantage of this system was that only the rams were heated, thus they were the only components which had to be made of heat resistant materials, and since they were loaded in compression they could be made of any

suitable materials, including ceramics. The rest of the jig remained cold, avoiding problems of misalignment and distortion due to heating and oxidation.

2.4.3. The Compression Cage.

The basic requirements for a compression test are that a specimen, at constant temperature, must be compressed between two parallel, co-axial surfaces in such a way that the relationship between load and compression may by measured, and that no part of the apparatus, particularly the compression surfaces should undergo plastic deformation.

Both these and the special requirements previously discussed were met by the compression cage designed for this investigation, and illustrated in Figs 2.6 and 2.7. It consisted of two interpenetrating frames. The upper one was bolted to the underside of the moving crosshead, and carried the dead weight of the furnace with its water, atmosphere and electrical connections. Strain was transmitted to the specimen by the upper ram attached to the bottom of this frame and ending in the hot zone of the furnace. The lower frame was connected to the load cell by a universal coupling and long connecting rod which passed through the centre of the moving crosshead. The load was transmitted from the specimen to this frame by a second ram attached to the top of its lower plate. There were no other fixtures on this frame, thus, apart from the load exerted on the test piece, the load cell sensed only the constant weight of the frame and ram; the Instron

recorder had facilities for "backing off" this load.

Each frame consisted of two circular end plates bolted to 1" diameter joining rods. Adjustable roller bearing, fitted to the bottom plate of the upper cage and upper plate of the lower cage made contact with these rods and could be adjusted to align the compression surfaces parallel to and co-axial with each other. This alignment was checked with feeler gauges, the maximum deviation from parallel over a one inch diameter being 0.0005 in., the tolerance to which the compression surfaces could be ground. The pressure exerted by the roller bearing could be adjusted, so that strong aligning forces could be applied when testing hard materials, where high loads were likely to cause lateral movement of the jig but friction in the bearings could be tolerated. When testing softer materials the bearings were adjusted less tightly, because friction could have been a considerable fraction of the total load, and because smaller aligning forces were required. A typical value of the friction, measured as the change in load when the motion of the crosshead was reversed was 100 g, with moderate aligning forces and a typical testing crosshead speed (0.01 cm min^{-1}). With a specimen of standard size this corresponded to a change in stress of 16 $g.mm.^{-2}$ which is negligible compared with the flow stresses normally measured.

To minimise atmospheric corrosion and maintenance problems the jig was made of En 58 B welding grade stainless steel. The size of the cage was dictated by two requirements. It had to be sufficiently large for the furnace to be fitted inside the lower cage and yet as short as

possible to minimise elastic distortion. As a result of early experiments, the pre-straining of material for the growth of single crystals by the strain-anneal technique, the cage was designed to sustain a maximum load of two tons without itself deforming plastically. The end plates, joining rods and bolts have however been made far thicker than required for this load in order to minimise elastic distortion. The measured elastic deflection of the cage and load cell varied between 6.5 and 8.5 x 10^{-4} mm Kg^{-1} according to the type of ram and hardness of the load cell used. While this distortion was large compared with that of the load cell (1 x 10^{-4} mm Kg^{-1} for the softest cell used) and the elastic distortion of the specimen (typically 1.5 x 10^{-4} mm Kg^{-1}) it was small compared with the plastic distortion of the specimen; and since it was elastic and reproducible it could be allowed for in the calculation of plastic strain.

2.4.4. The Furnace.

The mechanical testing furnace used in this investigation (Figs 2.8 and 2.9) was designed to operate at temperatures of up to 1000°C with minimum thermal gradients while remaining as small as possible. It was a simple vermiculite insulated resistance furnace with two independent nichrome windings on concentric silica tubes, the tops and bottoms of which were fitted into water cooled brass end plates. Temperature gradients were reduced by varying the distance between adjacent turns of the furnace winding, so that more heat was obtained from the top and bottom turns, and by careful choice of the

power supplied to each winding. The temperature gradient, measured by a thermocouple passing through a hollow ram was 1 deg C over a typical specimen length (7.5 mm) and 4 deg C over 25 mm at 575°C.

Precise temperature control is essential for mechanical testing because thermal expansion of the specimen and other heated members would be additional to the strains caused by the motion of the crosshead. An anticipatory temperature controller was used to control the power supplied to the outer winding, and "high-low" power switching used to eliminate "hunting". The chromel-alumel control thermocouple was placed between the two windings for maximum sensitivity. With this combination the temperature could be maintained constant to within ± 1 deg C throughout the normal duration of a test.

The small thermal mass of the furnace allowed equilibrium to be reached in a short time, usually fifteen to thirty minutes depending upon the magnitude of the temperature change. For testing purposes the temperature was considered to be steady when a thermocouple close to the the specimen had registered a constant reading for five minutes and a small load applied to the specimen had stabilised.

To enable tests to be made in inert atmospheres, gas seals could be fitted at the ends of the silica furnace tubes and between the furnace and upper ram; the lower end of the furnace was sealed with a polythene tube. To prevent cooling the specimens the gas was pre-heated by passing it between the two windings. Although commercial purity argon was most commonly used any inert or reducing gas could be substituted. Facilities were available for working or purging with

vacuum, but were not normally used because of the additional friction resulting from sliding O ring or flexible bellows vacuum seals.

A similar furnace, designed for testing oxides up to 1800°C and utilising a molybdenum heating element, was also used for a few tests at temperatures above 1000°C in conjunction with a similar compression cage. An atmosphere of 75% N_2 25% H_2 was used to protect both the windings and the specimen.

2.4.5. The Compression Rams.

The rams, which were the only stressed components to be heated, were very simple in design (Fig 2.6). They consisted of a long stem, which fitted inside the furnace, attached to a flange which was fixed to the compression cage. The flange and stem were normally bolted together, but if a good gas seal was required they were machined as one integral unit. Rams of this design were easily removed and their compression faces re-ground should any indentation occur.

A number of materials have been used as rams, these are listed in Table 2.1 with their operating temperatures and limitations. It was found that metal rams, with high thermal conductivity, caused a considerable loss of heat above 400°C, resulting in marked thermal gradients. Ceramic rams were therefore used for all high temperature tests although metal rams of sufficient hardness were available.

Table 2.1 Ram materials

Material	Hardness at 20°C	Temperature Range °C	Limitations
'Nonvar' tool steel	650 VPN	-196 to 100	tempering temperature 100°C
Nimonic 80A	250-350 VPN	20 to 500	thermal conductivity, high temperature strength and oxidation
Nimonic 115	450-500 VPN	-196 to 500	thermal conductivity
Pyrophyllite (Al_2O_3:SiO_2)	MOH 6	20 to 700	creeps under small load at 800°C
Sintox (95% Al_2O_3)	MOH 9	400-1000	high conductivity
Recrystallised Alumina (99% Al_2O_3)	MOH 9	above 800	poor thermal shock resistance
Refrax (silicon nitride bonded silicon carbide)	MOH 8	above 800	poor surface finish, high thermal conductivity

2.4.6. Low Temperature Tests.

A separate jig, designed by R.D. Rawlings, was used for tests at low temperatures (Fig 2.10). It was similar in design to the high temperature cage, except that the width was considerably reduced, so that the complete lower cage could be immersed in a liquid bath. This reduction in width also resulted in an increase in elastic stiffness, the measured deflection was 5×10^{-4} mm Kg^{-1} at room temperature.

An electrically heated oil bath, controlled and powered from the same supply as the 1000°C furnace, was used for temperatures in the range 20-200°C. For tests at lower temperatures the standard cooling mixtures listed in table 2.2 were used. Temperatures were measured by a calibrated thermocouple in contact with the specimen, and checked by a low temperature thermometer.

Table 2.2 Standard Low Temperature Baths

Coolant	Temperature	
	°C	°K
Ice and Water	0	273
Boiling Isceon 12	-30	243
Solid CO_2 in Acetone	-72	201
Solid-liquid Isceon 12	-158	115
Solid-liquid isopentane	-160	113
Boiling liquid nitrogen	-196	77

2.4.7. Testing Techniques.

All tests were performed on a floor model TT-CM Instron equipped with push button controls for "instantaneous" changes of strain rate and a $\frac{1}{4}$-second response recorder, which allowed load changes at a strain rate of 2×10^{-3} sec^{-1} to be followed without any appreciable time lag. With the normal size of specimen, and a decade speed reducer a minimum strain rate of 1×10^{-4} sec^{-1} was possible. Rapid cross-head speeds, up to 50 cm min^{-1} allowed the furnace to be raised rapidly clear of the lower ram, so that the minimum time elapsed between tests.

The use of load-cycling controls allowed a small load to be maintained on the specimen during heating or cooling. This technique was useful at high temperatures as an indication of the approach to equilibrium and it was essential for tests at temperatures below $0^{\circ}C$ where boiling liquids could dislodge the specimen.

A number of authors (Kelly, 1961; Kocks et al., 1964) have recommended the use of hard hemispheres between the specimen and upper compression surface. While realising that this system could give very accurately parallel compression faces for soft materials near room temperatures it was rejected for this investigation because it was thought that the high stresses at the small contact area would cause the spherical surface to indent the upper ram. Furthermore it would have been difficult to prepare accurate hemispheres in many of the materials used, thus this system could not have been used at all temperatures.

The use of lubricants at the specimen/ram interfaces was avoided for a similar reason, that no lubricant (except graphite if a good inert atmosphere was used) could have been employed over the full temperature range thus making comparisons between tests at different temperatures difficult. A thin film of PTFE was used as a lubricant for some single crystals tests at room temperature; as this caused some irregularities in the load-compression curve in the elastic region results in the plastic region were also suspect, and the specimens were only used for slip line observations.

2.5. Determination of Composition.

As a rough check on composition the density or lattice parameter was measured and compared with the values of Bradley and Taylor (1937). Densities were determined by weighing in air and in water, and lattice spacings by a standard Debye-Scherrer X-ray technique.

Chemical analyses for both nickel and aluminium were made on all single crystals grown and to check the nominal compositions of extruded material. Nickel was determined by precipitation with dimethylglyoxime, and aluminium by a controlled precipitation of the succinante. All compositions quoted in the results are those obtained from these analyses and are probably accurate to $\pm$ 0.5%.

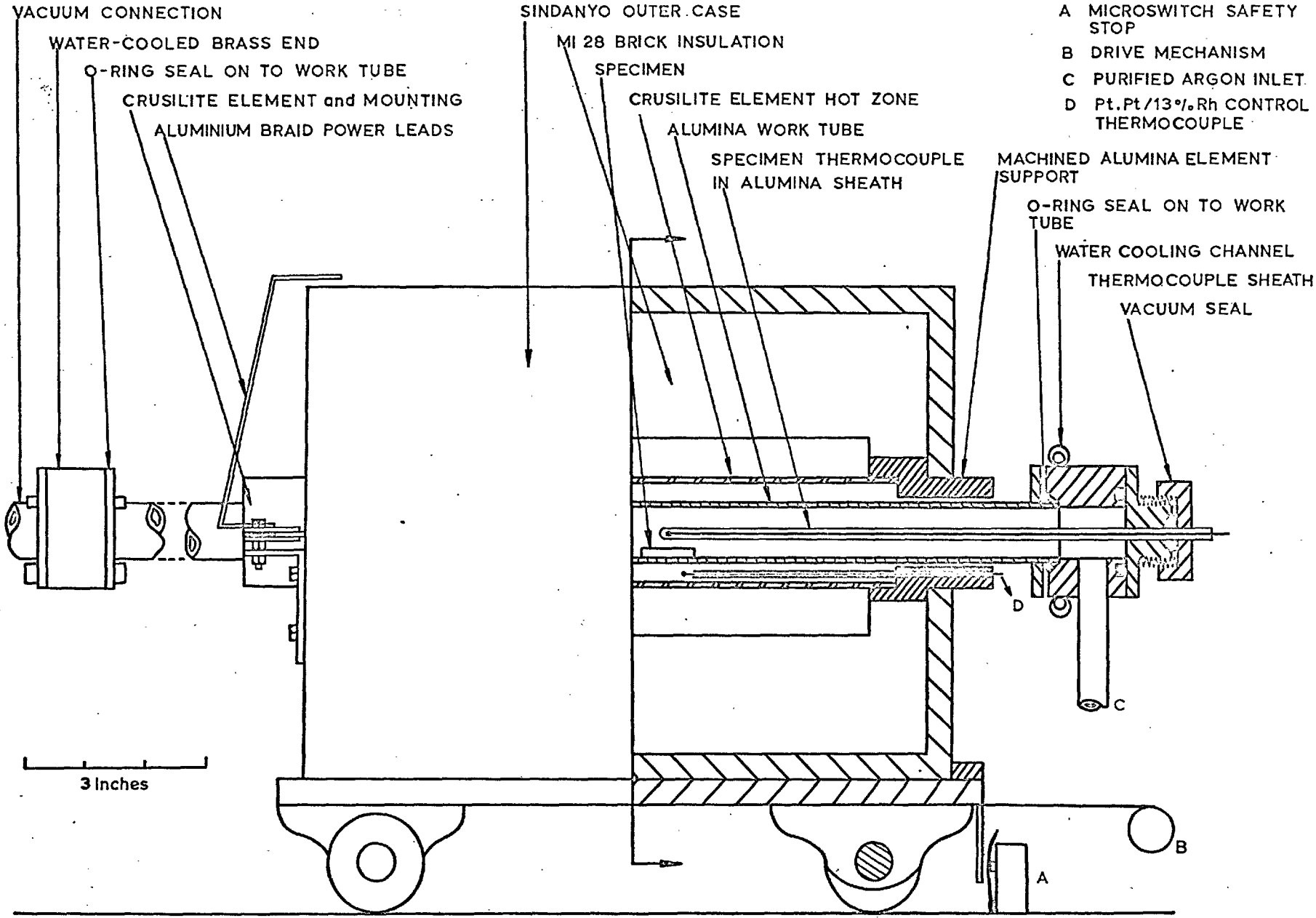

Fig 2.1 Gradient Annealing Furnace.

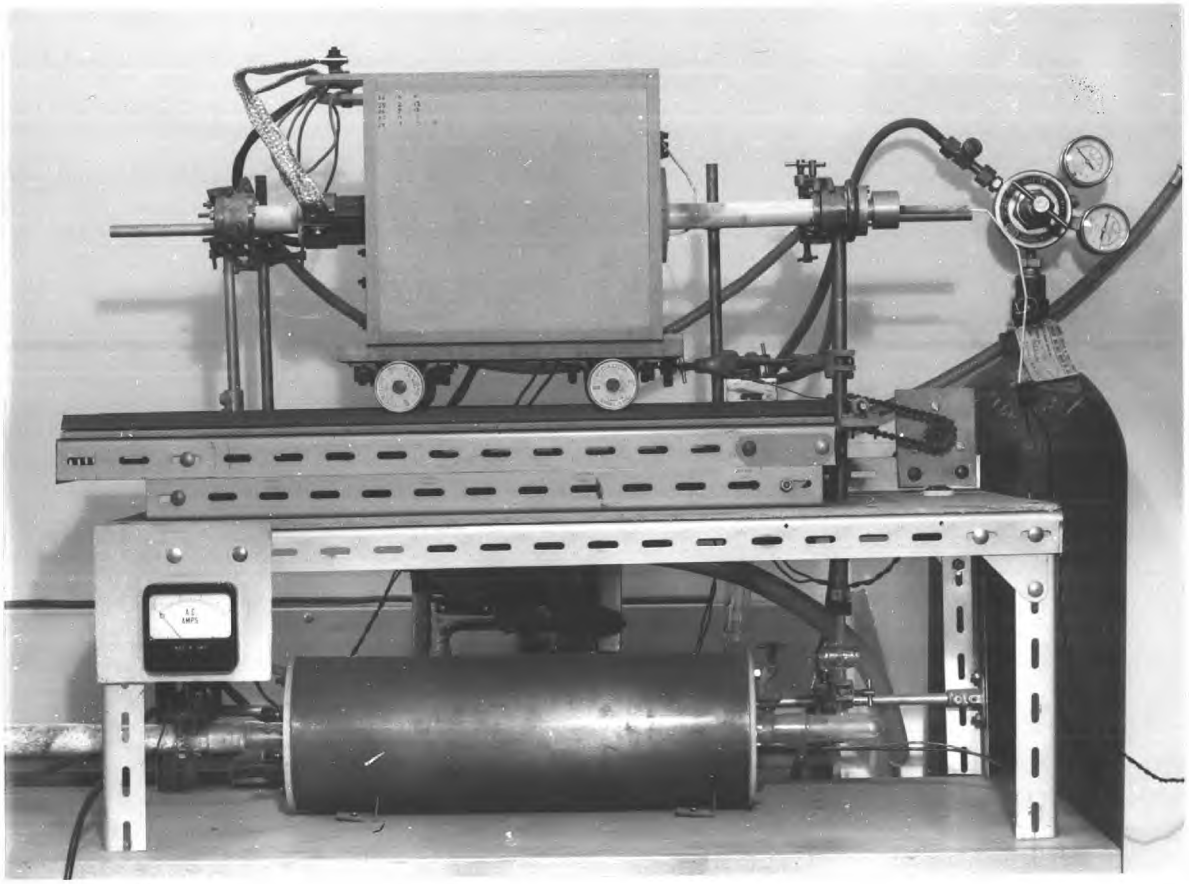

Fig 2.2 The Gradient Annealing Furnace Showing the Argon Purification Train

Fig. 2.3 Grain Size after Strain-Anneal Treatment (x 5).
Upper: Not Deformed Lower: Compressed 1%.

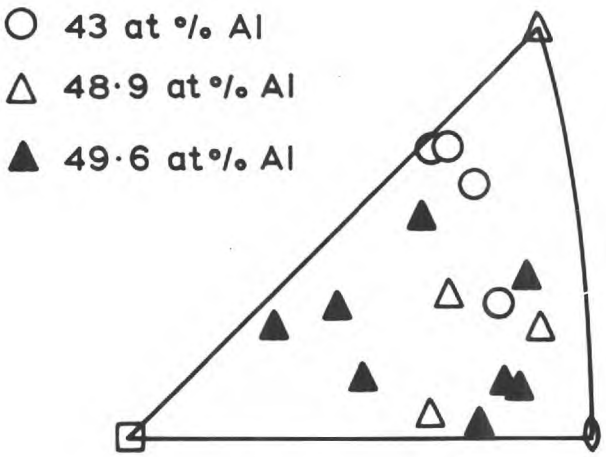

Fig. 2.4 Orientations of Single Crystals Grown by the Strain-Anneal Technique.

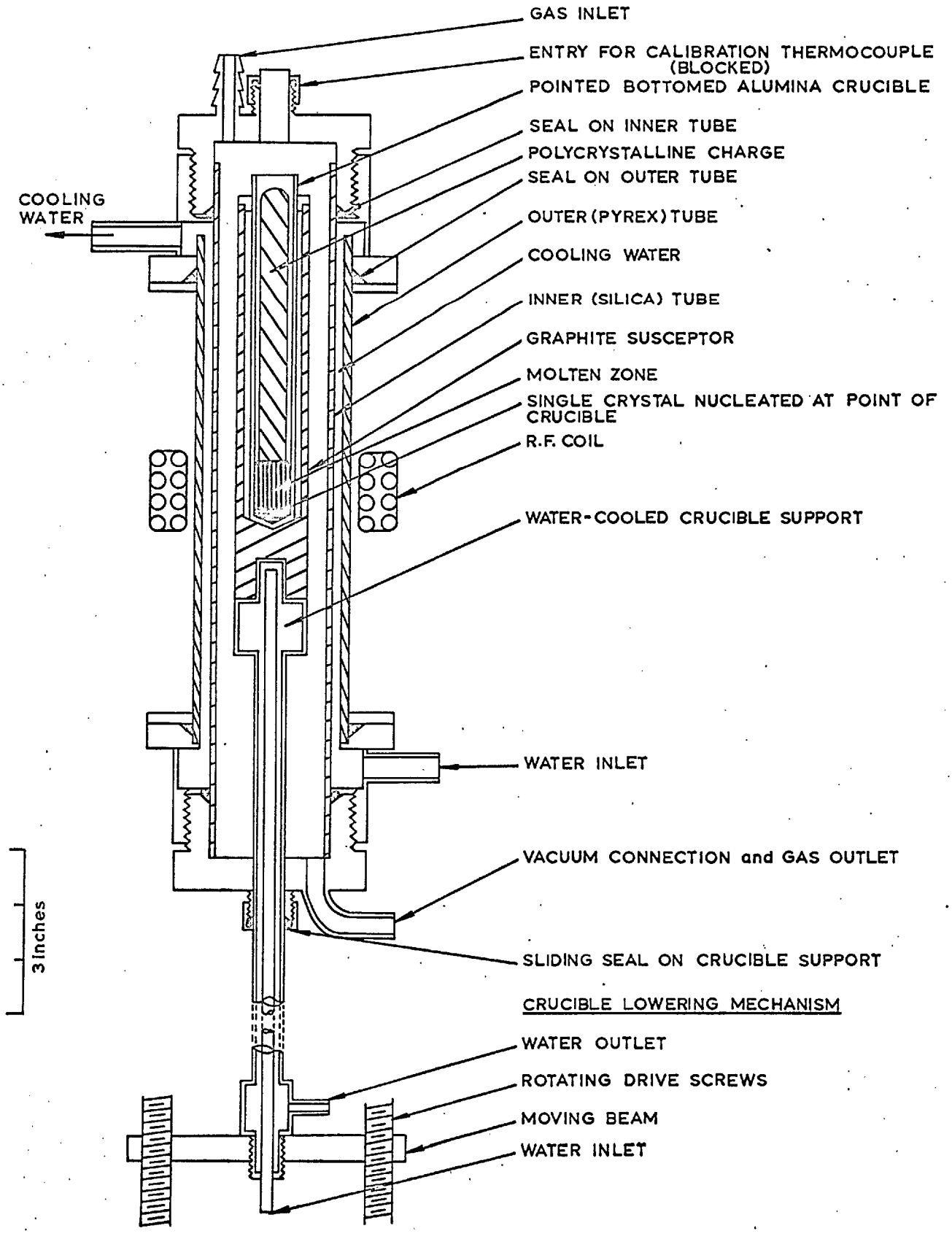

Fig 2.5 Apparatus for the Growth of Single Crystals from the Melt.

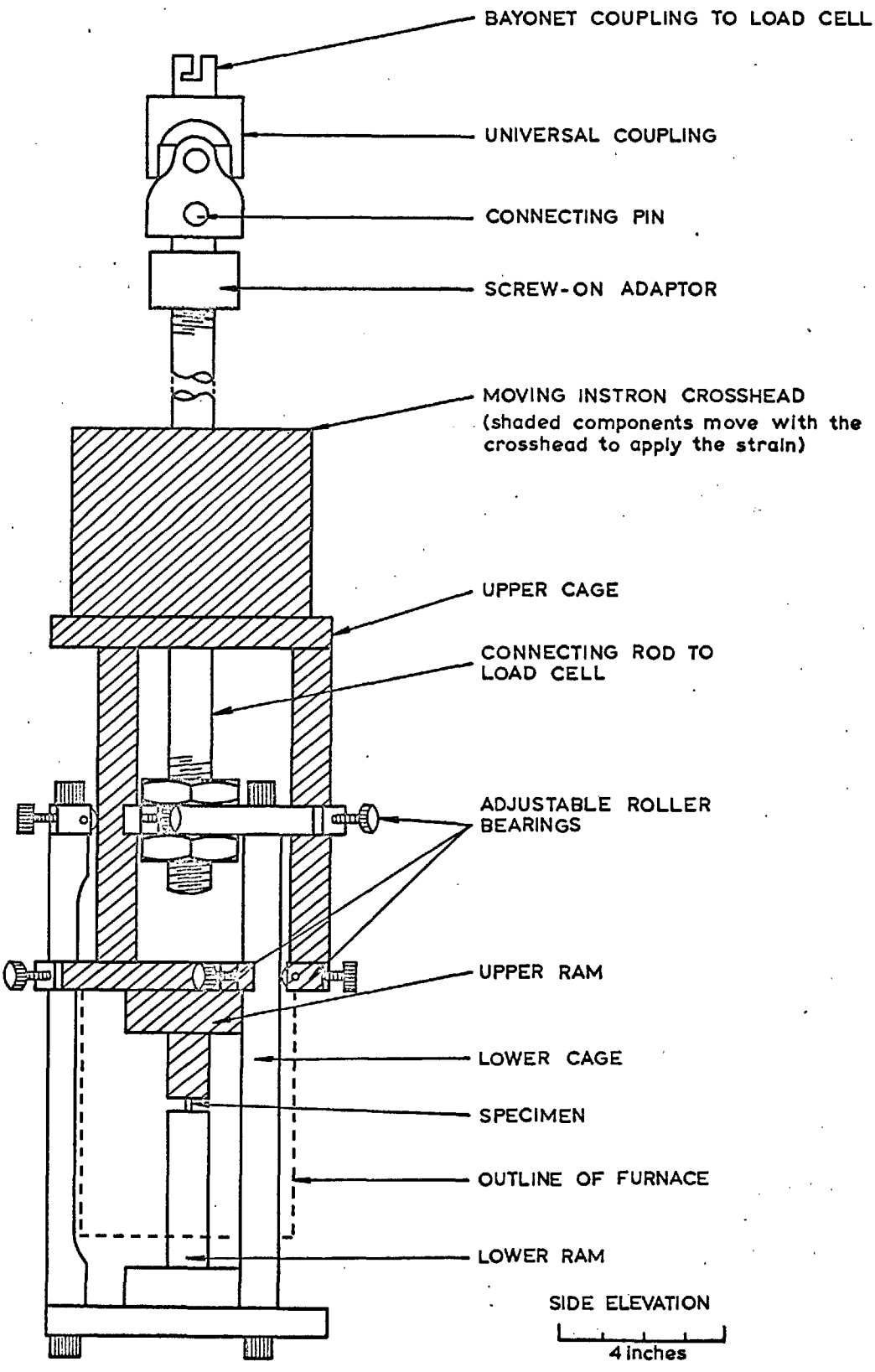

Fig 2.6 High Temperature Compression Testing Apparatus.

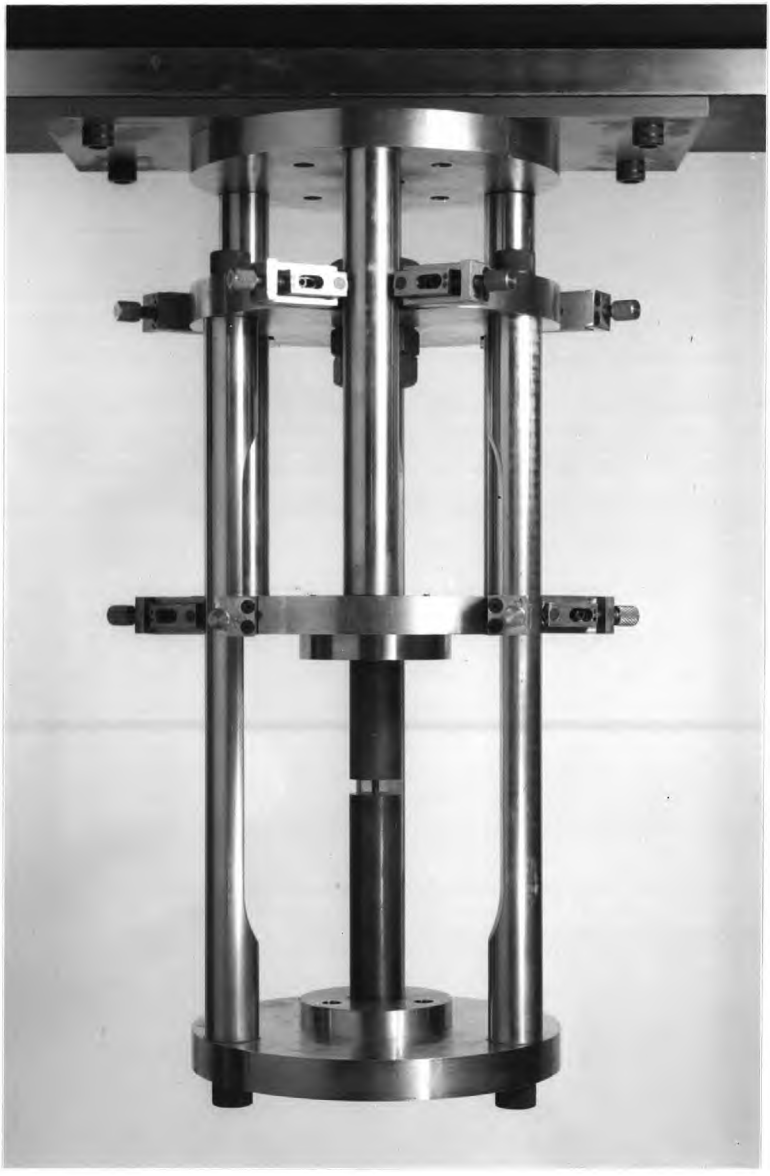

Fig 2.7 High Temperature Compression Cage (Furnace Removed)

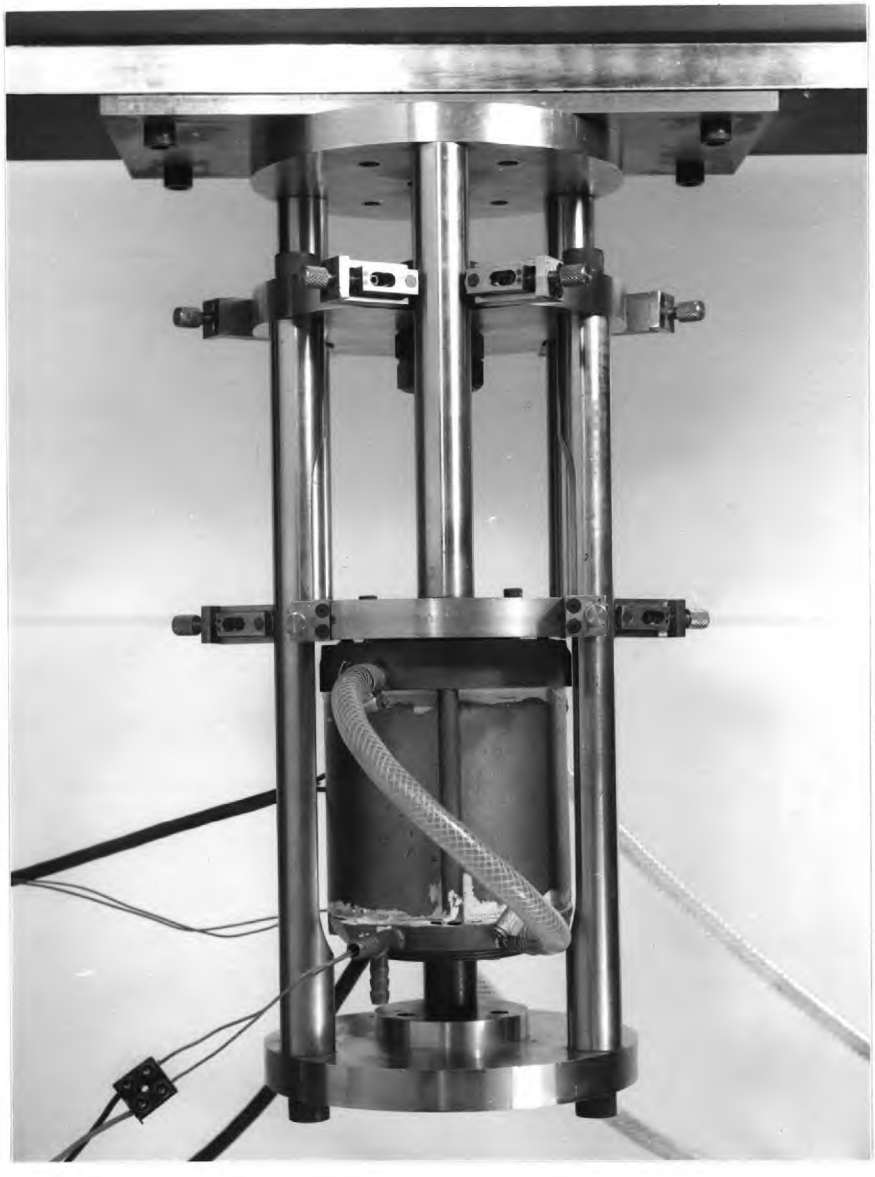

Fig 2.8 High Temperature Compression Apparatus with Furnace

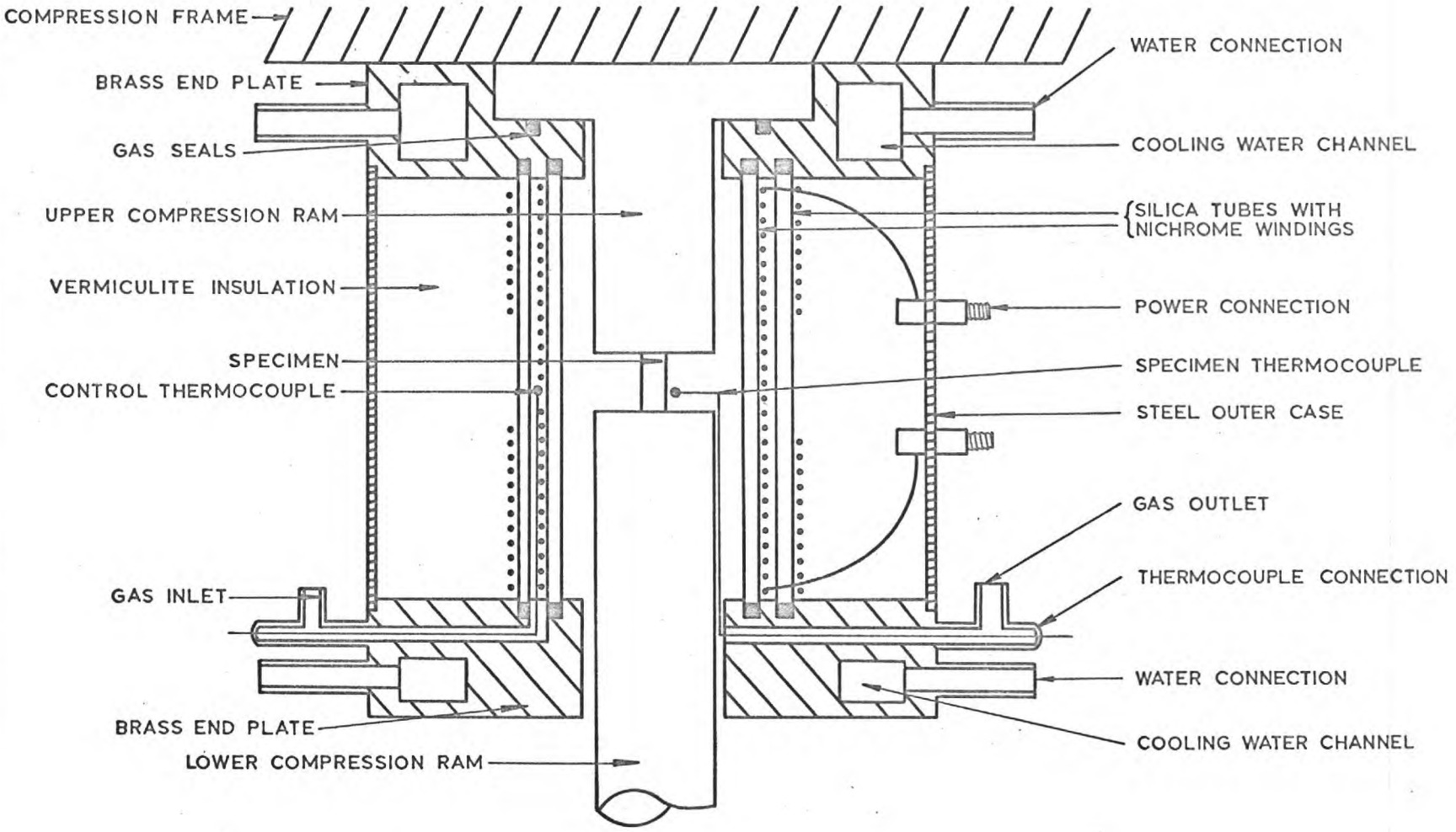

Fig. 2.9 1000°C Furnace for Mechanical Testing.

Fig 2.10 Low-Temperature Compression Cage

Chapter 3 Crystal Plasticity.

A knowledge of the slip plane and direction, and the way in which these vary with temperature, composition, and orientation, is an essential prerequisite to an understanding of the deformation behaviour of any material. It is particularly important in NiAl, where the crystal plasticity is extremely complex, and slip has been observed in ⟨100⟩, ⟨110⟩, and ⟨111⟩ directions and on numerous planes.

The special techniques used to determine slip systems are described in section 3.1. and examples of the application of these techniques in 3.2. and 3.3. It was found that the preferred slip direction in NiAl was ⟨100⟩; orientations which permit slip on this system will be referred to as "soft orientations". Straining along an axis close to ⟨100⟩ constrains slip on this primary system, resulting in a high flow stress; therefore orientations in which slip does not occur with a ⟨100⟩ vector will be called "hard". Slip, when observed, in these orientations was in a ⟨111⟩ or occasionally ⟨110⟩ direction. The observed slip systems are summarised in Table 3.1.

3.1. Experimental Techniques Used in the Determination of Slip Systems.

3.1.1. Slip Traces and Change of Specimen Shape.

The study of surface markings produced by deformation is a very useful and well established technique for the determination of slip systems, and has been applied to most crystalline materials which undergo deformation by slip. In principle the method is very simple, the slip plane can be found from the surface traces caused by the relative movement of atomic planes, and the slip direction from the direction of greatest shear. In practice this analysis is not so straight forward because slip traces are often not straight and because slip markings, being a macroscopic manifestation of atomic movements, represent the average displacement of a large number of atoms.

Slip lines in body-centred cubic materials, NiAl and the refractory metals, are frequently very wavy because of the ease with which cross slip can occur. This may lead to difficulties in recognising and indexing the primary slip plane. To help solve this problem single crystals were cut, whenever possible, with the slip direction diverging from one face by about 5°. Had the slip vector been parallel to the surface no step would have been formed on deformation, thus slip lines would not have been seen on this face. If any slip band is considered to be the result of many dislocation loops reaching the surface from a single source, then it may be seen that the slip traces almost parallel to the slip direction should be

straight, because they are due to the movement of dislocations of predominantly edge character, which are unable to cross-slip. Similarly traces on the orthogonal faces could be wavy because they are largely due to the motion of screw dislocations, which can cross-slip freely. These two types of face will be referred to as "edge" and "screw" faces respectively.

The appearance of slip markings varied considerably with deformation conditions, from coarse slip bands visible to the unaided eye to fine traces on edge faces that could only be detected with special microscopic techniques. The simple metallurgical microscope is not the ideal tool for detecting fine slip lines on a highly polished surface because of the small differences in reflected intensity across the slip steps. Therefore special techniques were used to emphasise such markings, these include oblique and dark field illumination, and phase and interference contrast methods. The latter technique, using the Nomarski principle, proved particularly useful as it revealed small differences in level as a difference in colour.

Slip lines were indexed by measuring the angles between the slip traces and a reference line (on the specimen holder and parallel to the compression faces) with a goniometer eye piece in the microscope. Crystallographic orientations were measured by a standard Laue back reflection method, aligning the specimen and film with the same reference mark to aid comparison. The slip planes were then determined by a method similar to that of Chen and Maddin (1951), plotting the normals to the slip traces (i.e. the locus of all possible

positions of the pole of the slip plane) on a steregraphic projection. The point of intersection of the normals from orthogonal faces is the pole of the slip plane. Occasionally slip markings from only one face could be used, thus the slip plane could not be determined unambiguously, since the poles of several possible slip planes may lie near the normal to the slip trace. However if the slip direction was assumed, the determined slip planes were usually those that would have been predicted by "two trace" observations and the Schmid law. Wavy traces were difficult to index, often a most frequently observed slip plane was all that could be determined, although under some conditions individual segments could be identified.

Further information on slip systems could be obtained from the change of specimen shape and dimension. The movements in various directions could be measured and hence the slip direction computed as the direction of greatest shear in the slip plane. This simple calculation was often complicated by multiple slip, a problem which was partially overcome by cutting specimens with "edge" and "screw" faces. No slip would be expected perpendicular to the slip direction, thus all the change in cross-sectional area, and any barrelling, should take place by increasing the distance between the "screw" faces. A particular example of change of shape is the kink formation which was sometimes observed on straining hard orientations, this was evidence for the difficulty of slip in such orientations, and hence the operation of a $\langle 100 \rangle$ slip vector.

The Schmid law, that slip will occur on the slip plane and in the

slip direction of highest resolved shear stress (Schmid and Boas, 1950) has also been used as indication of slip systems. Resolved shear stress, τ, is defined as the stress resolved on the slip plane in the slip direction by the relationship:

$$\tau = \sigma \cos\phi \cos\lambda \qquad (3.1)$$

where σ is the engineering stress (applied load per unit area)

ϕ is the angle between the straining axis and the normal to the slip plane

λ is the angle between the axis and the slip direction

The term $\cos\phi \cos\lambda$ is known as the Schmid Factor (S.F.). It follows directly from the Schmid law that slip will occur first on the system with the highest S.F. The maximum possible value of $\cos\phi \cos\lambda$ is 0.5 when $\phi = \lambda = 45^{\circ}$. It was generally found that this law was obeyed in NiAl, and that slip was observed on the plane of a particular type on which the resolved shear stress was a maximum. Some experiments on very coarse grained polycrystals showed that slip markings were most predominant in grains in which the resolved shear stress was highest, although the constraints applied by the grain boundaries were an unknown factor in these cases.

3.1.2. X-Ray Asterism.

When a single crystal is strained, the combined effects of lattice rotation and constraint at the grips can lead to bending of the atomic

planes, which may be observed experimentally as asterism - the smearing out of spots in a Laue X-ray photograph. Taylor (1928), using a transmission X-ray technique, showed that in both aluminium and tungsten the axis of this rotation lay in the slip plane and was perpendicular to the slip direction. Yamaguchi (1929) studied the asterism after deforming aluminium in tension at 500-600°C and found that the streaks could be explained by a rotation about an axis approximately in the expected direction. Chen and Maddin (1951) used the form of the asterism in deformed molybdenum single crystals to show that some slip on seemingly higher index planes could be resolved into components on two $\{110\}$ planes.

Deformed NiAl shows very distinct asterism, but attempts to correlate this with observed slip systems were often unsuccessful, unless the centre of rotation of the asterism could be clearly distinguished. Some crystals were cut in orientations that showed a distinct centre of rotation near the middle of the X-ray photograph. Two examples are shown in Fig 3.1, for a melt grown stoichiometric single crystal and a randomly oriented nickel-rich crystal (43 at % Al) grown by the strain-anneal technique. Similar results, when obtained, correlated well with the slip systems determined by other methods. If the centre of rotation lay outside the field of the photograph its exact position proved difficult to ascertain, making comparison difficult. Tilting the crystal to direct the beam in the expected direction was not possible because differences in film to specimen distance across the width of the X-ray beam gave rise to apparent asterism.

3.1.3. Lattice Rotation.

Fleischer (1953) has examined the lattice rotations occurring during compression, both theoretically and experimentally. It was found that for small height-to-width ratios, the observed lattice rotations are in agreement with those predicted and observed by Taylor (1927), i.e. the normal to the active slip plane rotates towards the compression axis. Fleischer showed that the difference between this behaviour and that observed in tension is due to a difference in the definition of the stress axis. If rotations were measured from an axis parallel to the side, rather than perpendicular to the compression face of the specimen, the lattice rotations were the reverse of those observed in tension, i.e. rotation of the slip direction away from the reference axis. It was also found that lattice rotations at the centre of long specimens, referred to an axis perpendicular to the compression surface, were the reverse of those observed in tension, whilst those near the ends of such specimens were of the type observed by Taylor.

Since short specimens (height-to-width ratio 2.6:1) were used in this investigation it was expected that the rotation of the compression axis would have been towards the active slip plane, thus giving a further method of identifying the slip plane. The lattice rotation was measured by determining the crystallographic orientation with a standard Laue back reflection technique after various increments of strain. The deformed specimens were held by their compression faces in a small vice mounted on the X-ray specimen holder to aid reproducibility.

This technique did not prove very useful for the determination of the slip planes in NiAl for the following reasons:

i) Most melt grown single crystals were cut in symmetrical orientations, and did not deform by single slip. This was particularly true in hard orientations where four or more similar slip planes were equally stressed.

ii) Asterism and inhomogeneous deformation made accurate determinations of the orientation difficult, orientations could be determined reproducibly to within 2° in undeformed material.

iii) The low ductility of the material meant that lattice rotations were small; the changes in orientation were often comparable with the accuracy of the technique.

Despite these difficulties lattice rotations were measured in a number of single crystals, mainly those of random orientation grown by the strain-anneal technique which deformed by single slip. It was generally found that the slip plane determined by other methods rotated towards the compression axis.

3.1.4. Prismatic Punching.

Rachinger and Cottrell (1956 A) in their study of compounds with the CsCl structure utilised the prismatic punching method of Smakula and Klein (1951) to determine the slip systems; NiAl was not included in the survey. They used a conical indenter to make an impression in a thin slice of single crystal (typically 1 mm thick), a pyramidal bump

was observed on the opposite surface when a ⟨100⟩ slip direction was operative.

The indenter causes displacement of material which may move as a prismatic block if this prism is bounded by slip planes lying in a zone of which the slip direction is the axis. Under these conditions a pyramidal bump, or bumps if more than one slip direction is favourably oriented, can be formed; otherwise the material is displaced in a more complex manner, as in a hardness test. It has been shown (Nabarro, 1950) that in a cubic system the requirement for the slip direction to be the axis of a zone containing more than one active slip plane is only met with a ⟨100⟩ slip direction.

Rachinger and Cottrell determined the slip direction geometrically from the direction joining the original indentation to the bump on the opposite face. They indexed the slip plane by the straight sides of the pyramidal impressions. The slip systems determined by this method were confirmed by an examination of the slip traces on single crystals deformed in tension or compression.

When the experimental method used by Rachinger and Cottrell (1956 B) was applied to NiAl the thin slices cracked because of the low ductility of the compound. To overcome this difficulty a simple clamping device (Fig 3.2) was constructed, this held the thin slice between two sheets of perspex while the indentation was made through a hole in the upper sheet. The Instron compression apparatus was used to apply the indentation load, because it was a convenient means of indenting and the load-distance relationships could be studied.

Typical impressions on a metallographically polished surface are shown in Fig 3.3 for faces cut near to {100} and {110} in a stoichiometric single crystal of NiAl. The slip direction was found to be ⟨100⟩, but the irregular outline of the impression indicated that no single type of slip plane was operative, slip occurred on several planes to accommodate the shape of the spherical indenter. Therefore this technique only confirmed the ⟨100⟩ slip direction, and gave no information as to the slip plane.

3.1.5. Etch Pits.

Dislocation etch pits have proved a useful tool in the identification of slip systems and the study of dislocation dynamics in many materials. The observation that different crystallographic faces in NiAl had different etching characteristics when etched with alcoholic ferric chloride indicated the possibility of using this etchant to reveal dislocations. Microhardness indentations were made on low index faces, {100} and {110}, on which square and rectangular etch pits respectively were formed. These were etched for long periods after various annealing treatments. No distinct pattern, of the type observed in LiF (Gilman and Johnston, 1957), was seen, but after an anneal at 100°C followed by a 2 hour etch the nebulous cross shown in Fig. 3.4 was revealed. The form of the cross was consistent with a ⟨100⟩ slip direction, but gave no indication of the slip plane. Similar markings could not be obtained on any other face.

The technique was not considered for quantitative measurements

because of the high background density of attack, the difficulty of revealing individual etch pits, and the uncertainty that the pits were due to the presence of dislocations. Although it appeared that etching was accelerated by plastic deformation, attempts to reveal slip traces on "edge" faces of deformed single crystals proved unsuccessful.

3.2. Macroscopically Observed Slip Systems in Soft Orientations.

3.2.1. Melt Grown Stoichiometric Crystals with a [111] Compression Axis.

This orientation, with polished faces cut near to $(1\bar{1}0)$ and $(\bar{1}\bar{1}2)$, was selected for slip system determinations because the resolved shear stress on the $(110)[00\bar{1}]$ system is close to the maximum possible (S.F. = 0.48).

At 77°K straight coarse slip traces were observed on all faces (Figs 3.5 and 3.6) and there was no indication of wavy slip traces. The two observed slip planes were readily indexed as (110) and (101). The operation of two slip planes was not unexpected as the resolved shear stress on each was almost identical.

Slip traces, after deformation at 295°K, were less well defined than those from the lower temperature, but were found to be due to slip on the same planes (Fig 3.7). A poorly defined centre of rotation indicated that the primary slip system was $(110)[00\bar{1}]$ and this was consistent with the appearance of the deformation markings. Lattice rotations, although towards the $[1\bar{1}0]$ pole were too small (about 3°) to be significant.

3.2.2. Compression Axis Near to [122] in Melt Grown Stoichiometric Crystals.

The [122] compression axis was investigated because observations on a non-stoichiometric single crystal of similar orientation indicated that slip could occur on higher index planes than previously observed (see 3.2.4.).

On deforming at 77°K cleavage fracture occurred after a small strain (0.7%). Despite the low ductility distinct, coarse slip traces were seen (Fig 3.8) and the slip plane identified as (110) - the $\{110\}\langle 100\rangle$ system on which the resolved shear stress was highest (S.F. = 0.47).

Room temperature deformation produced a completely different set of slip traces, again less distinct than those from the lower temperature. The primary slip system was identified as (210) $[00\bar{1}]$ using the information which is summarised on the standard stereographic projection Fig 3.9. The resolved shear stress on the (210) plane is slightly higher than on the close packed (110) plane observed at low temperature (S.F. = 0.49).

3.2.3. Melt Grown Stoichiometric Crystals with $[01\bar{1}]$ Compression Axes.

Compression along an $[01\bar{1}]$ direction was selected for a determination of the temperature dependence of slip systems and flow stress, because it is the orientation at which the resolved shear stress is a maximum (S.F. = 0.5) on the (010) $[00\bar{1}]$ slip system. Early experiments, on single crystals of random orientation, indicated that this was the predominant slip system. Furthermore specimens could be cut in this orientation with a minimum of wastage, because the melt grown crystals used were found to have $[01\bar{1}]$ growth axes. This was the orientation used by Ball and Smallman (1966) and its use aided direct comparisons between results.

Slip Systems at 77°K.

Although several crystals of this orientation were deformed in liquid nitrogen only one showed any appreciable plastic strain before cracking, and that had not been prepared for metallographic observations (see Fig 4.13). Of the prepared specimens several had regions in which slip markings could be distinguished; a typical example, Fig 3.10, shows some coarse straight slip traces on a "screw" face. Traces on "edge" faces, although less numerous, were similar to those seen at higher temperatures (cf. Fig 3.11). These traces were found to correspond to slip on (110)[001] and (101)[010], the two systems of this type on which the resolved shear stress was highest (S.F. = 0.35). There was no indication of slip on (100) planes which would have caused traces parallel to the ends of a "screw" face (cf. Fig 3.12).

Slip Systems at 201°K.

Typical slip traces obtained after deformation at a temperature of 201°K are shown in Figs 3.11 and 3.12. Traces on the (100) "edge" face were straight and parallel to the expected slip directions [001] and [010]. Individual slip traces on the "screw" faces were very difficult to resolve, although there was a general tendency for traces to be parallel to the compression faces, particularly near the middle of the specimen. Higher magnifications revealed little extra detail (Fig 3.12) because barrelling and coarse slip markings combined to make individual slip lines indistinguishable. Thus the operative slip plane

when NiAl is deformed at this temperature remains in doubt, although the surface markings and a [100] axis of asterism rotation indicated that (010)[001] and (001)[010] were the most probable systems. It should be noted that if the slip system is of the type $\{010\}\langle 001\rangle$ there is always a second system $\{001\}\langle 010\rangle$ on which the Schmid factor is identical; thus duplex slip is invariably observed under these conditions.

Slip Systems Observed at Room Temperature and Above.

Slip systems in this temperature range have been studied by Ball and Smallman (1966 B) and Wasilewski et al. (1966). The former, using electron microscopy and slip trace measurements, identified the slip system in this orientation as $(110)[00\bar{1}]$. Wasilewski et al. noted that the slip system determined from slip line measurements was orientation dependent and that a $(010)[00\bar{1}]$ system was operative in crystals with an $[0\bar{1}1]$ deformation axis. This is in agreement with the present results, slip in this orientation was on an (010) plane and in an $[00\bar{1}]$ direction at all temperatures up to 1025°K. This slip system is the predominant one, determined by favoured directions of slip traces, asterism and, where possible, lattice rotations. A close inspection of wavy traces revealed that cross-slip on numerous other planes occurred. However part of the apparent waviness was due to slip on both (010) and (001) planes, because the surface was cut a few degrees off a true $(0\bar{1}1)$ plane, and because the slip planes do not make the same angle of intersection.

Typical slip traces are shown in Figs 3.14, 3.15 and 3.17, and the evidence used to determine the slip systems is summarised in Fig 3.16. The appearance of slip traces after deformation at high temperatures was sometimes obscured by slight oxidation, but in general the slip traces became finer (i.e. of smaller slip height and more closely spaced) with increasing deformation temperature. This behaviour is commonly observed in metals and may be seen from a comparison of slip traces at 200, 295 and 550°K (Figs 3.13, 3.15 and 3.17).

3.2.4. Slip Systems in Single Crystals of Random Orientation Grown by the Strain-Anneal Technique.

Single crystals of equiatomic and nickel-rich compositions (50, 48.9 and 43 at % Al) which had been grown by the strain-anneal technique were deformed at 295 and 875°K and their slip characteristics studied. Some determinations were also made on very coarse grained (grain sizes 2-5 mm.) polycrystalline material.

The slip systems observed are shown in Fig 3.21 together with details of the techniques used in their determination. Whilst the full range of techniques could be applied to some specimens others were only suitable for single trace measurements, confidence in these results is obviously less than those studied in greater detail. These results show that the operative slip system is orientation dependent, as in melt grown crystals. Although two specimens with axes inclined at 25° to $[\bar{0}01]$ exhibited kinking insufficient crystals were available to

determine the orientation at which this deformation mechanism became important.

In the regions of a standard stereographic triangle near $[0\bar{1}1]$ and $[\bar{1}11]$ slip was observed predominantly on (010) and (110) planes respectively. Slip was often detected on secondary slip planes which proved difficult to index because of the difficulty of matching the traces of different slip planes on orthogonal faces.

In a region between the $[0\bar{1}1]$ and $[\bar{1}11]$ corners of the triangle slip occurred on planes on which the resolved shear stress was higher than on either (010) or (110). Insufficient evidence was available to decide whether the slip plane was a particular high index plane, or the plane containing an $[001]$ slip direction of highest resolved shear stress. This uncertainty arose because of difficulties of measuring the exact position of the pole of the slip plane (to better than 5^{o}) due to asterism, barrelling and the wavy nature of the slip traces.

Two single crystals, one containing 43 and the other 48.9 at % Al were particularly well oriented for all the available measuring techniques to be employed. The second crystal had an orientation near to $[0\bar{1}1]$ and showed the same behaviour as a melt grown crystal with this axis. The extremely nickel-rich specimen had an axis between $[0\bar{1}1]$ and $[\bar{1}11]$. Clear slip traces were seen (Fig 3.18) mainly on one system; there was a distinct centre of rotation (Fig 3.1) and lattice rotations after several increments of slip could be measured. This information, which is summarised in Fig 3.22, indicated the operative slip plane was either (120), (230) or a plane between these containing

the [001] slip direction. The plane of highest resolved shear stress was (130).

Slip traces in non-stoichiometric compositions were similar to those in the equiatomic composition deformed at a lower temperature. Typical slip traces for a 43 at % Al alloy deformed at 295°K (Fig 3.18) and 800°K (Fig 3.19), and for a coarse-grained polycrystalline 54 at % Al compound deformed at 800°K (Fig 3.20) are illustrated. The straightness of the slip traces may be due in part to the random orientation of the observation surfaces, as well as to the defect structures and high flow stresses of the non-stoichiometric composition. The clearer slip traces enabled slip planes in nickel-rich compositions to be indexed more easily than those in stoichiometric compounds.

3.2.5. Summary of Slip Systems Observed in Soft Orientations.

The slip systems observed at all temperatures and in all orientations are summarised in Table 3.1. The orientation dependence of the slip systems in soft orientations at 77°K and in the temperature range 300 to 1000°K is shown in Fig 3.25. At 77°K all the soft orientations studied slipped on the system (110)[001]. At higher temperatures, i.e. above 150°K for stoichiometric compounds, slip occurred on a plane of high resolved shear stress. Values of the transition temperature, if one exists, were not measured for the other compositions because of their low temperature brittleness and the lack of suitable single crystals. The slip plane at high temperatures was

normally (110) or (010) if the Schmid factors on those planes were high. In some cases an intermediate slip pl-ne, between (110) and (010) was observed but there is insufficient evidence to decide whether this plane was (120), any other plane with rational indices (e.g. (230) or (130)) or the plane, containing the slip direction, of highest resolved shear stress. Deviations from stoichiometry, at least on the nickel-rich side had no effect on the observed slip systems.

3.2.6. Grain Boundary Sliding.

An additional deformation mode, which operated at high temperatures, was grain boundary sliding. Although this was difficult to observe in the fine grained polycrystalline material used to determine the temperature dependence of the flow stress because of the small sliding distances involved, it has been seen at high temperatures in the large grained polycrystals used for determinations of slip systems. Sliding occurred in all compositions starting at about $1000^{\circ}K$, although no survey has been made to determine the temperature at which it contributes significantly to the strain at normal strain rates (i.e. near 10^{-4} sec^{-1}). It has been noted that a 54 at % Al alloy shows sliding at $1075^{\circ}K$ (Fig 3.25) but not at $850^{\circ}K$ (Fig 3.20).

Evidence for the occurrence of grain boundary sliding is a change in surface level across grain boundaries and a lateral displacement of the boundary. This displacement can be seen by a relative movement of surface markings on opposite sides of the boundary; these markings may

be made deliberately or be scratches left by incomplete polishing. Examples of grain boundary sliding in NiAl are shown in Figs 3.23 and 3.24.

3.3. Deformation of Single Crystals with [001] Compression Axes.

In other studies of the deformation processes in single crystals of NiAl the temperature dependence of slip in specimens with [001] compression axes has not been very fully considered. Wasilewski et al. (1966), working in tension, found that there was considerable anisotropy of flow stress; and that the [001] orientation was much harder than any other. It was also noted that orientations near to [123] showed a discontinuous stress-strain curve, and that the sharp drops in stress coincided with the formation of discrete bands in the specimen. These were very similar in form to the kinks seen in compression. On compressing specimens of this orientation Ball and Smallman (1966 A) observed kinking, similar in form to kinks found in cesium halides. Neither Wasilewski et al., or Ball and Smallman reported any evidence of slip.

The results described below show that slip can occur in this orientation, although the flow stresses were considerably higher than those of soft orientations in certain temperature ranges. All determinations were made on stoichiometric melt grown single crystals.

3.3.1. Low Temperature Slip Systems.

In this temperature range, which extends from below 77°K to about 250°K, distinct slip markings were observed (Figs 3.26-3.31). Slip traces were very coarse, and on the "screw" faces wavy, although a closer inspection revealed that many of the individual segments of wavy slip were quite straight (3.29 and 3.30). These short segments could

be indexed and slip was found to have occurred on $\{\bar{2}\bar{1}3\}$ planes in $\langle 111\rangle$ directions. As there are eight slip systems of this type equally stressed some of the apparent waviness may be due to slip on more than one of these systems. The fourfold symmetry of the [001] deformation axis meant that pure "edge" and "screw" faces as such could not exist on specimens of square cross-section, Fig 3.31 shows "edge" and "screw" type traces on the same face. Kinking was observed at 201°K, after initial slip, but not at 77°K.

3.3.2. Intermediate Temperatures (250 to 600°K).

The deformation modes in this temperature region were extremely complex. Kinking was important although it was usually associated with slip, and under some conditions an apparent shear transformation was observed. The slip systems, and the problems involved in determining them, were very similar to those in the higher temperature region, and will be considered with these.

Kinking was similar to that observed in NiAl by Ball and Smallman (1966 A), and in CsBr by Johnson and Pask (1964). A coarse kink (Fig 3.32) formed simultaneously with a sharp drop in measured load, and was sometimes accompanied by a clearly audible click. This behaviour was shown to be due to kinking, and not any of the other observed deformation phenomena, by unloading immediately after a load drop and studying the surface, both optically and with X-rays. The sharp load drop and clicks were very similar to those noted when a b.c.c. metal twins; there was however no similarity between the

crystallography of the kinks and that of twinning. It may be seen from the kinks shown in Figs 3.27, 3.32, 3.33 and 3.35 that there is no consistent geometry of kinking. All the photographs are of {110} surfaces. Laue X-ray photographs of the kinked region revealed nothing of its structure because of high local deformation.

Two experimental observations were in agreement with the explanation of the structures of kinks given by Hess and Barnett (1949). In all kinked specimens seen the relative movement of material on either side of the band was in a ⟨110⟩ direction. This is consistent with a model of kinks being due to a concentration of $\frac{a}{2}\langle 001\rangle$ primary dislocations on {110} planes.

There appeared to be no critical stress for the formation of kinks as they were noted at very different stresses under apparently identical conditions. However kinking was found to occur in preference to slip at temperatures where the flow stress in hard orientations was considerably higher than in soft ones. (Fig 3.34). In the temperature range 350 to 500°K, where ratio of flow stresses was greater than 5.5:1, kinking was the prime mode of deformation and occurred before slip. There was a transition region, in which slip usually preceeded kinking, at temperatures just outside this range (flow stress ratio greater than 4.5:1). At lower values of the ratio, that is above 600 or below 250°K, the importance of kinking gradually decreased, occurring, if at all, at high strains, until at 77°K or above 725°K (ratio 2-3 : 1) it was not observed. This indicates that the stress required to cause kinking is related to the flow stress on

the primary system, and that kinking is due to the movement of primary (i.e. $\underline{a}\langle 100\rangle$) dislocations. This model also indicates that the kinking stress should be orientation dependent, reaching a maximum when compressed in the $[001]$ direction. This would explain why some single crystals with axes more than 20° from $[001]$ exhibited kinking at comparatively small stresses. (see 3.2.4.).

The other deformation process, illusteated in Fig 3.33, was observed between 250 and $450^{\circ}K$. The bands are local surface corrugations and not apparently due to slip, the peaks corresponded to $\{111\}$ planes which has not been observed as a slip plane under any other conditions. Furthermore the bands do not look like slip traces and there was a definite change of surface inclination across them. The behaviour was invariably associated with kinking so it was impossible to study its effects on the stress-strain curve.

The surface markings look very similar to either twins or a martensite. An X-ray examination revealed that the $\{111\}$ plane was not distorted, but spots on either side of this plane showed asterism. Cahn and Coll (1961) have shown that twinning in a CsCl lattice is difficult without disordering, and a martensite transformation has been observed in NiAl of greater nickel content. Therefore the most likely explanation is that the surface markings are due to stress induced martensite, as elastic stresses are known to raise the Ms temperature of martensitic transformations well above the normal values. However Cahn and Coll pointed out that the twinning process, if it did occur, could be more accurately described as a martensitic transformation, so

the dividing line between the two possible processes is very fine.

There are several inconsistencies in this explanation. No martensitic transformation was observed on cooling to 77°K, and similar markings were not seen after deformation at lower temperatures, thus it is possible that the process is one which requires thermal activation. Also no markings were seen after polishing off the surface corrugations and etching the new surface, and X-ray spots from this new surface were not distorted, although it is possible that an extremely unstable structure had reverted to its original form on polishing.

3.3.3. Slip Systems Observed Above 250°K.

The high symmetry of the $[001]$ axis means that several slip systems of the same type have the same Schmid factor. Added to this several different types of slip system have been observed, so that the total number of possible slip systems in this orientation are as follows:

8 x $\{\bar{2}\bar{1}3\}\langle 111\rangle$ (S.F. = 0.46)

4 x $\{\bar{1}\bar{1}2\}\langle 111\rangle$ (S.F. = 0.47)

8 x $\{0\bar{1}1\}\langle 111\rangle$ (S.F. = 0.41)

4 x $\{0\bar{1}1\}\langle 011\rangle$ (S.F. = 0.5)

In addition a misorientation of the axis of only 4° would allow the applied stress to exceed the critical resolved shear stress for slip on $\{100\}\langle 100\rangle$ and $\{110\}\langle 100\rangle$ systems, at the highest ratio of flow stresses on hard and soft systems. Although the initial axes were all within 2° of $[001]$ the addition misorientation could have been caused by kinking.

Thus it can be seen that indexing slip traces in these orientations could be very difficult. This was particularly so if slip took place on several systems and traces on orthogonal faces could not be matched. In general two preferred slip systems were noted, either $\{112\}\langle 111\rangle$ or $\{110\}\langle 110\rangle$, although the behaviour was seldom simple. For example one specimen showed faint but distinct slip on a $\{110\}\langle 110\rangle$ system and a $[100]$ centre of rotation; after further straining under identical conditions, in an attempt to emphasise these markings, slip traces corresponding to a $\{112\}\langle 111\rangle$ system and a $[110]$ centre of rotation were seen.

In kinked specimens slip traces were coarse and paralled to the end of one face (Fig 3.35 and 3.36). These could have been due to slip on $\{112\}$, $\{110\}$ or $\{100\}$ planes or the formation of small kinks, although slip traces on two orthogonal faces permitted the identification of the slip system as $\{112\}\langle 111\rangle$ for these two examples. On increasing the temperature the slip traces became finer and more difficult to distinguish. (Figs 3.37 and 3.38). The slip system was generally identified as $\{112\}\langle 111\rangle$; the information used to determine this system is summarised in Fig 3.39 for a series of specimens. However some slip traces and other deformation effects were observed which could have only been due to slip on $\{110\}\langle 110\rangle$ systems. These were often associated with a rounded yield point on the stress strain curve as shown in Fig 4.16 ($716^{\circ}K$). There was no obvious systematic variation of slip system with temperature, it appeared that slip could occur equally easily on $\langle 111\rangle$ or $\langle 110\rangle$ systems at temperatures above $300^{\circ}K$.

Table 3.1 Observed Slip Systems (cf. Fig 3.34 for Conditions for Kinking).

Temperature Range ^{o}K	Soft Orientations (Slip Planes)				Hard Orientations
Compression Axes	[111]	[122]	[011]	Random	[001]
77	(110)	(110)	(110)	(110)	$(\bar{2}\bar{1}3)$ [111]
77-150	?	?	(110)	Plane of	$(\bar{2}\bar{1}3)$ [111]
150-300	(110)	(210)	(010)	High	?
250-600	?	?	(010)	Resolved	$(\bar{1}\bar{1}2)$ [111] $(0\bar{1}1)$ [011]
Above 600	?	?	(010)	Shear Stress	$(\bar{1}\bar{1}2)$ [111] $(0\bar{1}1)$ [011]

Slip Directions for Soft Orientations [001]

3.4. Discussion of Observed Slip Systems.

3.4.1. Comparison of Slip Systems in Hard and Soft Orientations with the Theory of Ball and Smallman.

The operation of a ⟨100⟩ primary slip direction is now well established (Wasilewski et al. 1966, Ball and Smallman, 1966) but slip in orientations where the primary system is constrained has not been previously reported. In a study of the low temperature deformation of AgMg Mukherjee and Dorn (1964) observed that the slip plane was {123} and occasionally {112}, but never {110}; the slip direction was ⟨111⟩. Thus the slip systems of NiAl in hard orientations are similar to those of AgMg. The preference for {123} and {112} slip planes could explain the observations of Mohanty and Wert (1963), and Mohanty (1966), that faulting was not detected on {110} planes in NiAl, but was significant on {112}.

If the arguments of Ball and Smallman (1966 B) are extended to cover the slip systems observed in hard orientations, a problem arises in determining the value of the anisotropic elasticity factor $\underline{K}$ (eqn. 1.10) for edge dislocations on {123} planes, because no analytical solution exists for this condition. Since $\underline{K}$, for screw dislocations, is independent of slip plane, the values for {123} and {112} planes are the same as for {110}. $\underline{K}$ for edge dislocations on {112} planes may be estimated from the equations of Foreman (1955). The energies and mobilities of the $\underline{a}$ ⟨111⟩ unit dislocation on these planes may be calculated from equations 1.10 and 1.11, using the elastic

constants of NiAl measured by Wasilewski (1966). There parameters are listed in Table 3.2 together with values from Ball and Smallman for comparison.

Table 3.2 Mobilities and Energies for Unit Dislocations in NiAl.

b.	Plane	Edge or Screw	K x 10^{-12} dynes cm^{-2}	Energy x 10^{4} erg cm^{-1}	$\frac{d}{b}$	C x 10^{-12} dynes cm^{-2}	$\frac{\zeta}{b}$	Mobility S
001	110	S	1.12	9.3	$1/\sqrt{2}$	1.12	0.356	0.46
		E	1.06	8.8	$1/\sqrt{2}$	1.12	0.355	0.51
001	010	S	1.12	9.3	$1/2$	1.12	0.25	0.67
		E	0.92	7.7	$1/2$	1.12	0.207	0.71
011	$0\bar{1}1$	S	0.62	10.3	$1/2$	0.336	0.463	0.32
		E	0.92	15.3	$1/2$	0.336	0.685	0.06
111	$0\bar{1}1$	S	0.56	13.9	$1/\sqrt{6}$	0.598	0.187	0.98
		E	1.17	29.3	$1/\sqrt{6}$	0.598	0.4	0.42
111	$\bar{1}\bar{1}2$	S	0.56	13.9	$1/3\sqrt{2}$	0.598	0.22	0.69
		E	1.11	27.7	$1/3\sqrt{2}$	0.598	0.11	0.70
111	$\bar{1}23$	S	0.56	13.9	$1/14\sqrt{3}$	0.598	0.115	0.70

A difficulty in applying equation 1.10 is in assigning suitable values to the cut-off radii R and r_o. For the purposes of comparison all energies listed in Table 3.2 have been calculated assuming $\frac{1}{4\pi} \ln \left(\frac{R}{r_o}\right)$ is equal to unity. When extending this treatment to superdislocation arrays the problem cannot be avoided so easily, because $\underline{E}_{APB}$ (Eqn. 1.6) is independent of $\underline{R}$ and $\underline{r}_o$, and $\underline{E}_{int}$ (eqn 1.4) has no $\underline{r}_o$ term. The inner cut-off radius is that of the dislocation core in which classical elasticity theory does not hold, and is conventionally taken as being of the same order as the Burgers vector, $\underline{b}$. A value of $\underline{R}$ may be estimated from the dislocation density, $\underline{\rho}$, but as this is seldom uniform and varies with strain, comparison is difficult. Furthermore the significance of $\underline{R}$ for the imperfect dislocations in a superdislocation is open to question because the distance to the next dislocation varies around the dislocation line (from the distance between the imperfect dislocations, $\underline{w}$ to $1/\underline{\rho}$).

The importance of the $\underline{E}_{APB}$ term to the total energy should depend on $\underline{R}$ and $\underline{r}_o$ because a change in these radii would affect $\underline{E}_1$, $\underline{E}_2$ and $\underline{E}_{int}$ but not $\underline{E}_{APB}$. As a result the increase in the dislocation density during deformation should reduce the energy of a unit dislocation more rapidly than a superdislocation, (providing that the applied stress does not constrict the ribbon of APB).

The energies of various unit dislocation and superdislocation configurations that might be expected in NiAl are listed in Table 3.3. $\underline{R}$ was taken as 2.5×10^{-5} cm which corresponds to a uniform dislocation density of 1.6×10^{9} cm^{-2}, which is typical of the densities observed

by Ball (1964) at small strains; $\underline{r}_o$ was assumed to be equal to $\underline{b}$ (2.5×10^{-8} cm). The width of the stacking fault ribbon, required in the calculation of $\underline{E}_{int}$, may be determined from eqn 1.8. It should be orientation dependent because of variations in the geometrical factor $\underline{\alpha}$, but the differences are smaller than those due to many of the other assumptions (e.g. $\underline{R}$ and $\underline{r}_o$) and will be neglected. Values of $\underline{w}$ were taken as 2.5×10^{-7} cm for screw and 5×10^{-7} cm for edge dislocations in drawing up Table 3.3. It was not necessary to know $\underline{w}$ to calculate $\underline{E}_{APB}$. The force tending to constrict the APB ribbon is equal to the surface energy of the boundary (i.e. $\frac{E_{APB}}{w}$); at equilibrium this is just balanced by the force due to the interactions between the dislocations. Therefore using the notation of 1.3:

$$\frac{E_{APB}}{w} = \frac{K\, b_1\, b_2}{2\pi\, w} \qquad (3.2)$$

Table 3.3. Energies of Dislocation Arrays in NiAl.

b	Plane	Edge or Screw	A.P.B width w x 10^7 cm	$E_1 = E_2$ x 10^4 erg cm^{-1}	E_{APB} x 10^4 erg cm^{-1}	E_{int} x 10^4 erg cm^{-1}	Energy x 10^4 erg cm^{-1}
001	110	S	unit				5.1
		E	unit				4.9
001	010	S	unit				5.1
		E	unit				4.2
011	$0\bar{1}1$	S	unit				5.7
		E	unit				8.4
111	$0\bar{1}1$	S	2.5	1.9	0.56	2.0	6.4
		E	5.2	4.0	1.2	3.4	12.6
111	$\bar{1}\bar{1}2$	S	2.9	1.9	0.56	2.0	6.4
		E	5.7	3.8	1.1	3.2	11.9
111	$\bar{1}\bar{2}3$	S	2.8	1.9	0.56	2.0	6.4

$\underline{R} = 2.5 \times 10^{-5}$ cm

$\underline{r}_o = \underline{b} = 2.5 \times 10^{-8}$ cm.

The energies in Table 3.3 are in agreement with the conclusions of Ball and Smallman that the a ⟨100⟩ dislocation has the lowest energy and should therefore be most stable. The conclusions with regard to the hard orientations are not so clear cut, the lowest energy dislocations are:

1) an a ⟨110⟩ screw dislocation
2) an a ⟨111⟩ screw superdislocation
3) an a ⟨110⟩ edge dislocation in a {110} plane.

Therefore from energy considerations there should be little to choose between ⟨110⟩ and ⟨111⟩ slip directions, this is in agreement with the experimental observations at temperatures above 300°K. The small difference in energy (5.7×10^{-4} against 6.4×10^{-4} erg cm^{-1}) could easily be reversed by a modification of the assumptions. For example a change in R on straining could explain the observed change from a {110} ⟨110⟩ slip system to {112} ⟨111⟩ on re-testing under identical conditions, but as there are so many other variables involved such an explanation would be pure surmise. Since mobilities of the superdislocations could not be calculated a comparison with those of a ⟨110⟩ unit dislocations is not possible.

One phenomenon which cannot be explained by Table 3.3 is the {123} low temperature slip plane, and the tendency for high temperature slip to be restricted to {123} and {112}, to the exclusion of {110} ⟨111⟩ slip. The energies of dislocations on all three planes are similar; as are the mobilities, if the assumption is made that the mobility of a superdislocation is proportional to that of a unit dislocation.

However the stacking fault width of an edge superdislocation is greater than a screw, and this would be expected to affect the mobility. An explanation of the $\{123\}$ plane could possibly be found if mobilities for all conditions were known. The $\{112\}$ may be predominant at higher temperatures because it is the slip plane on which the resolved shear stress is highest; it is also the observed slip plane in b.c.c. metals with $\langle 100 \rangle$ axes.

3.4.2. Comparison with Body-Centred Cubic Metals.

There is a marked similarity between the mechanical properties of NiAl and the pure b.c.c. metals. This may be seen in the temperature and orientation dependence of the slip systems, the appearance of slip traces, and the stress-temperature relationships. The main difference is that the primary slip direction in NiAl is $\langle 100 \rangle$, not $\langle 111 \rangle$, so the deformation of hard orientations, where slip on the primary system is constrained, has to be considered.

In the b.c.c. metals at low temperatures slip is restricted to $\{110\}$ planes, under specific but uncertain conditions, slip traces are normally very straight. At higher temperatures cross-slip becomes significant and the slip plane can be any which contains a $\langle 111 \rangle$ direction, (i.e. $\{110\}$ $\{112\}$ $\{123\}$). At still higher temperatures slip is not always observed on a low index plane, and has been noted on non-crystallographic planes in a $\langle 111 \rangle$ zone on which the resolved shear stress is highest (Foxall and Duesbury, 1965). Slip in NiAl soft orientations is very similar, slip traces at low temperatures are

straight on {110} close-packed planes. At higher temperatures the observed slip plane is any one, containing a ⟨100⟩ slip direction, on which the resolved shear stress is high. There is a comparable change in hard orientations from {123} to a plane of higher resolved shear stress, {112}. Slip traces in both b.c.c. metals and NiAl are straight when parallel to the slip direction, and very wavy perpendicular to that direction.

One problem in common with b.c.c. metals is the significance of the observed slip plane. It is not certain whether atomic movements occur on this plane, or on short sections of most closely-packed planes, which appears as macroscopic slip on planes other than {110}. This idea, known as "pencil glide" because of the analogy of sliding rows of hexagonal pencils over each other, was first proposed by Taylor and Elam (1926) to explain the slip markings of α-iron. There has been considerable discussion as to whether b.c.c. metals deform by pencil glide, and most of these arguments may be extended to NiAl.

Chen and Maddin (1951) studied the fine structure of X-ray asterism and concluded that slip on {112} planes in molybdenum could be resolved into slip on two {110} planes. No such substructure has been observed in NiAl, e.g. in Fig 3.1 one photograph is of a specimen which slipped on a {320} plane. Any substructure could usually be attributed to multiple slip.

The electron microscope observations of Ball (1964), in which the slip plane was identified as {110} from the geometry of dislocation concentrations and by following the movement of dislocations, indicated

that slip on the atomic scale was on planes of the closest packing. However it is difficult to determine definitely the plane in which a group of dislocations was slipping before the specimen was thinned for observation; and the stressing system causing dislocation motion in a thin foil may be very different from that applied to the bulk specimen. Moreover cross-slip on planes such as $\{310\}$ was observed, indicating that atomic movements on planes other than $\{110\}$ are possible.

Mitchell and Spitzig (1965) have studied wavy slip traces in tantalum by carbon replica techniques, and found that there was no indication of traces separating into discreet slip on $\{110\}$ planes at magnifications of up to x 20,000.

There are two arguments against the occurrence of pencil glide. If this type of mechanism is operative, why are planes other than those of highest resolved shear stress ever observed? Secondly there would be no reduction in energy by adopting this configuration, and the energies (and mobilities) of dislocations on cube planes are not very different from those on $\{110\}$ planes (Table 3.2). The effective area of the slip plane would be approximately the same as for slip on $\{110\}$ planes, and the effective Schmid factor would be unchanged. Flow stress of single crystals (Chapter 4) are largely quoted as compressive stresses, rather than resolved shear stresses, because of the uncertainty of the Schmid factor. This problem also arises with b.c.c. metals and Noble and Hull (1965) have shown that although slip traces corresponding to higher index planes are observed the critical resolved shear stress for slip is constant if the Schmid factor for $\{110\}$ is used.

3.4.3. Availability of Independent Slip Systems.

Copley (1963) and Ball and Smallman (1966 B) have discussed the independent slip systems available with a ⟨100⟩ slip direction in the CsCl lattice. They showed that there are only three independent slip systems available. This number is insufficient for ductility in a polycrystal since Von Mises (1928) suggested that five are required to accommodate a general strain. Groves and Kelly (1963) showed that two independent slip sytems are available with a {110} ⟨110⟩ slip system (as observed in NaCl), and that five are available in b.c.c. metals, with a ⟨111⟩ slip direction.

There should be sufficient slip systems to accommodate a general strain in polycrystalline NiAl, because additional slip systems can operate in the highly stressed region near the grain boundary. The reasons for the low temperature brittleness should therefore be sought elsewhere. It may be seen that there are sufficient slip systems from a comparison of the stress-strain curves of polycrystalline NiAl (Fig 4.10) with those of NaCl, in which there is known to be insufficient slip systems. These curves show very rapid initial hardening and fracture after small strains (1-2%) (Stokes, 1965).

It should be noted that although sufficient slip systems are available at high stresses only three are available at low stresses, and high flow stresses are known to favour brittle behaviour (see 1.5.).

3.5. Atomic Mechanisms of Fracture.

The two atomic mechanisms of fracture described below have been observed in single crystals and coarse grained polycrystals. The importance of these mechanisms, and their relevance to overall ductility will be considered in Chapter 5, together with low temperature intergranular fracture.

3.5.1. Cleavage.

The common form of failure in single crystals was by cleavage on $\{110\}$ planes. As most melt grown crystals were cut with one $\{110\}$ face the fracture was normally seen as a vertical crack parallel to this face, as in Figs 3.8, 3.11 and 3.16; typical cleavage faces are shown in Fig 3.40. Since the fracture surface often bisects two slip planes, it would be possible to explain its crystallography by the coalesence of dislocations on intersecting slip planes to form a microcrack, which propagates along $\{110\}$ planes (Cottrell, 1958). However fine grained polycrystals often fail by vertical intergranular cracking, so the significance of such cracks in single crystals is questionable. An alternative site for the nucleation of cracks, at a kink, is shown in Fig 3.41.

The cleavage plane differs from the $\{100\}$ normally observed in b.c.c. metals (Gilman, 1959). Cleavage on $\{110\}$ planes involves breaking fewer Ni-Al bonds per unit area, so this may be a further indication of the high ordering energy of NiAl. Cleavage in AgMg has been observed on $\{112\}$ planes (Wood and Westbrook, 1961) and cracks on

bending on {100} planes (Kurfman, 1965).

The overall stresses required to cause cleavage were quite small, and a gentle tap could cause fracture. Cleavage was sometimes noted on machining single crystals, particularly when cutting {110} planes. Unlike ionic crystals the cleaved surfaces were never very smooth, and always showed considerable substructure, they were therefore unsuitable for surface studies.

3.5.2. Triple Point Cracking.

When grain boundary sliding occurred at comparatively low temperatures, in the range 0.5 to 0.6 Tm (where Tm is the melting temperature) cracks opened at grain boundary triple points due to the relative movement of grains. These could propagate and lead to failure. This mechanism is thought to be the cause of the anomalously low ductility of the 54 at % Al alloy near 935°K. At higher temperatures diffusion processes and slip cause grain boundary migration, thus preventing cracks from nucleating (Nield and Quarrell, 1957).

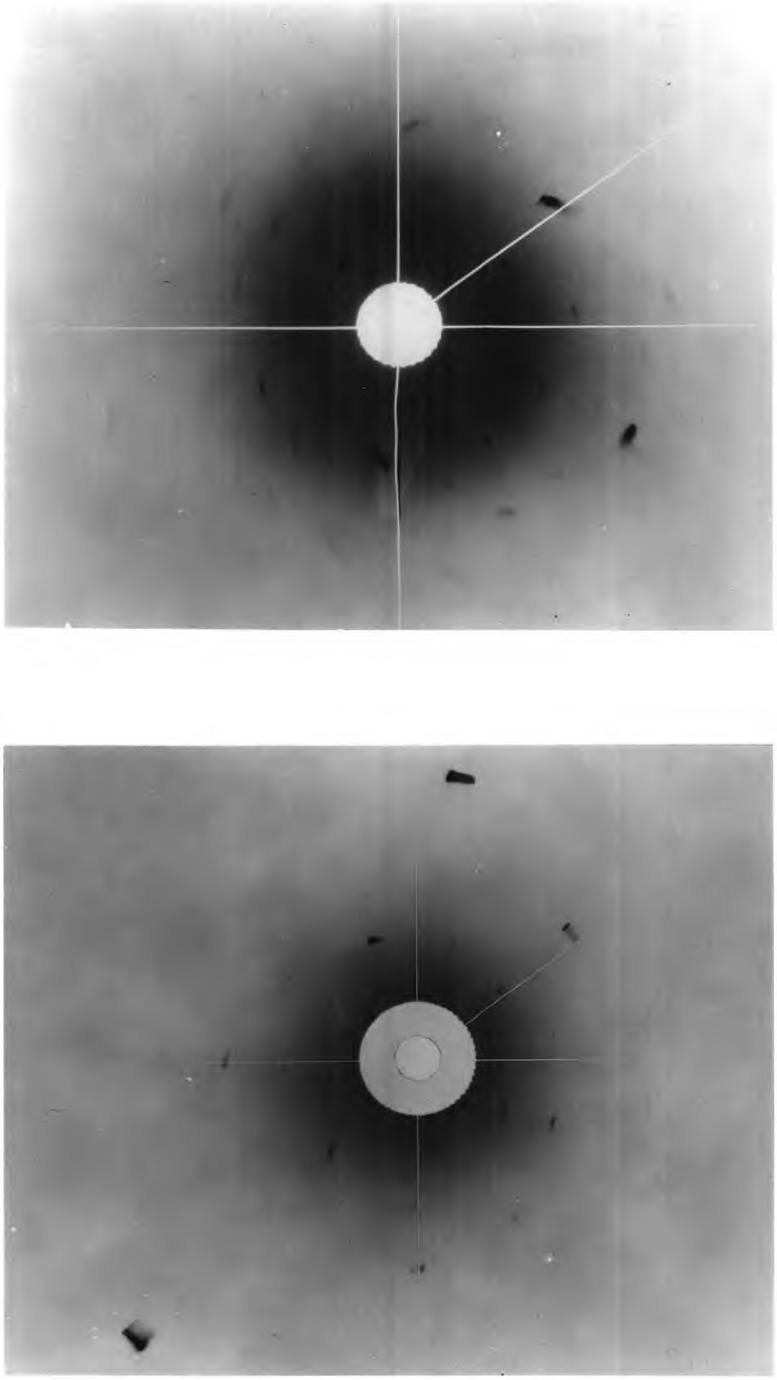

Fig. 3.1 Typical Centres of Rotation of X-Ray Asterism. A: Melt grown 48.9 at.% Al, deformed at 550°K, (100) face [011] axis vertical. B: Strain-anneal grown, 43 at.% Al, deformed 295°K, (101) face.

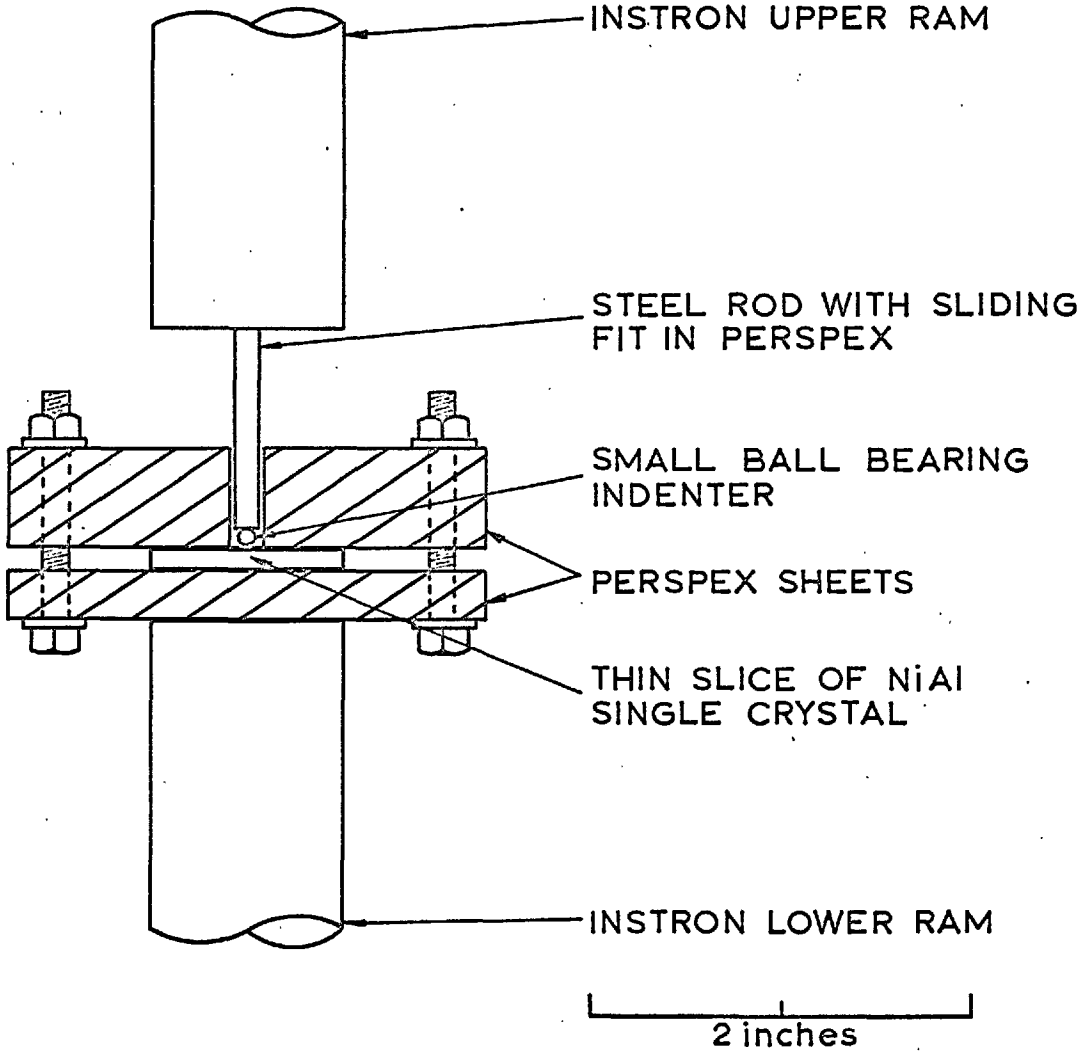

Fig 3.2 Prismatic Punching Jig.

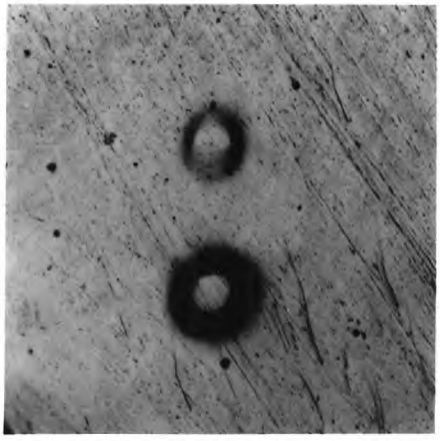

A

B

Fig. 3.3 Prismatic Punching Impressions. A: (110) face. B: (100) face. (x 50).

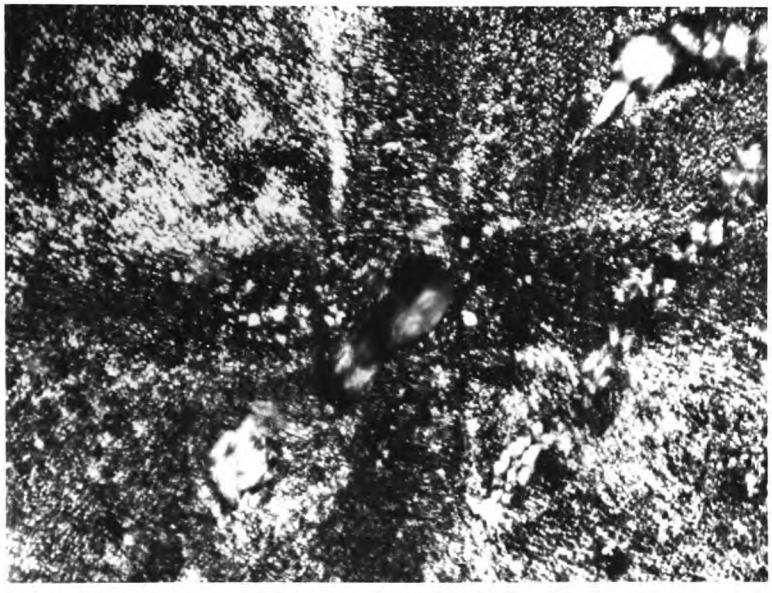

Fig. 3.4 Markings around a microhardness indentation etched in alcoholic ferric chloride. (x 195).

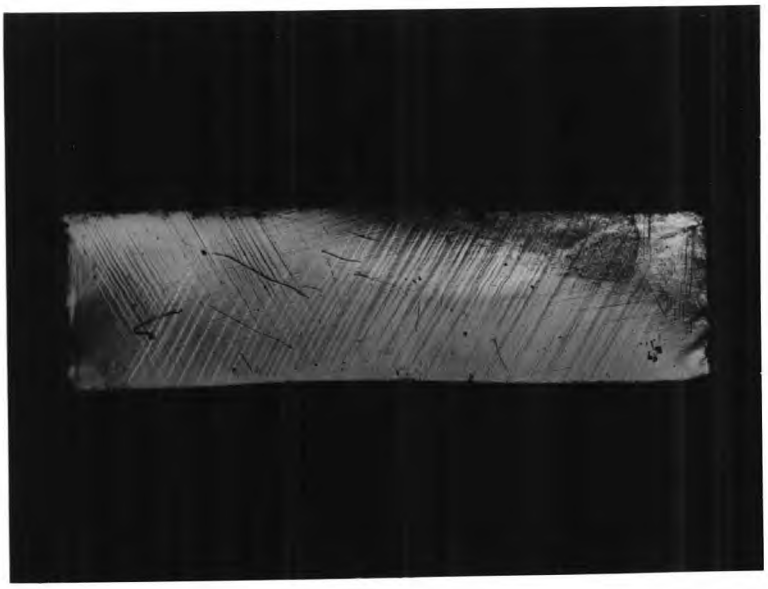

Fig. 3.5 Slip Traces at 77°K (x 11).

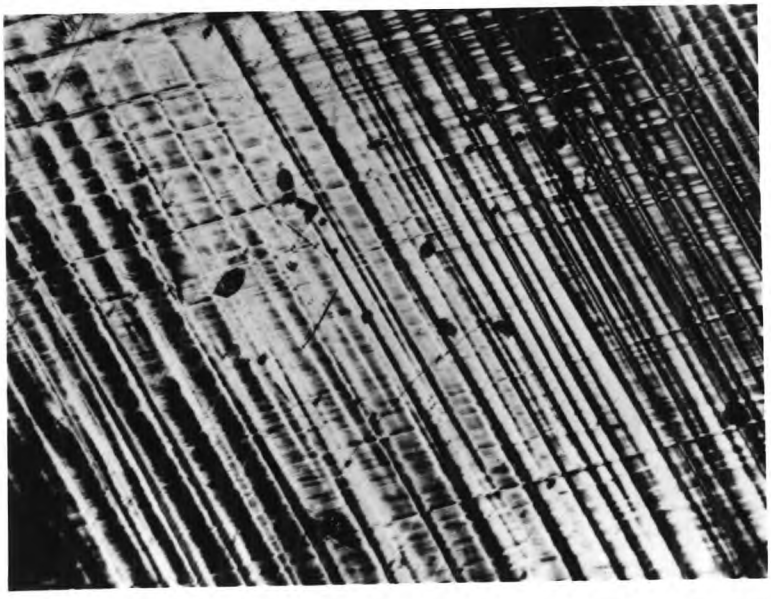

Fig. 3.6 Slip Traces at 77°K (x 75).

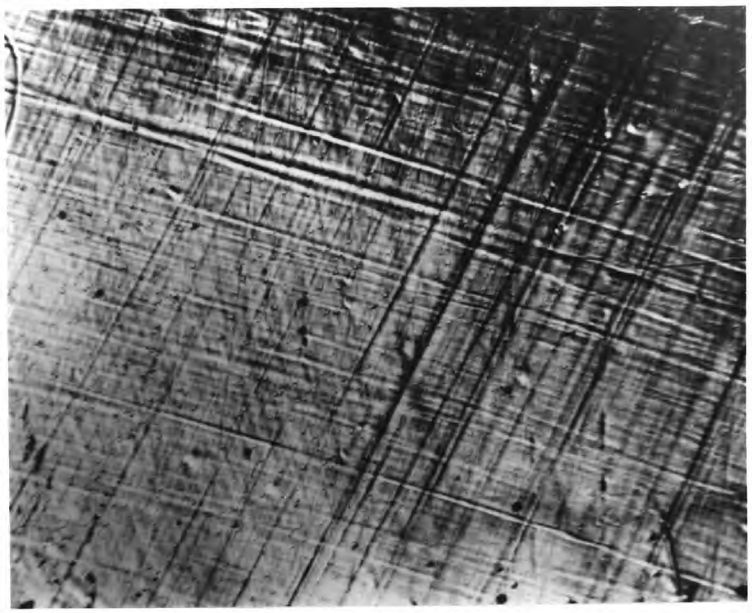

Fig. 3.7 Slip Traces at 295°K (x 75).

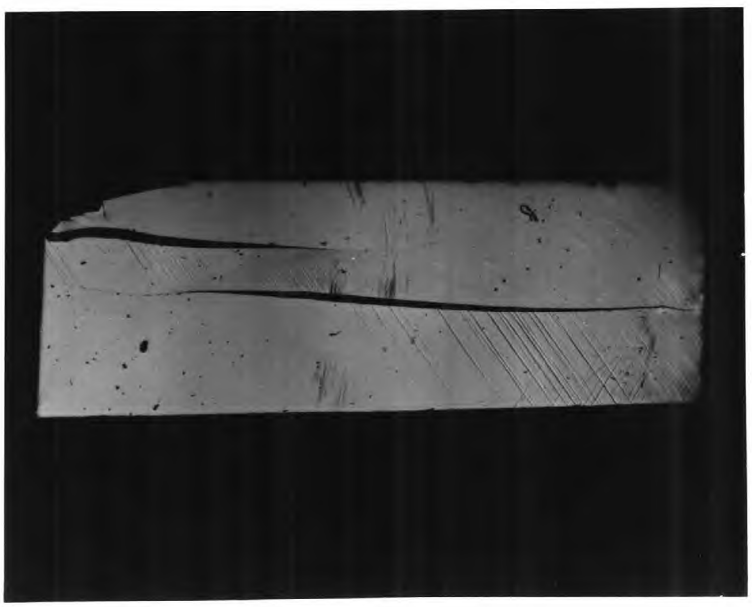

Fig. 3.8 Coarse Slip Traces at 77°K (x 11).

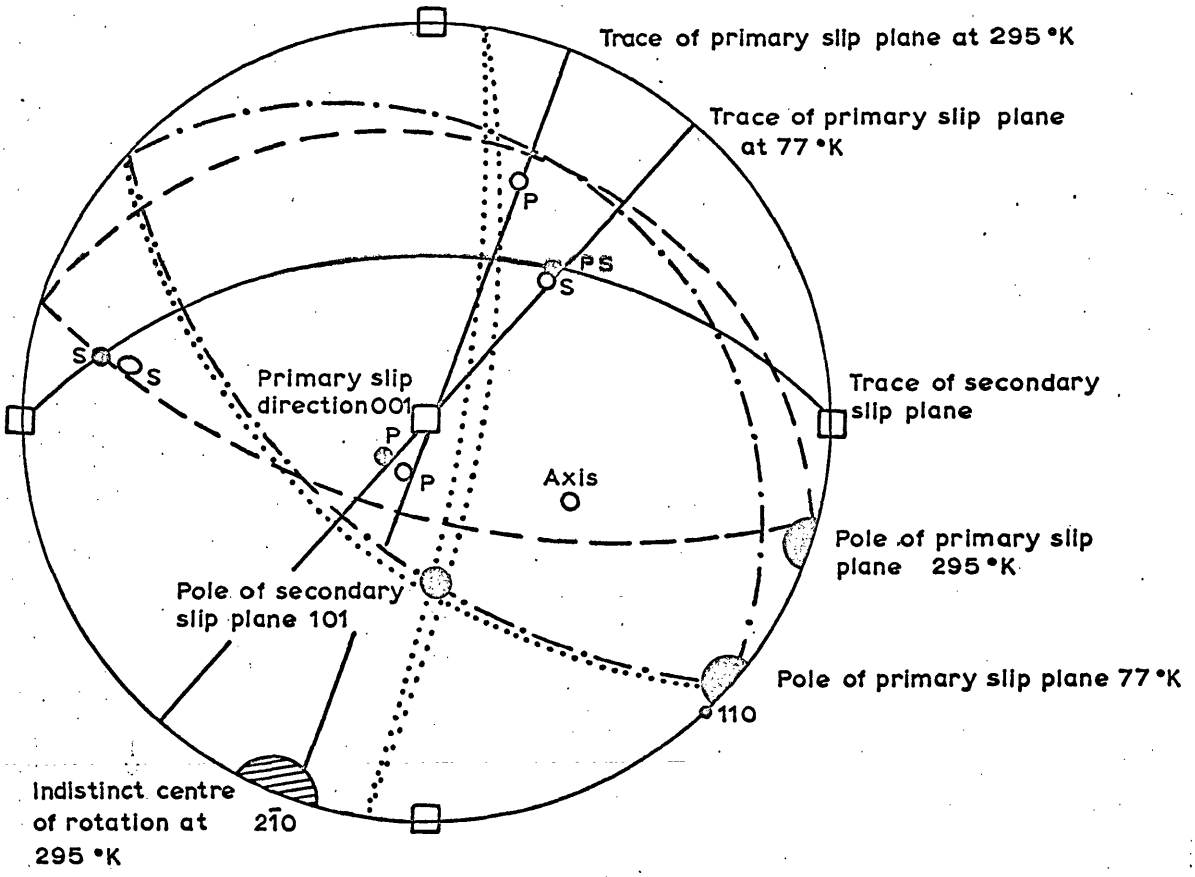

⊙ Slip traces at 77 °K

O Slip traces at 295 °K

P Primary slip traces

S Secondary slip traces

– – – Normal to primary slip trace 295 °K

–·–· Normal to primary slip trace 77 °K

····· Normal to secondary slip traces

Fig 3.9 Summary of Slip Systems Observations at 77° and 295°K for a Compression Axis Near 122 .

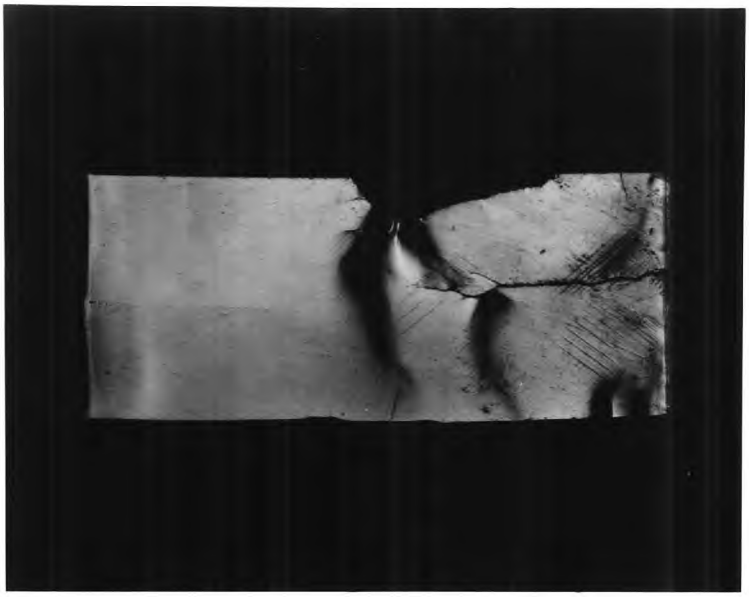

Fig. 3.10 Slip Traces and Cracking after Deformation at 77°K (x 11).

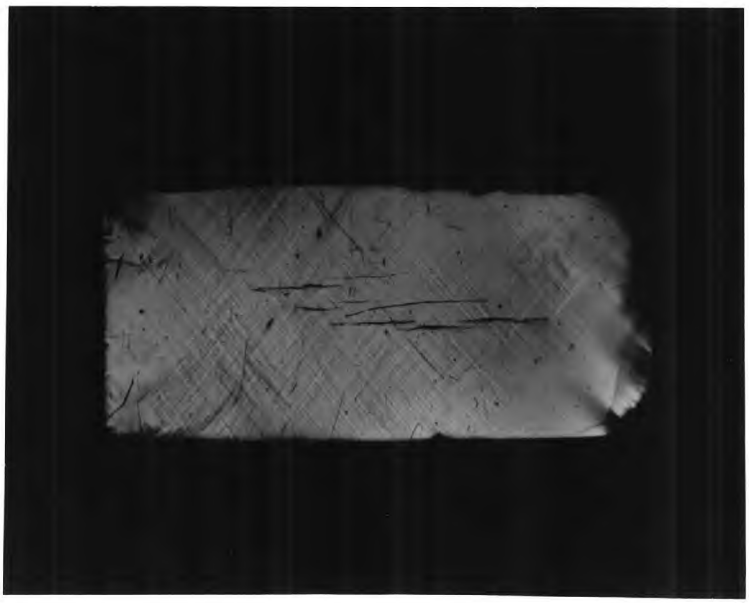

Fig. 3.11 Markings on an "Edge" Face after Deformation at 195°K (x 11).

Fig. 3.12 Markings on a "Screw" Face after Deformation at 195°K (x 11).

Fig. 3.13 Coarse Slip Markings on a "Screw" Face after Deformation at 195°K (x 75).

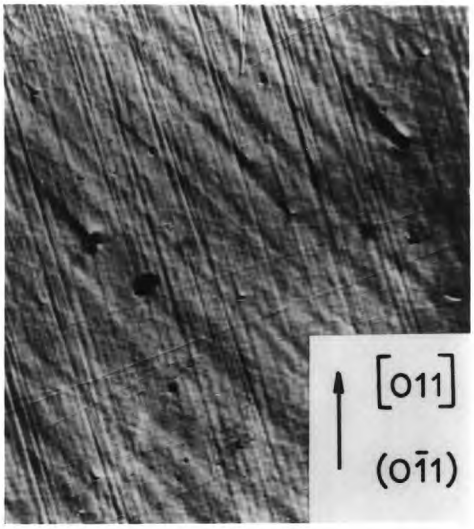

Fig. 3.14 Slip Traces at 295°K on an 'Edge' Face (x 150 Interference Contrast)

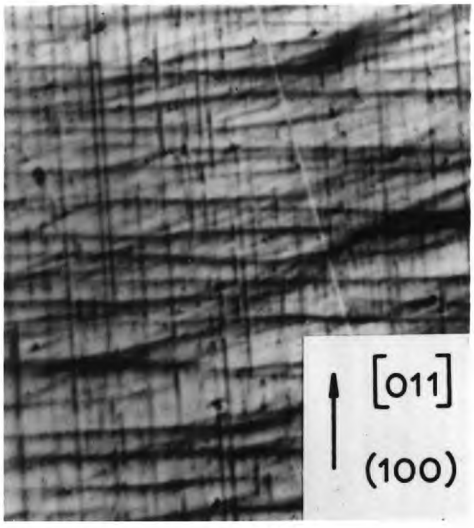

Fig. 3.15 Slip Traces at 295°K on a 'Screw' Face (x 150)

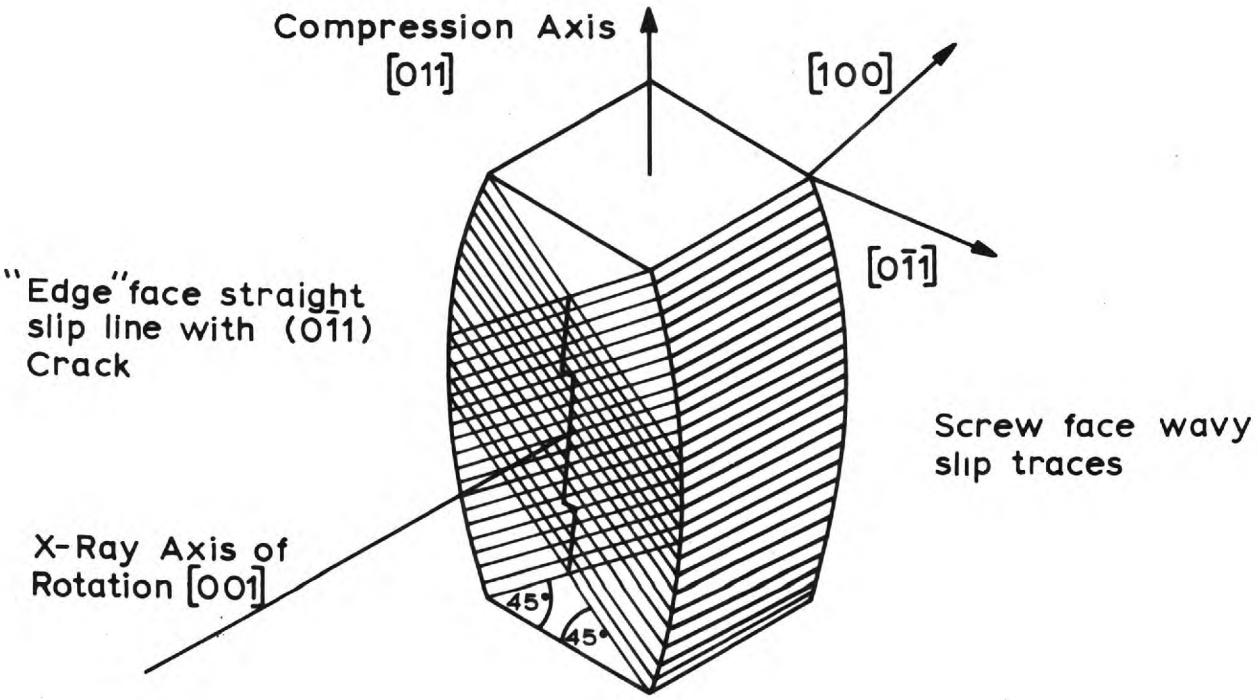

Fig. 3.16 Deformation Behaviour of a Specimen with an [011] Axis

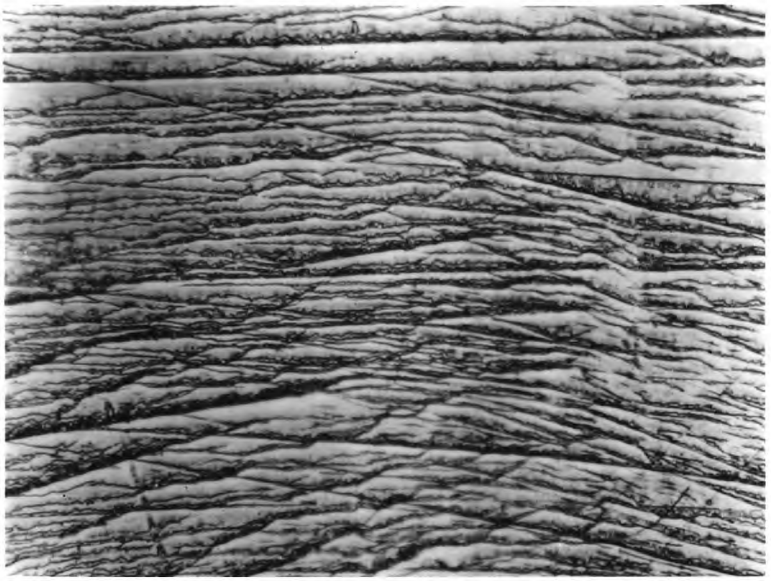

Fig. 3.17 Wavy Slip Traces on a "Screw" Face after Deformation at 550°K (x 380).

Fig. 3.18 Slip Traces in a Coarse-Grained, Nickel-Rich Polycrystal (43 at.% Al) (x 75).

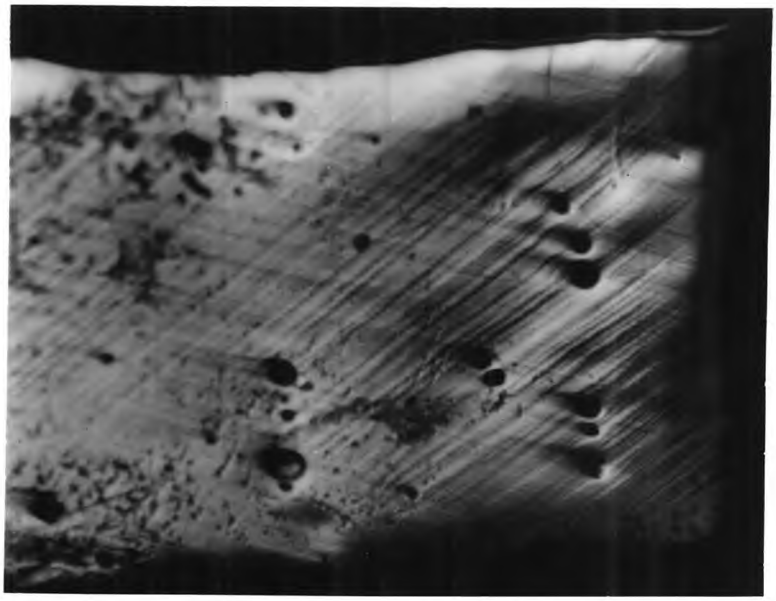

Fig. 3.19 Slip Traces in a Nickel-Rich Single Crystal (43 at.% Al) (x 96).

Fig. 3.20 Slip Markings in an Aluminium-Rich Polycrystal Deformed at 850°K (54 at.% Al) (x 75).

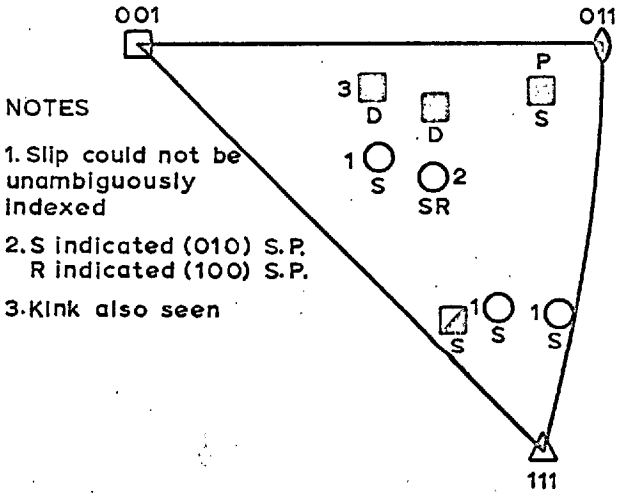

A Ni 50 at °/. Al, 295 °K

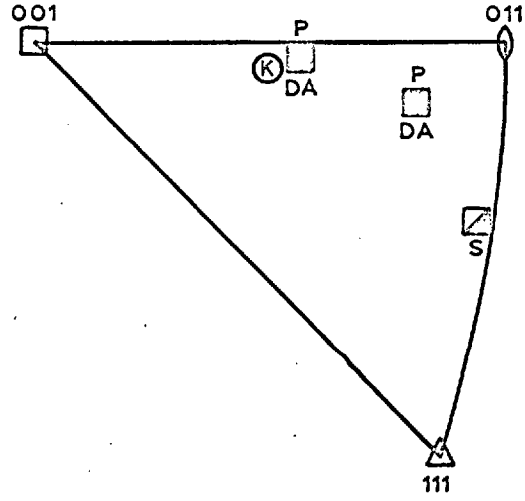

B Ni 50 at °/. Al, 875 °K

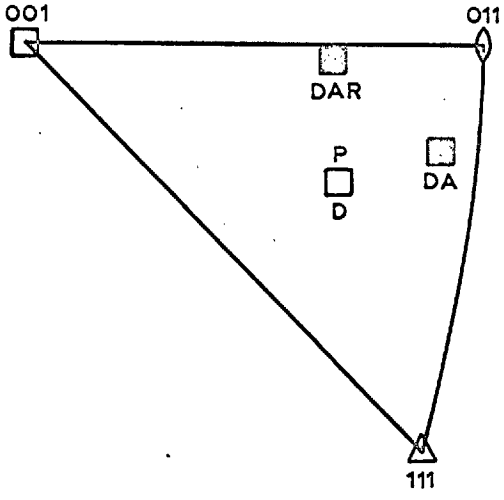

C Ni 48·9 at °/. Al, 295 °K

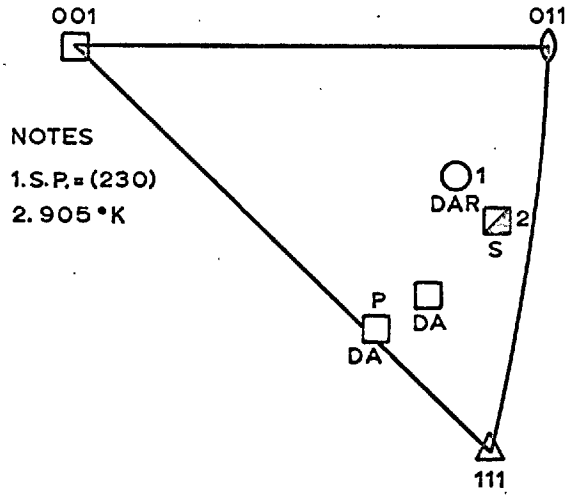

D Ni 43 at °/. Al, 295 °K

SLIP SYSTEMS

- □ (110) [001]
- □ (010) [001]
- ▨ Duplex slip on (010) [001] and (110) [001]
- Ⓚ Kink
- ○ Other

TECHNIQUES USED

- S Single Trace Method
- A Asterism
- D Double Trace
- R Lattice Rotation
- P Course Grained Polycrystal

Fig 3.21 Slip Systems in Single Crystals grown by the Strain Anneal Technique.

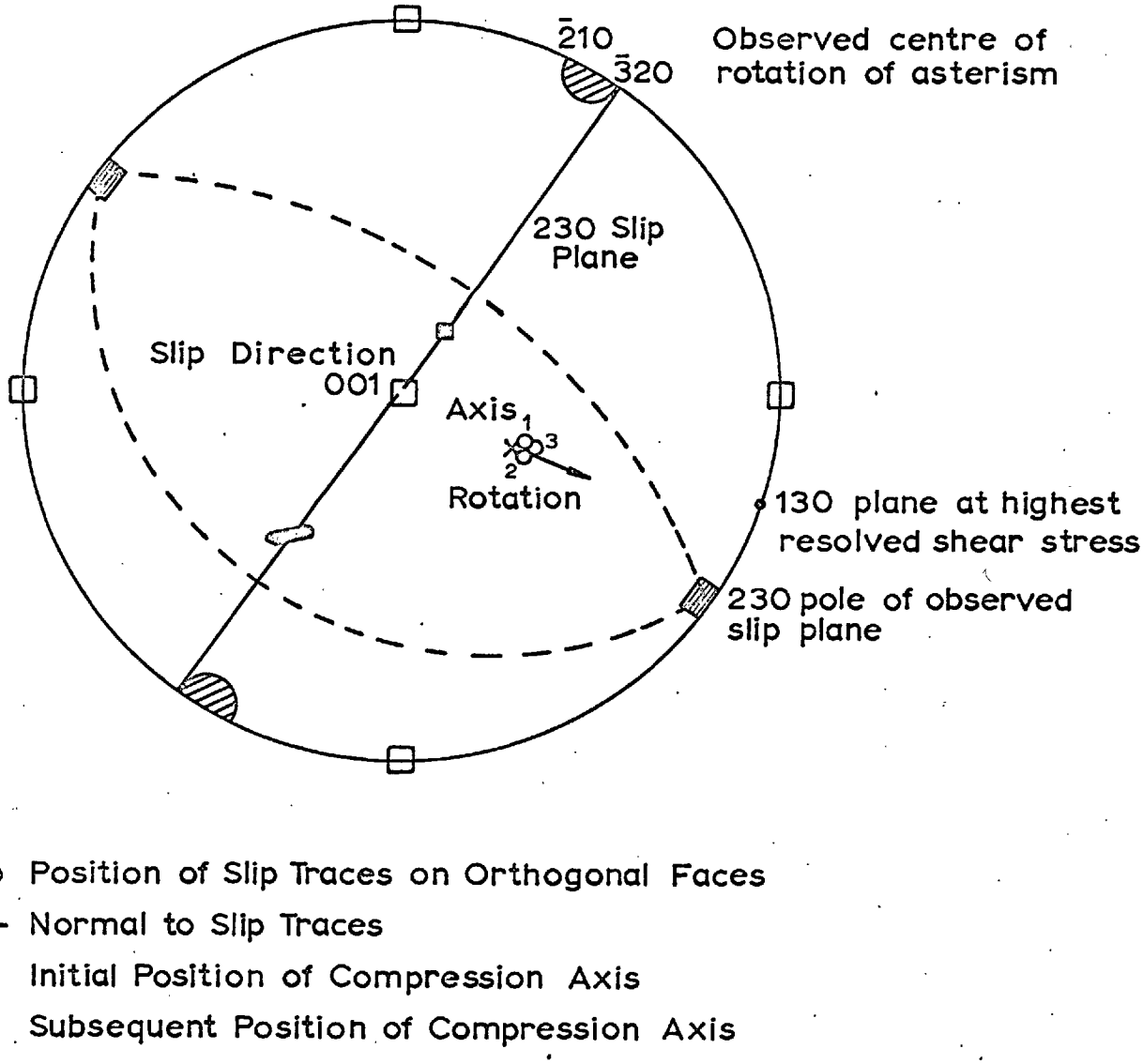

Fig 3.22 Summary of Slip System Observations in a Strain-Anneal Grown Single Crystal of Ni. 43 at % Al.

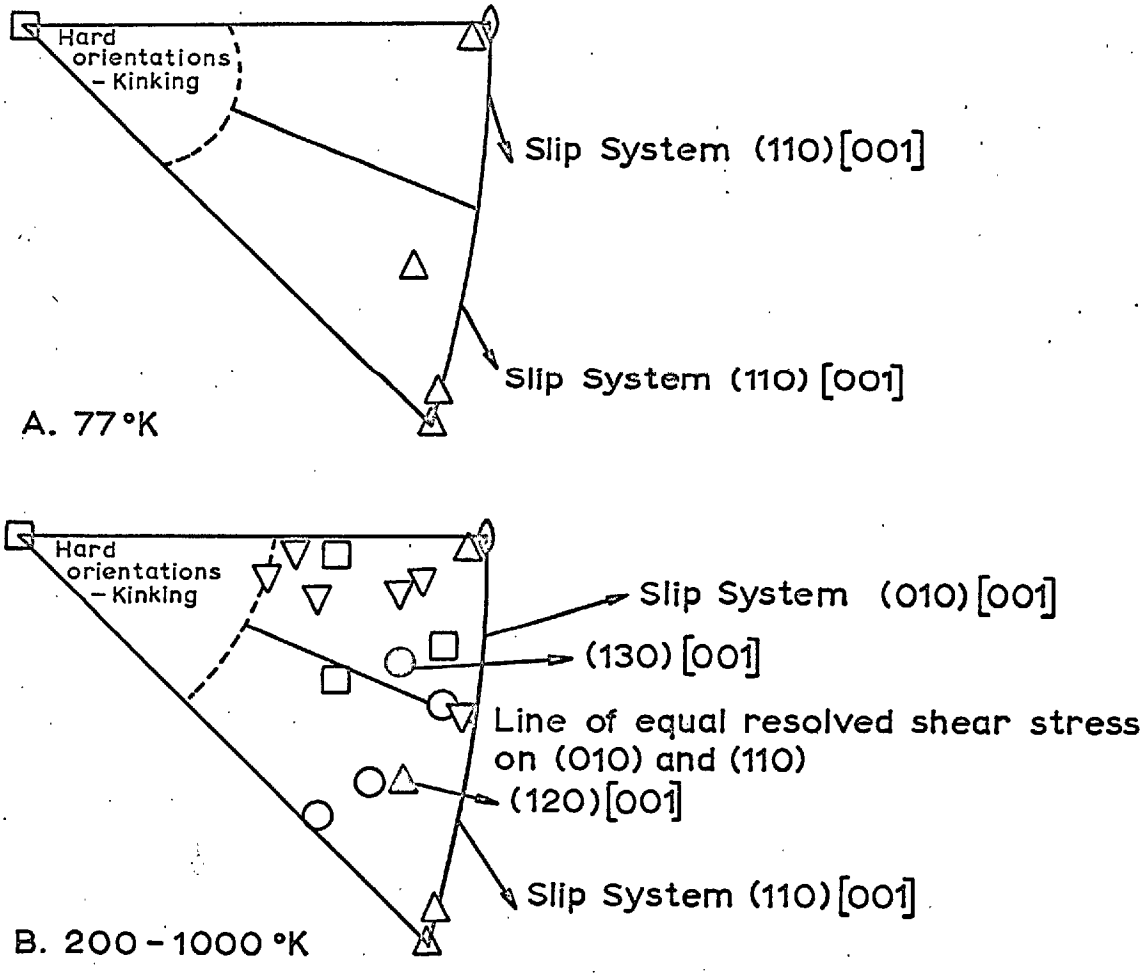

△ Melt Crystals Ni 50 at °/o Al

▽ Ni 50 at °/o Al

□ Ni 48·9 at °/o Al

○ Ni 43 at °/o Al

Open symbols: Primary slip on indicated system

Filled symbol: Primary slip on other systems

Fig 3.23 Orientation Dependence of Slip Systems.

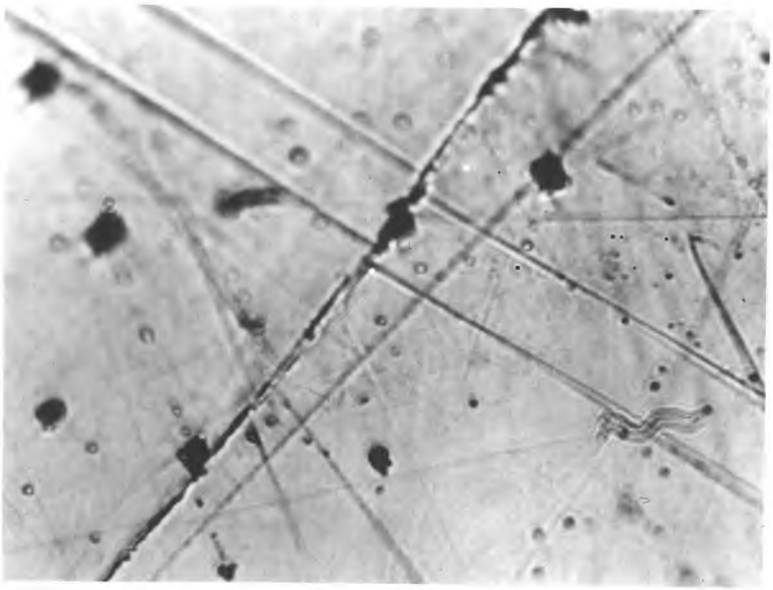

Fig. 3.24 Grain Boundary Sliding in Ni 43 at.% Al Deformed at 875°K (x 840).

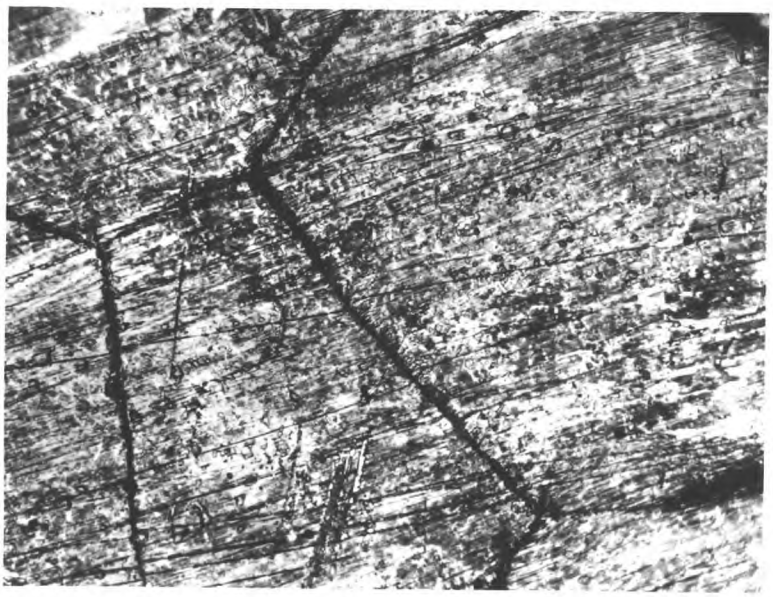

Fig. 3.25 Grain Boundary Sliding in Ni 54 at.% Al Deformed at 1075°K (x 840).

Fig. 3.26 Slip Traces on a Crystal of a Hard Orientation Deformed at 77°K (x 11).

Fig. 3.27 Slip Traces on a Crystal of Hard Orientation Deformed at 195°K

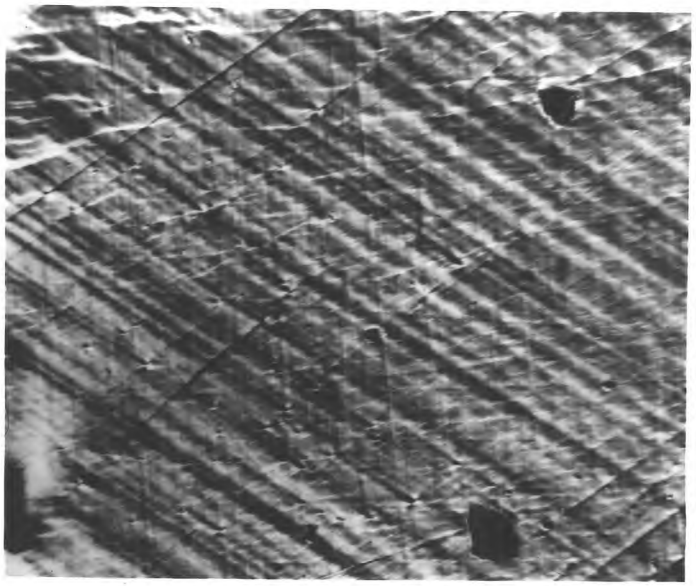

Fig. 3.28 Straight Slip Traces on an "Edge" Face of a Hard Crystal Deformed at 77°K (x 150).

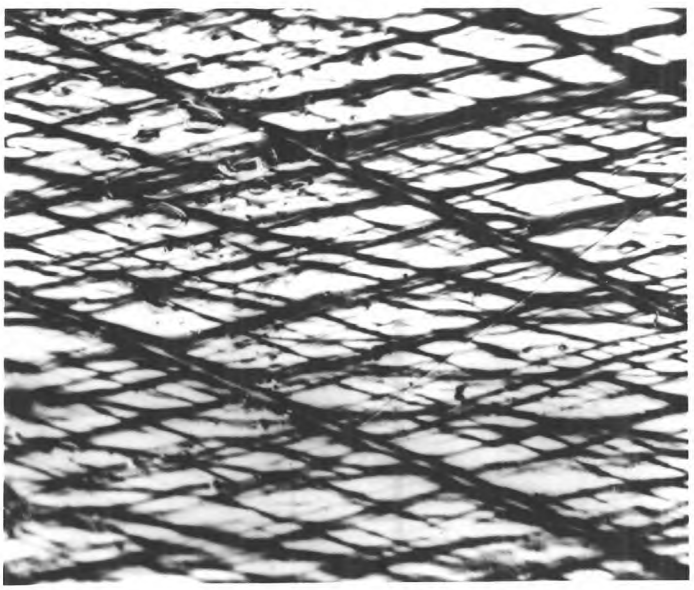

Fig. 3.29 Wavy Slip Traces on a "Screw" Face of a Hard Crystal Deformed at 77°K (x 300).

Fig. 3.30 Slip Traces after Deformation of a Hard Crystal at 201 °K (x 150).

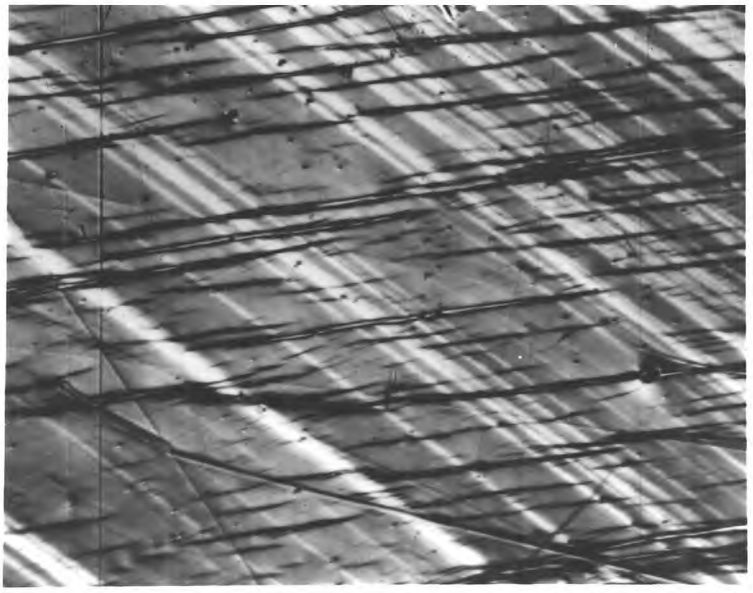

Fig. 3.31 "Edge" and "Screw" Type Slip Traces on the Same Face of a Single Crystal of Hard Orientation Deformed at 201 °K (x 150).

Fig. 3.32 Kinking of a Hard Orientation at 376°K (x 11).

Fig. 3.33 Kinking and Transformation in a Hard Crystal at 420°K (x 11).

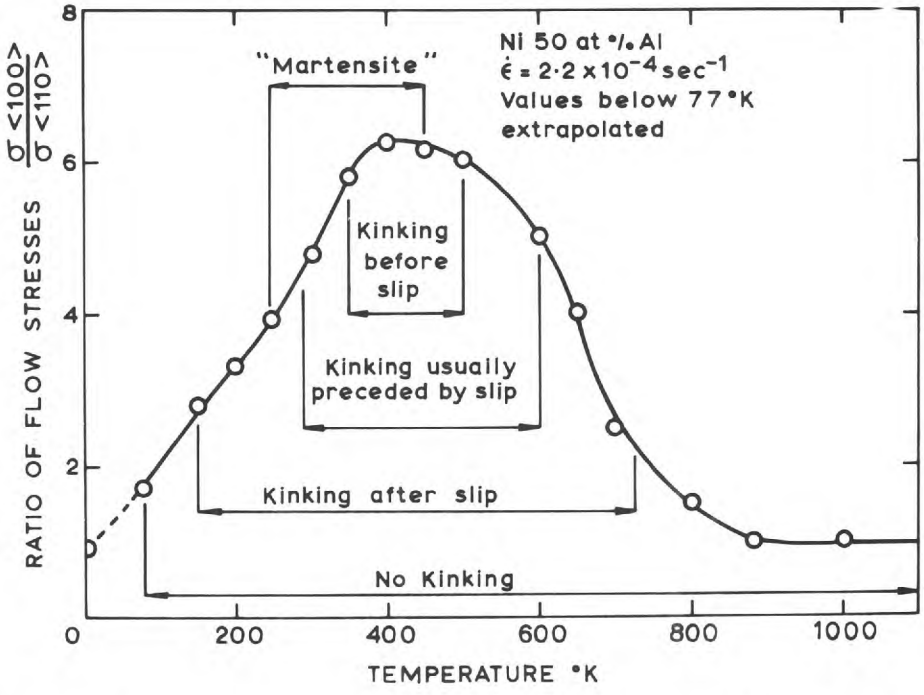

Fig. 3.34 Temperature Dependence of the Ratio of Flow Stresses on Hard and Soft Systems and its Relation to Kinking.

Fig. 3.35 Slip Traces on a Kinked Specimen (x 13).

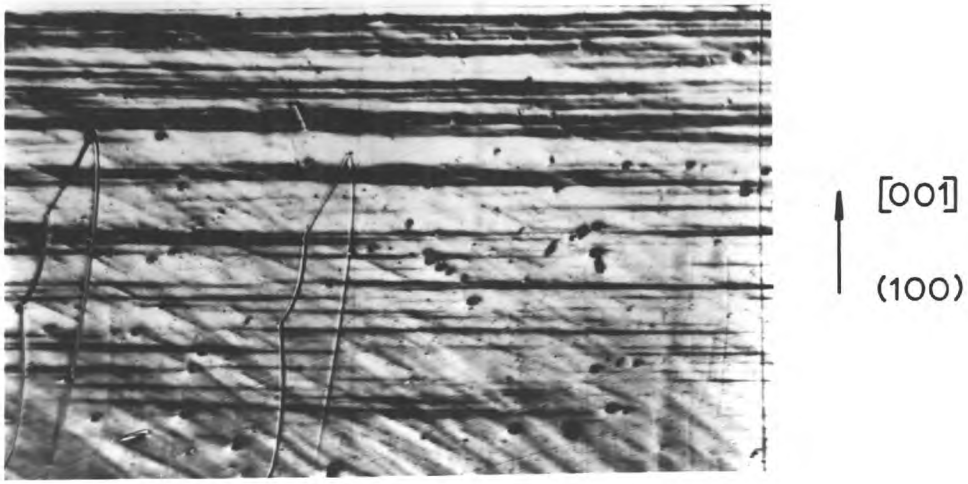

Fig. 3.36 "Edge" and "Screw" Type Slip Traces on a Kinked Specimen (x 150).

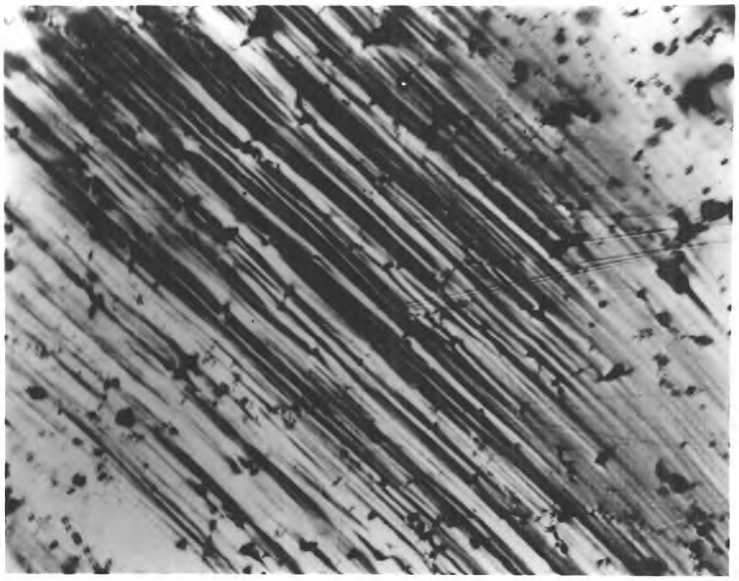

Fig. 3.37 Slip Traces on a Hard Orientation Crystal Deformed at 821°K (x 150)

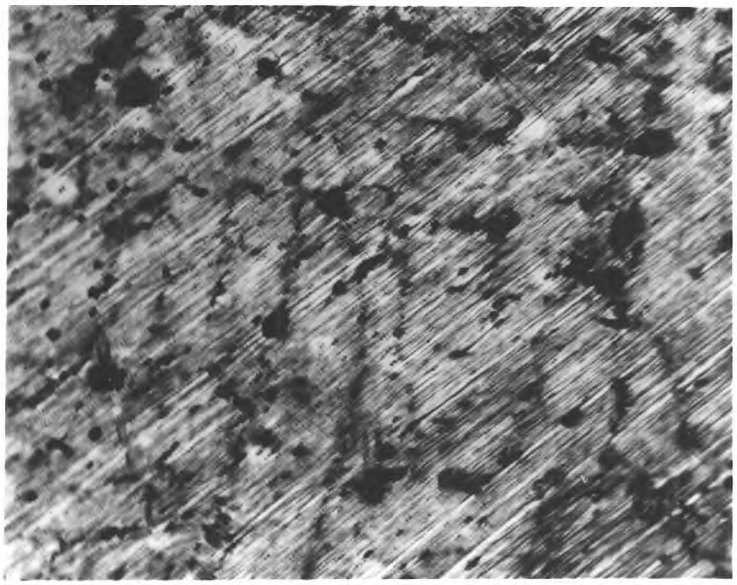

Fig. 3.38 Slip Traces on a Hard Crystal Deformed at 1025°K (x 150).

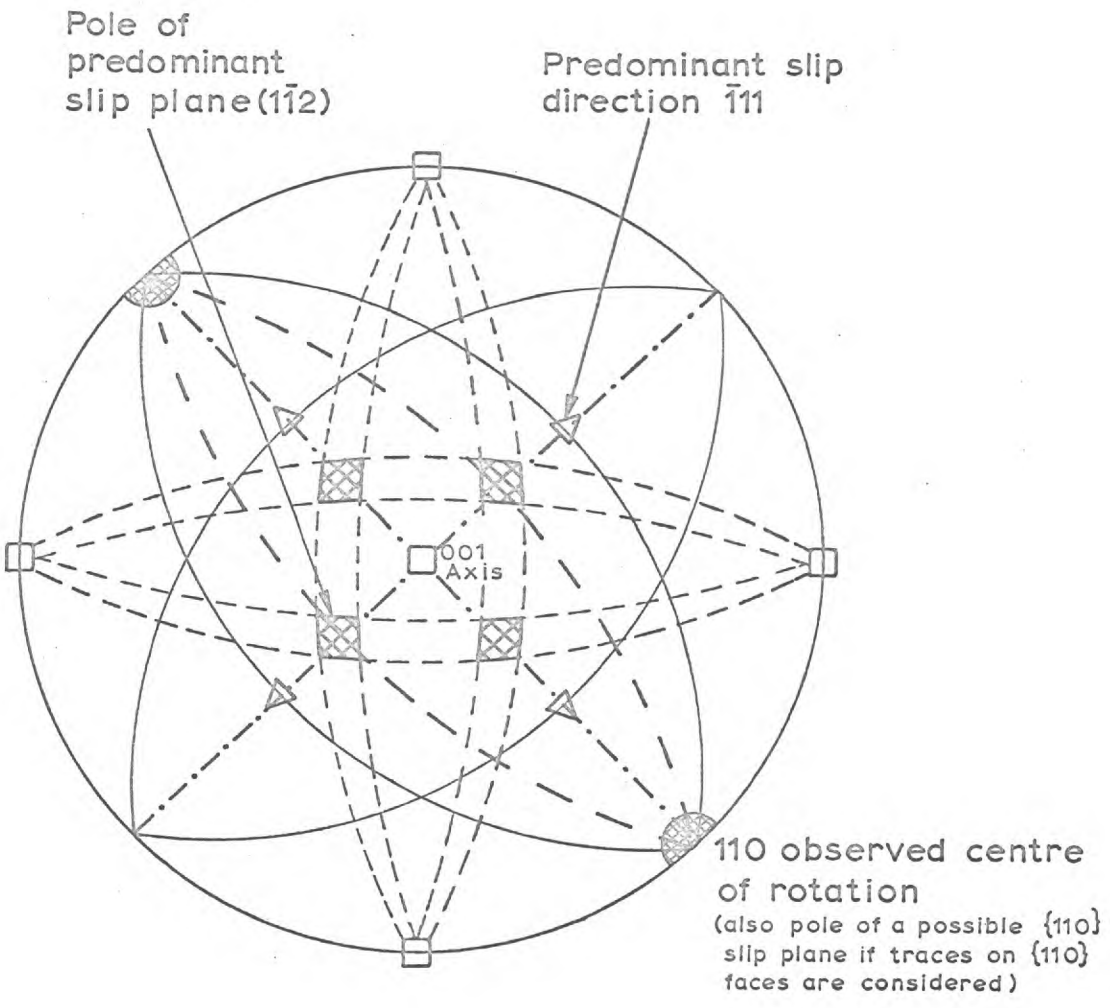

⊗ Pole of observed {112} slip planes

—— Trace of observed slip planes

---- Normals to slip traces on {100} faces (7 specimens)

-·-·- Normals to slip traces on {110} faces (2 specimens)

△ Slip direction <111>

Fig 3.39 Summary of Slip System Observations in Hard Orientations between 295 and 1070°K.

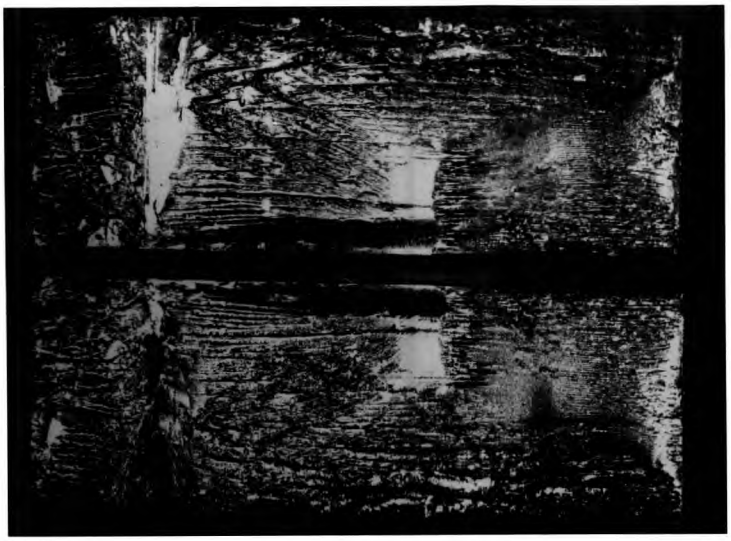

Fig. 3.40 Vertical Cleavage Surface of a Soft Crystal Compressed at 77°K (x 11).

Fig. 3.41 Crack Formed at a Kink in a Hard Crystal (x 11).

Chapter 4: The Mechanical Properties of NiAl.

4.1. Parameters Measured and their Significance.

4.1.1. Strain-Rate.

The strain rate, $\dot{\varepsilon}$, may be calculated from the cross-head speed and the length of the test piece. This strain-rate is an overall one, $\dot{\varepsilon}_T$, and is a combination of three terms:

$$\dot{\varepsilon}_T = \dot{\varepsilon}_M + \dot{\varepsilon}_E + \dot{\varepsilon}_p$$

where $\dot{\varepsilon}_M$ is the component of strain-rate due to the elastic distortion of the compression cage (measured in a blank experiment forcing the compression surfaces together without a specimen).

$\dot{\varepsilon}_E$ is the strain-rate component leading to elastic strain in the specimen.

$\dot{\varepsilon}_p$ is the plastic strain-rate in the specimen.

The important parameter when considering plastic deformation is the plastic strain-rate which varies continuously throughout a test - from $\dot{\varepsilon}_p = 0$ in the elastic region to $\dot{\varepsilon}_p = \dot{\varepsilon}_T$ where the work-hardening rate is zero. When required, the exact value of $\dot{\varepsilon}_p$ could be measured from a comparison of the elastic and plastic stress-strain relationship. This comparison was often unnecessary because strain-rate enters most calculations as a $\Delta \log \dot{\varepsilon}$ term; if the rate of work-hardening is the same immediately before and after a change of strain rate it can be

seen that:

$$\Delta \log \dot{\varepsilon}_p = \Delta \log \dot{\varepsilon}_T = \Delta \log V_{x.h.}$$

where $V_{x.h.}$ is the speed of the moving cross-head.

Strain-rates will be quoted as $\dot{\varepsilon}_T$ values because of the variation of $\dot{\varepsilon}_p$ with strain.

4.1.2. Stress-Strain Relationships.

The Instron recording system indicates the relationship between the load applied to the specimen and time. This may be converted into the accepted form of a stress-strain curve knowing the specimen dimensions and the speeds of the moving cross-head and chart. Stress-strain data are shown in the form of true-stress/natural-strain curves. True stresses (σ) were measured from the applied load and instantaneous cross-sectional area, which was calculated from the measured change in length by assuming the volume of the specimen to be constant. True stress measured in this way was found to be meaningless at strains greater than 0.1 because barrelling and other inhomogeneous forms of deformation led to variations in cross-sectional area along the specimen length.

Resolved shear stresses, τ, in single crystals were calculated from the applied stress and the Schmid factor on the observed slip system (cf. 3.1.1). Values of τ for polycrystals were obtained by assuming a mean orientation factor, $\bar{m}$, of 2 ($\tau = \sigma/\bar{m}$). This value is

probably low for NiAl because it requires every grain to be in the most favourable orientation for slip. It was used because it gave reasonable agreement between single and polycrystal results and because the complexity of the slip systems in NiAl prevented a more accurate calculation of $\bar{m}$.

The strain measured from the Instron chart had components due to the elastic deformation of the jig and specimen as well as to the plastic deformation of the specimen (cf the components of strain-rate); and allowance had to be made for these elastic contractions in the calculation of the permanent change of length. Strains are largely quoted as natural strains ϵ, defined by:

$$\epsilon = \log_e (l/l_o)$$

where l and l_o are respectively the instantaneous and original lengths of the specimen.

4.1.3. Flow Stresses.

The following parameters were measured to describe the stress at which plastic flow became significant at the applied strain-rate:

i) The initial flow stress, σ_f, the stress at which the first deviation from a linear stress-strain relationship was noted.

ii) The proof stress, σ_p, the stress after 0.2% plastic strain.

iii) A 1% proof stress, $\sigma_{0.01}$, was also measured when an irregularity, such as a yield point, obscured the initial plastic stages of

the stress-strain curve. Where a yield point occurs the normal practice is to measure the lower yield stress, σ_y. This could not be done with NiAl because the appearance of the yield point varied markedly and a classical yield drop was often not observed.

The behaviour of each of these parameters was found to be identical under most conditions; results are quoted as 0.2% proof stresses because these were found to be the most reproducible. An indication of the reproducibility of these stresses can be gained from the typical values listed in table 4.1. Errors in flow stresses arise from variations in cross-section, inhomogeneities of deformation and from the difficulty of estimating the stress at which the first deviation from linear elastic behaviour occurs in materials with high initial rates of work hardening.

4.1.4. Work-Hardening Parameters.

The initial rate of work-hardening, Θ, is the slope of the stress stress-strain curve at low strains; in practice Θ is measured from the difference between the initial flow stress and the proof stress. The reproducibility of this parameter was expected to be low because the differences in stresses were not much greater than the errors in their measurement (see table 4.1).

An alternative way of considering work-hardening is to express the relationship between stress and strain in the form:

$$\sigma = K\epsilon^{n} \qquad (4.1)$$

The parameter n, the work-hardening exponent, is a measure of work-hardening and may be evaluated from the slope of log σ against log ϵ plot, which should be linear if a relationship of this type is obeyed.

4.1.5. Fracture Data.

"Fracture" data in compression are difficult to interpret because of the constraints on crack propagation. However two parameters were measured to enable the fracture behaviour under various conditions to be compared. These were the stress and strain at the point where the applied load showed the first drop that could be attributed to cracking (i.e. not kinking or a yield point); metallographic examination revealed that some cracking occurred prior to this. The stress will be referred to as the fracture stress, or the maximum stress in compression, σ_M; and the strain as the ductility, ϵ_M. The term ductility should strictly be applied only to deformability in tension, but as there is no alternative in general use it will be used to describe compression behaviour. The reproducibility of these parameters is indicated by some typical values listed in table 4.1.

4.1.6. Change of Strain-Rate Experiments.

The basic information that can be derived from a change of strain-rate experiment is the change in stress, $\Delta\sigma$, corresponding to a

change of strain rate $\Delta\dot{\epsilon}$; this is conventionally expressed as the strain-rate sensitivity $\frac{\Delta\sigma}{\Delta \log \dot{\epsilon}}$. The thermal activation and dislocation dynamic parameters were obtained from $\Delta\sigma$ using the equations of section 1.6.

Under certain conditions local peaks in the flow stress, resembling yield points, were observed on changing strain-rate. Peaks of this type have been reported in many materials and there are two schools of thought about their significance (Christian and Masters, 1964 A). One of these is that the peaks are due to dislocation multiplication to accommodate the higher stresses, and because the equations of 1.6 require a constant dislocation structure to be valid the peak values should be measured. The alternative view is that the peaks are machine effects, or other local transients, which would not be seen under "perfect" testing conditions and have no significance. In this case the smooth flow curve should be extrapolated to the strain before the strain-rate was changed to measure $\Delta\sigma$ (Conrad et al, 1965). Both "yield point" and "extrapolated" values were measured because of this uncertainty.

Table 4.1 Typical Errors in Measured Parameters

Parameter	Source	Composition at % Al	Temp °K	$\dot{\epsilon}$ T_1 sec^{-1}	Value	Units	Standard Deviation	percentage error	No. of readings taken
τ_f	SS	50.0	295 ± 3	2.5×10^{-4}	12.3	Kg mm^{-2}	1.0	8	5
θ_f	SA	49.6	725 ± 5	4.2×10^{-5}	5.2	Kg mm^{-2}	0.4	7.5	8
θ_f	SA	48.9	295 ± 3	4.2×10^{-4}	23.5	Kg mm^{-2}	2.2	9.5	9
θ_f	PL	48.9	295 ± 3	2.2×10^{-4}	24.6	Kg mm^{-2}	1.4	6	4
θ_p	PL	48.9	295 ± 3	2.2×10^{-4}	25.9	Kg mm^{-2}	1.6	6	4
$\sigma_{0.01}$	PL	48.9	295 ± 3	2.2×10^{-4}	34.5	Kg mm^{-2}	3.2	9.5	4
σ_m	PL	48.9	295 ± 3	2.2×10^{-4}	80	Kg mm^{-2}	5	6	4
ϵ_m	PL	48.9	295 ± 3	2.2×10^{-4}	16.7	%	1.8	11	4
σ_f	PT	48.9	294	2.2×10^{-4}	30.8	Kg mm^{-2}	2.1	7	3
ϵ_m	PT	48.9	294	2.2×10^{-3}	11.0	%	1.0	9	3
σ_f	SA	43.0	295 ± 3	1.1×10^{-3}	71.1	Kg mm^{-2}	3.5	5	17
σ_p	SA	43.0	295 ± 3	1.1×10^{-3}	81.3	Kg mm^{-2}	3.9	5	10
	SA	43.0	295 ± 3	1.1×10^{-3}	4.7×10^{3}	Kg mm^{-2}	0.6×10^{3}	13	10

Sources:

SA Pre-strain for the growth of single crystals by the strain-anneal technique
PL Mechanical Property measurement on a polycrystal (longitudinal axis)
PT Mechanical Property measurement on a polycrystal (transverse axis)
SS Mechanical Property measurement on a "soft" single crystal

4.2. Flow Stresses.

4.2.1. Temperature Dependence of Flow Stress of Polycrystals and Soft Orientation Single Crystals.

The temperature dependence of the 0.2% proof stress of single crystals of hard and soft orientations is shown in fig 4.1. Comparison with that of polycrystalline material of various compositions, fig 4.2, shows that the temperature dependences of soft single crystals and of polycrystals are very similar. A complete study of the properties of aluminium-rich compositions was prevented by the low temperature brittleness of this material (below 700°K no specimen could be strained more than 0.5%). Each curve could be divided into three distinct regions:

i) At low temperatures the flow stress was strongly dependent on temperature and strain-rate, indicating that a strongly thermally-activated process was operative. A linear relationship was observed between the logarithm of the thermally activated component of flow stress ($\log \sigma^*$) and temperature for all conditions (fig 4.3).

ii) Intermediate Temperatures: The flow stress in this region was relatively independent of temperature and strain-rate, indicating that the operative deformation process was not strongly thermally activated. This region was subdivided further for the 48.9 at % Al alloy; the slight temperature dependence noted at comparatively low temperatures coincided with the

occurrence of an initial yield point (fig 4.10). A similar temperature dependence was observed with a 1% proof stress.

iii) High Temperature: A further thermally activated process occurred at high temperatures and the flow stresses were again dependent on temperature and strain-rate. A linear relationship (fig 4.4) was obtained between log. flow stress and temperature of the form:

$$\sigma_p = A \exp(-\alpha T) \qquad (4.2)$$

Values of $\underline{A}$ and $\underline{\alpha}$ are listed in Table 4.2 with comparative values from Rozner and Wasilewski (1965). The temperature dependence of aluminium-rich compositions was found to be divided into two regions with different values of $\underline{A}$ and $\underline{\alpha}$.

The temperature dependence is similar to that observed by Wasilewski et al (1966) on single crystals. It is also similar at intermediate and high temperatures to the polycrystalline results of Ball (1964) and Rozner and Wasilewski (1966), although these investigations reported insufficient ductility for measurements to be made at low temperatures.

4.2.2. Effects of Deviations from Stoichiometry.

Deviations from stoichiometry had two effects, they raised the flow stress at all temperatures studied and altered the temperatures at which the processes listed above became operative. It may be seen

from figs 4.2 and 4.3 that the major effect of lattice defects was to increase the athermal flow stress, σ_μ, in the intermediate temperature region. Insufficient information was available to allow a detailed study of the effects of defect concentration on the flow stress; although it was apparent that vacancy defects caused greater hardening than substitutional atoms at intermediate temperatures (fig 4.5). This is in agreement with the hardness results of Westbrook (1957) and the flow stress values of Ball (1964).

In the high temperature region the rate of softening with increasing temperature was greater for aluminium-rich alloys than for any other. Above 1300°K Ni. 53 at % Al alloys were softer than those containing excess nickel (Ni 43 at % Al).

The flow stresses of polycrystals have been measured over the full range of composition (from 40 to 54 at % Al) by Lautenslager et al (1965) in the temperature range 950° to 1200°K. It was found that flow-stress against temperature plots passed through a peak on either side of the equiatomic composition at any temperature, in a manner similar to that observed in AgMg by Wood and Westbrook (1962). This behaviour may be partly explained by the choice of a working temperature range where several different processes are operative. The temperature, T_c, at which the high temperature process becomes operative is dependent on composition and decreases with increased defect concentration. Ball and Smallman (1966 A) showed that the temperature dependence of stoichiometric and non-stoichiometric NiAl could cross because of the comparatively high T_c of stoichiometric alloys.

Defects also affected the temperature, $\underline{T}_A$, at which the change from the low temperature process to athermal flow occurred. $\underline{T}_A$ was determined as the temperature at which the strain-rate effect on the initial flow stress disappeared. It could not be determined to any great accuracy as may be seen from the change of strain rate experiments. This temperature was increased by the presence of substitutional defects, and probably by vacancy defects also.

Typical values of $\underline{\sigma}_\mu$, $\underline{T}_A$ and $\underline{T}_c$ are listed in table 4.2.

4.2.3. Hard Orientations.

Although the temperature dependence of flow stress of hard orientations (fig 4.1) was similar in outline to that of polycrystals it was completely different in detail. At low temperatures, where $(\bar{1}\bar{2}3)[111]$ slip occurred, the flow stress was not as strongly temperature dependent as in soft orientations. The flow stress, if extrapolated to $0^\circ K$, was lower than of soft crystals (fig 4.6). At high temperatures, where the predominant deformation mode was slip on $(\bar{1}\bar{1}2)[111]$ or $(0\bar{1}1)[01\bar{1}]$, the flow stress depended sharply on temperature and obeyed a $\sigma_p = A \exp(-\alpha T)$ relationship (fig 4.6). Values of $\underline{\alpha}$ and $\underline{A}$ are given in table 4.2. The scatter in hard orientation flow stresses was considerable (fig 4.6); this is probably because the high flow stresses and strong orientation dependence emphasised the effects of any misorientation or variation in composition.

The behaviour at intermediate temperatures was complex. Kinking

did not occur at a reproducible stress and that there was considerable scatter from a smooth curve.

The temperature at which the high temperature process became operative, $\underline{T}_c$, was lower than for any other condition.

Table 4.2 Effect of Composition on the Temperature Dependence of Flow Stress.

Composition at % Al	Axis	$\sigma_0{}^{\circ}K$ Kg mm^{-2}	σ_{μ} Kg mm^{-2}	T_A $^{\circ}K$	T_c $^{\circ}K$	A	α x 10^{-3}
50	[001]	220	(125)	350	550	2850	2.98
50	[011]	260	20	(350)	(950)	-	-
53	Poly	-	(100)	(500)	600	690	5.8
		above T_D = 980°K				9245	3.2
49.6	Poly	-	8	(300))	(900)	-	-
48.9	Poly	290	18	325	815	710	4.5
43	Poly	285	6.1	470	720	1060	4.5
Rozner and Wasilewski (1966)							
50.6	Poly	-	14	400	873	800	4.15

4.3. Form of the Stress-Strain Curve and Work-Hardening.

Although all polycrystalline specimens showed similar work hardening behaviour, in that equation 4.1 was obeyed, the form of the stress-strain curve varied with composition and was very different to that of single crystals.

4.3.1. Nickel-Rich Polycrystals (43 at % Al).

Typical stress-strain curves for nickel-rich polycrystals at several temperatures are shown in fig 4.7. They all obeyed a $\sigma = K \epsilon^n$ relationship at strains greater than 0.01 and both K and n were dependent on temperature. Values of the work-hardening exponent, which rose to a maximum at about 600°K (fig 4.8), were in the range 0.1 to 0.2, which is typical of most metals. Above 1200°K the work hardening rate was effectively zero. The temperature dependence of the initial rate of work-hardening was similar to that of the flow stress (fig 4.9).

4.3.2. Near-Stoichiometric Polycrystals (48.9 and 49.6 at % Al).

The stress-strain curves of polycrystals of near-stoichiometric compositions were more strongly dependent on temperature than those of the nickel-rich alloys (fig 4.11); this is particularly apparent from the logarithmic plot (fig 4.12). The strain-hardening exponent was strongly temperature dependent rising to a maximum of 0.5 near room tmmperature; this value is very high compared with most metals.

Initial yield points were exhibited by a 48.9 at % Al alloy up to

585°K; this temperature corresponds to a change in slope of the temperature dependence of flow stress (T_B). The yield points were generally very flat and a classical yield drop was seldom seen; the strain over which irregularities in the stress-strain curve were observed increased with decreasing temperature, to 0.05 at 77°K. The presence of these yield points excluded any meaningful measure of the initial rate of work-hardening and obscured the true value of the flow stress. The characteristics of the yield points were not studied in detail, but it was noted that they occurred only over a limited range of composition and that the usual strain ageing phenomena were associated with them - a yield point did not occur on unloading and immediately reloading, but it reappeared after ageing at 350°K for about one hour.

4.3.3. Aluminium-Rich Polycrystals (53 at % Al).

Aluminium-rich compositions were very brittle below 750°K and normally shattered before any appreciable plastic flow occurred, although a few specimens deformed slightly before fracturing. Four different forms of stress-strain curve were observed with increasing temperature (fig 4.13). At low temperatures the initial rate of work hardening was extremely high and fracture occurred at low strains. At slightly higher temperatures this rising stress-strain curve developed into a broad rounded "yield point" (~790°K) the height of which decreased with increasing temperature. At 875°K the peak had disappeared and a "normal" stress-strain curve was observed. The work

hardening exponent, measured outside the yield point strain, was low and increased to a maximum value of 0.08 between 900 and 950°K. At higher temperatures the stress-strain curve passed through a broad peak and then dropped continuously. Equation 4.1 was obeyed beyond the peak with negative values of strain-hardening exponent.

4.3.4. Soft Orientation Single Crystals.

The stress-strain curves of single crystals of soft orientations (fig 4.13) were very different from those of polycrystals. Equation 4.1 was not obeyed, the stress-strain relationship was linear after a rounded initial flow region. The linear work-hardening rate, Θ_L, decreased with increasing temperature and became almost zero above 1050°K (fig 4.14).

The flow stress and the shape of the stress-strain curve were dependent on the orientation of the compression axis (fig 4.15). With axes other than [011] the stress-strain relationship was neither linear or exponential. Both the ductility and flow stress appeared to be dependent on orientation, but as the dependence changed between 77° and 295°K further work is required to determine whether this is a genuine effect, and not due to slight variations in composition or purity (which were not detected by chemical analysis).

4.3.5. Hard Orientations.

The stress-strain curves observed in single crystals with [001] compression axes were extremely varied (fig 4.16) as might be expected

from the many deformation modes available. Two general features of the curves were apparent. Kinking, when it occurred, resulted in a relaxation of stress which was usually very sharp at low strains; when a kink formed after initial plastic flow it often formed quite gradually. Work-hardening followed equation 4.1 where it could be studied and the work-hardening exponent increased with increasing temperature. The detailed behaviour of $\underline{n}$ could not be determined because it was often necessary to make measurements across the small range of strain before kinking occurred.

A broad, rounded yield point was occasionally seen (e.g. that at 716°K). This behaviour was generally associated with slip on a $(0\bar{1}1)[011]$ system.

4.4. Change of Strain-Rate Experiments.

4.4.1. Strain-Rate Sensitivity.

The effects of changes of strain-rate on various stress-strain curves are illustrated in figs 4.13, 4.16 and 4.17. Fig 4.18 shows the temperature dependence of strain-rate sensitivity. It may be seen that the strain rate sensitivity of polycrystals and soft orientation single crystals is high where the flow stress is strongly temperature dependent and low at intermediate temperatures. The boundaries between the regions of high and low sensitivity correspond closely to $\underline{T}_A$ and $\underline{T}_c$ measured from the temperature dependence of the flow stress.

At low temperatures the strain-rate sensitivity exhibited a maximum at 120°K in near-stoichiometric compositions. In nickel-rich alloys it increased with decreasing temperature, down to the minimum temperature (200°K) at which the ductility allowed changes of strain-rate to be made. At any temperature the change of stress due to changing the strain-rate by a constant factor was almost invariant with stress or strain; although this $\underline{(\Delta\sigma)}_T$ was often anomalously high for the first change at low strains. A similar effect has been noted in pure b.c.c. metals (Christian and Masters, 1964 A).

The intermediate temperature range was associated with low strain-rate sensitivities and peaks on changing strain-rate. It seems unlikely that these peaks were a machine effect, even though they were only observed at low strain-rate sensitivities, because they have not been noted in other materials under similar conditions (including

small $\Delta\sigma$) and using the same apparatus. Furthermore the height and appearance of the peaks was dependent on strain (figs 4.17 and 4.19) and unloading experiments indicated that their magnitude depended on the time of unloading. These peaks were first observed below T_A and they ceased abruptly at T_c.

The change is stress, $(\Delta\sigma)_T$, increased with increasing stress or strain in this region (fig 4.19) and values of zero were observed at low strains in near-stoichiometric alloys if the flow stress curve was extrapolated through the peak.

The strain-rate sensitivity above T_c rose rapidly with increasing temperature to a peak and then decreased gradually. It was independent of stress or strain (fig 4.19) but it varied with the magnitude of the strain rate change.

The effects of strain-rate on aluminium-rich polycrystals (54 at % Al) was rather different from any other composition (fig 4.18 B). Measurements could only be made above T_c because of low temperature brittleness and a very low sensitivity was noted near 900°K (i.e. close to T_D - the change in slope of the logarithmic stress-temperature curve). At higher temperatures the sensitivity rose to a maximum at 1100°K.

Strain-rate change experiments in hard orientations could only be made above T_c. At lower temperatures the change in stress was masked by kinking which appeared to occur in preference to slip at high strain-rates. The rate sensitivity decreased with temperature above 600°K to a broad minimum at about 1000°K. It was independent of

strain within the limit of the number of strain-rate changes that could be made (fig 4.16).

4.4.2. Dislocation Velocity Stress Exponent.

Values of $\underline{m}'$ have been calculated from equation 1.32 and extrapolated to zero strain to give the dislocation velocity stress exponent, $\underline{m}$. The variation of $\underline{m}$ with temperature is shown in fig 4.20 and typical plots of $\underline{m}'$ against strain in fig 4.21. The exponent $\underline{m}'$ increased rapidly with strain at low temperatures, reaching an approximately constant value if a sufficiently high strain could be achieved. The strain at which the change of slope occurred decreased with increasing temperature so that $\underline{m}'$ was independent of strain above $\underline{T}_c$.

The temperature dependence of $\underline{m}$ was the inverse of that of the strain-rate sensitivity, being low in the temperature dependent region and rising to a maximum which approaches infinity at intermediate temperatures. In the aluminium-rich composition a peak was observed in the high temperature region at 900°K, with very low values (3 - 10) on either side of the peak. In hard orientations $\underline{m}$ rose continually with increasing temperature.

4.4.3. Thermal Activation Parameters.

The activation parameters measured in this investigation were the activation volume, $\underline{v}^*$, defined by equation 1.24 and the activation enthalpy, $\underline{H}$, measured from equation 1.25. It was found that the

additional terms in equations 1.22 and 1.23 that involved the shear modulus were small compared with $\underline{H}$ and that for practical purposes equation 1.25 also defined the activation free energy, $\underline{G}$ under all conditions. The thermally activated component of stress, or effective stress $\underline{\sigma}^*$, was determined by subtracting the athermal stress measured above $\underline{T}_A$ from the applied stress, allowing for the effects of yield points and the variation of μ with temperature. The independence of strain-rate sensitivity of strain implies that $\underline{\sigma}^*$ does not increase with strain and therefore that the work-hardening is due to an increase in the long-range interaction stress, $\underline{\sigma}_i$. This assumption was not verified by making change of temperature tests. The $(\partial\sigma/\partial T)_\varepsilon$ term in equation 1.25 was evaluated from the temperature dependence of the initial flow stress.

At low temperatures polycrystals that were not brittle behaved in a very similar manner to soft orientation single crystals. The activation volume was found to depend on effective stress in the same way as most b.c.c. metals (Conrad, 1963) and results from all compositions and grain sizes, including one hard orientation single crystal, could be fitted to the same curve (fig 4.22). This volume rose to a maximum of 50-100 b^3 at low stresses and decreased rapidly to 5 b^3 at high stresses. The modified formula (eqn 1.29) for v^* was not used to account for the possibility of back jumps because the effective value of v^* depends critically on σ^* which cannot be determined accurately (i.e. $\pm$ 1 Kg mm^{-2}). The measured activation enthalpy was dependent on stress (fig 4.23), rising to a maximum of

1.4 eV in a 43 at % Al alloy and 1.0 eV near to stoichiometry (single and polycrystals).

In utilising the relationships of 1.6.2 the question of the validity of the analysis often arises, particularly with regard to the operation of a unique rate controlling process. The validity may be checked by comparing values of one of the activation parameters measured in two different ways, e.g. v^* could be determined from the slope of the stress dependence of H (= G) and by equation 1.24. Arsenault (1966) used a similar method to show that a single process is rate controlling in tantalum alloys. Assuming that entropy is small equation 1.15 becomes:

$$v^* = \left(\frac{\partial H}{\partial \tau}\right)_T$$

The activation energy at zero effective, $\underline{H}_o$, stress may be determined by integration as

$$H_o = H + \int_{\tau_i}^{\tau} v^* \, d\tau \qquad (4.3)$$

which should be independent of stress if a single process is operative. Values of H_o (fig 4.24) were measured by integrating fig 4.22 graphically and adding this energy to the curve of fig 4.23. It may be seen that although H_o is independent of strain at high stresses this constancy disappears when $\tau^* < 15$ Kg mm^{-2}. Therefore it appears that a single dislocation process is not rate controlling at

low effective stresses in the low temperature region.

At intermediate temperatures the finite strain-rate sensitivity allowed an activation volume to be measured. This varied with applied stress in the classical manner (fig 4.25) but its interpretation is not clear because the small temperature dependence of flow stress indicates a very high activation energy of deformation.

Above $\underline{T}_c$ a similar stress dependence of v^* was observed for near stoichiometric polycrystals (fig 4.26 A), and soft and hard orientation single crystals. Non-stoichiometric alloys showed marked differences. Activation volumes in nickel-rich compositions remained almost constant up to 1350°K rising only slightly with decreasing stress (fig 4.26 A). Aluminium-rich alloys exhibited a sharp maximum of v^* at about 40 Kg mm^{-2} (fig 4.26 B).

These differences in activation volume were reflected in differences in activation enthalpy. $\underline{H}$ of a near-stoichiometric alloy (48.9 at % Al) remained constant with increasing stress or temperature (fig 4.27 A) whilst both nickel and aluminium-rich compositions exhibited a peak at 900-1000°K. This peak was sharp and very high (up to 20 eV) in the 53 at % Al alloy but very broad in Ni 43 at % Al (fig 4.27 B). The activation energy, when extrapolated to zero stress, was very close to that for self-diffusion (Berkowitz et al, 1954). Comparative values are listed in table 4.3.

The activation enthalpy of hard orientation crystals was considerably higher than that of polycrystals, excluding the peaks, and varied linearly with temperature (fig 4.27 B).

The total activation energy was not evaluated according to equation 5.3 because no measurements were made above 1350°K.

Table 4.3. Activation Enthalpies of Deformation at Zero Effective Stress, H_o.

Composition at % Al	Orientation	Activation Enthalpy, H_o				Activation Energy for Self Diffusion, H_{SD} K cal mole^{-1}
		below T_A		above T_c		
		eV	K cal mole^{-1}	eV	K cal mole^{-1}	
53	Polycrystal	-	-	2.5	58	57
50	[001] axis	-	-	6.8	156	90
50	[011] axis	1.0	23	-	-	90
48.9	Polycrystal	1.0	23	3.5	80	80
43	Polycrystal	1.4	32	1.6	37	40

4.4.4. Comparison with Previous Work.

The effects of changes of strain-rate on the flow stress has not been studied in detail in any of the previous investigations of NiAl. Wasilewski et al (1966) made change of strain-rate tests from which they measured extremely large activation volumes (100-3000 b^3) although their values of $(\Delta\sigma)_T$ were comparable with those in figs 4.18 and 4.19. Ball (1964) measured m over a limited range of

temperature (700 to 1100°K) and observed a similar temperature dependence to fig 4.20.

The activation energies and volumes are comparable with those measured in b.c.c. metals (Conrad, 1963; Christian and Masters, 1964 A) and in AgMg (Mukherjee and Dorn, 1964). Activation energies in other materials at high temperatures have been measured mainly in creep tests. They are usually close to the energy of self-diffusion, at least over a limited range of temperature (Ishida et al, 1966; Conrad, 1961 A).

Ball and Smallman (1964) studied the kinetics of the annealing of dislocation loops in deformed NiAl and found that the temperature dependence of loop density after isochronal anneals was similar to that of the flow stress. The activation energy for the collapse of these loops was close to that of self-diffusion indicating that dislocation climb was a rate controlling mechanism in the high temperature deformation of NiAl.

4.5. The Effects of Grain Size and Temperature on Ductility.

Both the ductility and "fracture" stress of NiAl are sensitive to changes in temperature, composition (figs 4.28 and 4.29) and grain-size (figs 4.30 to 4.32). The maximum stress in compression (fig 4.28) decreased with increasing temperature without passing through any obvious stages corresponding to the different deformation processes. A similar temperature dependence was noted by Savitsky et al (1964) at high temperatures.

The increase of ductility with an increase of temperature or a decrease in defect concentration (fig 4.29) was probably a disguised effect of stress. If ductility is taken as a measure of deformability equation 1.12 may be re-written:

$$\epsilon_m \propto \gamma \sigma^{-1} d^{-\frac{1}{2}} \qquad (4.4)$$

Fig 4.33 is a plot of ductility against the reciprocal of fracture stress. It may be noted that although the scatter is considerable, as expected from compressive fracture data, the relationship is approximately linear; this confirms that a relationship of the form of equation 4.4 is obeyed. Furthermore results from near-stoichiometric and nickel-rich compositions lie on the same line. The fracture data obtained from the aluminium-rich composition could not be fitted to fig 4.33.

The low ductility of the aluminium-rich composition does not seem to be associated with its susceptibility to failure by the "pest"

phenomenon. Polycrystalline specimens were kept in air for many weeks without visible deterioration and no grain boundary hardening was detected without previous high temperature anneals.

An increase of grain size had no appreciable effect on the flow stress (table 4.4, fig 4.30) but caused a sharp drop in ductility (fig 4.31 and 4.32) and changes in the stress-strain curve (fig 4.30). The reduction in ductility was in agreement with the predictions of equation 4.4, although a $d^{-\frac{1}{2}}$ relationship was not observed because the decrease in ductility was accompanied by a decrease in fracture stress. The changes in the stress-strain curve took two forms, a reduction of the strain hardening exponent (table 4.4) and serrations at moderate strains. These serrations appeared to be due to local cracking because metallographic examination revealed many cracks at stresses below σ_m. The change in grain size also resulted in a change of crack morphology. Cracking in fine-grained material was always intergranular (fig 4.32) whilst that in large grained specimens was both intergranular and transcrystalline (fig 4.34).

A reduction in ductility was also observed on deforming a polycrystalline specimen cut with its axis normal to the extrusion direction (see table 4.4). This effect was probably due to a deformation or annealing texture, or to the distribution of impurity particles, because the grains appeared quite equiaxed and grain sizes were the same in all directions. All Debye rings in a back reflection X-ray photograph (polycrystalline specimen, Cu K_α radiation) were of uniform intensity, indicating that the grains were randomly oriented.

This result is rather surprising because the violent extrusion process would be expected to produce a marked texture, although it is possible that some information was lost by studying high index lines using a back reflection technique.

The ductility observed below room temperature is very different to that observed by Ball (1964), who noted no significant strain before fracture (i.e. $\epsilon_m < 1\%$) below 200°C. No explanation can be found for this difference because the material was obtained in a similar form and from the same source. The annealing conditions were not identical to those used by Ball, but his anneals were not as severe as those used to produce very large grain sizes. Rozner and Wasilewski (1966) were able to deform stoichiometric polycrystalline NiAl in compression at room temperature. It was completely brittle in tension, in agreement with the results of Grala (1960).

The effects of grain-size on ductility were confirmed by Westbrook et al (1964) who noted that when mechanical working operations reduced the grain size they also lowered the ductile-brittle transition temperature.

Table 4.4 Effects of Annealing Treatment on the Grain Size and Mechanical Properties of Ni 48.9 at % Al at 295°K.

Annealing Conditions		Grain Size microns d	Micro-hardness Kg mm^{-2}	Proof Stress Kg mm^{-2} σ_p	Max Stress Kg mm^{-2} σ_m	Ductility % ϵ_m	Strain hardening exponent n
Time hours	Temperature °C						
Longitudinal Sections							
As Extruded		45		34.1	90	16	
1	900	43	300	27.2	87	17	0.44
1	1100	45	290	27.5	90	18	
1	1200	75	300	27.0	71	13	
1	1300	125	300	25.4	72	12	0.39
1	1400	250	340	28.3	64	10	
1	1500	350	325	31.2	57	7	
24	1500	300	320	24.6	60	9	0.27
(24 (prestrained	1500	Single Crystal [110] Axis	320	20.8	57	12	linear hardening
Transverse Section							
1	900	40	300	30.8	81	11	
Scatter			± 20	± 2	± 5	± 2	

N.B. The change in flow stress is largely accounted for by an increase in microhardness and is probably due to contamination or loss of aluminium.

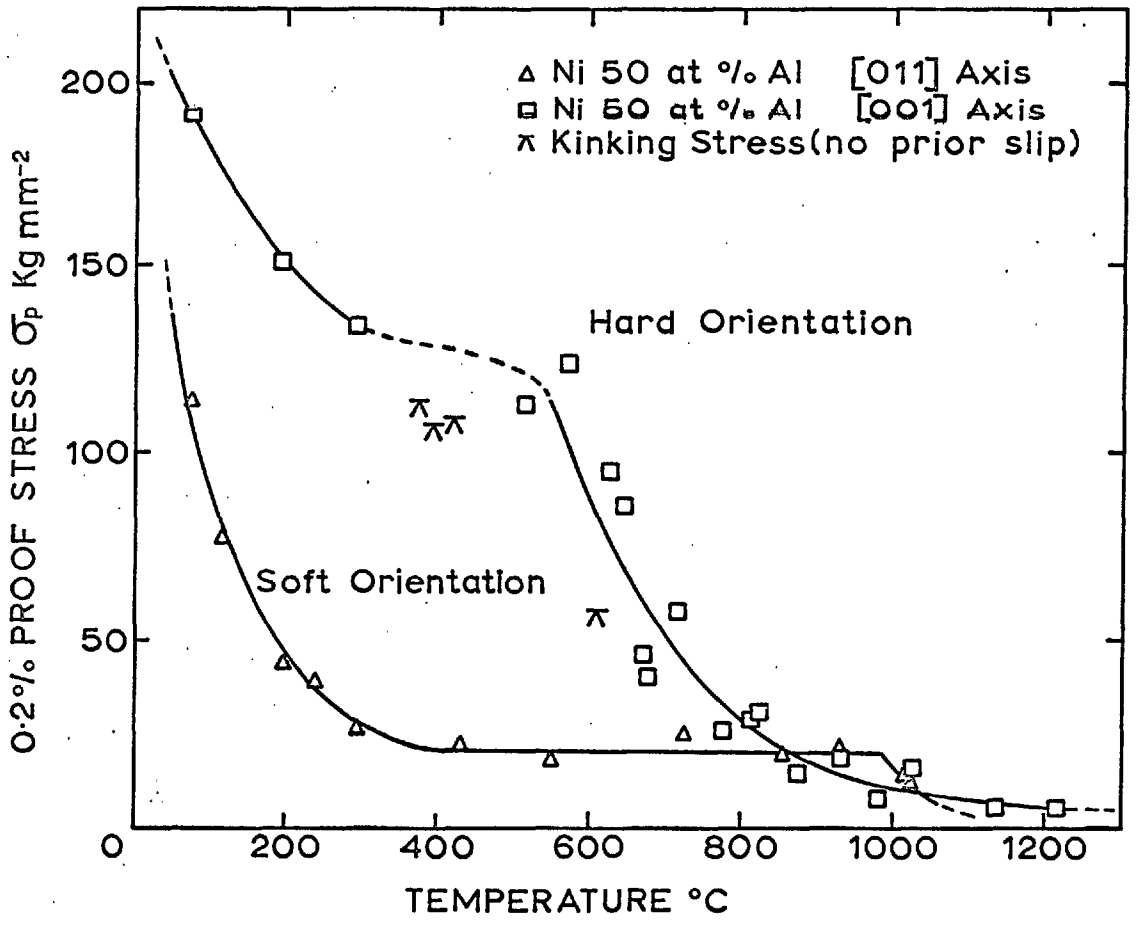

Fig 4.1 Temperature Dependence of Slip in Stoichiometric Single Crystals.

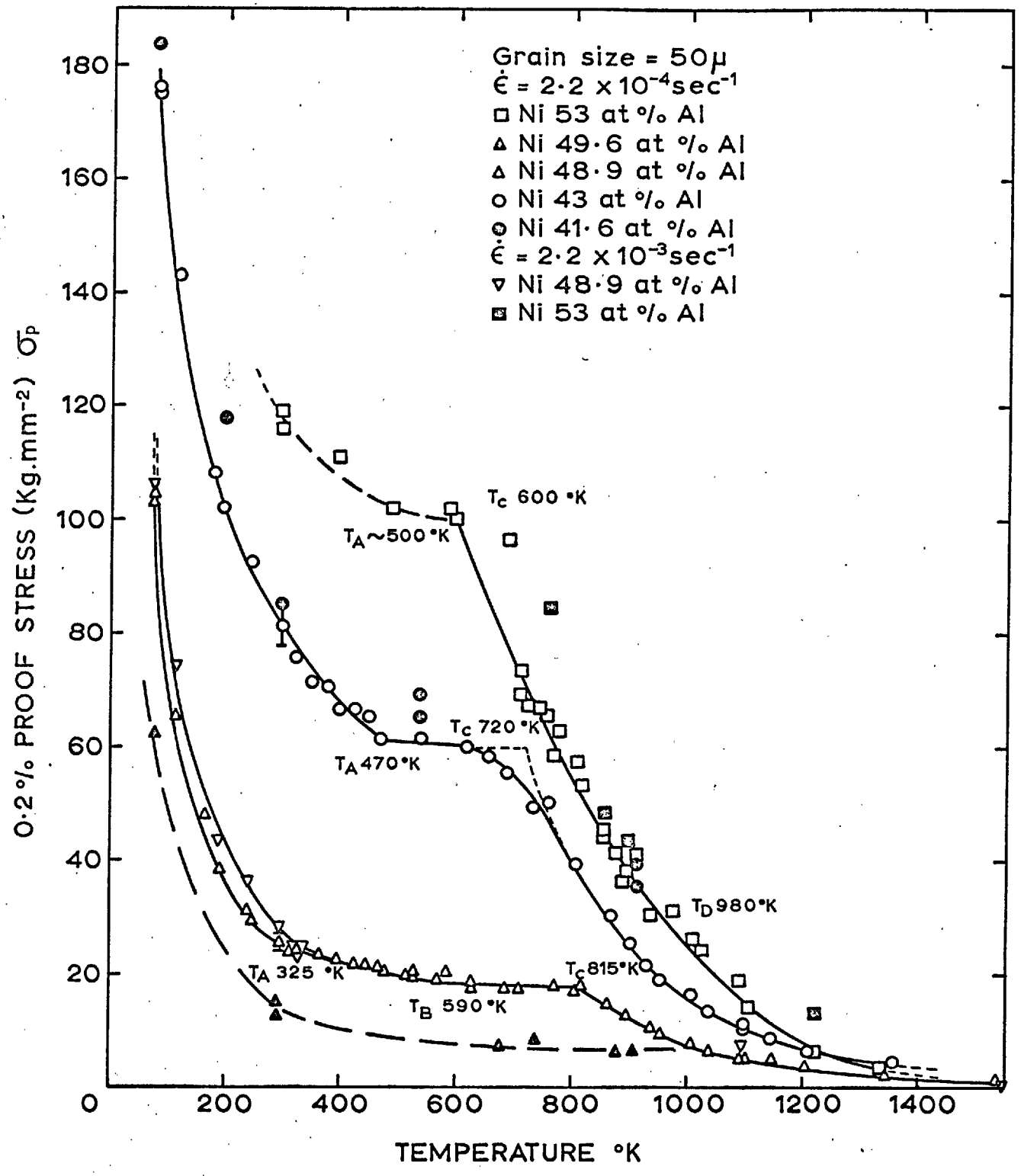

Fig 4.2 Temperature Dependence of Flow Stress of Polycrystalline NiAl.

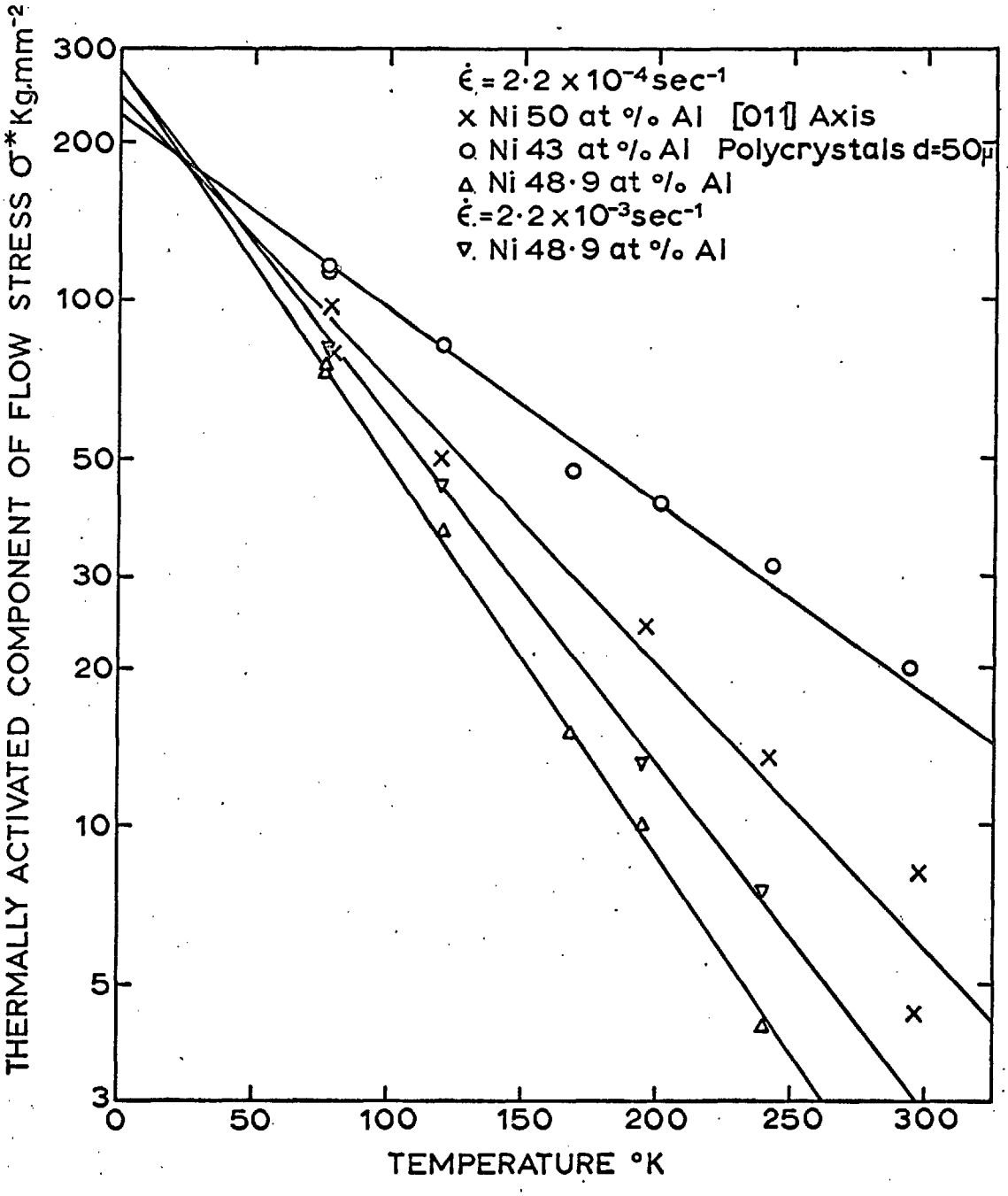

Fig 4.3 Temperature and Strain Rate Dependence of Flow Stress at Low Temperature.

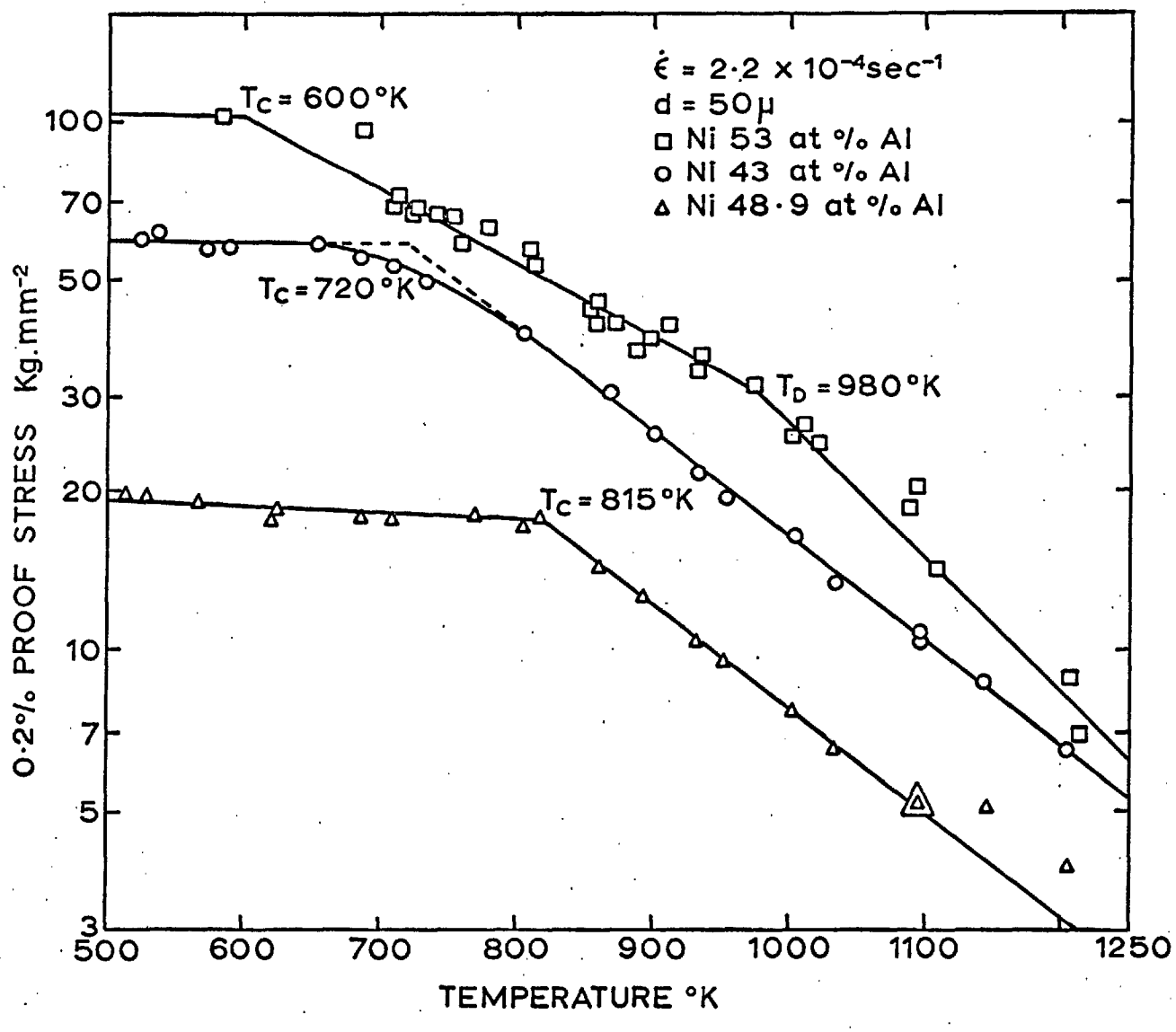

Fig 4.4 Flow Stress - Temperature Relationships at High Temperatures.

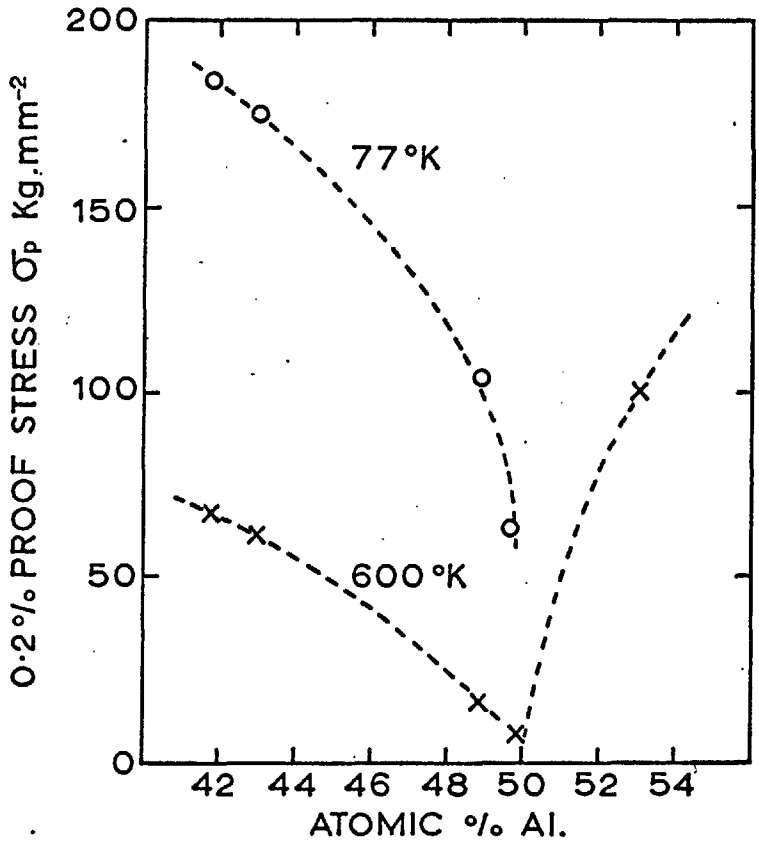

Fig 4.5 Variation of Flow Stress with Composition.

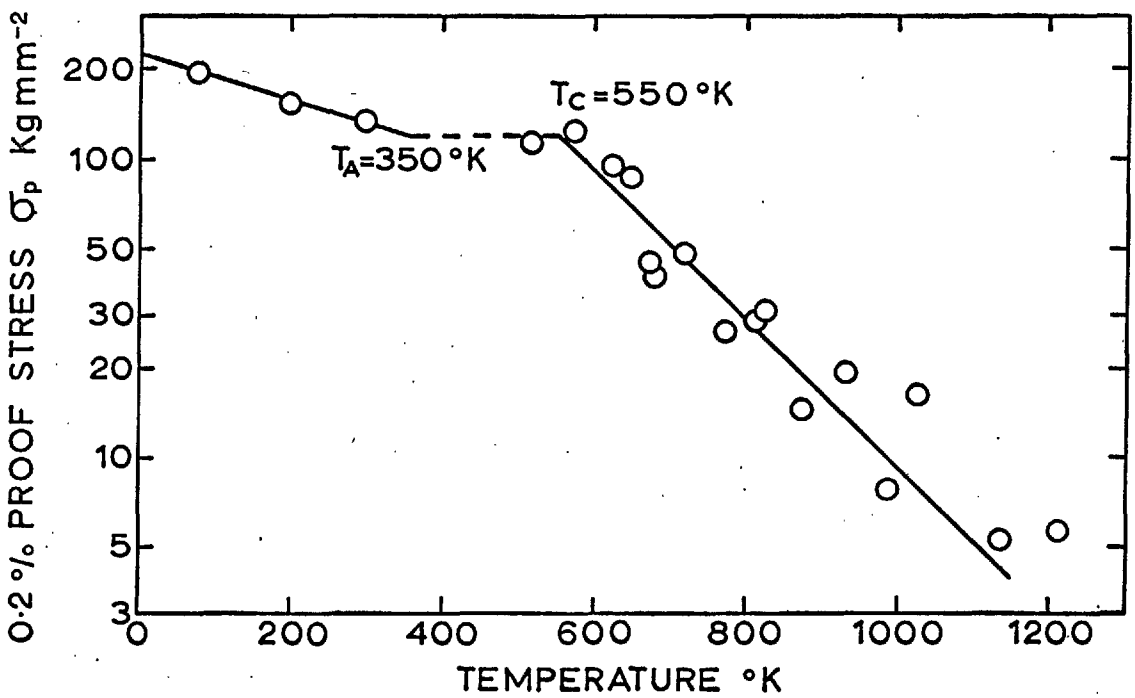

Fig 4.6 Temperature Dependence of Flow Stress of Single Crystals of Hard Orientation.

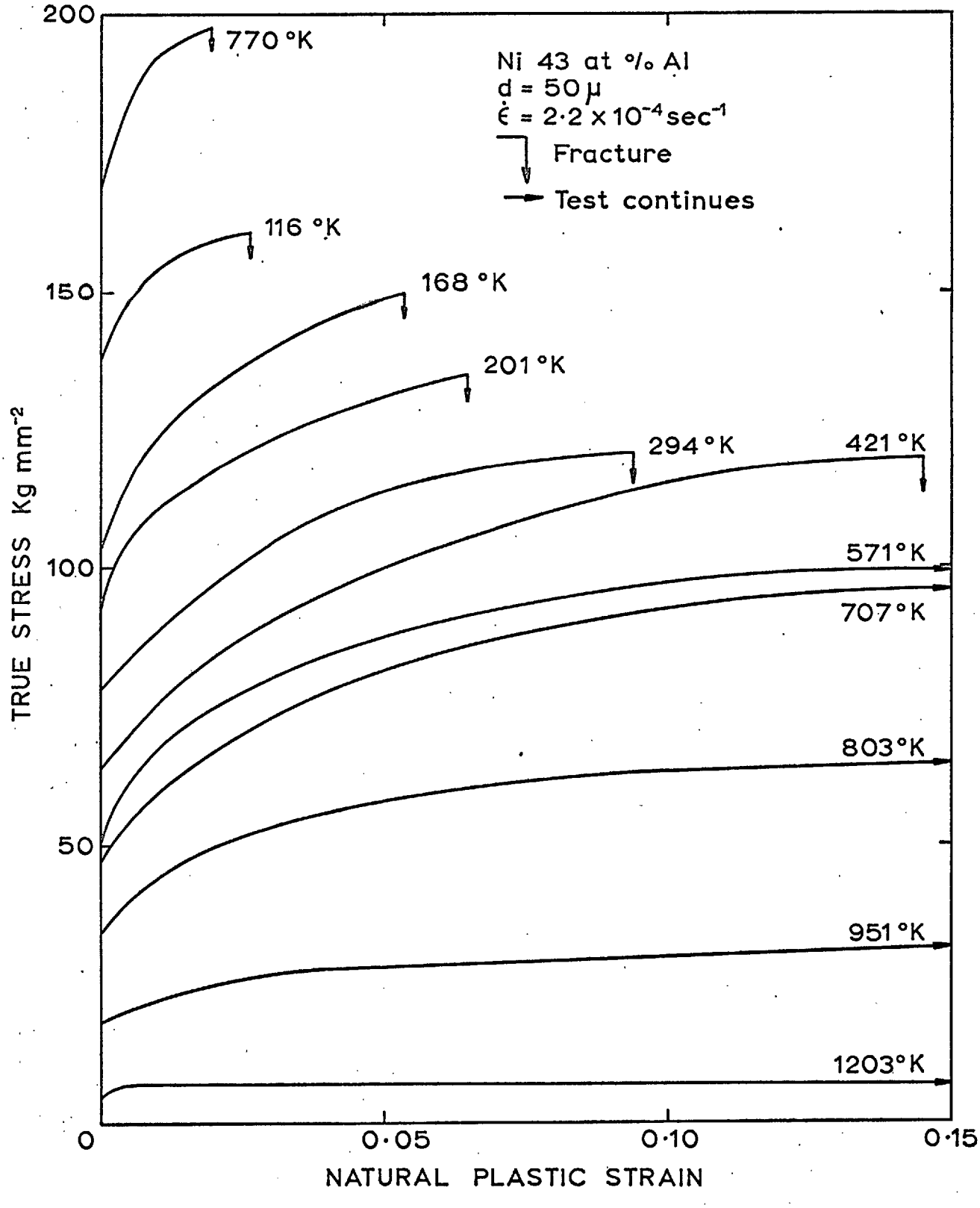

Fig 4.7 Typical Stress-Strain Curves for Nickel-Rich NiAl.

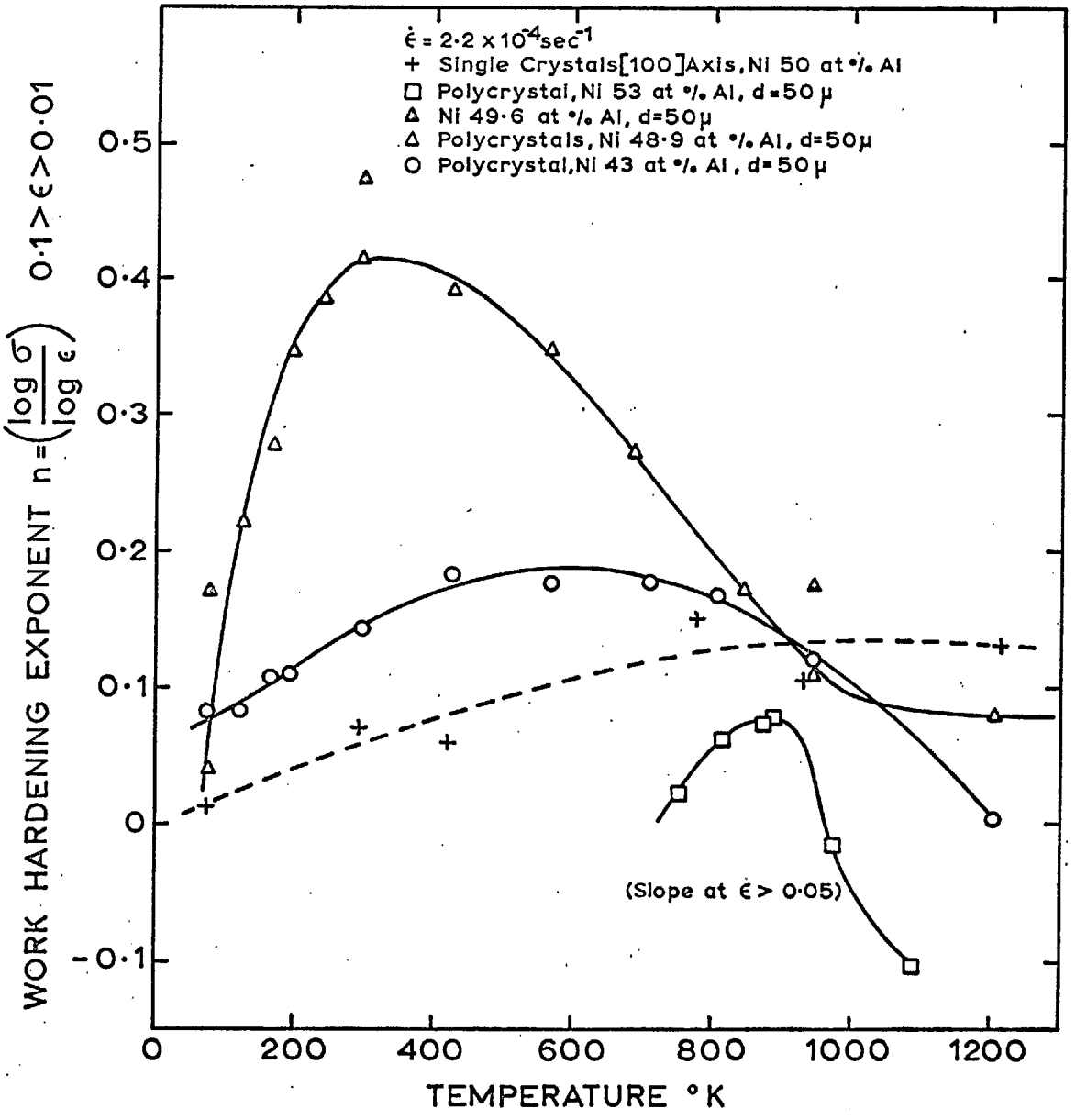

Fig 4.8 Temperature Dependence of the Work Hardening Exponent.

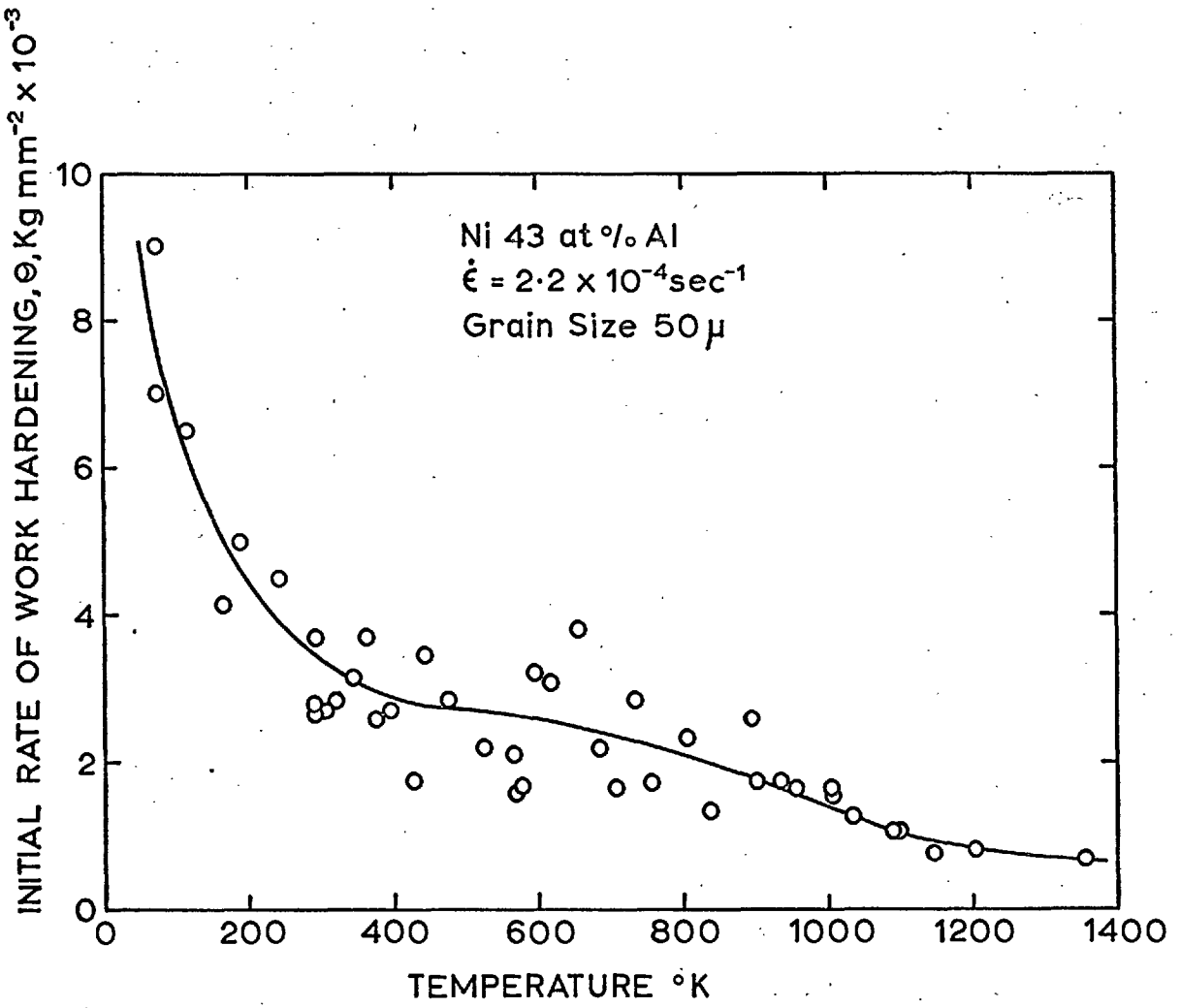

Fig 4.9 Temperature Variation of Initial Rate of Work Hardening with Temperature.

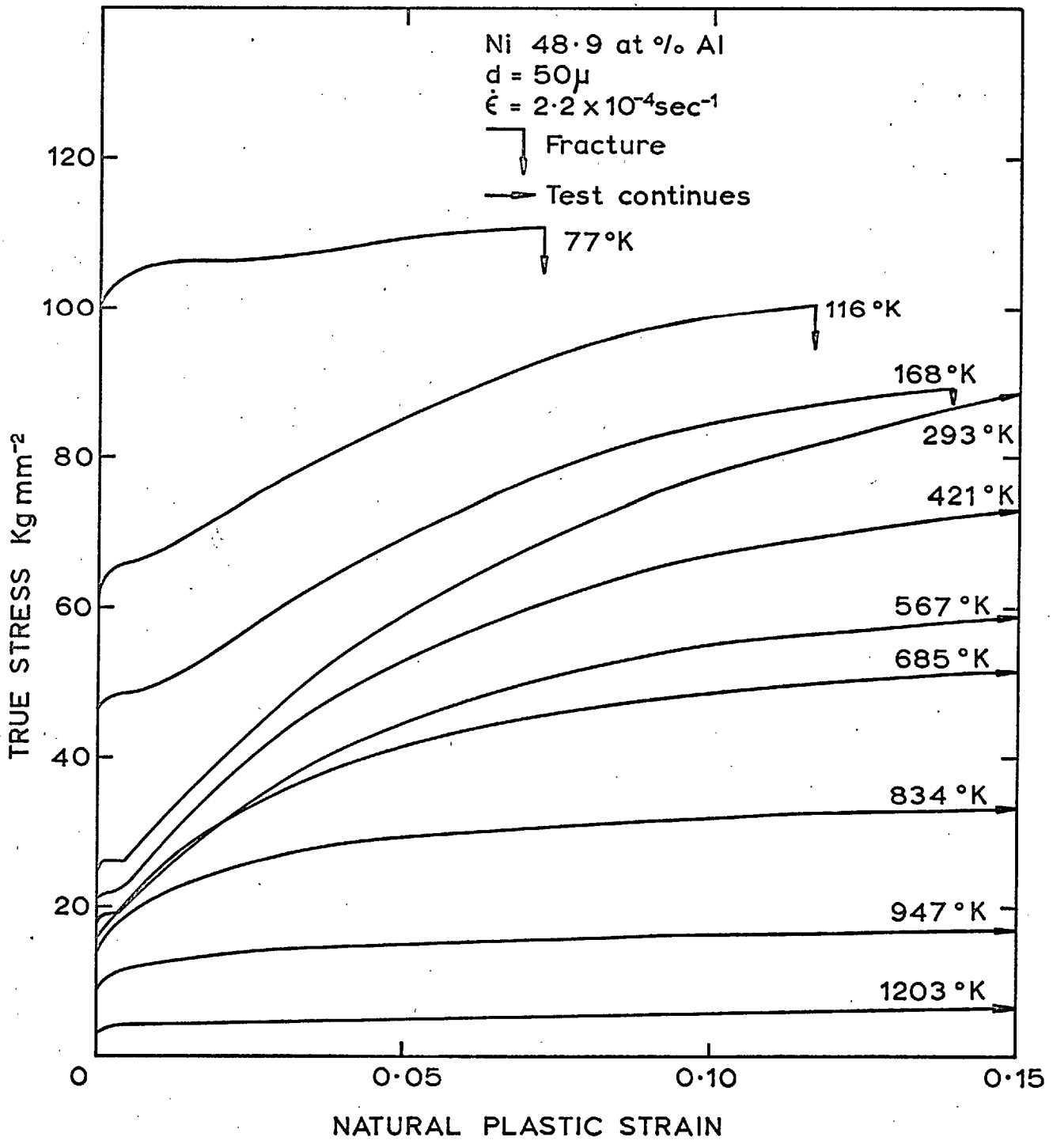

Fig 4.10 Typical Stress-Strain Curves for Near-Stoichiometric NiAl.

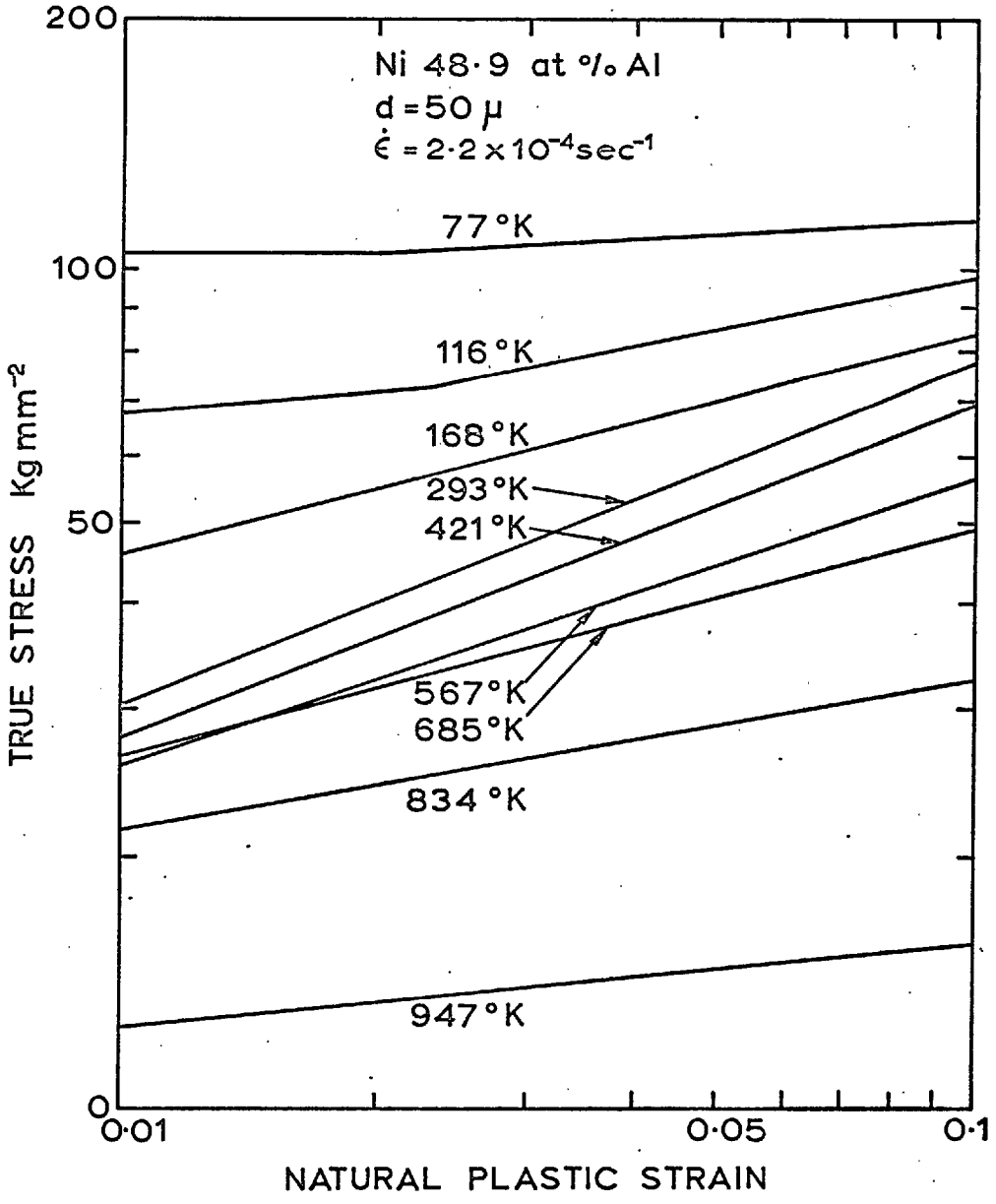

Fig 4.11 Typical Logarithmic Stress-Strain Curves.

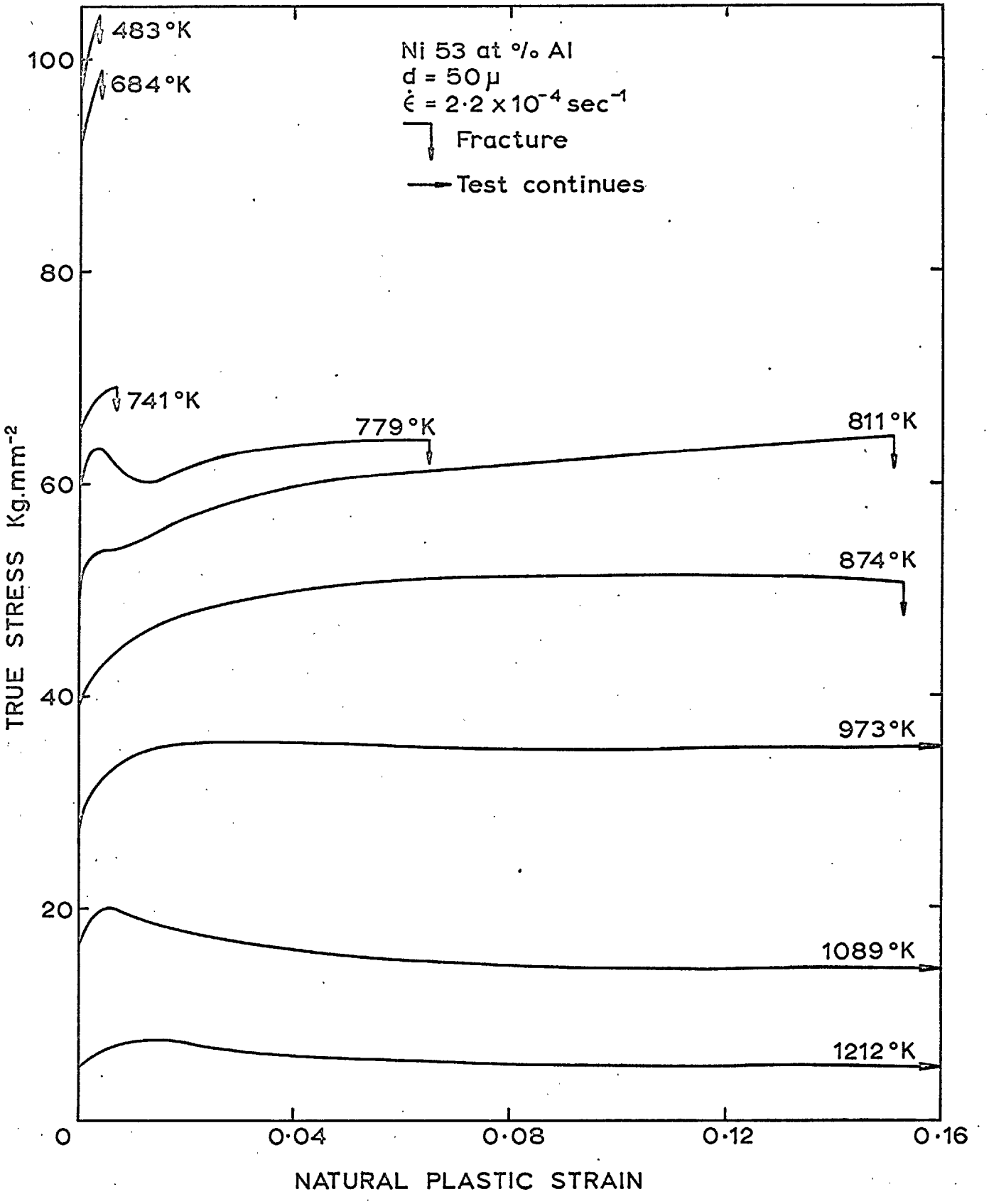

Fig 4.12 Typical Stress-Strain Curves for Aluminium-Rich NiAl.

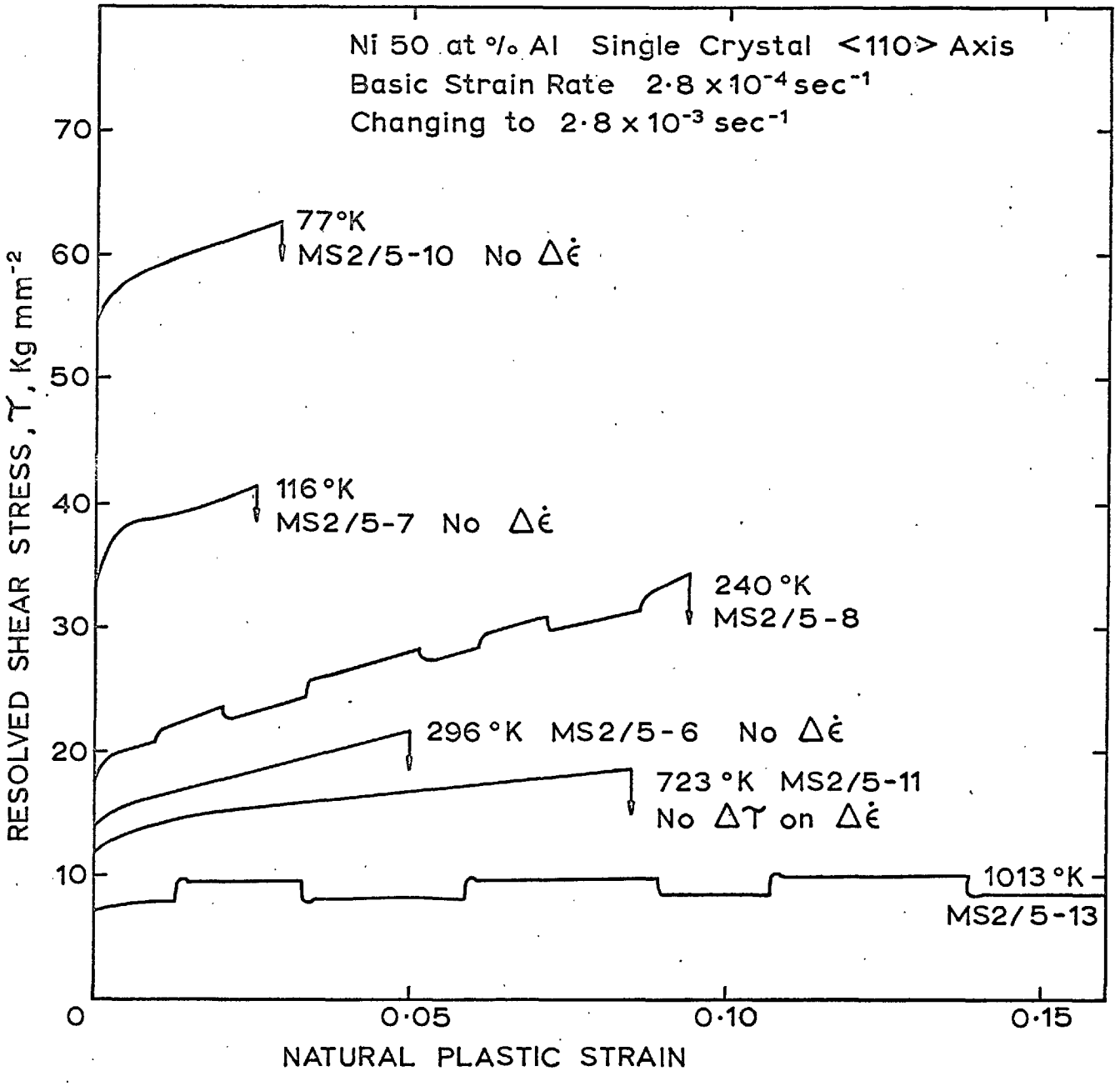

Fig 4.13 Typical Stress-Strain Curves for Stoichiometric Single Crystal of Soft Orientations.

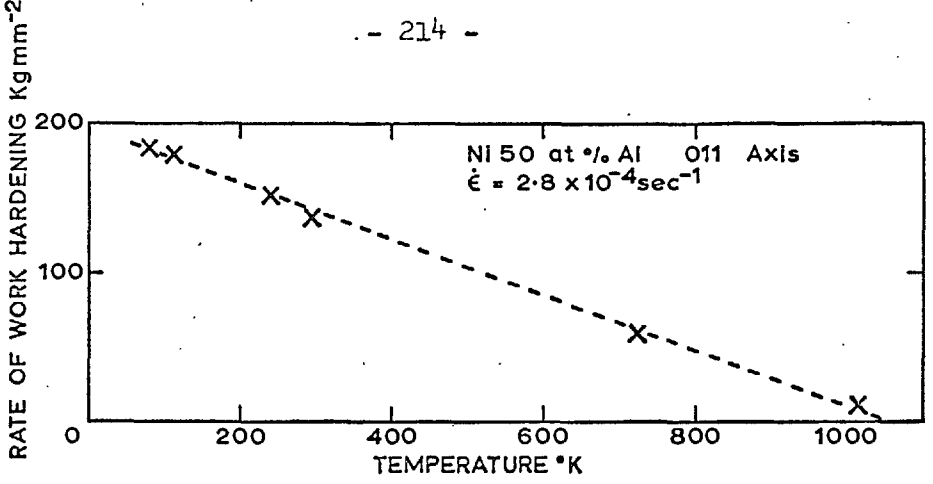

Fig 4.14 Linear Work Hardening Rates in 'Soft' Single Crystals.

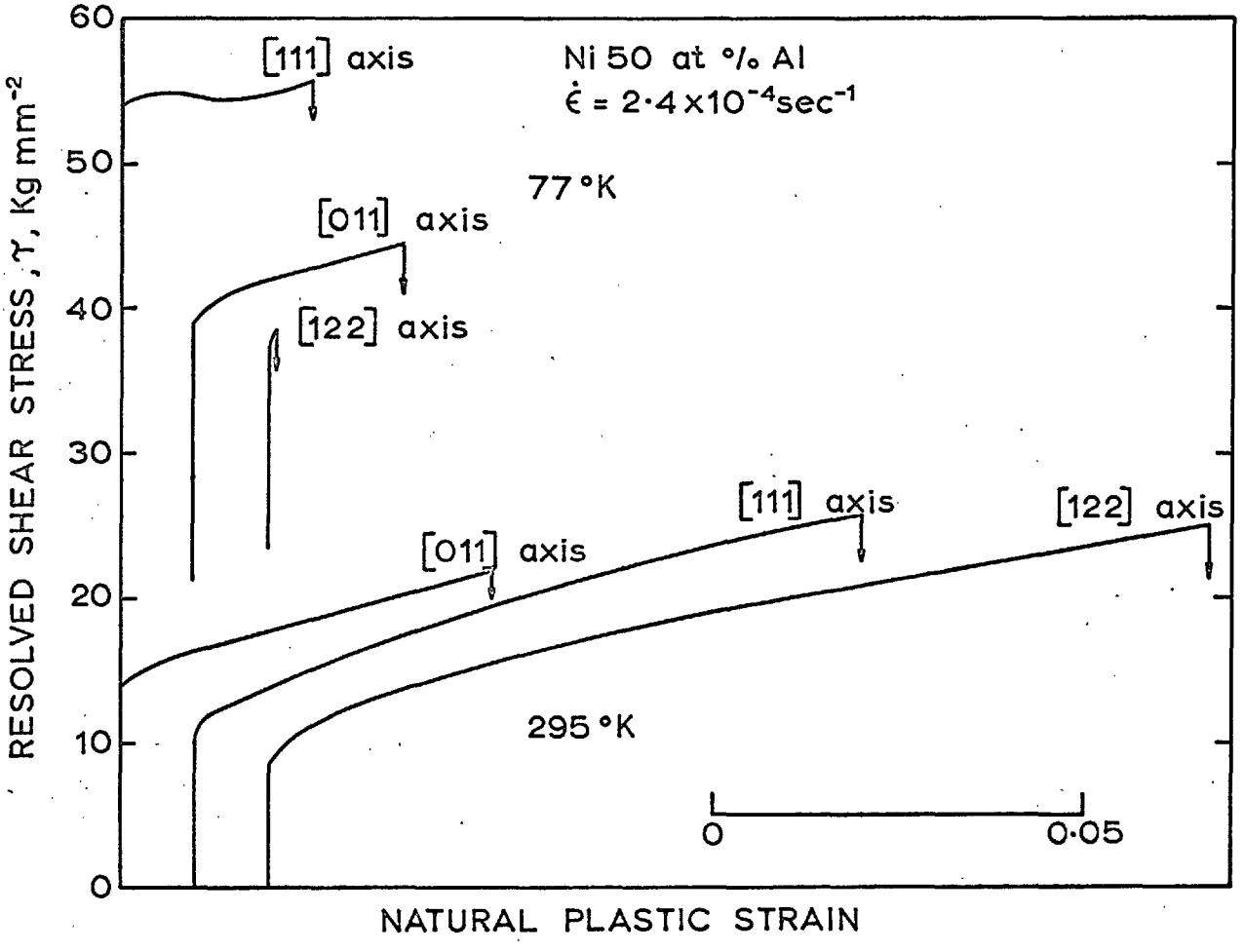

Fig 4.15 Orientation Dependence of Stress-Strain Curves of Stoichiometric NiAl.
(Stress Resolved on observed slip system).

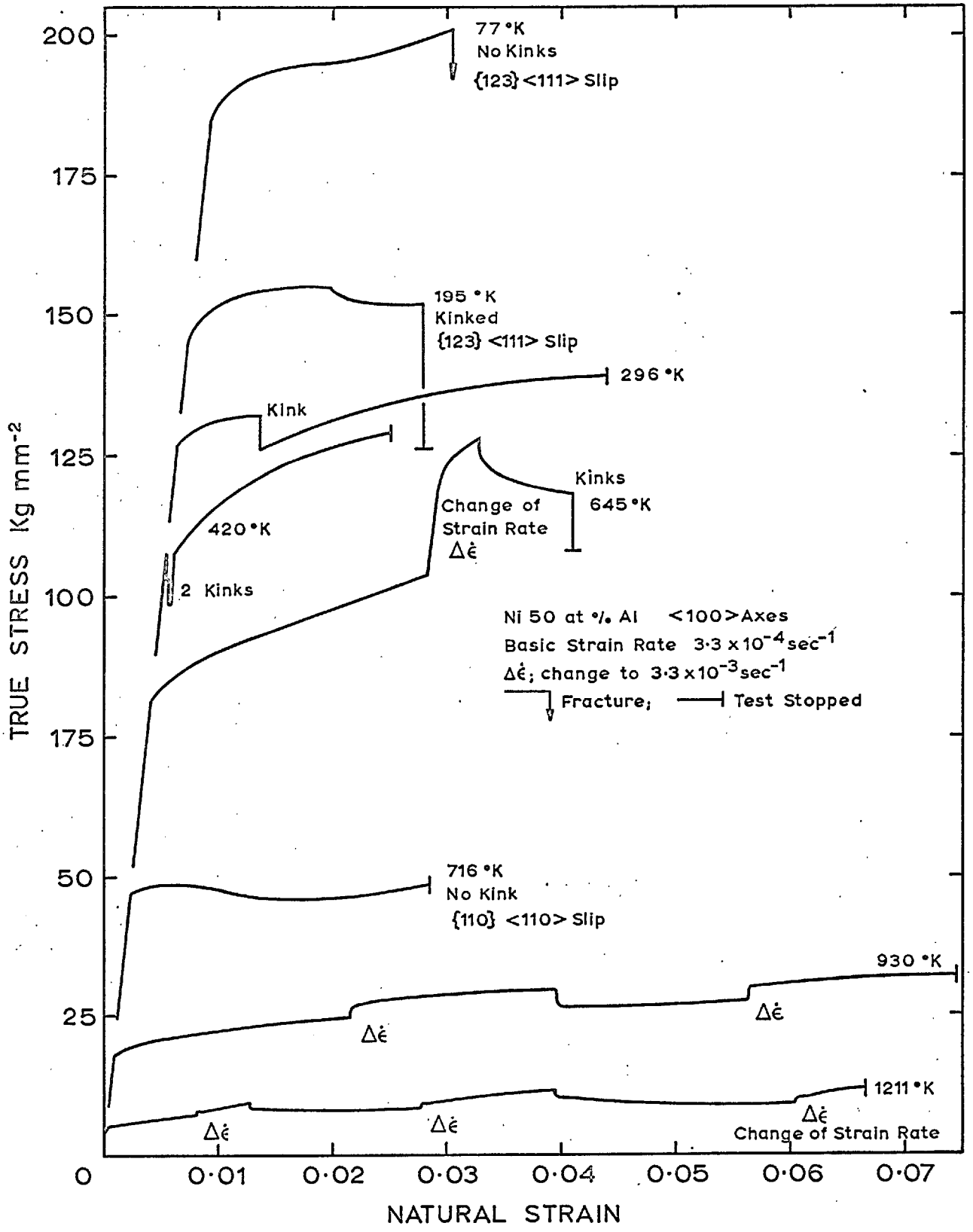

Fig 4.16 Typical Stress Strain Curves of Hard Orientation Single Crystals.

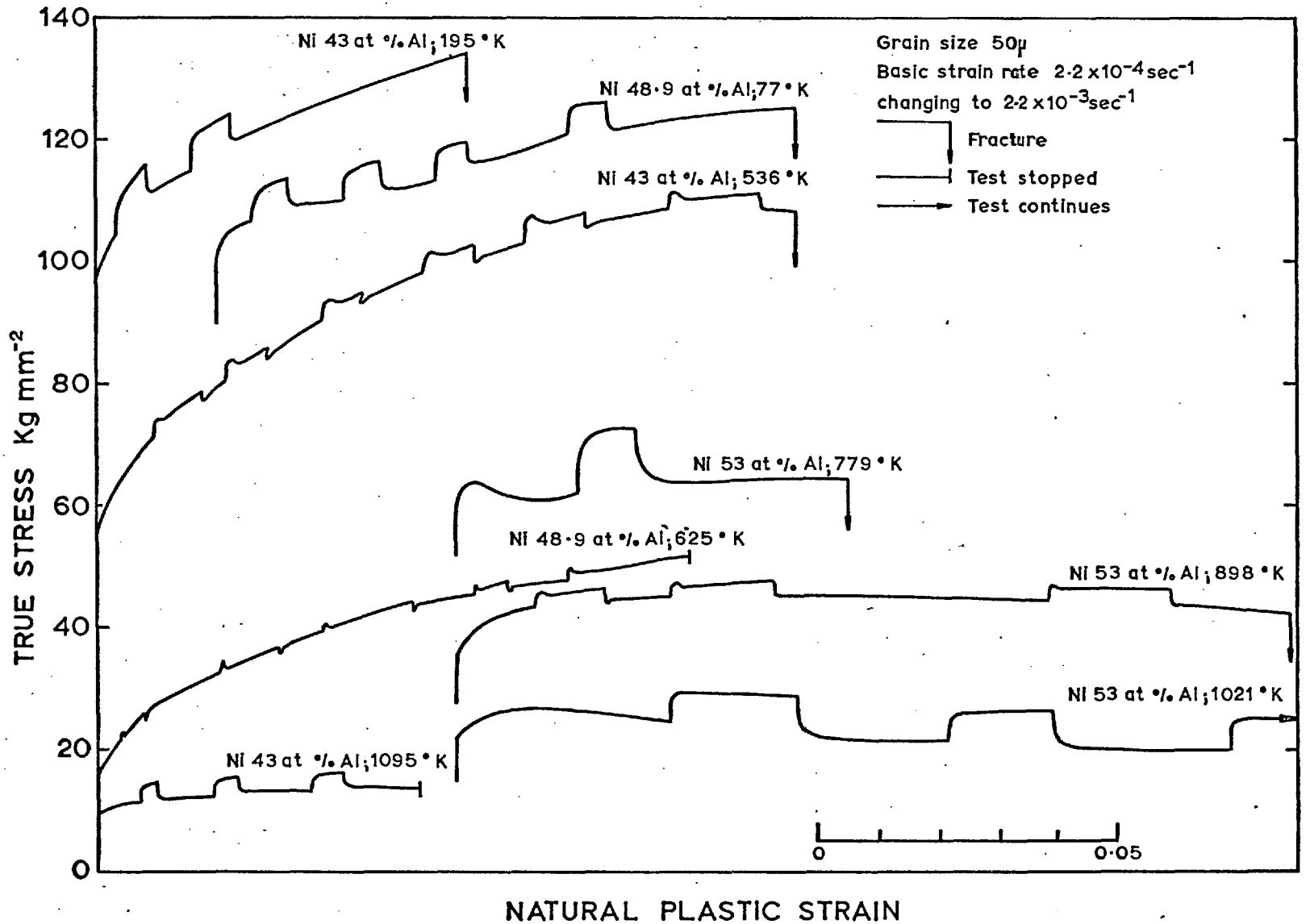

Fig 4.17 Effects of Changes of Strain Rate on the Stress-Strain Curves of Polycrystals.

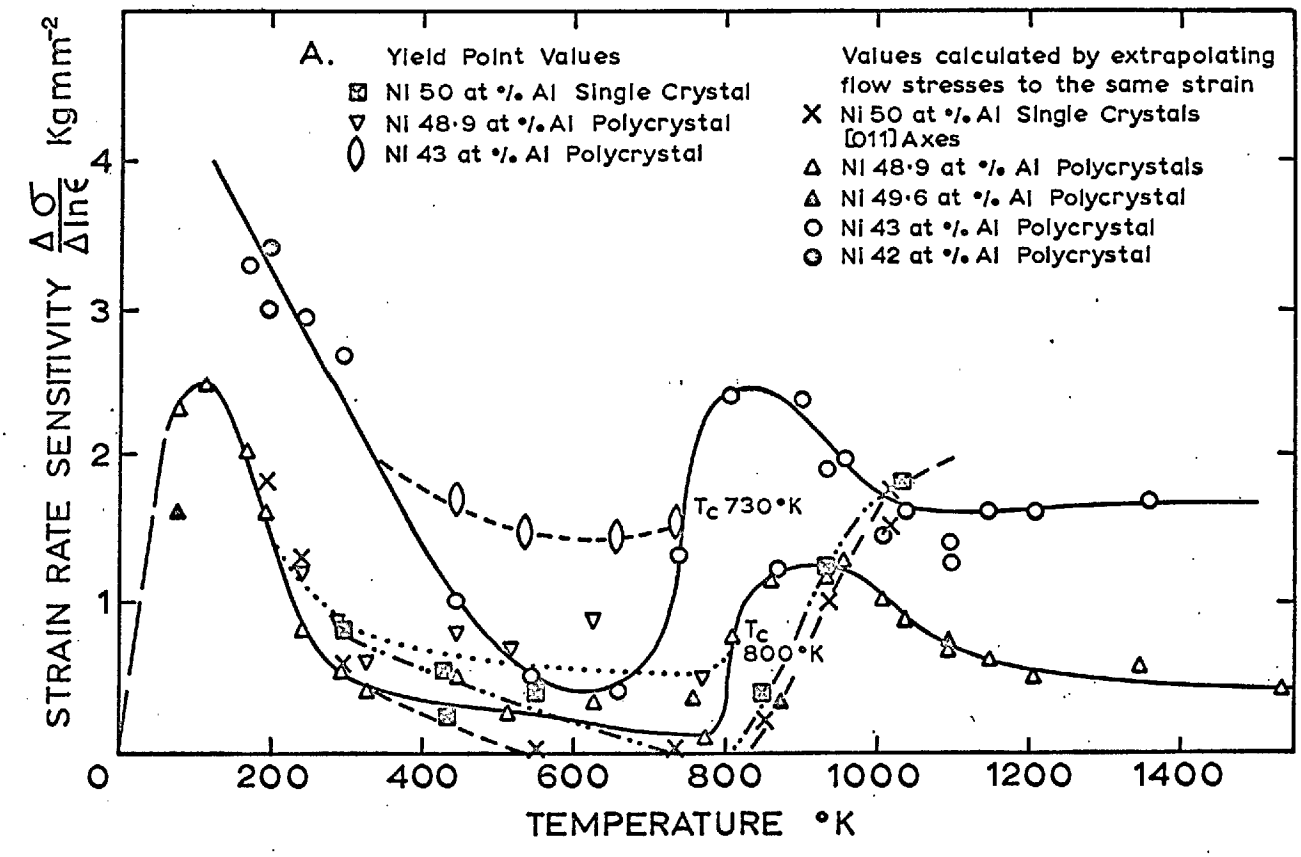

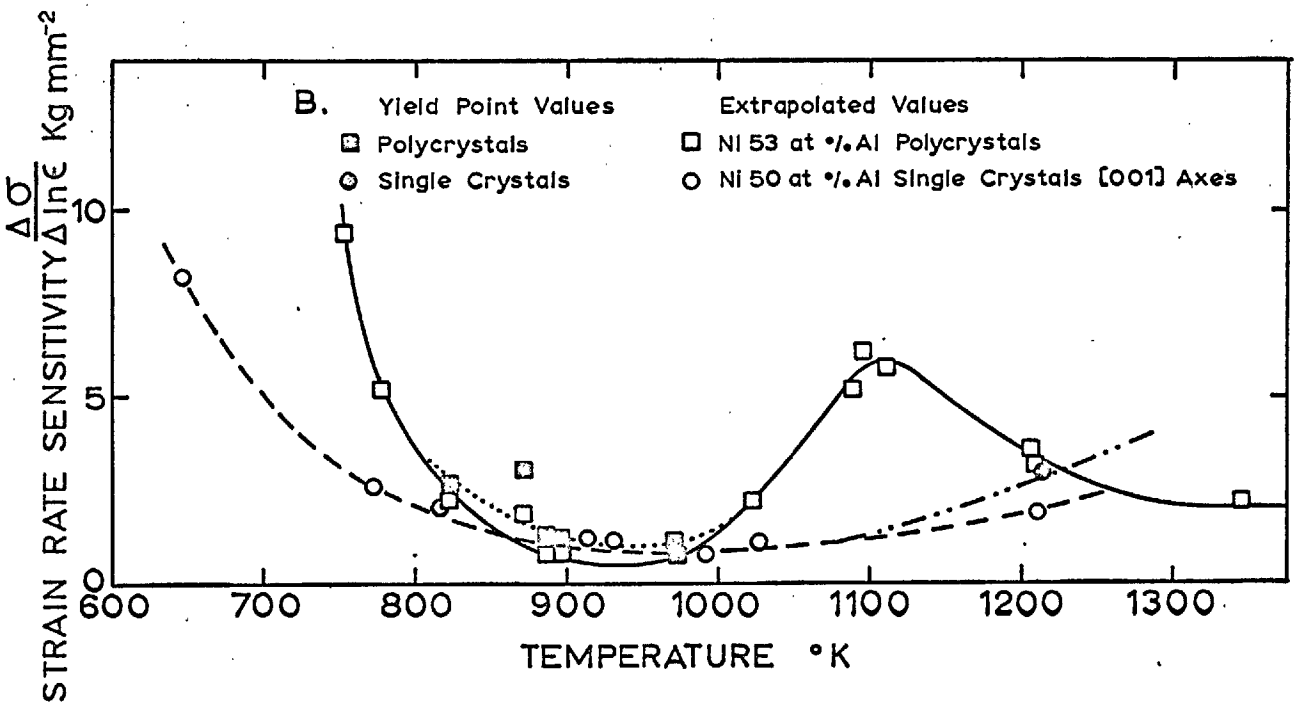

Fig 4.18 Temperature Dependence of Strain-Rate Sensitivity.

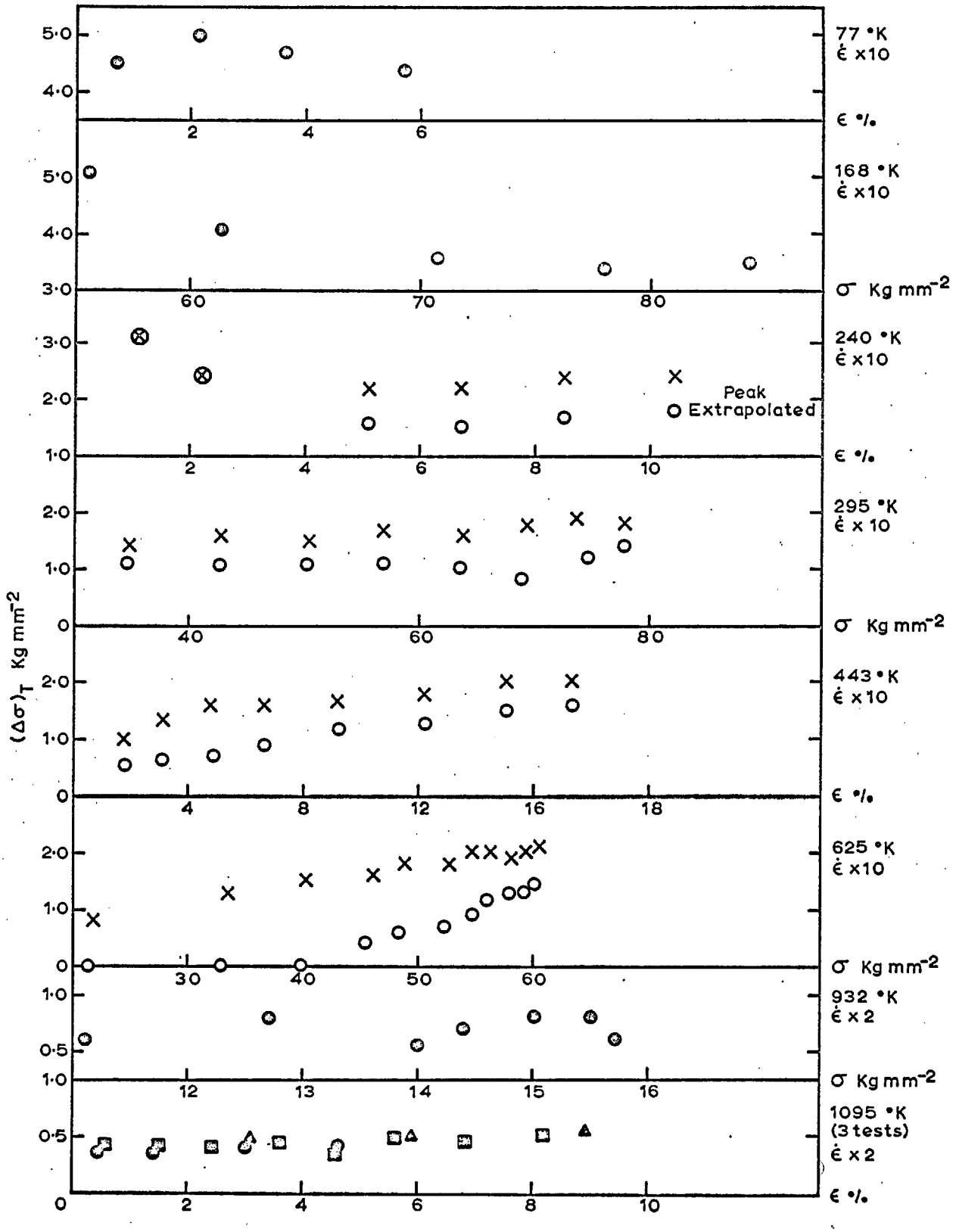

Fig 4.19 Typical Plots of Changes of Stress on Changing Strain-Rate. (Ni 48.9 at % Al Polycrystals).

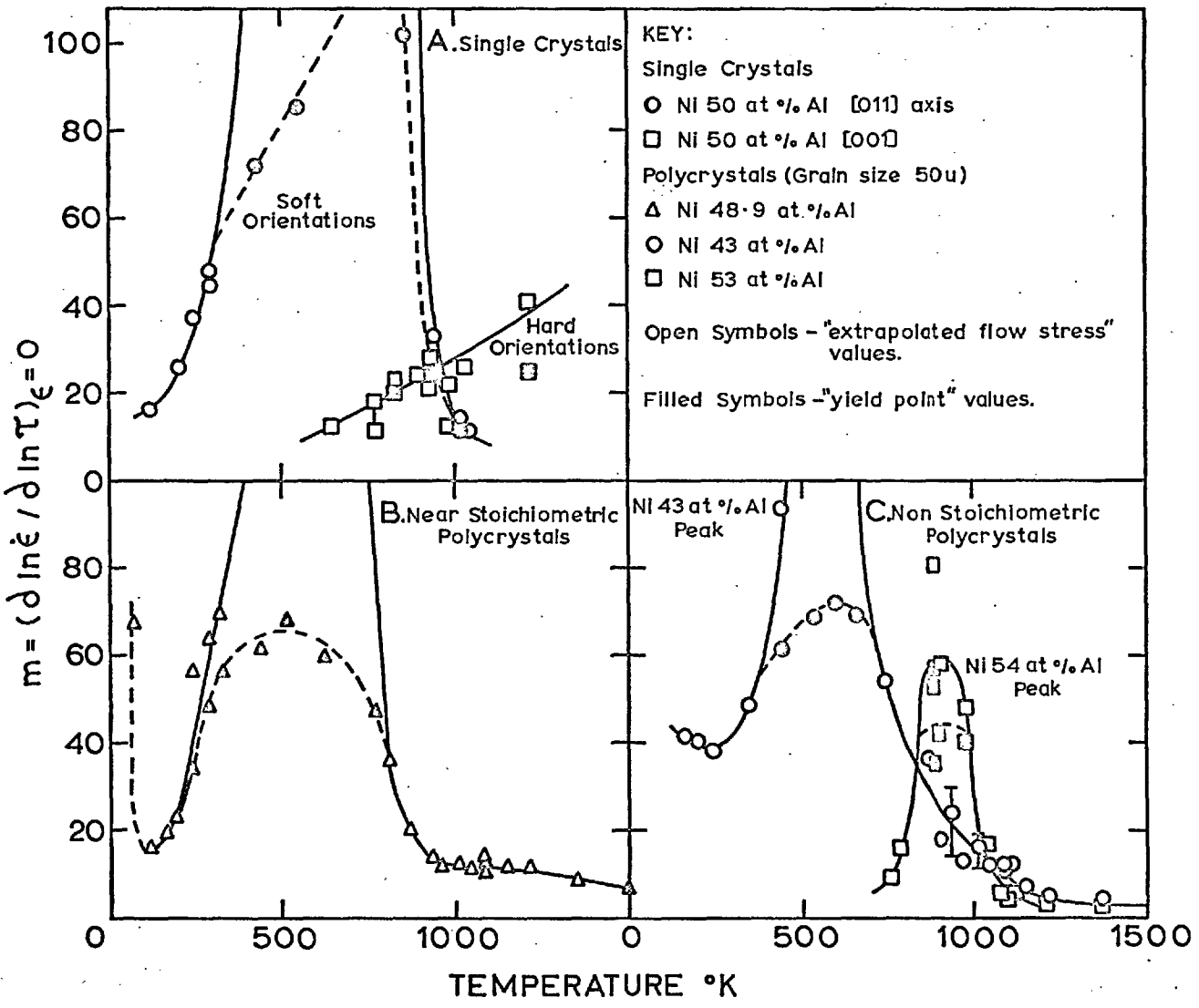

Fig 4.20 Temperature Dependence of m.

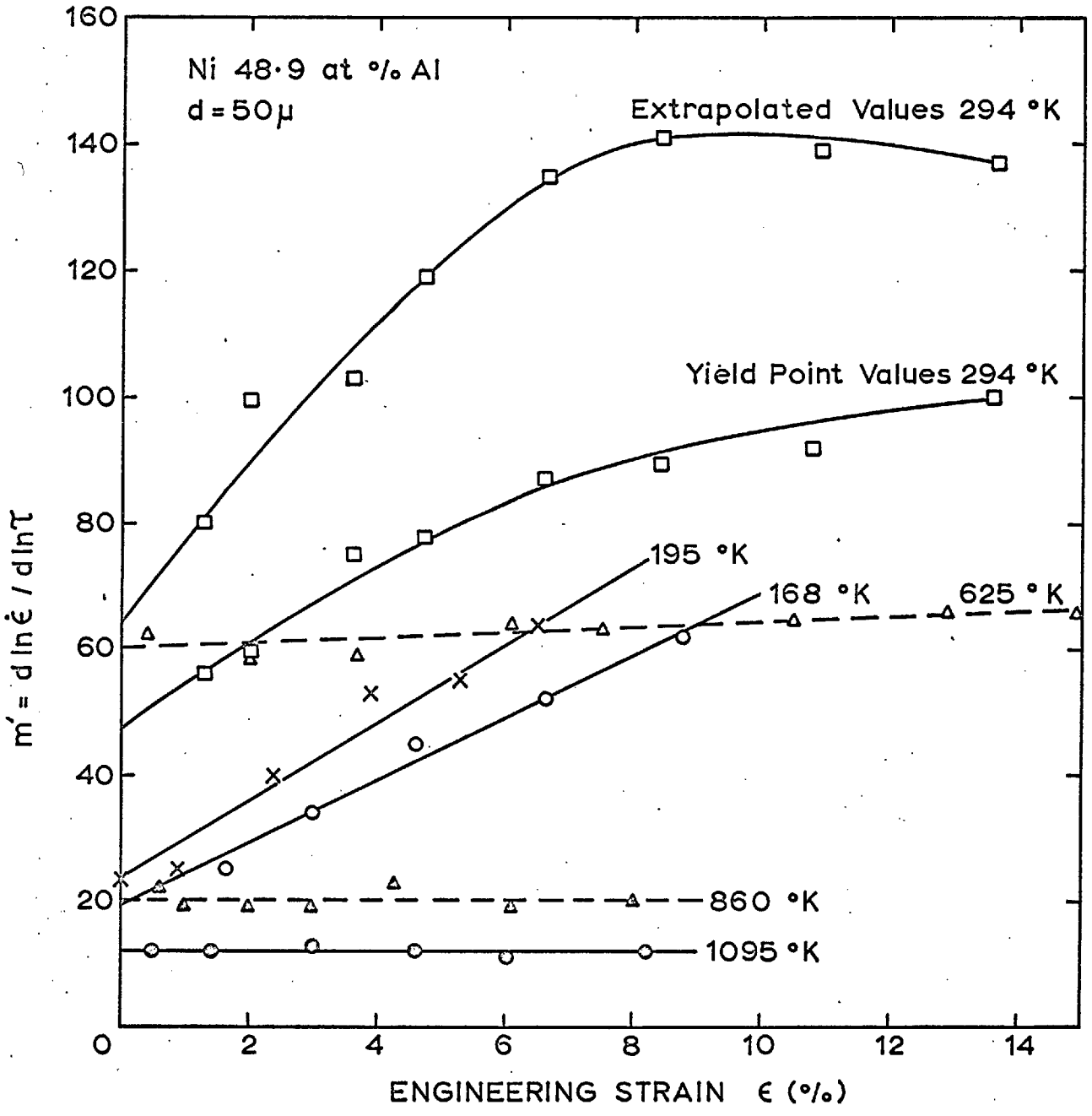

Fig 4.21 Typical variations of m' with strain.

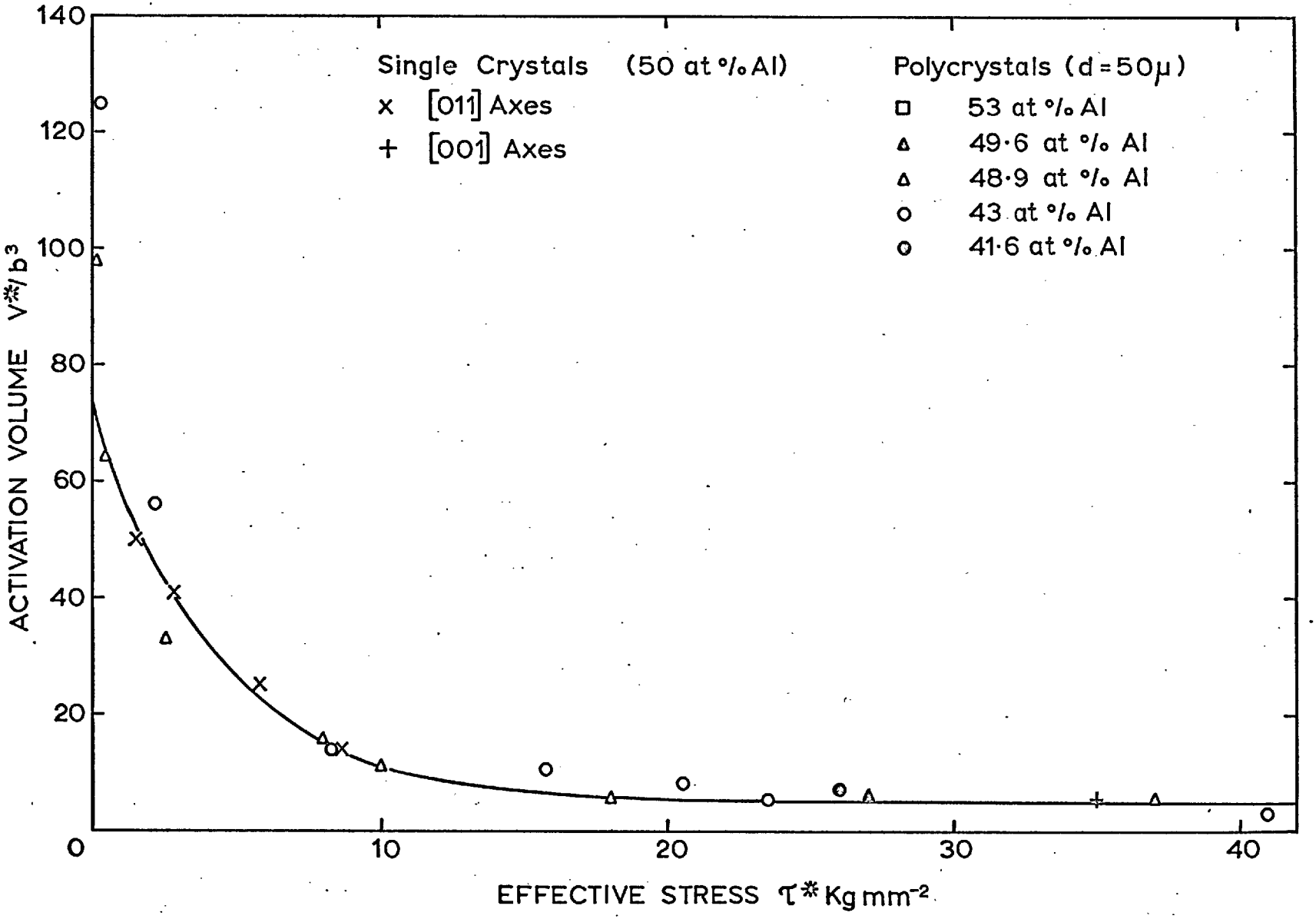

Fig 4.22 Variation of the Activation Volume with Stress at Low Temperature.

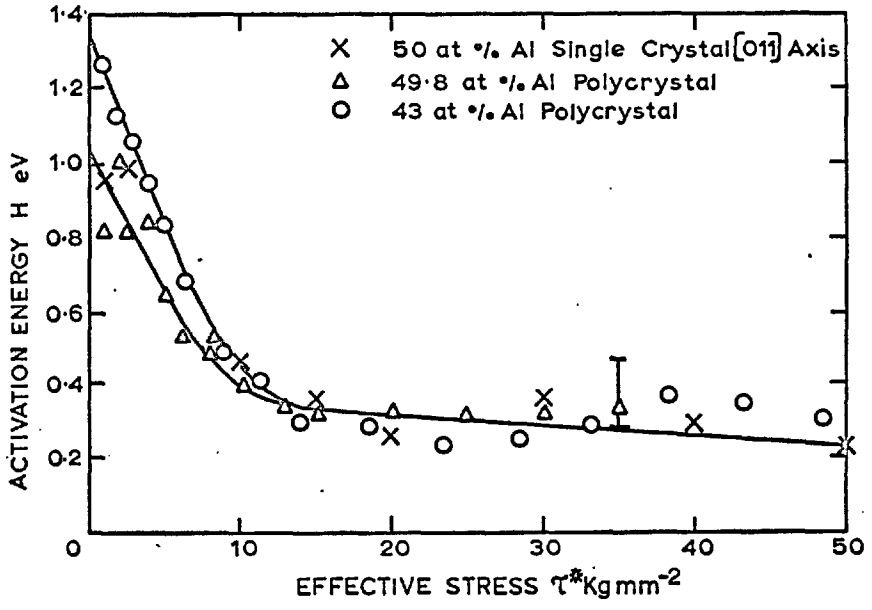

Fig 4.23 Stress Dependence of the Activation Energy at Low Temperature ($T < T_A$)

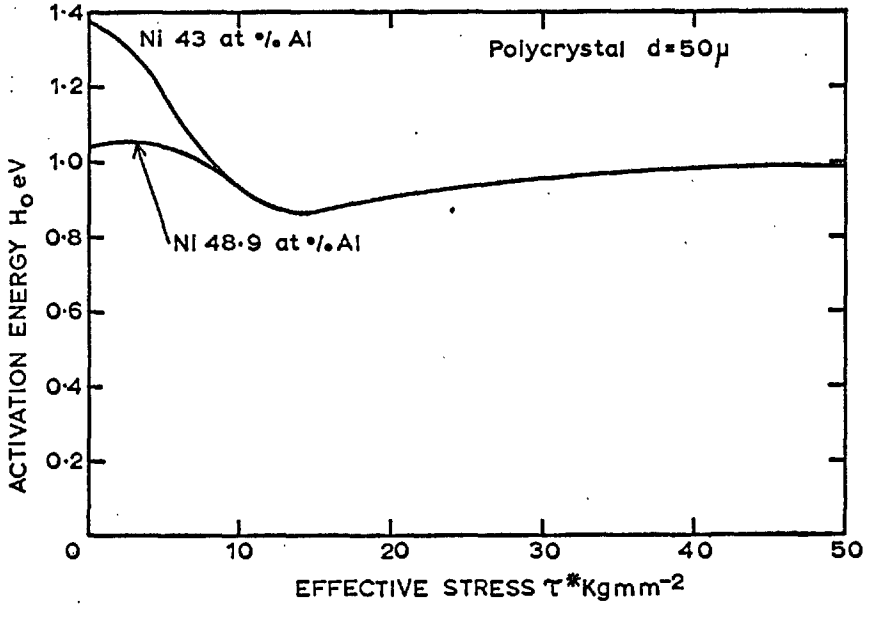

Fig 4.24 Variation of Activation Energy at Zero Stress with Stress at Low Temperatures ($T < T_A$)

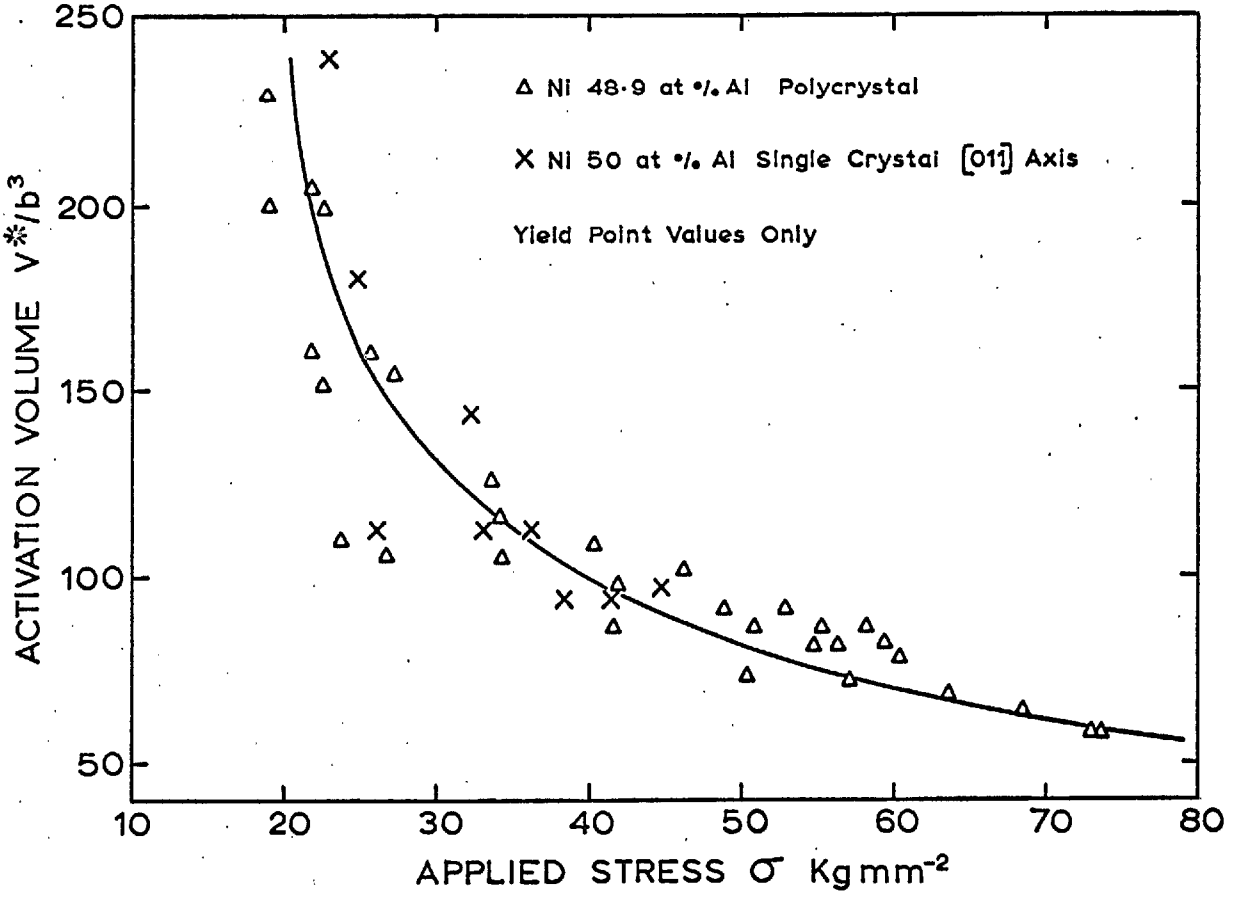

Fig 4.25 Activation Volumes between T_A and T_c.

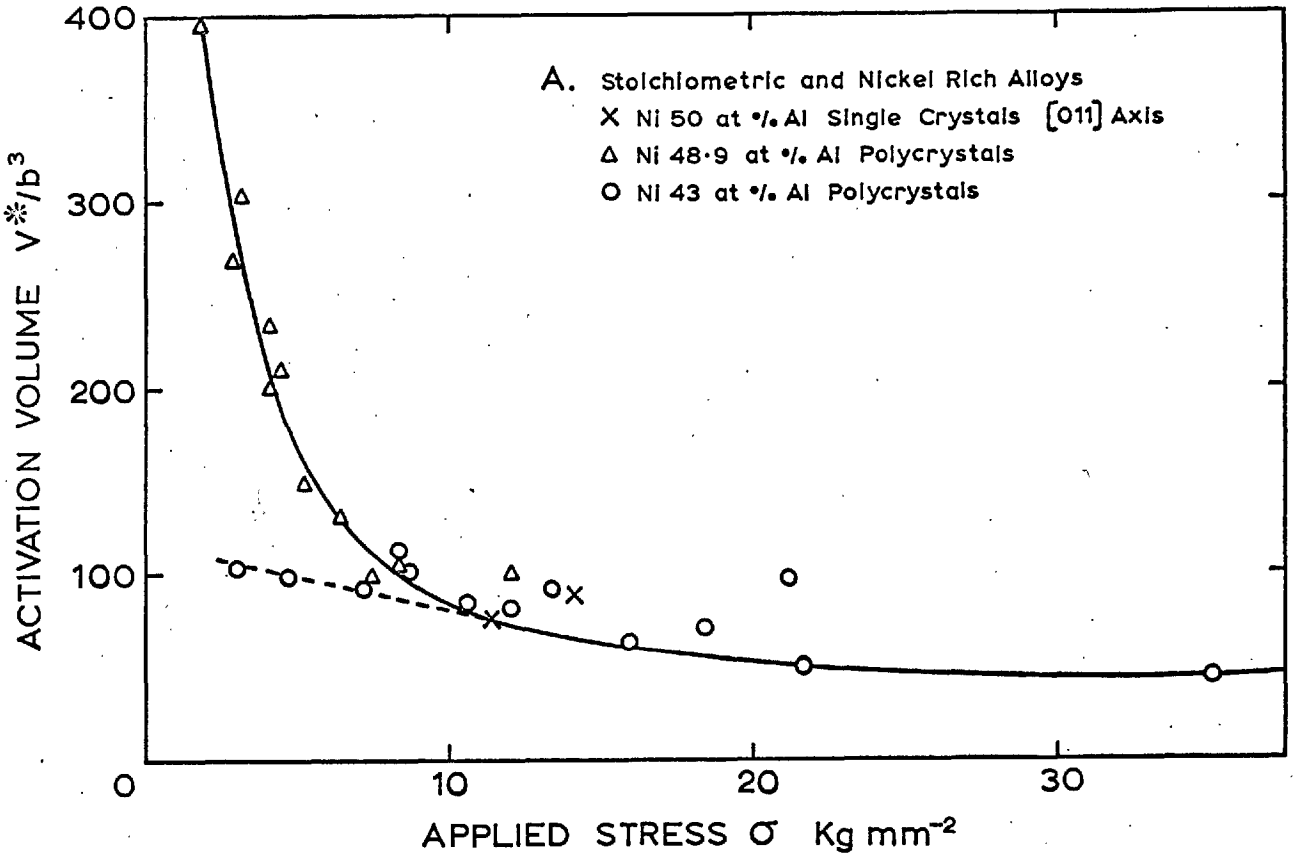

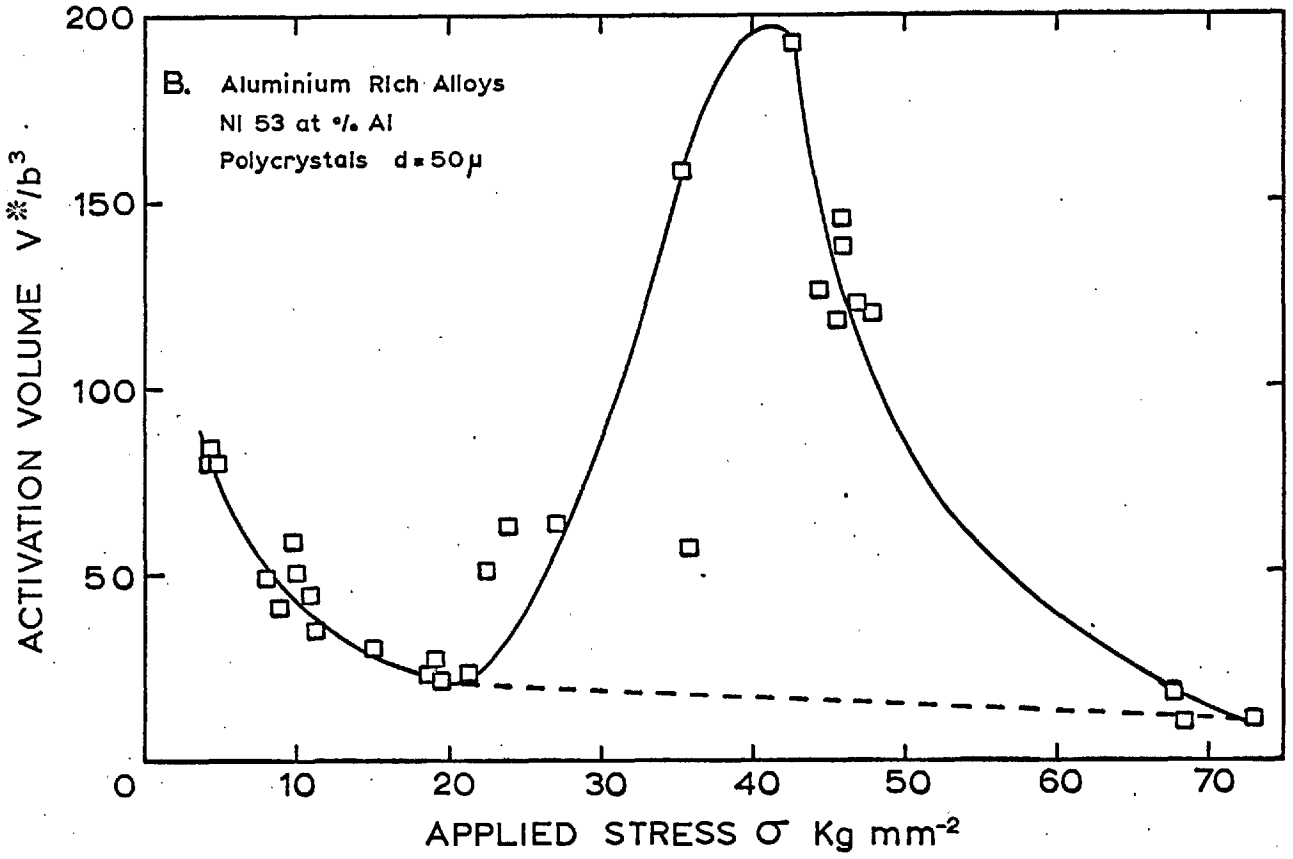

Fig 4.26 Activation Volumes at High Temperatures.

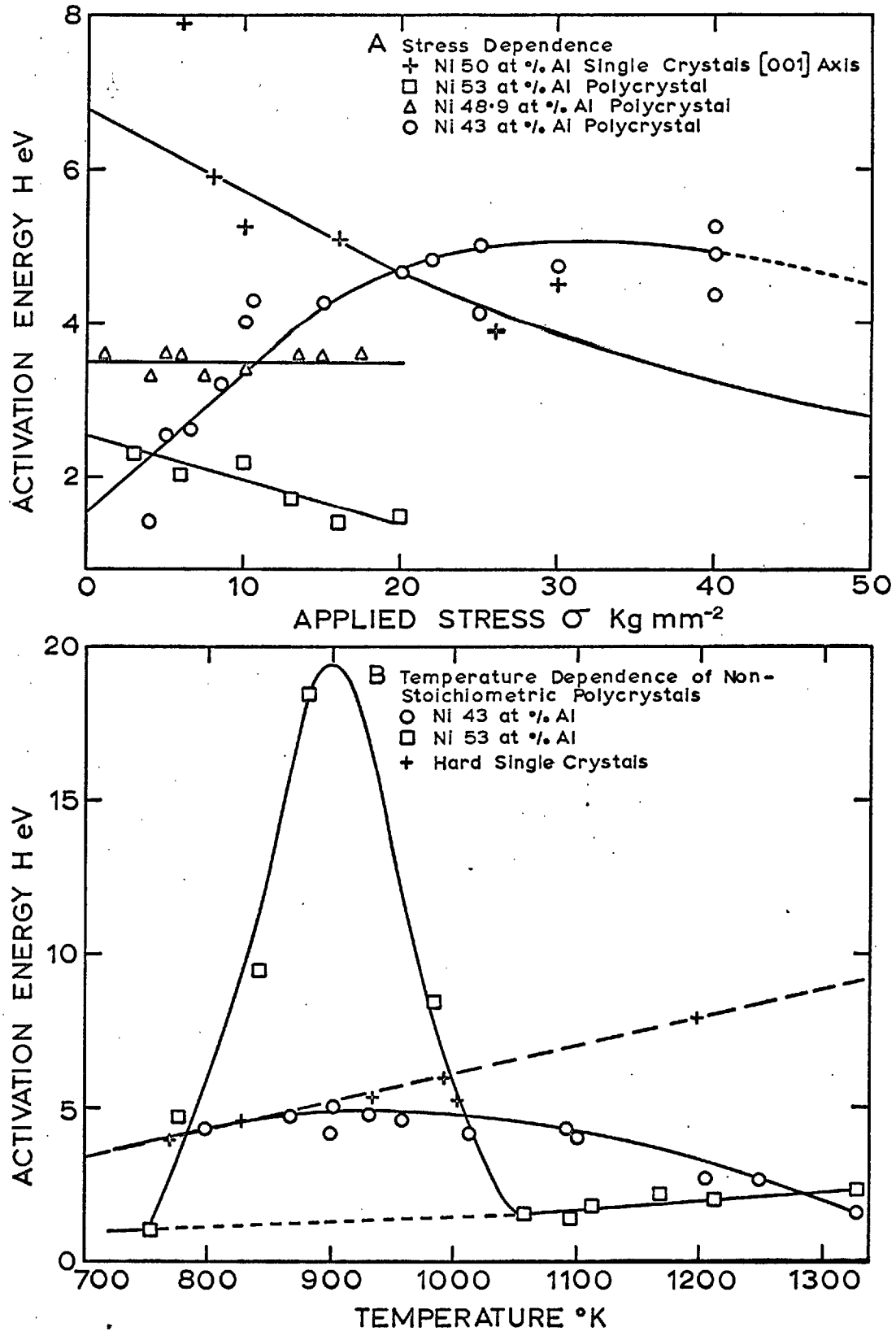

Fig 4.27 Activation Energies at High Temperatures ($T > T_c$)

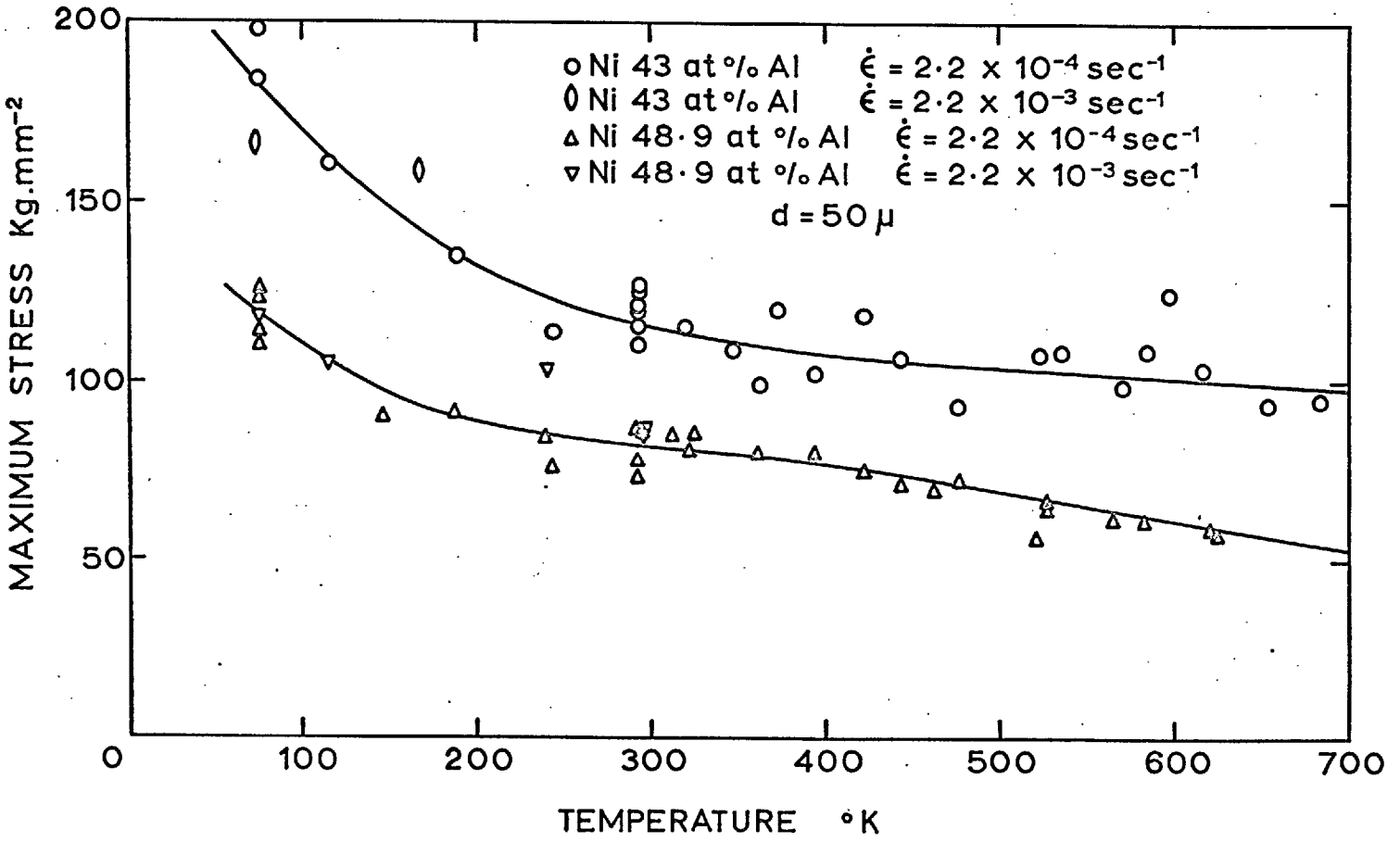

Fig 4.28 Temperature Dependence of Maximum Stress in Compression.

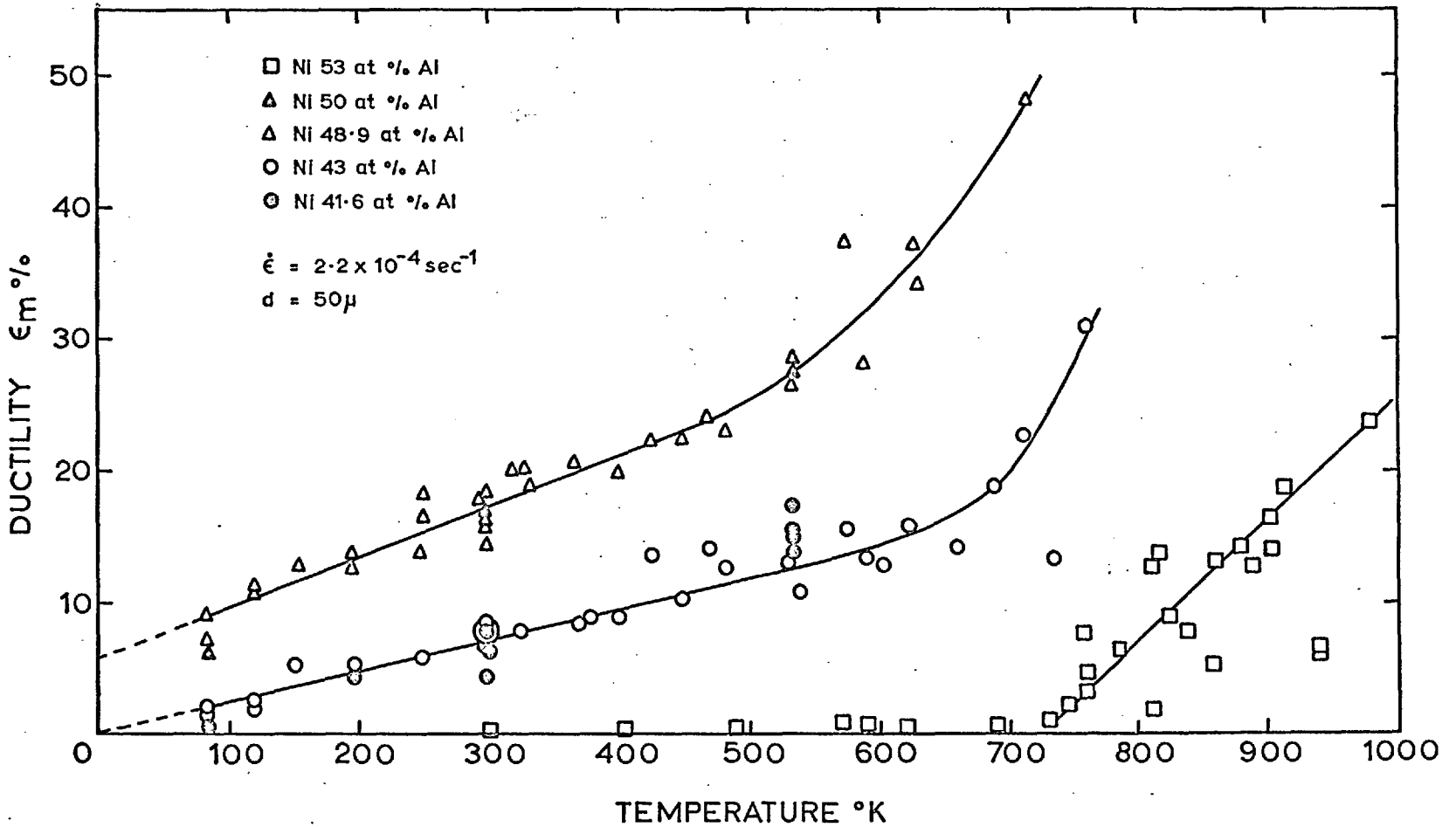

Fig 4.29 Temperature Dependence of Ductility of Polycrystals.

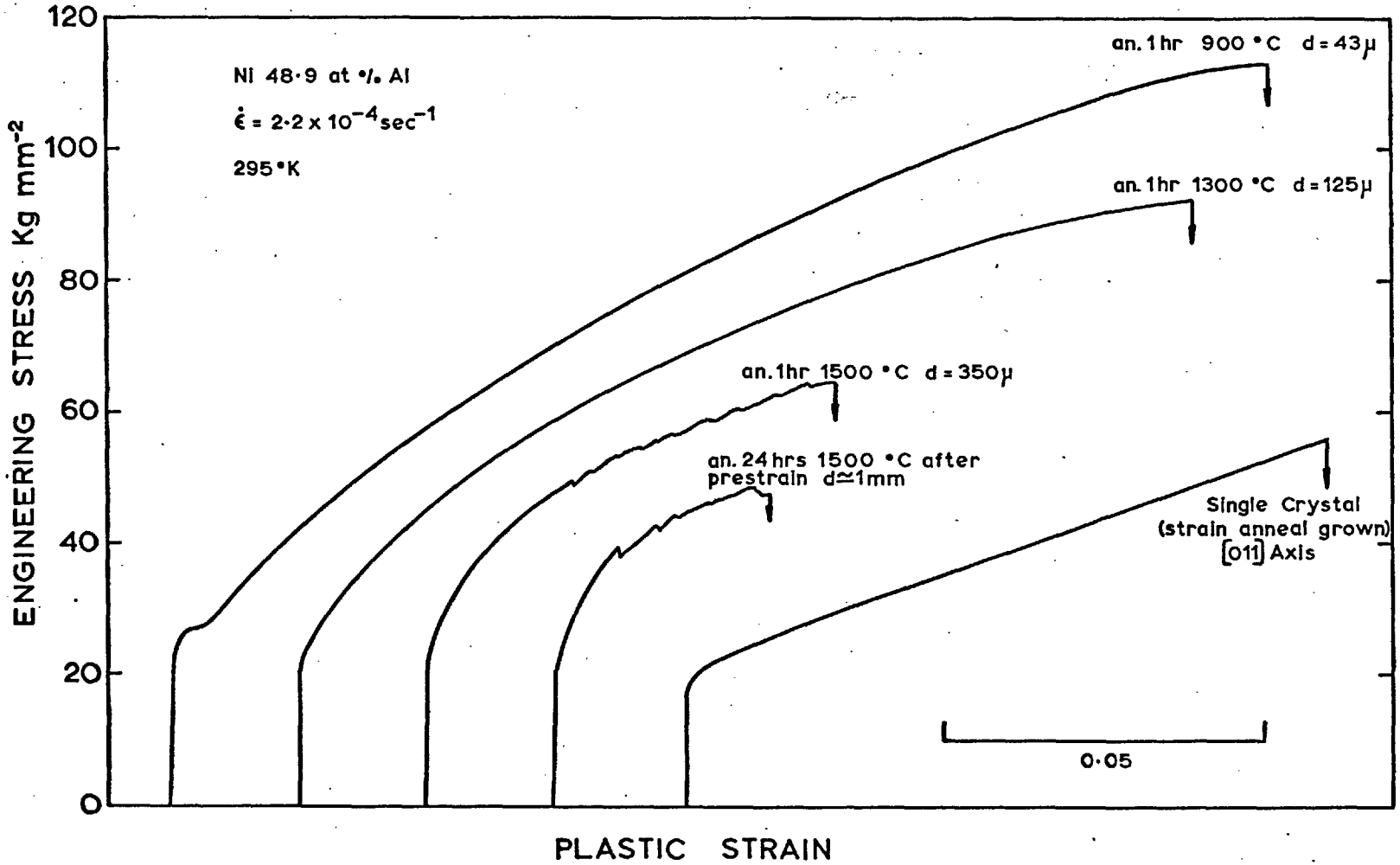

Fig 4.30 Effects of Grain Size and Annealing Treatment on the Stress-Strain Curve.

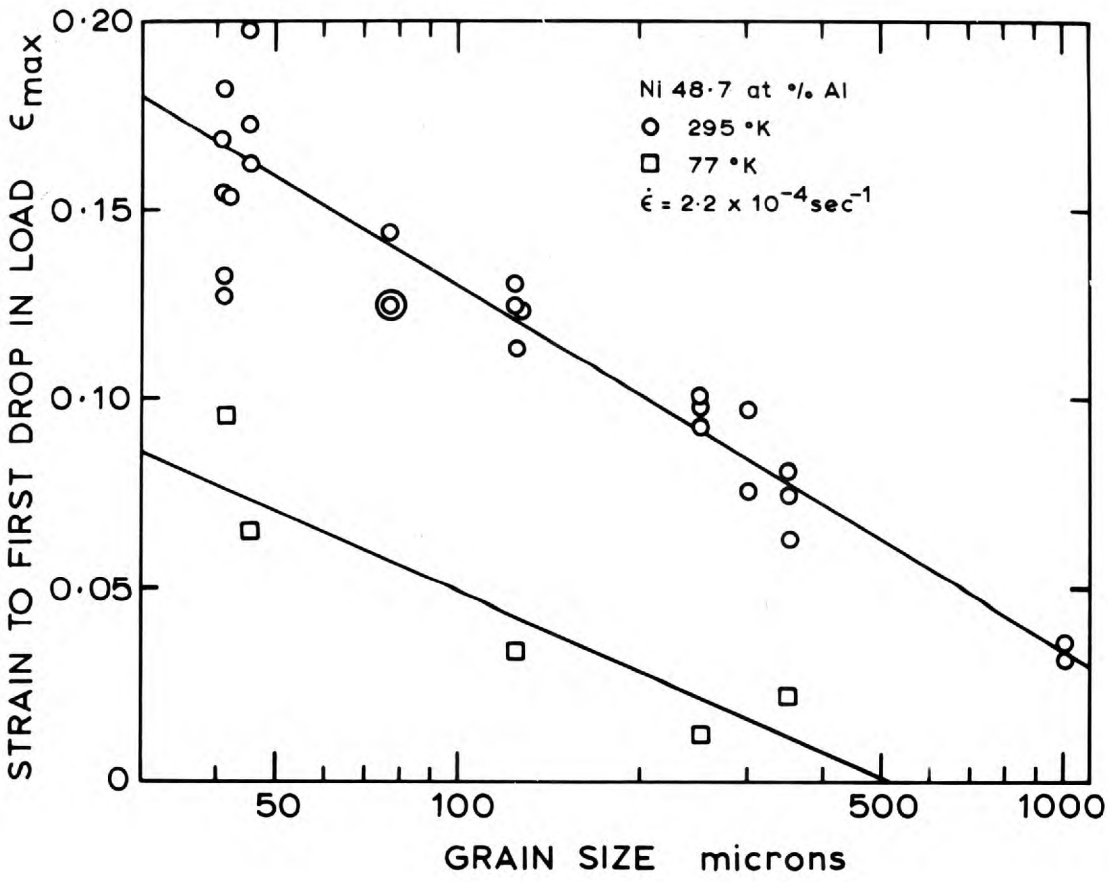

Fig. 4.31 Variation of Ductility with Grain Size

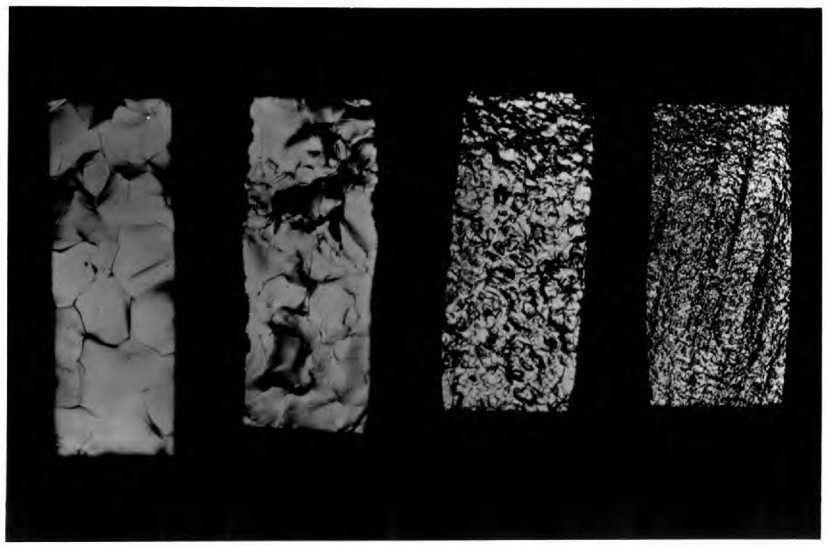

Fig. 4.32 Effect of Grain Size on Ductility (Initial Length of Each Specimen was the Same).

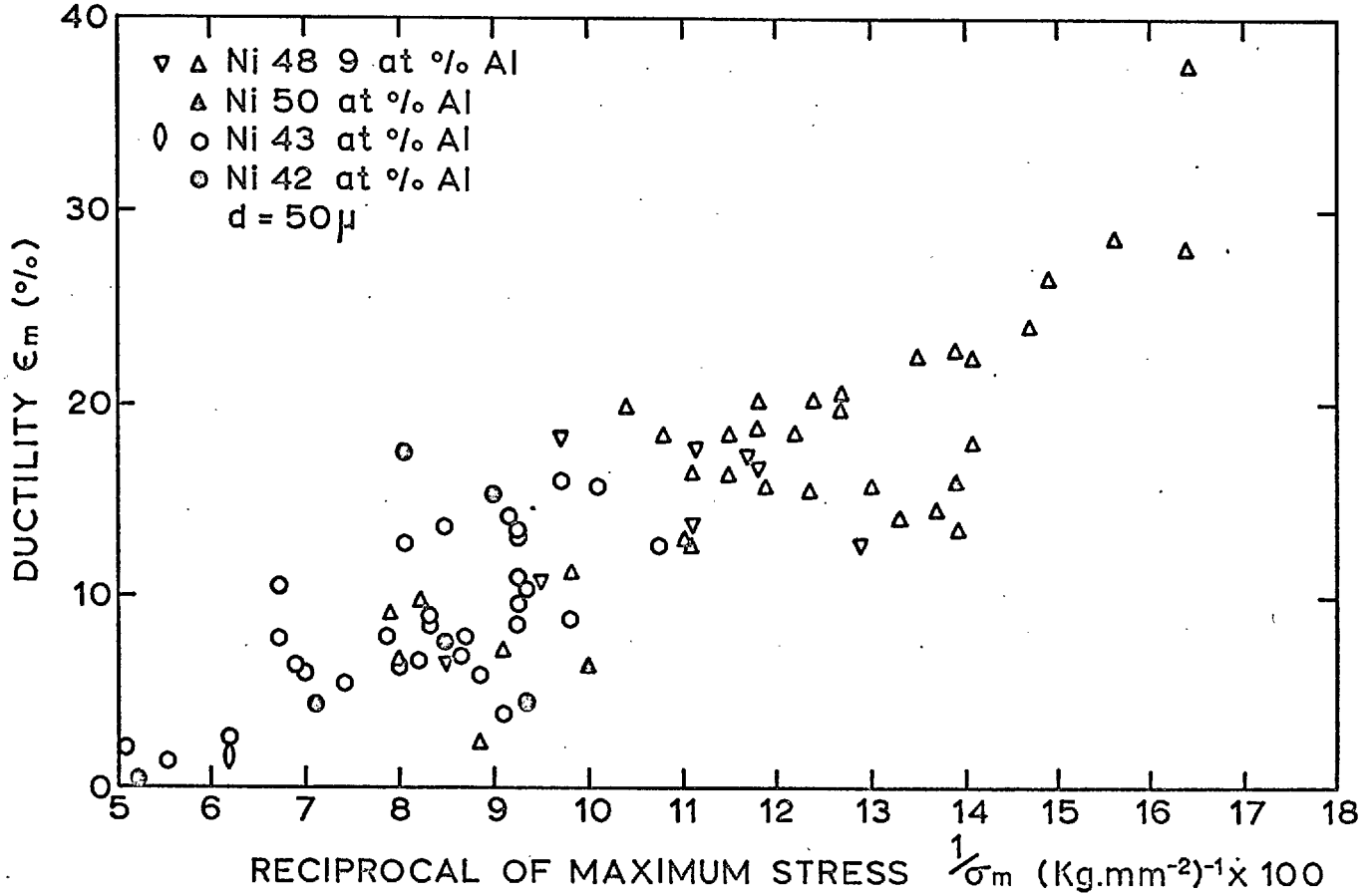

Fig 4.33 Effect of Maximum Stress on Polycrystalline Ductility At Constant Grain Size.

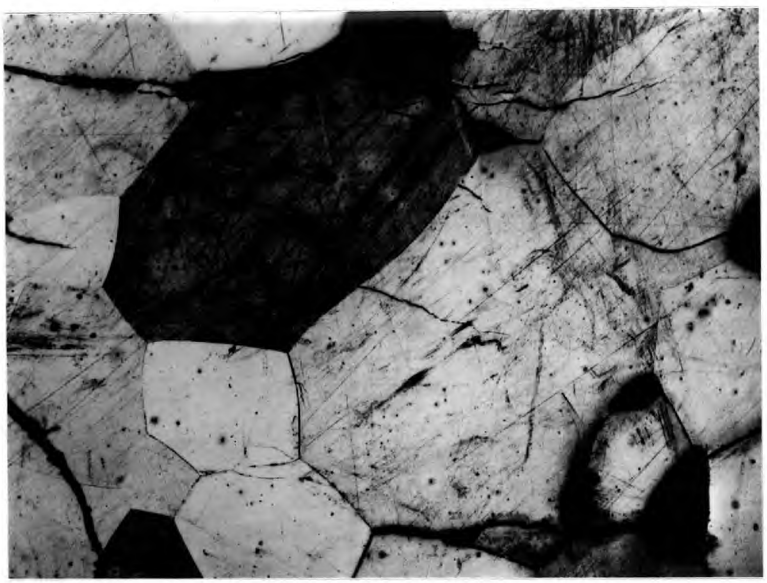

Fig. 4.34 Intercrystalline and Transcrystalline Cracking in Large Grained Material (x 25).

Chapter 5 Deformation Processes in NiAl.

From a comparison of the results presented in the preceding chapter it may be seen that variations of temperature and strain-rate affect certain parameters in a very similar manner for different material conditions. Therefore it would appear that the deformation processes under the various conditions are similar, if not identical. For example the form of the temperature and strain-rate sensitivities of polycrystals of several compositions and of soft orientation single crystals are identical at low temperatures. This suggests that the same processes control the deformation rate in each of these compositions and that the deformation of polycrystals is controlled by the motion of a [100] dislocations. These processes will be discussed below together with those in other temperature ranges and in hard orientations. Consideration is also given to the work hardening and fracture behaviour of polycrystals.

5.1. Factors Influencing the Flow Stresses of Polycrystals and Soft Orientation Single Crystals.

5.1.1. Low Temperatures.

At temperatures below T_A all soft single crystals and polycrystals which had a reasonable degree of ductility, (i.e. near stoichiometric and nickel-rich compositions) exhibited a markedly temperature dependent flow stress. This indicated that the processes which controlled the rate of dislocation motion were strongly

thermally activated. The similarity of the temperature dependences and of the variations of activation volume with stress indicated that these processes were the same in all the compositions and conditions listed above.

In order for the thermal activation parameters defined in 1.6.3 to be valid it is necessary that only one process is rate controlling. This condition is not satisfied at low stresses, as may be seen from fig 4.24, although a single process may be operative at high stresses. Li (1965) has shown that if more than one process occurs the measured activation energy and activation volume will be a mean value weighted in the ratios of the number and type of dislocations involved in each process. A consideration of the effective values of activation parameters can therefore give an indication of which processes do not influence a significant number of mobile dislocations.

Mechanisms that are likely to be rate controlling at low temperatures are:

i) Interactions with solute atoms or other lattice defects.

ii) Intersection of forest dislocations.

iii) Cross-slip.

iv) Motion of jogged dislocations.

v) Overcoming the Peierls-Nabarro force.

The first of these may be discounted because the thermally activated component of flow stress at $0^{\circ}K$ was found to be almost independent of composition, the effects of deviations from stoichiometry being to decrease $\underline{\sigma}_p^*$ rather than increase it.

Furthermore the activation volumes are not dependent on composition other than through the effects of stress. Activation volumes are found to vary with both stress and temperature. Although in most materials it is not clear how much of this effect is due to the mutual dependence of σ^* and T, effective stresses measured in this investigation have been varied through the effects of composition as well as of temperature. Thus the observation that activation volumes measured at different temperatures and in different compositions were the same for a given effective stress indicates that the activation volume is primarily a function of stress rather than temperature.

The intersection of forest dislocations can also be discounted because the activation volumes are small compared with theoretically predicted values. A typical spacing between the "trees" would be 10^3 b (Ball, 1964, has measured a dislocation density of 10^9 cm^{-2} in the early stages of deformation). An activation volume of 10 b^3 would therefore require the activation distance to be about 10^{-2} b which would imply an improbable force-distance relationship (Christian and Masters, 1964 B).

In addition it would be expected that v^* would decrease with strain because dislocation multiplication would reduce the distance between the trees. A strain dependent activation volume is found in close packed metals where this process is believed to be rate controlling (Cottrell and Stokes, 1955). Fig 4.19 shows that $(\Delta\sigma)_T$ in NiAl is almost independent of strain; at very low temperatures it decreases with increasing strain, which corresponds to an increase in activation volume.

Cross-slip would only be expected to be effective as a rate controlling mechanism if a dissociated dislocation has to constrict for cross-slip to occur and there is no indication of any dissociation of the a [001] dislocation in NiAl. Numerous cross-slip planes are available in NiAl and microscope observations indicate that copious cross-slip occurs.

It has been shown that the activation energy required at zero effective stress for jogs to move non-conservatively, i.e. with the formation of point defects, is of the order of the energy of point defect formation (Conrad, 1961 B). The energy to form a vacancy in stoichiometric NiAl has been estimated to be about 1 eV (Berkowitz et al. 1955). The distance between jogs in a b.c.c. material has been calculated to be about 50 b (Schoeck, 1961 A), hence the activation volume would be expected to be of the order of 50 b^3. These values are close to those observed at low effective stresses in NiAl; it is therefore possible that the thermally activated motion of jogs contributes to the observed flow stress in this region. The effect of stress on the activation volume is uncertain because of two conflicting influences. Schoeck (1961 A) showed that l^*, which is of the order of the spacing between jogs at zero stress, should increase with increasing stress because of bowing of the dislocation line pinned at the jogs. This bowing effect will be offset by a reduction in the spacing between jogs on straining, which will tend to decrease l^*. The combined effect is that v^* could increase or decrease with increasing stress depending on the relative importance of each term.

The small activation volume ($\sim 5\ b^3$) and high flow stress at $0^\circ K$ ($\sim 0.01\mu$) indicate that the most probable deformation mechanism is the nucleation of a dislocation line across a Peierls-Nabarro barrier. The Peierls-Nabarro force is the force exerted by the lattice to oppose the motion of a dislocation. Kuhlmann-Wilsdorf (1960) suggested that this force should decrease with increasing temperature because of the increasing uncertainty of the position of the dislocation. However Fridel (1963) has shown that this effect is not as important as was thought and that the temperature dependence should arise through the nucleation process being aided by thermal fluctuations.

Several models have been developed to estimate the critical activation energy. A recent one due to Dorn and Rajnak (1964) is based on a suggestion by Fridel (1963) that the interaction between kinks in a dislocation line can be accurately expressed in terms of the line energy as the kinks approach each other. The activation energy for the process is the saddle-point energy for the nucleation of a pair of kinks and is a function of the applied stress, the lattice constants and the height and shape of the Peierls barrier. The shape of the barrier is described by a purturbation factor α ($-1 < \alpha < +1$) which indicates the divergence from a pure sinusoidal variation. No simple analytical solution could be determined for H, but numerical integration gave universal curves of $H/2E_K$ against τ^*/τ_p^* for various α. E_K is the energy to nucleate an isolated kink and τ_p^* the Peierls stress (the effective stress at $0^\circ K$) which was

assumed to change with temperature only through variations in the shear modulus. It was further shown that $^{H}/_{2E_K}$ was almost equivalent to $^{T}/_{T_o}$ where T_o is the temperature where $\tau^* = 0$ i.e. where thermally activated flow ceased.

Fig 5.1 shows a plot of experimental values of $^{T}/_{T_o}$ against τ^*/τ_p^* ($= \sigma^*/\sigma_p^*$) with the theoretical curve for $\alpha = -1$ superimposed. Fig 4.3 was used to determine $\underline{\tau}_p^*$ and $\underline{T}_o$ was determined by fitting this and one experimental value to the theoretical curve; changes of shear modulus with temperature were neglected.

The agreement between the theoretical and experimental curves is very good up to temperatures of 0.6 T_o; beyond which the flow stress is higher than predicted by the Dorn-Rajnak analysis. A further result of this analysis is that experimental points from several compositions, grain sizes and strain-rates lie on the same curve; this is further evidence that the same processes operate under the various experimental conditions.

Kink energies (E_K) can be measured from the effect of strain rate on the critical temperature. Dorn and Rajnak have shown that if the effects of temperature on the elastic moduli are neglected

$$2 E_K = k \left(^{1}/_{T_{01}} - {}^{1}/_{T_{02}}\right) \log \dot{\epsilon}_2/\dot{\epsilon}_1 = H_o$$

the subscripts 1 and 2 refer to the fast and slow strain-rates respectively. Inserting typical values of $\underline{T}_o$ and $\dot{\underline{\epsilon}}$ for NiAl

$2 E_K$ = 0.36 eV for Ni 48.9 at % Al

= 0.54 eV for Ni 43 at % Al

These energies are of the expected order of magnitude (cf. Mukherjee and Dorn, 1964) and compare with those measured by equation 1.25 at high stresses (cf. fig 4.23). The difference between the compositions may not be significant because of inaccuracies in the measurement of $\underline{T}_o$ ($\pm$ 5 deg K where $\underline{T}_{02} - \underline{T}_{01}$ = 15 deg K).

A common argument against the operation of a Peierls mechanism is that it would require the dislocations to lie in straight lines along most closely packed directions, while experimental observations often show that they do not. No electron microscope evidence on the dislocation configurations in NiAl at low temperatures is available but it may be noted that surface slip traces are very straight at 77°K (0.37 T_o) whilst those above 195°K (0.95 T_o) are wavy.

Therefore, from a consideration of the activation energy and activation volume of deformation, the comparison between the measured flow stresses and the Dorn-Rajnak analysis, and the appearance of the slip traces, it may be concluded that the flow stress of NiAl at low temperatures is controlled by the thermally aided nucleation of dislocation kink pairs across a Peierls-Nabarro barrier. However variations in the activation energy at zero stress, $\underline{H}_o$, with stress and the deviation of the theoretical and experimental curves in fig 5.1 indicate that an additional mechanism operates at low effective stresses.

The shape of the temperature dependence of flow stress, particularly as represented by fig 5.1, indicates that the two (or more) processes are interdependent. When more than one mechanism is operative the overall rate will be controlled by the easier one for parallel (independent) processes and by the more difficult one for series (interdependent) processes (Schoeck, 1961 B). It may be seen from fig 5.1 that the more difficult process is predominant. This observation provides little additional information to identify the second mechanism because all dislocations require nucleation past a Peierls-Nabarro barrier before further interactions can occur. Of the mechanisms considered the one which fits the observed behaviour most fully is the non-conservative motion of jogged dislocations.

The mechanisms observed in b.c.c. pure metals are similar. The Peierls mechanism is thought to be rate controlling although the Dorn-Rajnak analysis does not give exact agreement over the full range of temperatures (Christian and Masters, 1964 B), and there is evidence for more than one mechanism under certain conditions (Guiu and Pratt, 1966).

Ball (1964) explained the temperature dependence of the critical resolved shear stress for slip in stoichiometric NiAl by a model of cutting bonds between unlike atoms, similar to that developed by Haasen (1957) to explain the plasticity of germanium. The model is based on the formation of a crack of atomic dimensions when an extra half plane of atoms is introduced into the lattice. The rate of motion of the dislocation is therefore restricted by the diffusion of

the crack through the lattice and a rate equation similar to 1.17, but with a temperature dependent pre-exponential term, may be derived. The activation energy for the process can be evaluated from the slope of a log (τ/T) against ^{1}/T plot. Ball showed that a plot of this type was linear over a temperature range 300-1000^{o}K in NiAl and that the activation energy was close to the bond energy. Application of this analysis to the results of chapter 4 does not give a linear relationship over any wide range of temperature. Therefore the flow stresses appear more consistent with a model of a conventional dislocation restrained by a high Peierls force than the diffusion of atomic cracks in a highly covalent material.

5.1.2. Intermediate Temperatures.

The dislocation mechanisms that control the rate of deformation at low temperatures in b.c.c. metals, and other materials with similar temperature dependent flow stresses, have been studied in detail and are well documented. There is however little information available about the deformation processes that occur in the athermal region in these materials.

The general features that have been noted in b.c.c. metals are that the athermal process is dependent upon purity (Christian and Masters, 1964 A) and grain size (Conrad, 1963). Dorn and Mitchell (1964) have studied the deformation behaviour of a series of alloys with a hexagonal close packed crystal structure. They concluded that, where the temperature dependence was of the type illustrated in fig 1.8,

the athermal flow stress was controlled by the presence of solute atoms, through processes such as Suzuki locking or short range order strengthening (Fisher, 1954). In a comprehensive study of compound AgMg Mukherjee et al. (1965) were unable to determine the processes which controlled the athermal flow stress.

From the results of the present investigation it may be seen that the athermal flow stress of NiAl is dependent upon the concentration (c) of lattice defects - substitutional atoms and vacancies. The exact form of this dependence could not be determined, because of the lack of sufficient compositions of extruded (fine grained) polycrystals; a $\tau \propto c$ or $\tau \propto c^{\frac{1}{2}}$ relationship could have been obeyed equally well. This increased strength was probably due to solid solution hardening, rather than fine precipitates, because there is no evidence of the lattice defects forming large clusters (although there is some for small clusters of vacancies cf. 1.2.2).

Fleischer and Hibbard (1963) have noted that solutes which produce hardening may be divided into two classes. "Rapid" hardening is observed when the defects produce a tetragonal strain-field; the hardening rate is about two orders of magnitude higher than observed with symmetrical defects which give rise to "gradual" hardening. The rates of hardening observed in NiAl ($\frac{d}{dc} \simeq \frac{\mu}{10}$ for vacancies and $\frac{\mu}{20}$ for substitutional atoms) are comparable with those observed in the second category. This is consistent with the symmetrical form of defects in NiAl.

Fleischer and Hibbard have derived a relationship between flow

stress and solute concentration from a model of a fairly rigid dislocation line interacting with a solute particle of different size and shear modulus to the solvent. This relationship could not be tested on NiAl because the required information, particularly the composition dependence of shear modulus, was not available. However a $\tau_f \propto c^{\frac{1}{2}}$ dependence is predicted and τ_f should not be strongly dependent on temperature.

A number of alternative mechanism are described by Haasen (1965); of these the destruction of short range order (Fisher, 1954) appears at first sight to be a possible hardening mechanism in NiAl - a quadratic composition dependence and small temperature dependence are predicted. However a consideration of the geometry of slip in NiAl shows that this mechanism is unlikely to be important because one sub-lattice is always fully ordered, even in non-stoichiometric compositions, and slip in a $\langle 100 \rangle$ direction would not affect the solute distribution on the other.

In addition to the frictional force exerted on a moving dislocation a solute atom may also influence the flow stress by locking the dislocations. Locking effects are usually observed as an initial yield point; although at sufficiently high temperatures the solute atoms may diffuse at the same rate as the dislocations move, causing a frictional drag and often a serrated stress-strain curve.

Dislocation locking is probably the cause of the yield point observed in Ni 48.9 at % Al alloys. It is uncertain whether the locking is caused by excess nickel atoms or by impurities such as

oxygen; this difficulty could possibly be resolved by studying the kinetics of strain-ageing. Of the mechanisms of dislocation locking listed by Haasen (1965) elastic (Cottrell) locking appears to be the most reasonable explanation of the yield points - Suzuki locking requires the presence of stacking faults, and stress induced ordering involves non-symmetrical defects, neither of which are expected in NiAl.

5.1.3. High Temperatures.

There appears to be no single deformation mechanism that is rate controlling over the complete range of experimental conditions at temperatures above T_c. The complexity of the deformation behaviour in this region may be gauged from composition and temperature dependence of the form of the stress-strain curve, the flow stress, and the activation energy and activation volume of deformation.

In attempting to interpret this data and determine the rate controlling processes a difficulty arises in obtaining comparative information from other materials. Most of the data that is available has been obtained on face-centred cubic metals under creep conditions. Constant strain-rate tests have only been performed at high temperatures on a limited number of materials, e.g. aluminium and copper (Sellars and Tegart, 1966), alumina (Conrad et al., 1965) and AgMg (Mukherjee et al., 1965).

Weertman, in a series of papers, has developed creep relationships of the form:

$$\dot{\epsilon} = C \sigma^{m} \exp - \left(\frac{Q}{kT} \right) \qquad (5.1)$$

where C and m are constants, Q is an activation energy and all other symbols have their usual meaning. This was derived from a model of dislocations being emitted from a source to be held up at an unspecified barrier. Dislocation climb around the barrier may lead to mutual anhilation of dislocations and the emission of further dislocations from the source leads to steady state creep. The activation energy is near to that for self-diffusion (H_{SD}) because the diffusion of vacancies is a necessary step in dislocation climb. The stress exponent m depends on the rate-controlling process: if it is climb m = 4.5 Weertman (1957 A); if the deformation rate is determined by the motion of the dislocations, limited by the viscous drag of solute atoms, m = 3 (Weertman, 1957 B). The creep of a series of lead and indium alloys was studied by Weertman (1960) who observed a change of stress exponent from 4.5 to 3 with increasing alloy content, and a breakdown of the simple power law at high stresses.

It may be noted that equation 5.1 is similar in form to 1.14. This similarity has permitted Q to be measured using the analysis outlined in 1.6.2. Sherby et al. (1957) measured apparent activation energies for creep in aluminium, by measuring the change in creep rate on changing the temperature at constant stress, and found that Q was equal to H_{SD} above 0.5 T_m (T_m is the melting temperature) and that it was independent of stress or temperature.

A similar observation has been made in near-stoichiometric NiAl,

using change of strain-rate tests, - $\underline{H}$ was found to have a value of 3.5 ($\pm$ 0.2) eV compared with $\underline{H}_{SD}$ of 3.4 eV and was independent of stress and therefore temperature. This indicates that the rate controlling process at high temperatures is the climb of dislocations past obstacles. The form of these obstacles could not be determined, but they were probably the same as in the athermal region. Further evidence for this mechanism is provided by Ball and Smallman (1964) who studied the kinetics of the annealing out of dislocation loops by electron microscopy. They noted that the loop concentration after isochronal anneals had the same temperature dependence as the flow stress, and that the activation energy for the process was that of self diffusion.

However two experimental observations are not consistent with this explanation. The slope of the stress dependence of activation energy is small, as predicted theoretically for climb (Conrad, 1964). The activation volume, as defined by equation 1.15, must also be small because the difference between G and H are negligible even at 1000^{o}K. The activation enthalpy was determined using equation 1.25, which includes a term in v^{*} measured in this case by the effects of a change of strain-rate (equation 1.2.4). This second activation volume has a high value and is strongly dependent on stress (fig 4.26). This difference in activation volume measured in different ways implies that the analysis described in 1.6.2 is not valid at high temperatures. The analysis does however give a measure of the activation energy that is in agreement with a theoretical model of a

process that is observed in other materials, and for which there is independent experimental verification in NiAl. The differences may be due to the strong stress dependence of the pre-exponential term.

The second objection is that if Q in equation 5.1 is independent of stress and temperature then m is equal to $\frac{\partial \log \dot{\varepsilon}}{\partial \log \sigma}$ if all other terms in C are independent of stress. This same equation defines the dislocation velocity exponent (cf. eqn 1.32) values of which have been measured in the temperature range in which the mechanism operates and found to be about 11 and independent of strain. This is rather higher than predicted by Weertman, although m does decrease at higher temperatures, and the simple power law breaks down at high stresses (Weertman, 1960).

The behaviour in non-stoichiometric compositions is complex and several processes are probably involved. The activation energies extrapolate to values close to those of self-diffusion at low stresses. The exponent m has values between 3 and 5, if the stress dependence of the activation enthalpy is neglected. It may also be noted that it is at temperatures at which the stress is low that grain-boundary sliding is thought to be important, although this process would be expected to have an activation energy close to that for self-diffusion.

As the stress increases H increases in nickel-rich alloys, but decreases in the aluminium-rich composition. The 53 at % Al composition also exhibits a high energy peak, superimposed on the above behaviour, and a change of slope of the temperature dependence

of log flow stress. It is at these higher stresses that several processes are probably operating and the thermal activation analysis is invalid.

The close coincidence of the stress and temperature dependences of $\underline{H}$ for the 43 at % Al polycrystals and hard orientation equiatomic single crystals suggests that similar processes could be operative at high stresses. Peaks in the activation energy of creep, similar to that noted in the aluminium-rich composition, have been noted in other materials at temperatures at which an atomic change occurs, e.g. the Curie point in iron (Ishida et al., 1966), although such effects can usually be explained by a similar anomaly in the activation energy of diffusion. It might therefore prove profitable to study the atomic order and defect structure in a 53 at % Al alloy in the temperature range of the peak.

5.1.4. Grain Size.

The flow stress of NiAl is not strongly dependent on grain-size, as may be seen from table 4.4, there is a slight softening at large grain sizes. This is in agreement with the findings of Ball (1964) in NiAl and of Terry and Smallman (1964) in AgMg. A mean orientation factor $\underline{\bar{m}}$ = 2.8 may be obtained from a comparison of the flow stress of a fine grained polycrystal with the critical resolved shear stress of a single crystal of the same composition.

A comparison of the flow stresses of a 49.6 at % Al polycrystal (fig 4.2) and a 50 at % Al soft single crystal (fig 4.1) reveals that

the single crystal is harder, even though it was oriented with a Schmid factor of 0.5 and is closer to the equiatomic composition. This discrepancy is believed to be due to contamination of the single crystal during melting, mainly with oxygen from the alumina crucible; no analyses for gaseous impurities could be made. This contamination could also explain the low ductility of these crystals compared with those of Ball (1964) who found that single crystals were completely ductile; the single crystal flow stresses measured by Ball were similar to those reported in chapter 4. The hard orientation single crystals did not suffer from this disadvantage because they were grown by the high frequency induction melting technique described in chapter 2.

5.1.5. The Composition Dependence of T_A and T_c.

Both T_A - the temperature where the flow becomes athermal - and T_c - that at which diffusion controlled flow starts - are dependent on composition. Increasing defect concentration increases T_A but decreases T_c; thus the behaviour of T_c is different to that found in the hardness study of Westbrook (1957) who noted that it rose continually with increasing nickel content across the complete phase field.

The increase in T_A is probably a result of an increase in T_o - the critical temperature for the Peierls-Nabarro mechanism. Fig 5.1 indicates that all temperature dependences may be made to coincide if suitable values of T_o are selected. Dorn and Rajnak (1964) introduce

$\underline{T}_o$ into their analysis through the relationship

$$\frac{T}{T_o} \simeq \frac{H}{2 E_K}$$

Thus the composition dependence of T_o reflects the composition dependence of E_K-the energy to nucleate a kink against a Peierls-Nabarro potential.

Terry and Smallman (1964) have derived a relationship between T_c and the activation energy of self diffusion, based on a jog theory of work-hardening. This explains why T_c for AgMg is 0.4 T_m (where T_m is the melting point) compared with 0.5 ~ 0.65 $\underline{T}_m$ in pure metals. This explanation cannot be extended to NiAl, at least in soft orientations, because it relies on the additional energy of a superdislocation. An explanation for the low T_c of NiAl (about 0.4 $\underline{T}_m$ depending on composition) will have to be sought elsewhere, particularly when it is realised that $\underline{H}_{SD}$ is higher in NiAl than in most pure metals. An alternative calculation by Schoeck (1961 B), which makes no assumption about the process other than it is diffusion controlled, also concludes that $\underline{T}_c$ is a function of $\underline{H}_{SD}$.

The composition dependence of $\underline{T}_c$ may therefore be explained by the variation of the activation energy for diffusion with creep. There is however no direct empirical relationship of the type $T_c = C\ H_{SD}$; $\underline{T}_c$ for the 53 at % Al alloy is lower than that of 43 at % Al although $\underline{H}_{SD}$ is higher in the aluminium rich alloy. In the theories of Schoeck and of Terry and Smallman $\underline{T}_c$ is not simply

dependent on $\underline{H}_{SD}$ but on a number of other parameters, any of which could vary with composition.

An alternative explanation of the composition dependence, based on the variation of the melting temperature, also lacks direct correlation and will not explain the difference between NiAl and pure metals. Furthermore at compositions close to stoichiometry $\underline{H}_{SD}$ and $\underline{T}_{c}$ vary rapidly with composition, while $\underline{T}_{m}$ shows it smallest sensitivity to composition.

5.2. Flow Stresses of Hard Orientation Single Crystals.

It has not been possible to study the activation energies and volumes of deformation of single crystals with [001] axes in detail because of the limited number of single crystals available, and the small range of strain over which strain-rate changes could be made before kinking, or fracture, occurred.

The flow stresses measured at low temperatures were consistent with the nucleation of kink pairs across a Peierls-Nabarro barrier being the rate controlling process. Values have been fitted to the theoretical curve of Dorn and Rajnak (1964) using the experimentally determined value of $\underline{T}_A$ as $\underline{T}_o$; the agreement was close over the entire temperature range, and there was no evidence of a second process (fig 5.1). The only measurement made of activation volume was also consistent with a Peierls mechanism (fig 4.22). The deformation behaviour of hard orientation NiAl therefore seems very similar to that of AgMg at low temperatures (Mukherjee and Dorn, 1964), because the same slip systems are observed and the same rate controlling mechanism operates.

The relationship between kinking and the flow stress at intermediate temperatures has been discussed in 3.3.2. The occurrence of kinking prevented an analysis of the factors controlling the deformation rate at intermediate temperatures.

The deformation process operating at high temperatures is very different to that in soft orientations; the activation energy is considerably greater than that for self-diffusion and strongly

dependent on stress and temperature. Mechanisms which rely on diffusion may therefore be discounted; as may the non-conservative motion of jogs because the energy is considerably higher than that required to form a vacancy. Intersection processes are also unlikely because of the independence of $(\Delta\sigma)_T$ on strain, although this may be due to a continual reduction of the dislocation density by recovery processes. The effects of composition could not be studied.

The remaining alternative mechanisms are the constriction of the ribbon of anti-phase boundary to allow a superdislocation to cross-slip or a Peierls mechanism. The stress dependence and absolute values of the activation volume are consistent with both mechanisms ($v^* = 5\ \underline{b}^3$ at high stresses and $200\ \underline{b}^3$ at low stresses, where $\underline{b} = \underline{a}\ [111]$) and either mechanism could be responsible for the observed slip markings (fine and relatively straight). An objection to a Peierls mechanism is that the nucleation of [111] dislocations appears to be rate controlling at low temperatures and [111] is the predominant slip direction in the high temperature range, although [011] slip is also observed. In addition $\underline{H}$ is linearly dependent on temperature and extrapolates to zero at about 400°K (fig 4.27); $\underline{H}$ would be expected to extrapolate to zero at 0°K for a Peierls mechanism (Dorn and Rajnak, 1964).

The stress required to constrict a superdislocation and permit cross-slip at temperatures where thermal activation is negligible may be estimated from a modification to equation 3.2. The force, due to the applied stress, tending to constrict the dislocation will be aided

by the anti-phase boundary energy, and opposed by the mutual repulsion of the two imperfect dislocations. Therefore at equilibrium:

$$\tau b + \frac{E_{APB}}{w} = \frac{K\, b_1\, b_2}{2\pi w} \qquad (5.2)$$

If the width of the ribbon of APB is reduced to one atomic spacing then w = b, and the superdislocation becomes an $\underline{a}\,[11\bar{1}]$ unit dislocation capable of cross-slip. Rearranging equation 5.2 and substituting values of $\underline{K}$, (for a screw dislocation on a $(\bar{1}\bar{1}2)$ plane) and $\underline{E}_{APB}$ from tables 3.3 and 3.2 gives

$$\tau = 8.9 \times 10^{10} - 8.0 \times 10^{10} \text{ (dynes cm}^{-2}\text{)}$$

This estimated stress to constrict a superdislocation - 90 Kg mm^{-2} - is in reasonable agreement with observed flow stress at 400°K of 65 Kg mm^{-2}. Schoeck and Seeger (1955) have shown that the activation energy for the constriction of an extended dislocation should be strongly dependent on stress, reaching a very high value at low stresses. Therefore it appears that the rate controlling mechanism in hard orientation single crystals is the constriction of screw type superdislocations so that they may cross-slip around obstacles.

A process of this type has not been observed in any other superlattice. The creep properties of ordered materials, that deform

by the motion of superdislocations, have been summarised by Stoloff and Davies (1966). They note that although the activation energies for creep are higher in the ordered state than when disordered the increase may be explained by a corresponding change in the activation energy for self-diffusion. Mukherjee et al. (1965) were unable to determine a controlling process for the high temperature thermal region in AgMg (region B in fig 1.5); activation energies were stress dependent though no values were quoted. A further process, identified as the viscous glide of dislocations modified by the presence of the anti-phase boundary ribbon, has been noted at very high temperatures in AgMg ($T > 0.75\ T_m$) by Mukherjee and Dorn (1965). The measured activation energy was independent of stress and slightly higher than H_{SD}, the difference was explained by the presence of the APB ribbon.

5.3. The Form of the Stress-Strain Curve and Work-Hardening.

5.3.1. Work-Hardening Relationships.

The independence of strain-rate sensitivity on strain indicates that work-hardening results in an increase in the athermal stress, σ_μ. The hardening mechanism is probably a long range interaction with the increased number of dislocations created during deformation. Ball (1964) has shown that the dislocation density increases linearly with strain, and that the flow stress varies as the square root of the dislocation density. Combining these relationships gives:

$$\sigma = \sigma_f + K' \epsilon^{\frac{1}{2}} \qquad (5.3)$$

where σ_f is approximately the initial flow stress and K' is a constant dependent on composition and temperature. Relationships of this type are predicted by several work-hardening theories (Weertman and Weertman, 1965). If stress-strain data is plotted logarithmically according to equation 5.3 (i.e. log $(\sigma - \sigma_f)$ against log ϵ) rather than equation 4.1 ($\sigma = K\epsilon^n$) a straight line of slope ~ 0.5 is obtained at low temperatures and in the range of composition 42 to 50 at % Al.

The reason for the decreasing values at low temperatures of work-hardening exponent, as defined by equation 4.1, is therefore apparent - this equation does not consider the effects of flow stress. Further evidence for this explanation is that materials with similar flow

stresses have similar work-hardening exponents and that n approaches 0.5 when the flow stress is low. Equation 5.3 is therefore a better representation of work hardening behaviour; although experimental results have been presented plotted according to equation 4.1 rather than 5.3 because of considerable scatter in the latter values.

This scatter arises largely from the breakdown of the linear relationship between strain and dislocation density at low strains ($\epsilon < 0.01$) and to the occurrence of yield points. A number of parameters were found to show anomalous values at low strains, e.g. the initial rate of work-hardening was temperature dependent and $(\Delta\sigma)_T$ was different to the constant high strain value. It seems probable that any simple model of deformation mechanisms was not applicable at low strains.

At high temperatures the work-hardening exponents defined by either equation have similar values because of the decrease of flow stress. The reduction of n, to values smaller than 0.5, is due to a further breakdown of the linear relationship between strain and dislocation density at high temperatures when dynamic recovery may occur during deformation. At sufficiently high temperatures the rate of recovery becomes equal to the rate of work-hardening and an effective hardening rate of zero is observed. This is equavalent to creep occurring at the applied strain-rate.

The work-hardening behaviour of hard orientation single crystals may be explained in the same way. There is, however, no obvious explanation for the linear hardening of soft single crystals. These

were deformed in a symmetrical orientation and duplex slip was observed to occur, - these are the conditions that should lead to parabolic hardening. An explanation of the linear hardening would require additional information from electron microscopy.

5.3.2. The Stress-Strain Curve of Aluminium-Rich Polycrystals.

The complex variations of the stress-strain curves of Ni 53 at % Al polycrystals with temperature may be explained by the methods of Johnston and Hahn outlined in 1.6.3. At the lowest temperatures at which reproducible deformation is obtained the dislocation velocity exponent is low ($\underline{m}$ = 9 at 750°K) and appears to decrease further with decreasing temperature. A comparison with the theoretical curves derived by Johnston (1962) shows that a yield point of the observed shape would be expected with values of $\underline{m}$ of this order, and an initial dislocation density of 10^9 cm^{-2} and a strain-rate of 10^{-4} sec^{-1}. An increase of temperature is accompanied by an increase of $\underline{m}$ which results in a decrease in the height of the yield drop and eventually a smooth curve, the work hardening behaviour of which is similar to that described in 5.3.1.

A further broad maximum in the stress-strain curve is observed above 950°K; the flow stress beyond this peak continues to decrease with increasing strain. Curves of this type have been noted in many other materials at high temperatures (Sellars and Tegart, 1966). This behaviour could be explained by a Johnston-Hahn multiplication process because it is associated with a decrease of $\underline{m}$ to values near 3; the

continuous decrease of flow stress with strain could be due to the low rate of work hardening. This explanation is unsatisfactory because other compositions, which have similar m values, do not show the same shape curve. The additional observation that this behaviour starts at the same temperature as grain-boundary sliding in coarse-grained polycrystals suggests that grain boundary effects could be responsible for the falling stress-strain curve. Similar curves have been reported in $TlBi_2$ by Robinson and Bever (1966); these curves are associated with a transition from brittle to ductile behaviour that is achieved by grain boundary sliding.

5.4. Fracture Behaviour.

Several features of the fracture behaviour of NiAl are apparent although no systematic study has been undertaken because of the restrictions imposed by the compression test.

The dependence of ductility on stress (through composition and temperature) and on grain-size indicates that an equation of the form of 1.12 ($\epsilon_m \propto \gamma \sigma^{-1} d^{-\frac{1}{2}}$) is a valid representation of the fracture behaviour. Therefore NiAl is brittle because the stress required to propagate a crack is smaller than that for plastic deformation. This explanation is not altogether surprising because the flow stress of Ni 43 at % Al is higher at any temperature (below 600°K) than that of tungsten (Schnitzel, 1965), the brittleness of which has been explained in the same way.

It should be noted however that equation 1.12 was derived for cleavage fracture and intergranular fracture occurred in all fine-grained materials. This may be interpreted as indicating that slip on the three independent soft slip systems results in high local stresses at grain boundaries. These stresses may be relieved by slip on hard systems, giving the five independent slip systems required for general ductility, but this process has to compete with crack propagation. An alternative explanation - surface effects - has been given by Westbrook et al. (1964) who noted a transition from intergranular to transcrystalline fracture after careful surface preparation.

The stress-ductility relationship observed in the aluminium-rich alloy could not be fitted to the same curve as the other compositions, -

the ductility is considerably smaller than that predicted from the flow stress. This embrittling effect is similar to that observed in radiation damaged material and arises from the same cause - a large concentration of point defects. Although Cottrell (1958) has explained radiation damage embrittlement by the effect of increased flow stress on equation 1.12 Evans et al. (1963) have attributed it to a decrease in the surface energy term. The latter explanation is unsatisfactory for NiAl because it would require a decrease of surface energy by 50% to explain the observed ductility.

A further explanation is that the number of independent slip systems is effectively reduced to three because of a high flow stress in hard orientations, although this mechanism would be expected to give a small plastic strain before fracture. Alternatively the dislocation velocity exponent is small in this composition, therefore cracks may be able to propagate more rapidly than plastic deformation can remove stress concentrations, and the brittleness would be associated with the initial yield point.

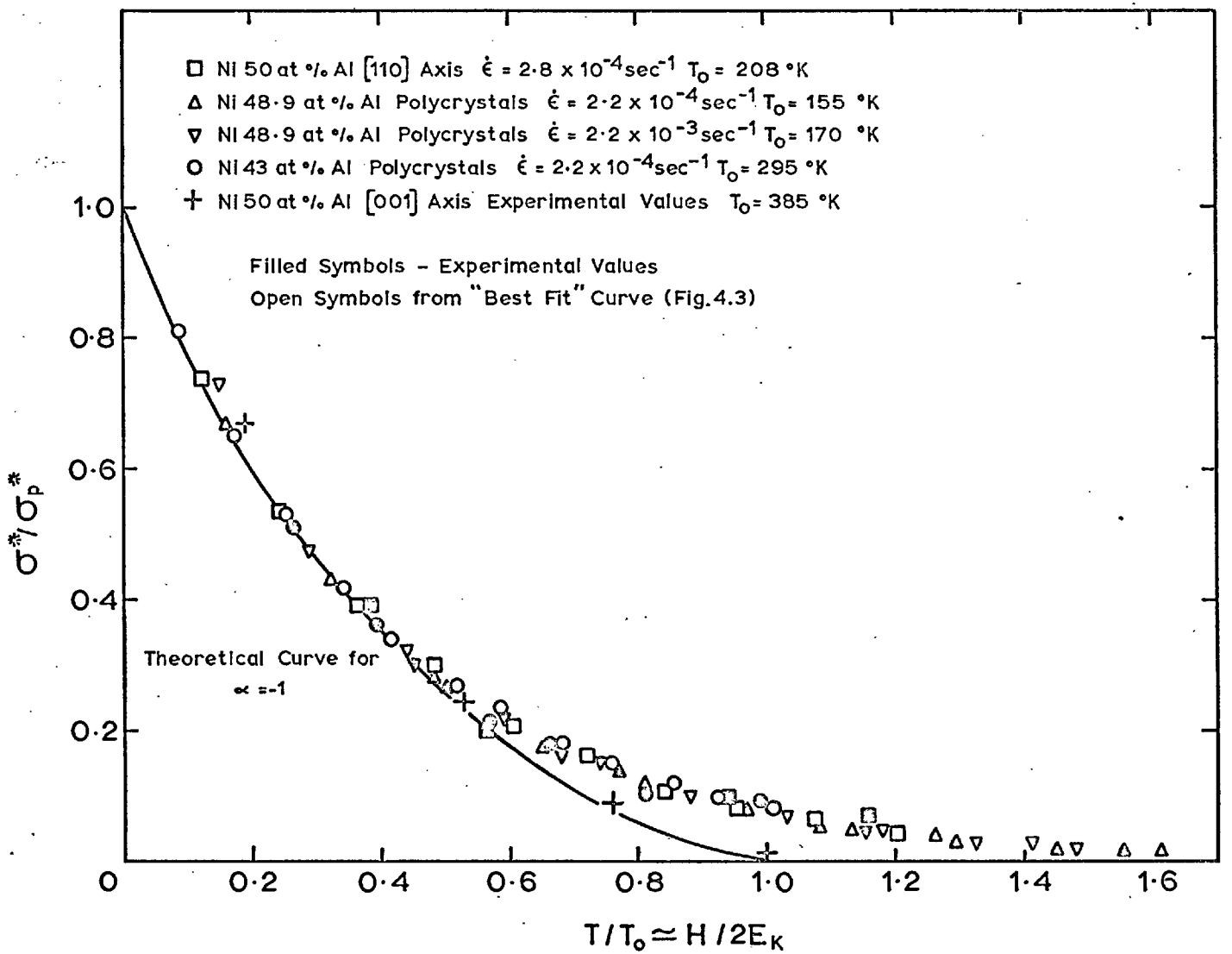

Fig 5.1 Temperature against Thermally Activated Component of Flow Stress in Dimensionless Units.

Chapter 6 Conclusions and Suggestions for Future Work.

6.1. Conclusions.

The Bridgman technique may be used to grow single crystals of the intermetallic compound NiAl of stoichiometric composition. Single crystals containing excess nickel may also be grown by the strain-anneal technique.

The atomic mechanisms of deformation of these single crystals were extremely varied. The preferred slip direction was $[001]$; in agreement with the energies of possible dislocation arrays calculated from anisotropic elasticity theory. At low temperatures the most closely packed plane, (110), was the slip plane, but an increase of temperature permitted slip on any plane that contained an $[001]$ direction. Deviations from stoichiometry on the excess nickel side had no effect on the operative slip system.

The compression of stoichiometric single crystals along an $[001]$ axis resulted in zero resolved shear stress on any of the primary slip systems. Slip then occurred on a $(\bar{2}\bar{1}3)[111]$ system at low temperatures and $(\bar{1}\bar{1}2)[111]$ or $(0\bar{1}1)[011]$ above 700°K. At intermediate temperatures kinking was observed; the properties of these kinks were consistent with a model of their being caused by the motion of $\frac{a}{}[001]$ dislocations. An apparent shear transformation was also observed near room temperature.

The stress-strain relationships of single and polycrystals have been studied in compression, as a function of temperature, strain-rate,

composition, orientation and grain-size, between 77 and 1500°K. All specimens could be deformed at 77°K with the exception of polycrystals containing a large concentration of vacancies, i.e. those of excess aluminium compositions, which were completely brittle below 700°K. Aluminium-rich specimens were very similar to radiation damaged material - they showed high flow stresses, low ductility and low rates of work-hardening.

The similarity between the temperature and strain-rate dependence of polycrystals and of single crystals that slipped in an [001] direction indicated that the flow stress of polycrystals is controlled by the motion of a [001] dislocations. The temperature dependence of these flow stresses, for any composition or grain size, could be divided into three distinct regions. At high and low temperatures strongly thermally activated processes gave rise to steep temperature dependences; an athermal process at intermediate temperatures resulted in a flow stress plateau. Activation enthalpies and activation volumes of deformation were evaluated for the thermal processes from the effects of temperature and strain-rate rate on flow stress.

The activation parameters, flow stresses and slip markings at low temperatures were consistent with a model of the rate controlling process being the thermally activated nucleation of dislocation kink pairs against the Peierls-Nabarro force. There was also evidence for a second process operating at low effective stresses, this was possibly the thermally aided motion of jogs on dislocation lines.

The flow stress at intermediate temperatures was controlled by the concentration of atomic defects due to deviations from stoichiometry. The vacancy defects resulting from excess aluminium atoms proved more potent as hardening agents than did substitutional atoms.

The rate controlling mechanism in stoichiometric NiAl at high temperature appeared to be the climb of dislocations past obstacles. The mechanisms in non-stoichiometric alloys were more complex - several processes appeared to operate, one of which caused a large peak in the apparent activation energy of deformation of aluminium-rich compositions.

The flow stresses of single crystals with [001] compression axes were generally higher than those which slipped in an [001] direction. The flow stress was controlled by a Peierls-Nabarro mechanism at low temperature, but there was no evidence of a second process. Intermediate temperature processes were masked by kinking. The activation energy of deformation at high temperatures was strongly stress (or temperature) dependent and was much higher than that of self-diffusion. The rate controlling process was probably the constriction of superdislocations to cross-slip around obstacles.

Work-hardening behaviour in polycrystals was parabolic at low temperatures, where no recovery occurred, as predicted by theories of work-hardening. Linear hardening was observed at all temperatures in single crystals with [011] axes.

The observed slip in crystals with [001] compression axes

provided two additional independent slip systems to the three available from the (110)[00] system giving the five systems required for general ductility. The fracture behaviour of polycrystalline NiAl was consistent with the explanation that the brittleness was due to the stress for the propagation of cracks being lower than that required to continue plastic deformation.

6.2. Suggestions for Further Work.

The object of this investigation was to make a general survey of the deformation behaviour of NiAl. It was therefore expected that all aspects of the subject could not be covered in equal detail, and that many areas of research that merited further study would be revealed. These areas were found to include measurements of basic physical parameters, e.g. shear moduli of non-stoichiometric compositions, that are required to correlate experimental data with theoretical models. Apart from these and minor suggestions made in chapter five mechanical property measurements that could produce useful and interesting results include:

i) A detailed comparison, including electron microscopy, of slip in hard and soft orientations between $4^{o}K$ and T_A. The extrapolated temperature dependences of flow stress cross at low temperatures and hard orientations appear to have the lower flow stress. Furthermore the deformation of hard orientations should involve the motion of superdislocations, hence greater disordering than in soft orientations; this should be revealed by changes in physical properties such as electrical resistivity. This study could also include the effects of deviations from stoichiometry; the presence of lattice defects should reduce the ordering energy and therefore increase the width of superdislocations.

ii) A similar study made at high temperatures could be relevant to the creep behaviour of ordered alloys. It was noted that the activation energy for high temperature deformation was higher when

slip occurred by the movement of superdislocations. A study of slip systems above 850°K could be included because the lowest critical resolved shear stress above this temperature appeared to be that of the hard orientation.

iii) Measurements of the athermal flow stress in compositions between stoichiometry and the extreme of the phase field. These could give an insight into the solid solution hardening processes and hence the rate controlling mechanisms at intermediate temperatures.

iv) A comparison with the single crystal properties of CoAl in view of the reported disordering of this isomorphous compound.

v) A further study of the pest phenomenon; particularly the conditions which lead to grain boundary precipitation and its relevance to overall ductility.

ACKNOWLEDGMENTS.

The author would like to thank his supervisor, Dr. C.W.A. Newey, for advice and assistance throughout the investigation.

The provision of research facilities in the Metallurgy Department by Professor J.G. Ball, and the financial assistance of the Ministry of Aviation and Science Research Council, are also gratefully acknowledged.

A P P E N D I X

GRAIN BOUNDARY "PEST" IN THE INTERMETALLIC COMPOUND NiAl

Grain Boundary "Pest" in the Intermetallic Compound NiAl

The "pest" phenomenon – the susceptibility to severe intergranular attack, which in the limit causes complete disintegration of a material – has been observed in a wide variety of intermetallic compounds, particularly silicides, beryllides and aluminides. The conditions under which it occurs are not clear. Westbrook and Wood [1] have shown that intergranular embrittlement in a wide variety of intermetallic compounds is associated with anomalous grain boundary hardening effects, resulting from the segregation of gaseous contaminants to the boundaries. Grain boundary hardening was only observed in compounds containing more than the stoichiometric proportion of the electropositive component. In a detailed study of NiGa, Seybolt and Westbrook [2] concluded that the hardening was due to the presence of dissolved oxygen, and they suggested that the hardening mechanisms might involve the lattice distortion produced by the formation of a Ga–O complex, e.g. an oxide, a sub-oxide or a cluster of oxygen atoms. Thus grain boundary hardening, which seems to be a necessary condition for the occurrence of the pest, can only be accounted for in a very tentative manner and, to date, no suggestions for a pest mechanism have been published. The purpose of this letter is to propose a mechanism for the pest which is based on some of the results of an investigation of the compound NiAl.

Specimens of NiAl containing 54 at. % Al, i.e. excess of Al, the electropositive component, were prepared from extruded rod supplied by the International Nickel Co (Mond) Ltd. NiAl is known to be very resistant to oxidation at temperatures below about 1100° C, but annealing in air for 2 h at 1400° C produced a white powdery deposit on the surface of the samples which was optically active under polarised light. Using an X-ray powder method, the deposit was shown to be predominantly α-Al_2O_3. Micro-hardness traverses, similar to those used by other investigators [1, 2], on the oxidised surfaces of these samples and on surfaces freshly prepared by mechanical polishing did not reveal any grain boundary hardening. However, upon subsequent annealing in air at 800° C and mechanical polishing, hardening effects were found which were similar in character and magnitude to those observed in NiAl by Westbrook and Wood [1]. (From the experiments carried out to date, it would seem that an anneal in air at an elevated temperature, about 1400° C, is an essential prerequisite for the occurrence of the pest.) Metallographic studies revealed the presence of precipitates predominantly at the grain boundaries and also, occasionally, within the grains; a typical example is shown in fig. 1. These precipitates

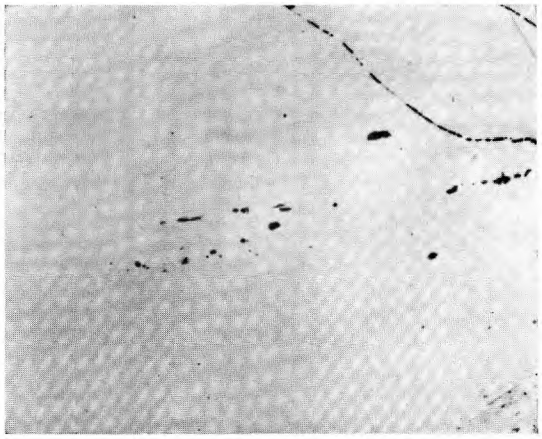

Figure 1 Distribution of precipitates (X152).

are inactive under polarised light and have a micro-hardness of about 2000 kg/mm^2. Preliminary electron microprobe traces across the precipitates have shown that they contain considerably more Al than the bulk specimen. This information suggests that the precipitates are of the sub-oxide Al_2O, a conclusion which is supported by the X-ray investigation of Hoch and Johnston [3], who established that when Al and α-Al_2O_3 were heated together a cubic phase of composition Al_2O was produced which was unstable at room temperature.

On exposure to the atmosphere at room temperature for a few days, the precipitates were observed to undergo a transformation. Initially, small regions of each particle became optically active under polarised light, and these areas spread until, eventually, the whole particle had transformed. This process is illustrated in figs. 2 and 3; the pested regions are the small very light areas within the grey particles. The darker grey appearance of these same particles in fig. 2 is merely a photographic effect. It was found that the transformation could be accelerated considerably in the presence of an oxidising agent, H_2O_2. The product of the transformation was white, powdery in form, optically active,

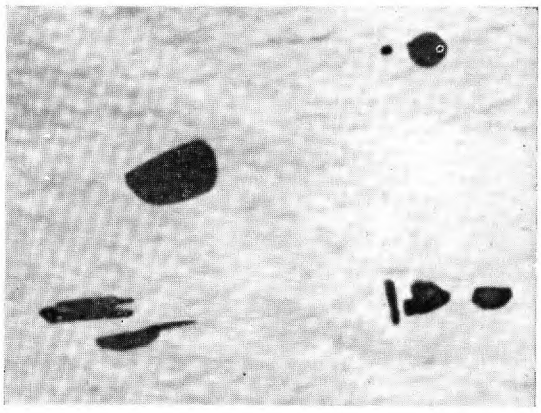

Figure 2 Al_2O precipitates before transformation (X1300).

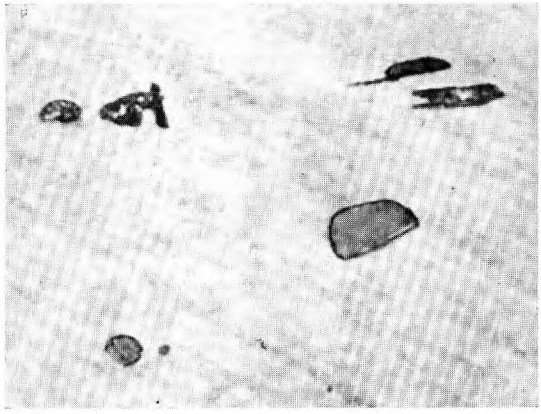

Figure 3 The same particles as shown in fig. 2 after 8 days exposure to the atmosphere at room temperature; the transformation to α—Al_2O_3 is more complete in the smaller particles (X1300).

and it could not be distinguished from the oxide layer present on the original surface. The initially flat surfaces of the Al_2O particles became so uneven that satisfactory electron microprobe traces could not be made; this feature indicates that a considerable volume expansion is involved in the transformation. It seems reasonable to assume that the product of the transformation is α-Al_2O_3. During the transformation the grain boundary hardening effects disappear and, in general, the grain boundary regions become softer than the grains.

These results indicate that the pest phenomenon is associated with the oxidation of Al_2O to α-Al_2O_3. This transformation probably occurs at internal boundaries by the diffusion of oxygen along the grain boundaries, and disintegration could then follow as a result of the internal strains produced by the volume expansion involved in the transformation. Such a process would open up the material along the grain boundaries and allow oxygen to diffuse further into the interior to continue the transformation.

A mechanism of this type is supported by the experimental observation that, when new surfaces were prepared in partially "pested" samples, precipitates in the bulk of the grains were still in the Al_2O form. The effect may be attributed to the extremely slow bulk diffusion of oxygen at room temperature, and would account for the striking feature of the pest observed by Westbrook and Wood [1] – that the individual grains in a "pested" sample could still undergo plastic deformation.

The factors which determine the formation of Al_2O and the mechanisms of grain boundary hardening will be discussed in detail in a later publication.

This work was supported in part by an SRC research grant and a Ministry of Aviation contract. One of us (R. T. Pascoe) is indebted to the Ministry of Aviation for the provision of a bursary.

References

1. J. H. WESTBROOK and D. L. WOOD, *J. Inst. Metals* **91** (1963) 174.
2. A. U. SEYBOLT and J. H. WESTBROOK, *Acta Met.* **12** (1964) 449.
3. M. HOCH and H. L. JOHNSTON, *J. Am. Chem. Soc.* **76** (1954) 2560.

15 November 1965

P. A. TURNER
R. T. PASCOE
C. W. A. NEWEY
Department of Metallurgy
Imperial College
London, SW7
UK

LIST OF SYMBOLS.

The following symbols have been used throughout this thesis. Others have appeared in specific instances and are defined where they occur.

a	lattice spacing
b	Burgers vector
C	shear modulus in the slip direction
d	grain size
d^*	activation distance
e/a	electron to atom ratio
E	energy
E_{APB}	anti-phase boundary energy
E_{int}	interaction energy between two dislocations
E_K	energy to nucleate a single kink across a Peierls-Nabarro barrier
$G = \Delta G$	Gibbs free energy
$H = \Delta H$	activation enthalpy of deformation
H_o	H at zero effective stress
H_{SD}	activation enthalpy of self-diffusion
K	energy factor which is a function of the elastic moduli and direction of the dislocation line in an anisotropic medium
k	Boltzmann's constant

l^*	length of dislocation line involved in thermal activation
m	dislocation velocity exponent defined by equation 1.30
m'	apparent dislocation velocity exponent defined by equation 1.32
$\bar{m}$	mean orientation factor
n	work hardening exponent defined by equation 4.1
Q	activation energy of deformation
R	outer cut-off radius of a dislocation stress field
r_o	inner cut-off radius (radius of dislocation core)
S	long range order parameter
$S = \Delta S$	entropy (of activation)
T	absolute temperature
T_A	temperature for the start of the athermal process
T_c	temperature for the onset of the high temperature deformation process
T_C	critical ordering temperature (Chapters 1 to 3)
T_m	melting point
T_o	temperature at which thermal fluctuations can overcome the entire Peierls force
u	dislocation velocity
V_{AA}, V_{BB}	bond energies between like atoms
V_{AB}	bond energy between unlike atoms
v^*	activation volume

w	distance between imperfect dislocations in a superdislocation
γ	surface energy
ϵ	strain
ϵ_m	maximum strain before fracture (ductility)
$\dot{\epsilon}$	strain-rate
$\dot{\epsilon}_o$	pre-exponential constant in equation 1.14, structure dependent
ζ	width of a dislocation
θ	work hardening rate
μ	shear modulus
ρ	mobile dislocation density
σ	stress
τ	resolved shear stress

Subscripts to stresses (used with either σ or τ)

f	flow stress
i	internal stress
m	maximum stress in compression
p	0.2% proof stress
μ	athermal stress
o	stress where dislocation velocity is unity (equation 1.30)
0.01	1% proof stress

$\tau^*(\sigma^*)$ thermally activated component of stress (effective stress)

$\tau_p^*(\sigma_p^*)$ Peierls-Nabarro stress (effective stress at $0^\circ K$)

$(\Delta\sigma)_T$ change of stress due to a change of strain-rate at constant temperature

REFERENCES.

N.V. Ageev and L.N. Guseva (1949) Izvest. Akad. Nauk. SSSR, Otdel. Khim. Nauk., 1949, 225.

G. Alefeld (1962) Z. Naturforschg. 17, 889.

W.O. Alexander and N.B. Vaughn (1937) J. Inst. Met. 61, 247.

N.P. Allen (1964) Rev. Metallurg. 61, 827.

S. Amelinckx (1961) Mechanical Properties of Engineering Ceramics, ed. Krigel and Palmour, Interscience

R.J. Arsenault (1966) Acta Met. 14, 831.

K.T. Aust (1963) The Art and Science of Growing Crystals ed. Gilman, Wiley, p. 452.

A. Ball (1964) Ph.D. thesis, Birmingham University.

A. Ball and R.E. Smallman (1964) Proc. 3rd Europ. Reg. Conf. on Electron Microscopy (Prague), p. 273.

A. Ball and R.E. Smallman (1966 A) Acta Met. 14, p. 1349.

A. Ball and R.E. Smallman (1966 B) to be published in Acta Met.

Z.S. Basinski (1957) Acta Met. 5, 684.

A.E. Berkowitz, F.E. Jaumot and F.C. Nix (1954) Phys. Rev. 95, 1185.

H.A. Bethe (1935) Proc. Roy. Soc. A150, 552.

K.C.A. Blasdale and R. King (1965) Phys. Stat. Sol. 10, 175.

A.J. Bradley (1951) J.I.S.I. 168, 233.

A.J. Bradley and A. Taylor (1937) Proc. Roy. Soc. A159, 56.

W.L. Bragg and E.J. Williams (1935) Proc. Roy. Soc. A151, 540.

N. Brown (1959) Phil. Mag. 4, 693.

N. Brown and M. Herman (1956) Trans. Met. Soc. A.I.M.E. 206, 1353.

R.W. Cahn and J.A. Coll (1961) Acta Met. 9, 138.

H.C.H. Carpenter and C.F. Elam (1922) Proc. Roy. Soc. A100, 329.

N.K. Chen and R. Maddin (1951) Trans. Met. Soc. A.I.M.E. 191, 937.

J.W. Christian (1964) Acta Met. 12, 99.

J.W. Christian and B.C. Masters (1964 A) Proc. Roy. Soc. A281, 223.

J.W. Christian and B.C. Masters (1964 B) Proc. Roy. Soc. A281, 240.

R. Collongues (1956) Inst. Intern. de Chimie Solvay - 10^{ieme} Conseil de Chimie, Brussels.

H. Conrad (1961 A) Mech. Behaviour of Materials at Elevated Temperatures, ed. Dorn, Wiley, p. 149.

H. Conrad (1961 B) J.I.S.I. 198, 364.

H. Conrad (1963) The Relation between Structure and Mechanical Properties of Metals, H.M.S.O., p. 476.

H. Conrad (1964) J. Metals, 16, 583.

H. Conrad, G. Stone and K. Janowski (1965) Trans. Met. Soc. A.I.M.E. 233, 889.

H. Conrad and H. Wiedersich (1960) Acta Met. 8, 128.

M.J. Cooper (1963 A) Phil. Mag. 8, 805.

M.J. Cooper (1963 B) Phil. Mag. 8, 811.

M.J. Cooper (1964) Phil. Mag. 10, 735.

S.M. Copley (1963) Phil. Mag. 8, 1599.

A.H. Cottrell (1953) Dislocations and Plastic Flow in Crystals, Oxford U.P.

A.H. Cottrell (1958) Trans. Met. Soc. A.I.M.E. 212, 192.

A.H. Cottrell (1963) The Relation between Structure and Mechanical Properties of Metals, H.M.S.O., p. 456.

A.H. Cottrell and R.J. Stokes (1955) Proc. Roy. Soc. A233, 17.

D.J. Dingley and K.F. Hale (1966) to be published in Proc. Roy. Soc.

H.A. Domian and H.I. Aaronson (1964) Trans. Met. Soc. A.I.M.E. 230, 44.

J.E. Dorn and J.B. Mitchell (1964) University of California, UCRL-11418.

J.E. Dorn and S. Rajnak (1964) Trans. Met. Soc. A.I.M.E. 230, 1053.

J.D. Eshelby (1949) Phil. Mag. 40, 903.

P.R.V. Evans, A.F. Weinberg and R.J. Van Thyne (1963) Acta Met. 11, 143.

H. Eyring (1936) J. Chem. Phys. 4, 383.

W.L. Fink and L.A. Willey (1934) Trans. A.I.M.E. 111, 293.

J.C. Fisher (1954) Acta Met. 2, 9.

R.L. Fleischer (1958) J. Mech. Phys. Sol. 6, 301.

R.L. Fleischer and W.R. Hibbard (1963) The Relation between Structure and Mechanical Properties of Metals, H.M.S.O., p. 261.

P.A. Flinn (1960) Trans. Met. Soc. A.I.M.E. 218, 145.

A.J.E. Foreman (1955) Acta Met. 3, 322.

R.A. Foxall and M. Duesbury (1965) Dresden Conf. on Pure Materials.

J. Fridel (1963) Electron Microscopy and the Strength of Crystals, ed. Washburn and Thomas, Interscience.

P.P. Gillis and J.J. Gilman (1965 A) J. Appl. Phys. 36, 3370.

P.P. Gillis and J.J. Gilman (1965 B) J. Appl. Phys. 36, 3380.

J.J. Gilman (1960) Aust. J. Phys. 13, 327.

J.J. Gilman (1963) editor The Art and Science of Growing Crystals, Wiley.

J.J. Gilman (1965) J. Appl. Phys. 36, 3195.

J.J. Gilman and W.G. Johnston (1957) Dislocations and Mechanical Properties of Crystals, ed. Fisher, Johnston, Thompson and Vreeland, Wiley.

E.M. Grala (1960) Symp. Mechanical Properties of Intermetallic Compounds, ed. Westbrook, Wiley, p. 358.

G.W. Groves and A. Kelly (1963) Phil. Mag. 8, 877.

R.W. Guard (1961) Acta Met. 9, 163.

R.W. Guard and A.M. Turkalo (1960) Symp. Mechanical Properties of Intermetallic Compounds, ed. Westbrook, Wiley, p. 141.

F. Guiu and P.L. Pratt (1966) Phys. Stat. Sol. 15, 539.

L.N. Guseva (1951) Doklady Akad. Nauk. S.S.S.R. 77, 145.

L. Guttman (1956) Solid State Physics 3, 415.

A.G.C. Gwyer (1908) Z. Anorg. Chem. 57, p. 113.

P. Haasen (1957) Acta Met. 5, 598.

P. Haasen (1965) Physical Metallurgy, ed. Cahn, North Holland Publishing Company, p. 821.

G.T. Hahn (1962) Acta Met. 10, 727.

R.C. Hall (1957) Trans. Met. Soc. A.I.M.E. 209, 1267.

J.B. Hess and C.S. Barrett (1949) Trans. Met. Soc. A.I.M.E. 185, 599.

M. Hansen (1958) Constitution of Binary Alloys, McGraw-Hill.

R.W.K. Honeycomb (1959) Met. Rev. 4, 1.

W. Hume-Rothery and G.V. Raynor (1962) The Structure of Metals and Alloys, Institute of Metals.

Y. Imai and M. Kumazawa (1959) Sci. Rep. Res. Inst. Tokahu Univ. A.11, 312.

Isaichev and Mirekskii (1940) J. Tech. Phys. U.S.S.R. 10, 316.

Y. Ishida, C-Y. Cheng and J.E. Dorn (1966) Trans. Met. Soc. A.I.M.E. 236, 964.

L.D. Johnson and J.A. Pask (1964) J. Am. Ceram. Soc. 14, 437.

W.G. Johnston (1962) J. Appl. Phys. 33, 2716.

W.G. Johnston and J.J. Gilman (1959) J. Appl. Phys. 30, 129.

W.G. Johnston and D.F. Stein (1963) Acta Met. 11, 317.

A. Kelly (1961) Instron Application Series H-6.

U.F. Kocks (1964) Phil. Mag. 10, 187.

U.F. Kocks, Y. Nakada and B. Ramaswami (1964) Trans. Met. Soc. A.I.M.E. 230, 1005.

J.S. Koehler and F. Seitz (1947) J. Appl. Mech. 14, A217.

M.A. Krivoglaz and A.A. Smirov (1964) Theory of Order-Disorder in Alloys, McDonald.

O. Kubaschewski (1958) Trans. Farad. Soc. 54, 814.

O. Kubaschewski and J.A. Catterall (1956) Thermochemical Data of Alloys, Pergamon Press.

D. Kuhlman-Wilsdorf (1960) Phys. Rev. 120, 773.

V.B. Kurfman (1965) Acta Met. 13, 307.

E.P. Lautenslager, D.A. Kiewit and J.O. Brittain (1965) Trans. Met. Soc. A.I.M.E. 233, 1297.

F. Laves (1952) Naturwissenschaften 39, 546.

J.C.M. Li (1965) Trans. Met. Soc. A.I.M.E. 233, 219.

H. Lipson and A. Taylor (1939) Proc. Roy. Soc. A.173, 232.

M.J. Marcinkowski (1963) Electron Microscopy and Strength of Crystals ed. Thomas and Washburn, Wiley, p. 333.

M.J. Marcinkowski and H. Chessin (1964) Phil. Mag. 10, 837.

M.J. Marcinkowski and R.M. Fisher (1963) J. Appl. Phys. 34, 2135.

N.D. Meakin and N.J. Petch (1963) Fracture of Solids, Interscience, p. 393.

T.E. Mitchell and W.A. Spitzig (1965) Acta Met. 13, 1169.

G.P. Mohanty (1966) Phys. Lett. 20, 224.

G.P. Mohanty and J.J. Wert (1963) Acta Met. 11, 217.

N.F. Mott (1937) Proc. Phys. Soc. 49, 258.

A.K. Mukherjee and J.E. Dorn (1964) Trans. Met. Soc. A.I.M.E. 230, 1065.

A.K. Mukherjee and J.E. Dorn (1965) J. Inst. Met. 93, 397.

A.K. Mukherjee, W.G. Ferguson, W.L. Barmore and J.E. Dorn (1965) University of California, UCRL-16433.

T. Muto and Y. Takagi (1955) Solid State Physics 1, 194.

F.R.N. Nabarro (1950) Phys. Rev. 79, 894.

B.J. Nield and A.G. Quarrell (1957) J. Inst. Met. 85, 480.

F.W. Noble and D. Hull (1965) Phil. Mag. 12, 777.

E. Orowan (1942) Nature 149, 643.

R.M. Paine, A.J. Stonehouse and M.B. Bever (1960) Wright Air Development Command Technical Report WADC TR 59-29.

H.W.L. Phillips (1942) J. Inst. Met. 68, 27.

W.A. Rachinger and A.H. Cottrell (1956 A) Acta Met. 4, 109.

W.A. Rachinger and A.H. Cottrell (1956 B) Acta Met. 4, 647.

A.E. Ray and J.F. Smith (1958) Acta Cryst. 11, 310.

C.N. Reid (1966) Acta Met. 14, 13.

P.M. Robinson and M.B. Bever (1965) Acta Met. 13, 647.

P.M. Robinson and M.B. Bever (1966) Acta Met. 14, 693.

A.G. Rozner (1965) Trans. Met. Soc. A.I.M.E. 233, 1646.

A.G. Rozner and R.J. Wasilewski (1966) J. Inst. Met. 94, 169.

E.M. Savitsky, Ch.V. Kopetsky and E.P. Arskaya (1964) Izvest. Akad. Nauk. S.S.S.R. Met. i. Gorne. Delo 1964, 129.

H.W. Schadler (1963) The Art and Science of Growing Crystals, ed. Gilman, Wiley, p. 343.

E. Schmid and W. Boas (1950) Plasticity of Crystals, F.A. Hughes and Co.

R.H. Schnitzel (1965) J. Less Com. Met. 8, 81.

G. Schoeck (1961 A) Acta Met. 9, 382.

G. Schoeck (1961 B) Mech. Behaviour of Materials at Elevated Temperatures, ed. Dorn, Wiley, p. 79.

G. Schoeck (1965) Phys. Stat. Sol. 8, 499.

G. Schoeck and A. Seeger (1955) Defects in Crystalline Solids, Physical Society, p. 340.

C.M. Sellars and W.McG. Tegart (1966) Acta Met. 14, 1136.

A.U. Seybolt and J.H. Westbrook (1964) Acta Met. 12, 449.

J.A. Sheppard (1963) Brit. Weld. Journ. 10, 603.

O.D. Sherby, J. Lytton and J.E. Dorn (1957) Acta Met. 5, 219.

A. Smakula and M.W. Klein (1951) Phys. Rev. 84, 1043.

E. Smith and P.J. Worthington (1965) Int. Conf. on Fracture Sendai Japan, p. A163.

D.F. Stein and J.R. Low (1960) J. Appl. Phys. 31, 362.

A. Steiner and K.L. Komarek (1964) Trans. Met. Soc. A.I.M.E. 230, 786.

R.J. Stokes (1965) O.N.R. Technical Report, Nonr-4076(00) NR-032-451.

N.S. Stoloff and R.G. Davies (1964) Acta Met. 12, 473.

N.S. Stoloff and R.G. Davies (1966) Prog. Matl. Science 13, 1.

C. Sykes and H. Wilkinson (1937) J. Inst. Met. 61, 223.

G.I. Taylor (1927) Proc. Roy. Soc. A.116, 16.

G.I. Taylor (1928) Trans. Farad. Soc. 24, 121.

G.I. Taylor (1938) J. Inst. Met. 62, 307.

G.I. Taylor and C.F. Elam (1926) Proc. Roy. Soc. A.112, 337.

J.C. Terry and R.E. Smallman (1963) Phil. Mag. 8, 1827.

J.C. Terry and R.E. Smallman (1964) J. Inst. Met. 92, 334.

Tret'yakov and Khomyakov (1959) Russ. J. Inorg. Chem. 4, 5.

P.A. Turner, R.T. Pascoe and C.W.A. Newey (1966) J. Matl. Sci. 1, 113.

A.A. Urusovskaya and R. Thyagarajan (1965) Phys. Stat. Sol. 10, 349.

A.A. Vertman and A.M. Samarin (1961) Izvest. Akad. Nauk. S.S.S.R. Met. i. Topl. 1961, 159.

A.E. Vidoz and L.M. Brown (1962) Phil. Mag. 7, 1167.

R. Von Mises (1928) Z. Angew. Math. Mech. 8, 161.

F.E. Wang, W.J. Buehler and S.J. Pickart (1965) J. Appl. Phys. 36, 3232.

R.J. Wasilewski (1966) Trans. Met. Soc. A.I.M.E. 236, 455.

R.J. Wasilewski, S.R. Butler and J.E. Hanlon (1966) to be published.

J. Weertman (1957 A) J. Appl. Phys. 28, 362.

J. Weertman (1957 B) J. Appl. Phys. 28, 1185.

J. Weertman (1960) Trans. Met. Soc. A.I.M.E. 218, 207.

J. Weertman and J.R. Weertman (1965) Physical Metallurgy, ed. Cahn, North Holland Publishing Company, p. 735.

G.W. West (1964) Phil. Mag. 9, 979.

G.W. West and L.E. Drain (1965) Phil. Mag. 12, 119.

J.H. Westbrook (1953) Trans. A.S.M. 45, 221.

J.H. Westbrook (1956) J. Electrochem. Soc. 103, 54.

J.H. Westbrook (1957) J. Electrochem. Soc. 104, 369.

J.H. Westbrook (1960) Symp. Mechanical Properties of Intermetallic Compounds, ed. Westbrook, Wiley, p. 1.

J.H. Westbrook (1965) High Strength Materials, ed. Zackay, Wiley, p. 724.

J.H. Westbrook, H.E. Grenoble and D.L. Wood (1964) Wright Air Development Division Technical Report WADD TR-60-184, Part V.

J.H. Westbrook and D.L. Wood (1963 A) J. Inst. Met. 91, 174.

J.H. Westbrook and D.L. Wood (1963 B) G. E. Res. Report 63-RL-3324M.

W.D. Wilkinson (1963) Laboratory Handbook, ed. Parr, Newnes, p. 5-105.

G.K. Williamson and R.E. Smallman (1953) Acta Met. 1, 487.

D.L. Wood (1960) Symp. Mechanical Properties of Intermetallic Compounds, ed. Westbrook, Wiley, p. 161.

D.L. Wood (1961) Mechanical Props. of Engineering Ceramics, ed. Krigel and Palmour, Interscience, p. 477.

D.L. Wood and J.H. Westbrook (1960) Wright Air Development Division Technical Report WADD TR-60-184, Part I.

D.L. Wood and J.H. Westbrook (1961) Wright Air Development Division Technical Report WADD TR-60-184, Part II.

D.L. Wood and J.H. Westbrook (1962) Trans. Met. Soc. A.I.M.E. 224, 1024.

K. Yamaguchi (1929) Sci. Pap. I.P.C.R. (Tokyo) 11, 151.